

# Master Thesis

Leopoldo Losa



**POLITECNICO**  
MILANO 1863

Comprehensive Analysis of Cryogenic Machining  
Application through the Development of a Finite  
Element Model of Ti6Al4V Milling

Machine Tools and Manufacturing Systems

Master degree student:

Leopoldo Losa

918524

Supervisor:

Paolo Albertelli

Co-supervisor:

Matteo Strano

**Academic year 2019/20**



# Contents

<b>1</b>	<b>Introduction</b>	<b>4</b>
1.1	Cryogenic Manufacturing Processes . . . . .	4
1.1.1	Cryogenic Forming . . . . .	4
1.1.2	Cryogenic Processing . . . . .	5
1.1.3	Cryogenic Machining . . . . .	5
1.1.4	Hybrid machining . . . . .	6
<b>2</b>	<b>Cryogenic Machining Fundamentals</b>	<b>8</b>
2.1	Cutting zone temperature . . . . .	9
2.1.1	Cutting zone temperature generation . . . . .	9
2.1.2	Temperature dependent tool wear mechanisms . . . . .	10
2.1.3	Material properties at cryogenic temperatures . . . . .	13
2.2	Cryogenic fluxes heat dissipation . . . . .	15
2.2.1	Workpiece Cooling . . . . .	16
2.2.2	Indirect Cooling . . . . .	17
2.2.3	Pressure jet cooling . . . . .	17
2.2.4	Hybrid Cooling . . . . .	19
2.3	Tribology and chip morphology . . . . .	20
2.3.1	Cutting forces . . . . .	20
2.3.2	Coefficient of Friction . . . . .	21
2.3.3	Chip morphology . . . . .	22
2.4	Productivity . . . . .	26
2.4.1	Tool wear, wear rate, life and failures . . . . .	27
2.4.2	Product quality and performances . . . . .	27
2.5	Economics and ecologies . . . . .	29
2.5.1	Cutting fluids consumption and impact . . . . .	30
<b>3</b>	<b>Application of Cryogenics</b>	<b>33</b>
3.1	Tool design . . . . .	33
3.1.1	Turning and Milling angles . . . . .	33
3.1.2	Cryogenic Tool design . . . . .	35
3.2	Cutting parameters and approach . . . . .	36
3.2.1	Natural process parameters . . . . .	36
3.2.2	Cryogenic parameters . . . . .	38
3.3	Cryogenic systems . . . . .	39
3.3.1	Cryogenic production units . . . . .	39
3.3.2	Cryogenic delivering system and issues . . . . .	40

<b>4</b>	<b>Cryogenic machining performance</b>	<b>49</b>
4.1	Workpiece material: cryogenic machining of Ti-6Al-4V . . . . .	49
4.1.1	Turning approach . . . . .	52
4.1.2	Milling operations . . . . .	62
4.1.3	Conclusion . . . . .	67
4.2	Insert materials . . . . .	67
4.2.1	High Speed Steels, HSS . . . . .	67
4.2.2	Carbides . . . . .	68
4.2.3	Ceramics, CBN, PCD . . . . .	68
4.3	Cooling media . . . . .	68
4.3.1	Liquid Nitrogen, LN2 . . . . .	70
4.3.2	Liquid Carbon Dioxide, LCO2 . . . . .	71
4.3.3	Chilled Air . . . . .	71
<b>5</b>	<b>Modeling Machining Processes</b>	<b>73</b>
5.1	Thermal models . . . . .	75
5.1.1	Temperature measurements . . . . .	75
5.1.2	Pure Thermal Models . . . . .	77
5.1.3	Temperature prediction in Milling . . . . .	78
5.1.4	Thermal behaviour in chip removal simulations . . . . .	83
5.2	Tribology . . . . .	85
5.2.1	Contact models for cutting simulations . . . . .	86
5.2.2	Friction determination for cutting simulations . . . . .	95
5.3	Material models . . . . .	105
5.3.1	Shear banding and damage models . . . . .	106
5.3.2	Models application to Titanium cutting . . . . .	108
5.4	Computational Fluid Dynamics . . . . .	125
5.5	Cryogenic machining simulations . . . . .	130
5.6	Hybrid Modeling . . . . .	133
5.7	Surface integrity prediction models . . . . .	135
<b>6</b>	<b>FEM models for Cryogenic Milling</b>	<b>139</b>
6.1	“Square shoulder” model . . . . .	139
6.1.1	Geometry generation . . . . .	140
6.1.2	Mesh generation . . . . .	143
6.1.3	Material and thermal properties . . . . .	143
6.1.4	Motions . . . . .	144
6.1.5	Interactions . . . . .	144
6.1.6	Calculation settings . . . . .	146
6.2	Experimental Campaigns . . . . .	146
6.2.1	Shoulder milling tests . . . . .	146
6.3	“Square shoulder” Model Fitting . . . . .	155
6.3.1	Material model and mesh size fitting . . . . .	156
6.3.2	Damage model . . . . .	163
6.3.3	Contact model set up . . . . .	165

<b>7</b>	<b>Model results</b>	<b>170</b>
7.1	Dry Environment . . . . .	170
7.1.1	Cutting parameters influence . . . . .	174
7.1.2	Cutting mechanics and tool stress analysis . . . . .	180
7.2	Cryogenic Environment . . . . .	185
7.2.1	Cryogenic cutting mechanics and tool stress analysis . . . . .	192
7.3	Summary . . . . .	196
<b>8</b>	<b>Summary and Conclusion</b>	<b>197</b>

# Abstract

The aim of this work consists in the simulation of cryogenically assisted milling of Titanium alloy Ti6Al4V to investigate the mechanisms responsible for inconsistent tool life performances. While cryogenic fluids have enhanced productivity for most studies in turning, in milling research is still at work due to increased process complexity.

Titanium, Nickel, Cobalt alloys, Stainless steels are designed for superior strength, fatigue, corrosion, toughness properties. They retain those properties at high temperature and present lower conductivity with respect to common steels. Cutting zone heat build up increases, without softening the material, promoting high wear rates. High strength alloys have been increasingly adopted in aerospace, chemical, structural, automotive fields who demands for high material removal rate technologies withstanding hard materials.

FE Simulations can provide information on machining processes hardly achievable with experiments. However, a numerical model need to be trustful. A good knowledge of machining and cryogenic applications can steer simulation toward the wanted targets in a reduced amount of time and discriminate on the goodness of the produced results. An introduction to cutting processes and Ti6Al4V machining is presented.

Many studies have analysed cutting performances considering various couples WP-Tool, but there are inconsistencies regarding cutting forces, friction coefficients, tool life. A critical analysis was made regarding experimental findings into the field of Cryogenic Machining application to Ti6Al4V.

The improvements regarding cutting performances seem to be strongly dependent on the cryogen delivery design. A review on delivery design solutions in relation with achieved performances is undertaken.

Many researchers focused on simulation of machining processes, trying to reproduce numerically their experimental findings, predict temperature and stress distributions in the tool-chip interface, combining them to forecast wear rates. A deep state of the art analyses (thermal, material and friction models) have been performed to help in the final model set up.

Experimental tool life tests were performed for dry, emulsion and cryogenic cooling with square shoulder mill. Cutting performances proved poor for cryogenic cooling if compared with emulsion. Measured quantities helped in setting up a FE model to better understand the aroused problematic.

Material models developed for orthogonal cutting simulations proved inefficient for heavy industrial-purpose numerical models. Stress flow response for Ti6Al4V were compared, exhibiting high variability. Simple Johnson-Cook material and Latham-Cockcroft damage models can predict square shoulder milling experimental results.

The FE Model could reproduce experimental chip morphology and cutting force ( $\sim 10\%$  error) for four different feed and speed combinations in dry and cryogenic cutting (8 different conditions). Lower friction needed to match cryogenic experiments. Results suggest the tendency of cryogenic machining to increase the local load on cutting edges. Tool geometries and materials need to be tougher. Attention should be given to smooth chip load evolution on cutting insert during engagement. A new interpretation of issues regarding tool wear and life results is therefore demonstrated. Work material exhibit lower plasticity. Simulated cutting temperature was slightly reduced. The portion of heat flowing into the tool increased due to lower temperature reached in the non-cutting phase rake face cooling. Consequently, the idle phase cooling action of jets on inserts is important.

# Map of concepts

## Introduction to Machining Processes:

**Chapter\_1:** Introduction of Cryogenic Manufacturing processes

**Chapter\_2:** Machining fundamentals. Mechanics of the cutting process: cutting forces and friction. Temperature generation and tool wear. Work material properties and chip morphology. Productivity, Economics and Ecologic

## Literature Review:

**Chapter\_3:** Cutting zone application of cryogenic fluids review. Tool design, cutting parameters and approaches. Cryogenic production and delivery systems

**Chapter\_4:** Review of experimental application of Ti6Al4V cryogenic turning and milling: cutting performances, insert materials, cooling media

**Chapter\_5:** Review of Machining oriented Modeling. Thermal measurement, models, thermal problem in chip forming simulations. Friction modeling, experimental friction evaluation for cutting models. Material modeling and application to machining simulation of shear bands affected materials. CFD and experimental cutting fluids cooling capacity. Analysis of FE Models and Hybrid CFD-FEM, for complete cryogenic machining simulations

## Numerical Model:

**Chapter\_6:** Model development based on experimental observations:

**Model set up:** Model objectives. Geometries, cinematics, dry and cryogenic interactions

**Experimental Campaign:** Dry, Emulsion cooling and Cryogenic cutting trials. Elaboration of cutting forces and comparison between cutting environments

**Model fitting:** Analysis of material model through orthogonal cutting simulations. Limits of material models developed for orthogonal cutting simulations. Variability of stress flow description for Ti6Al4V. Final choice through 3D simulation with damage model

**Chapter\_7:** Dry cutting results comparison with experiments. Evaluation of model prediction capability for achieved dry cutting technology. Cryogenic cutting comparison with experiments. Cryogenic and Dry comparison of simulated quantities, understanding of cryogenic machining issues through model results

## Conclusion:

**Chapter\_8:** Summary of findings. Future work concerning experimental trials, experimental quantities for modeling purposes and modeling objectives. Acknowledgments and tables ordering bibliography per subject



# Chapter 1

## Introduction

### 1.1 Cryogenic Manufacturing Processes

Cryogenic Manufacturing Processes are production oriented operations in which a cooling media is adopted in order to exploit advantages of material properties obtained at low temperatures. They can be divided into: Cryogenic Machining, Cryogenic Processing and Cryogenic Forming processes. Cryogenic Processing is somehow related with Machining as one of its more diffuse application relies in the study of procedures, involving low temperatures, for the enhancement of the performance characteristics of tools in metal cutting.

Cryogenics (Kryos: icy cold) refers to environments at very low temperature. There is no general agreement on the threshold where Cryogenics starts and refrigeration ends, [1, Jawahir 2016]. For what concerns machining, cryogenics refers to adoption of liquefied gases like LN2 ( $T_{lv} \cong -196^\circ C$ ), CO2 ( $T_{lv} \cong -78^\circ C$ ), while in general the term refers to temperature lower than  $-150^\circ C$  or  $-180^\circ C$ , being the liquation point of permanent gases colder (Nitrogen, Hydrogen, Helium, Oxygen, Air, Argon). Some applications of Cryogenic manufacturing, especially for Machining, make also use of chilled air up to  $-50^\circ C$ .

#### 1.1.1 Cryogenic Forming

Cryogenic Forming exploit the advantages coming from low temperature ductile to brittle transition of BCC metals. Less energy will be required to punch carbon steels at cryogenic temperature as a result of reduced fracture elongation. At the other side, for FCC metals that does not exhibit ductile to brittle transition, cryogenic temperature deformation can enhance properties by increasing dislocation density and work hardening abilities: when the material gets loaded dislocation arrange into cell structure. Cell structure size gets lower with decreasing temperature, therefore dislocation density of a low temperature formed FCC metal increase. High density of defects and consequent recrystallization lead to finer grain structure requiring less plastic deformation at cryogenic temperature, [1, Jawahir 2016].

### 1.1.2 Cryogenic Processing

Cryogenic Processing aims at the enhancement of material properties through developing heat treatment procedures at very low temperatures. In fact it would be more intuitive to call them Cold Treatments instead of Heat Treatments. Cryogenic Treatments can be adopted to enhance hardness, wear resistance properties, dimensional stability of tools for metal cutting, [2, Yildiz 2008]. By lingering some time at very low temperatures, with smooth cooling and warming rates to prevent residual stresses, allow metallurgical structure of metals to stabilize, relax or develop ultra fine and homogeneous texture, strengthening tools during cutting operations.

HSS Tools treated at low temperatures shows lower levels of retained Austenite (RA). With high pressure and temperature developed in the cutting zone, retained Austenite can transform into martensite with associated shrinkage and development of microcracks. Those phenomena enhances tool wear and chipping mechanisms, [3, Shokrani 2013]. Cryogenic processing help in transforming the RA almost completely into martensite, then a tempering treatment will compensate for the necessary toughness, [1, 4, Jawahir 2016, Deshpande 2018]. However there are inconsistent results regarding HSS drills and mills in comparison with the non-cryogenic treated counterparts. Tailoring cooling, lingering and heating phase have been done for trials and mechanisms explaining enhanced wear properties have to be clarified in depth, [3, 4, Shokrani 2013, Deshpande 2018].

Carbide containing inserts treated at low temperatures exhibit homogeneously dispersed ultra fine carbide particles. At low temperatures Carbon atoms tend to cluster, this clusters works as nuclei for the formation of disperse ultra fine carbides, richer in alloying elements, during the warming up of the piece to room temperature. This result in a denser, refined uniform structure, characterized by lower internal stresses, [1, 3, Jawahir 2016, Shokrani 2013]. Thermal conductivity raises for increase in size and dispersion of carbides and reduced bonding, [4, Deshpande 2018].

However, there is little mention in the literature regarding the application of cryogenic treated inserts in cryogenic machining. Do cryogenic treated inserts behave better than non-treated counterparts in cryogenic machining? Then little mention is done on cost and energy consumption comparison between treated and non treated inserts. Cutting tools are currently considered only through cost and time (time for change when worn). MT owners do not care about energy enclosed in them (consumption to realize them). Cutting inserts are consumed and thrown away. Anyway, the price to the environment we all will pay in the future. Therefore, additional cost-to-benefit ratio related to long-lasting and energy demanding cryogenic treatment of insert must be carefully analysed.

### 1.1.3 Cryogenic Machining

Cryogenic Machining can be considered as an evolution of classical Machining, where any sort of super-cool substances is applied to the workpiece (WP) or cutting zone. Mainly, cutting fluids are substituted, from usual lubro-coolants such as Mineral-Oil-Floods, by cryogenic liquefied gases: liquid nitrogen LN2, liquid carbon dioxide LCO2 are the most used.

Machining is defined as removal process: starting from a blank, through sharp, diversely

shaped tools and different approaches, the piece is processed and material is removed so to obtain the final shape. The different approaches refer to the technological achievement of relative speed between the tools and the workpiece:

- Turning: a sharp tool advances in the axial or radial direction while an axisymmetric workpiece rotates;
- Milling: the tool rotates while workpiece or the tool head moves in space;
- Drilling: a tool rotates and penetrates the piece making variously shaped axisymmetric holes;
- Grinding: an abrasive tool rotates removing by abrasion, ablation and ploughing, thin layers of material per cycle. Optimal tolerances with hard to cut materials can be achieved, but the process is highly energy demanding;
- Ultrasonic Machining: rotating abrasive tools vibrate in the axial direction (ultrasonic range) removing thin layers per cycle. Complex shape of hard to cut materials with tight tolerances can be machined;

Those, really in brief, are the machining approaches in which cryogenics acts a role. Other specific processes different from removal processes can be done at cryogenic temperatures such as Burnishing: a round shaped roller is pushed onto the surface of a machined WP to lower surface roughness and induce compressive residual stresses enhancing fatigue life. We will focus on the first three processes as the most wide-spread in the industrial manufacturing sector.

Cryogenic fluxes are fed to workpieces in order to vary their mechanical properties and/or to cool down the cutting zone. The first method is adopted for soft materials such as aluminum or polymers, in order to enhance compactness and brittleness in the piece to machine. The second approach is used to control the cutting region temperature in machining hard to cut materials such as Ti-alloys, Ni-alloys, Fe-Ni-Cr-alloys, Co-alloys, high strength steels and others.

Cryogenic techniques are also applied in machining of ceramics and composites, exotic metals such as tantalum and porous tungsten for electrodes. In composites low temperatures allow for better delamination control, for ceramics, it prolongs the life of the tool, for porous materials, it stabilizes the structure avoiding pores to close when cutting (smearing), [5, Pusavec 2009]. In machining magnesium alloys, the lower temperature avoids chip burning.

Low temperatures achieved during cutting can in their turn modify the metallurgical structure of the machined surface, promoting hard phases, compressive residual stresses, grain refinement and thinner deformed layers.

### 1.1.4 Hybrid machining

Progressive increase in material properties leads to increased complexity of machining strategies. At the frontier of machining processes, hybrid machining tries to fulfill performance demands by combining different manufacturing techniques. For what concerns Cryogenic Machining, in the last decade it has been applied in synergy with plasma heating and laser heating. The material is heated in the forefront of the tool, resulting

in partial softening and reduced shearing stress limits. On the other side, the tool is cryogenically cooled to preserve its compactness properties during cutting. Therefore, by appropriate balancing of parameters, benefits of the two processes can be exploited. On the other side, the complexity, cost and energy demand must be carefully considered and the cost-to-benefit ratio needs to justify the efforts.

In the next section, fundamentals of machining processes will be presented. Concepts of productivity, quality, tool life and more specific variables such as cutting forces, temperatures, tool wear, cutting fluids added to economic and ecologic aspects will be introduced and linked with the purpose of the present study.

# Chapter 2

## Cryogenic Machining Fundamentals

Knowing the fundamental phenomena of cryogenic machining is crucial for the set up of simulations and cutting tests, for the critical interpretation of their result, for the development of new designs, strategies exploiting our creativity and to make correct choices with responsibility. The effectiveness of Cryogenic Machining mainly focuses on three aspects:

- Economics and ecologics: tool life improvements (wear rate and mechanisms analysis, tribology, cutting forces), tool and fluids consumption in relation to achieved cutting performance. Often comparisons are done with other lubro-cooling strategies such as dry machining, conventional lubro-coolant floods, mists or high pressure systems, MQL, gaseous coolants, sustainable fluids, solid lubricants and nanofluids;
- Quality related issues: mainly Surface Integrity evaluation which embrace aspects like: achieved surface roughness, residual stresses, chemical and metallurgical surface alteration. This does not represent a separate aspect: high MRR roughing operation are not influenced by roughness limitation, however the surface morphology left after a tool passage vary with the cooling approach and could result in differences of material properties felt by the next cutting passage;
- Social and application related issues: cryogenic machining application need to be compatible with normal working legislation and of handy implementation.

During the initial part of our study we will focus mainly on the first aspect. In particular the tool life variation with the application of a low temperature fluid, being our final aim the characterization of the solicitation of different tools and their achieved life with LN2 cryogenic cooling. Higher tool life or same tool life at higher speed generates lower machine tool (MT) downtime, lower tooling cost and consumption, higher flexibility, lower energy consumption (MT), stabler processes. Higher tool life must be achieved with economic and ecologic cutting fluid parameters. When a CF strategy offer this, it is advantageous its application in the roughing regime. If surface properties are enhanced, also its application in the finishing regime could avoid additional material processing. Finally, if the strategy is socially bearable, it is ready for industrial implementation.

## 2.1 Cutting zone temperature

During machining of metals high temperatures are reached in the cutting zone. In metal cutting of ductile materials, the tool removes a layer of material, after called chip, by shearing action. Cutting zone temperature is described as the most relevant parameter influencing cutting forces, tool life, power consumption, surface finish and geometrical accuracy, [3, Shokrani 2013].

### 2.1.1 Cutting zone temperature generation

Cutting temperature generation in chip removal process is generally divided into three separated areas, depending on the location and the mechanisms promoting heat generation.

The primary deformation zone is the one interested by this phenomena. The grain structure of the chip is characterized by elongated oblique grains in the shearing direction. Moreover, for some materials, the high strains applied cause valley-peak structure in the upper part of the chip, called segmentation. For other materials, continuous chip are obtained at industrial speed, but raising speed segmentation can still be obtained. A secondary deformation zone is present where the newly formed chip rubs against the tool rake face. Metallurgical evidence of this is the recrystallization of grains in a narrow band in the lower portion of the chip, the one that slipped on the rake face of the tool. This area is the most detrimental in terms of temperature generation. Due to friction, temperature can reach up to  $700^{\circ}\text{C}$  during cutting common steel (dry cutting).

A tertiary deformation zone is located below the edge of the tool and in the flank face. The axial force applied by the MT needed to plough into the material cause the machined surface to be pushed down and scratched with the tool flank.

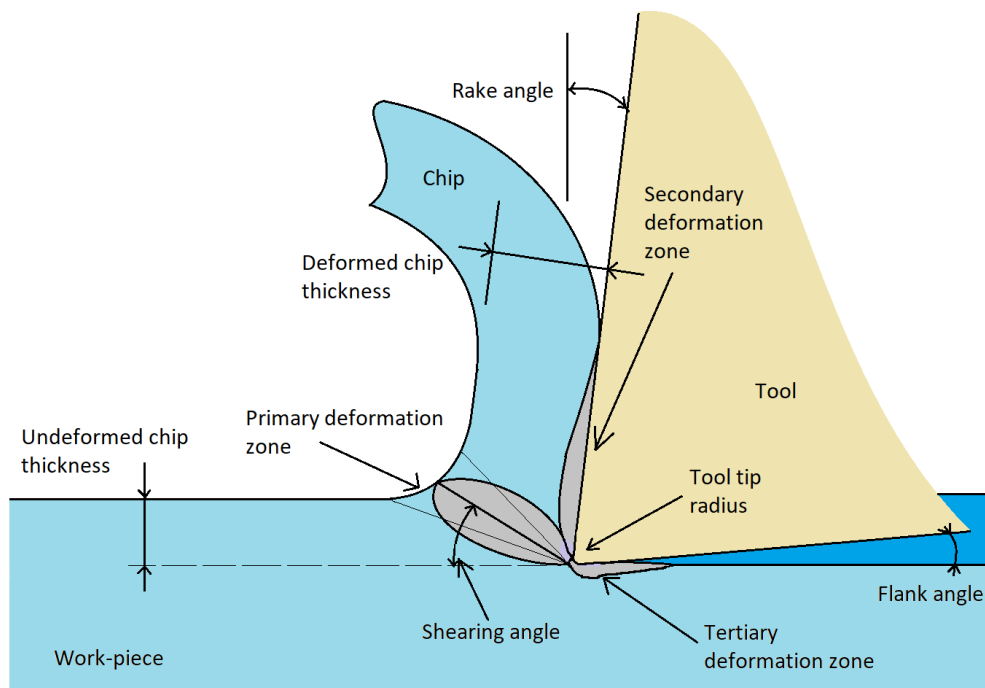


Figure 2.1.1: Chip formation mechanism and deformation zones, orthogonal cutting

Friction generates heat build up. Surface heating by this mechanism can induce detrimental stress states that lead to anticipate fatigue failure of components under cyclic loading. This effect increases as the tool wears out. However being the smallest region and the one with the lower temperatures, is in this area that tool wear is measured, because the portion of tool material removed by abrasion or chipping influence the geometry of the cutting edge and the final geometric tolerances of the workpiece.

Temperature definitely raises in the tool, workpiece surfaces and chip. Heat generation in primary and secondary zones is dependent on tool-workpiece materials and process parameters such as speed, feed, depth of cut, [6, Abukhshim 2006].

It has been proved by many researches that most of the generated heat is evacuated by the chip ( $\cong 80\%$ ), then some remain in the tool ( $\cong 10 \div 15\%$ ), while the remaining affect the machined surface ( $\cong 5 \div 10\%$ ). The proportion of heat shared between the three actors is variable depending on the material pairs and cutting parameters. The proportion of heat flowing into the tool is in generally dependent on tool and workpiece conductivity, specific heat, and interface conductance (perfect contact or not). At higher feed temperature is higher due to increased deformation and friction area. Raising speed, temperature raises because of increased strain rate, higher chip flow over the tool and lower time for heat dissipation. If higher cutting speed generates more heat, a larger portion of it is conveyed by the chip, due to the higher speed in comparison to the material conductivity. The heat fraction coefficient into the tool explains the portion of cutting heat, generally assumed as cutting force times cutting speed:  $Q = v_c \cdot F_c$ , flowing into the tool. It is an important value needed for cutting simulations that often need experimental trials to be determined.

## 2.1.2 Temperature dependent tool wear mechanisms

Tool materials must be harder than the material to be cut. This can be difficult for example when cutting ceramics. In any case, even if inserts are harder and tougher than the workpiece, they will undergo progressive degradation under cutting. The degradation rate depends on several factors like process parameters, workpiece and tool material properties, lubro-coolant strategy adopted. One of the most important parameter describing tool wear is temperature, and that is the reason why we will discuss wear mechanisms here.

Heat build up in the tool is responsible of several mechanisms that raise the wear rate, [7, 8, Hong 2001d, Hong 2001b]:

- High temperatures of the tool make it softer, thus closing the hardness gap between workpiece and tool materials, favoring abrasion wear;
- Chemical activity of tool and work material increase, diffusion mechanism are faster and the tool can loose the metallurgical structure that was achieved to guarantee its strength, wear resistance and toughness;
- Adhesion mechanism are enhanced, a hotter tool is stickier than a colder one and depending on the workpiece activity, adhesion and diffusion of elements in between tool and chip are enhanced.

The two latter mechanisms can lead to melted metal deposit on tool faces, modifying tool geometry (leading to dimensional deviation), influencing quality, raising cutting

forces and friction (and in turn temperature). When the BUE or BUL detaches because too big or embrittled by the coolant, it generates vibrations and unstable cutting, tool edge chipping or microchipping and deposit on the machined piece generating poor surface quality. Crater wear in the secondary deformation slipping zone and flank wear are recurrent progressive wear consequences. Friction forces are higher and higher cutting forces follow. Crater wear weaken the tool heightening sudden failure probability.

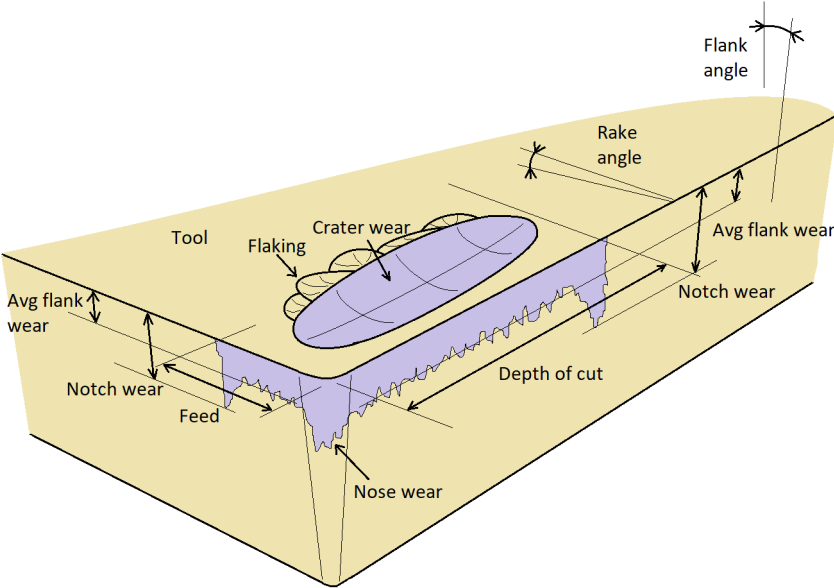


Figure 2.1.2: Tool wear characteristics

With respect to this, the application of lubro-cooling fluids have always had the function to reduce friction (Oil content of CCF, Conventional Cutting Fluids) and remove heat (Water content of CCF). Regarding this aspect, cryogenic fluids help in heat dissipation of hard to cut materials like Ti, Ni-Cr, Ni, Co alloys and High strength steels, where the higher force required for the shearing and the low heat transfer coefficient (low thermal conductivity) contribute with even higher heat generation in the cutting zone. Adversely, heightening temperature does not soften those materials which are designed to maintain high properties at elevated temperatures (hot side of engines). Cutting Titanium alloys in particular exhibit peculiar features. With respect to steel and other softer materials, crater wear is situated much more in the vicinity of the cutting edge. This cause another peculiar effect called edge recession. Edge recession happens when crater and flank wear meets, causing the actual cutting edge to be very weak and back off, [9, Sun 2015a].

Another recurrent mechanism happening when cutting hard materials, especially at higher speed with inefficient cooling technique, is edge plastic deformation. The heat build up near the edge and the weakening caused by the intense wear, sharpening the edge angles, cause the tool material to yield plastically, [9, Sun 2015a].



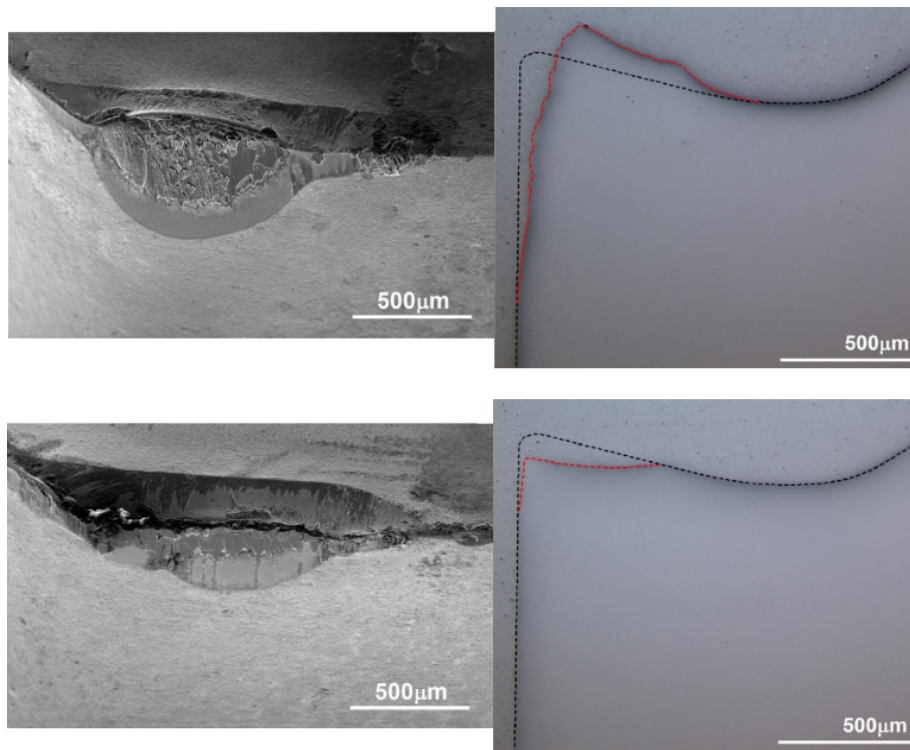


Figure 2.1.3: Plastic edge deformation when cutting Ti6Al4V (dry cutting) and edge recession (cryogenic chilled air)

Frequent when cutting high strength alloys, which are prone to chip segmentation and shear banding (see Chip Morphology section below), is flaking of the insert. It generally takes place in the proximity of the crater edge toward the interior of the insert. It is believed to be caused by alternate thermal loading generated by chip segmentation with consequent variation of the friction characteristics, from sticking to sliding, added to the alternate mechanical load, [10, Venugopal 2007].

### Turning and Milling wear issues

Some differences arise when talking about milling or turning wear issues. Added to the previously explained tool wear mechanisms and related causes, milling is affected by macroscopic thermal and mechanical cycling, due to the interrupted nature of the process. This causes warming up when cutting and chilling down in the idle phase. Cryogenic cooling could worsen the more this effect. A non precise nozzle configuration, not reaching the heat generating cutting zone, could result in warming the insert skin in cutting (hundreds of Celsius degrees) and cooling it to frozen temperatures in the idle phase (decades of Celsius degrees below zero). This thermal alteration of the inserts result in weakening of the tool and reduced improvements in life with respect to turning.

On the other hand, turning cutting tools are subjected to continuous erosion by the workpiece material during cutting, while milling inserts cut only on a variable (engagement dependent) portion of the process. Therefore, higher absolute tool life values are achievable, in theory, for milling inserts, independently of the cutting strategy. The more, adding a strong coolant could worsen the situation. The balance plays on the

reduction of friction and temperature while not increasing the thermal solicitations on the cutting edges. Emulsion and High Pressure emulsion prove to prolong tool life in milling with respect to dry cutting, even if features (like flaking) have generally been observed that witness the increase in edge thermal cycling. If thermal cycling become preponderant, intense edge chipping promote sudden insert failures.

Cryogenic machining pushed toward an increased cooling action of the tool, aiming at keeping its hardness and compactness properties, decreasing wear rates. Due to its strong cooling capacity, careful cooling design must be achieved. For instance, it could be detrimental to increase the thermal loading by placing the nozzle so to cool down during the idle phase. This could decrease the minimum temperature of the thermal cycle. On the other side a cooler tool would engage with the workpiece and the maximum temperature could be reduced as well. Accurate studies on thermal analysis of inserts will be presented in the modeling chapter, Chapter 5.

### 2.1.3 Material properties at cryogenic temperatures

Understanding material behavior at low temperatures is crucial for cryogenic machining purposes. At low temperature material properties change:

- As a general trend, Hardness, Yield strength, Tensile strength, Wear resistance, Fatigue strength increase. The material is definitely stronger [1, Jawahir 2016];
- FCC cell structures show a slight decrease in Ductility and Toughness, whereas BCC and HCP becomes brittle. For alloys like Ti and Ni toughness and ductility decrease at a much lower rate than the increase in strength properties, [11, Hong 1999];
- Residual stresses, at low temperature, tend to be lower, and dimensional stability increase [1, Jawahir 2016].

Cooling the tool will result in a harder and stronger cutter, more wear resistant, with reduced chemical activity, as the workpiece, with less sticky rake and flank faces leading to lower wear rates and BUE suppression in many cases, [12, Yasa 2012]. Carbides tools have been widely investigated in cryogenics because of economics and retention of toughness, transverse rupture and impact strength at low temperatures, [2, Yildiz 2008].

[11, Hong 1999] and colleagues started their study in the field of cryogenic machining by examining material properties at low temperature. In general, at the very low temperatures achieved with cryogenic cooling, hardness, wear resistance and strength rise, while chemical affinity and toughness decrease. For what concerns the tool side, indentation, three point bending, impact strength and microstructural observations tests were done on several carbide grades, all of them capable of maintaining their strength and toughness at low temperature, rising hardness and wear resistance. However, other tool materials were not considered, for example more expensive CBN, B-CBN, PCD, Ceramics, or cheaper HSS.

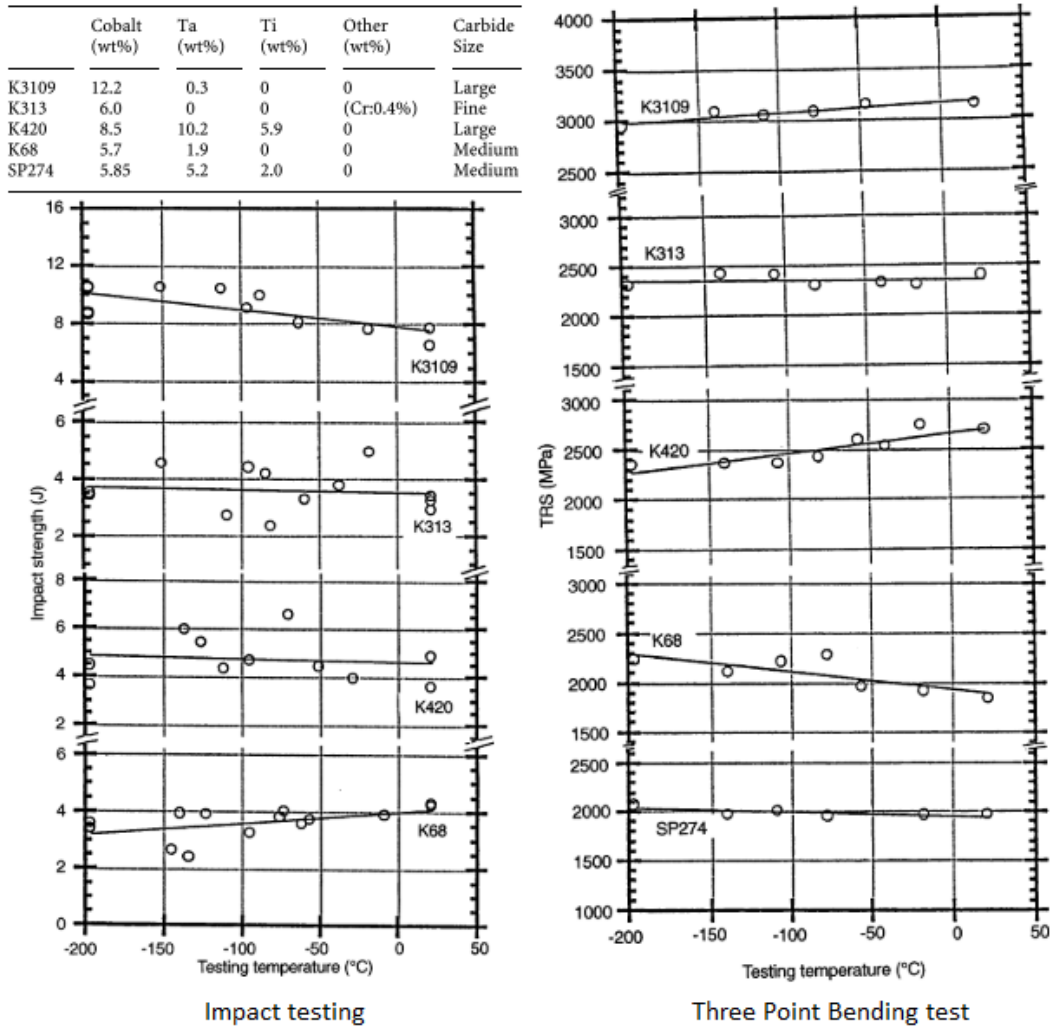


Figure 2.1.4: Different Carbide grades properties at low temperatures, [11, Hong 1999]

From the work material side several materials were tested:

- Mild-low carbon steels, AISI 1010, 1070: at low temperature has lower toughness and ductility: reduced elongation, reduction in area and impact strength, higher hardness and yield strength, therefore a smart solution is that of cooling only the chip;
- High strength steels AISI E52100, Al A390: they increase hardness and strength promoting higher tool wear, in this case a smart solution would be to cool the tool only to increase its wear resistance;
- Ti6Al4V: it doesn't markedly lose its toughness, elongation impact strength and ductility while increasing hardness and yield. In this case the best option is to cool the tool avoiding cooling of the workpiece or chip.

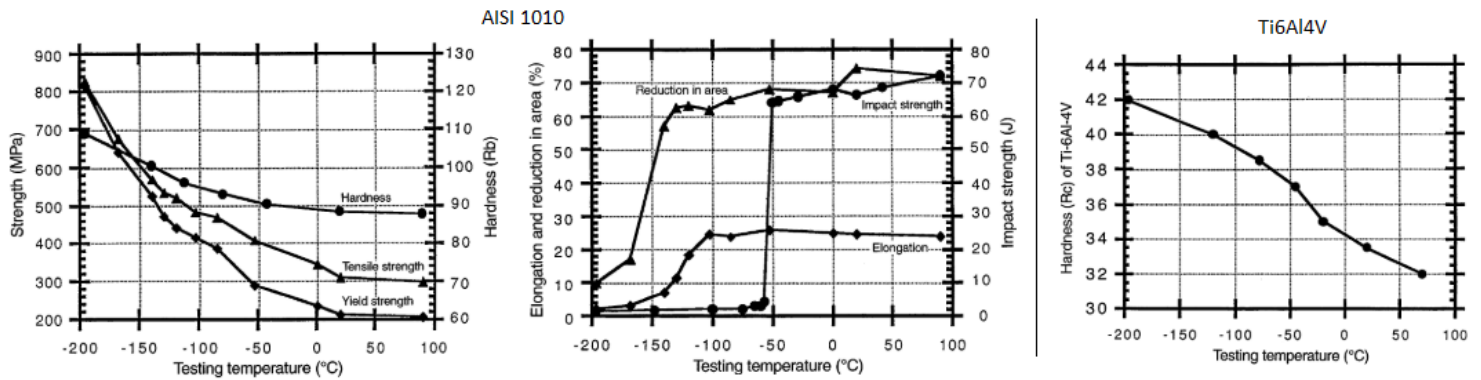


Figure 2.1.5: Different material's properties at low temperatures, [11, Hong 1999]

Other materials like Aluminium castings alloys, with Silicon content, have been difficult to machine because of hard Silicon phases causing high wear rates of tools. In this case, cryogenic cooling, by enhancing the wear resistance properties of inserts will increase tool life, [3, Shokrani 2013]. Cooling the workpiece is not the smartest idea for alloys that retain toughness and ductility at low temperatures, raising the shearing stress limits, [2, 12, 3, 13, Yildiz 2008, Yasa 2012, Shokrani 2013, Hong 2001c]. The position of nozzles for cryogenic cooling fluxes must be carefully tuned to avoid over-hardening of the workpiece material. Overhardening of the workpiece would lead to higher forces and power, increased energy consumption (the more the consumption if production of cryo-fluids is considered), increased wear rate of the tool. It is evident that a trade off must be achieved.

For ductile materials, soft and low strength, cooling the work material would reduce the fracture strain, having better control in chip formation. This materials have generally a precise temperature of ductile to brittle transition (like glass temperature for polymers). Welding tendency and BUE formation can be suppressed by cryogenic cooling, [3, Shokrani 2013]. However cooling indiscriminately the piece will lead also to higher strength, therefore a material soft to cut such as aluminum would be unreasonably hardened. A smart idea is to freeze locally the chip, in order to promote chip breakability without altering too much the properties of the workpiece.

## 2.2 Cryogenic fluxes heat dissipation

Cryogenic fluxes have high heat transfer capabilities, exploiting latent heat of vaporization and then the temperature difference up to room temperature. The Heat transfer ability and therefore the cooling capacity of cryogenic fluxes strongly depend on the way the fluxes interact with the surface: state of the flux (liquid, liquid and vapour, vapour), pressure, nozzle position and orientation. Moreover it was seen a general decrease in the cooling capacities of cryogenics when cutting at very high speed. This could be due to the obstruction of the cutting area by the chip and the impossibility of fluxes or jets to reach the heat affected zones, [2, Yildiz 2008]. Besides that, another reason could be that the rate of heat generation was not balanced by the correct flow rate or pressure of cryogenic fluid.

Theoretically, the combination of pressure, jet speed and spot size, vicinity of the nozzles, orientation, and fluid quality, should generate cooling rates that are balanced with the process heat generation rates. Additionally the correct locations of heat build up should be targeted. This so to cool down the tool without producing detrimental effects such as lack of fluid (simil-dry cutting) or fluid excess (overhardening of the workpiece, increased strength, hardness and wear rates of the tool).

Practically determining the cooling capability as a function of the exposed parameters is not trivial. It is necessary to know the cooling capacity of the flow depending on its properties in relation with the geometry and nozzle design. Then the heat generation in different zone, related to the targeting areas of the cooling flows, need to be modeled. The heat extraction and generation rates can then be compared and flow properties or nozzle design adjusted so to promote a balance.

Another problem recently addressed by researchers is the lower heat transfer capacity of vapor cushions that form when liquid Nitrogen come in contact with hot targets. This phase has significant lower thermal extraction action, definitely causing an insulating cap on the target, lowering the cooling effect of cryogenic coolant, [3, Shokrani 2013]. We can distinguish between three different techniques regarding how to approach the cooling of the cutting zone.

### 2.2.1 Workpiece Cooling

Workpiece cooling should be applied to materials that does not exhibit excessive hardening at low temperatures. Benefits to this technique come from cutting materials impossible to cut at ambient temperature due to melting or burr formations such as Aluminium or polymers, [14, Biermann 2010], materials subjected to delamination that require compactness such as composites, or materials that exhibit difficulties in controlling the newly formed chip: long chip causing entanglement with the tool, or burning chips (Magnesium). The main options to achieve low temperature in the piece are:

- Cooling bath: high energy demand and quantity of cryogenic fluid necessary, time demanding (also for the interrupted nature), in general the workpiece is overhardened, abrasion and cutting forces are generally higher, dimensional deviation must be considered;
- Flood cooling: less quantity of coolant necessary, less time demanding and more localized, but the shearing stress of the material is enhanced, abrasion is increased, dimensional deviation may be possible;
- Jet cooling: even less consuming and more localized, but cooling power can be insufficient. It can prove to be the best choice when needed to embrittle the newly formed chip so to promote chip breakability, or avoid burning, without undergoing in excessive hardening.

Evidence is showed on how is important to limit the consumption of cryogenic fluids. A correct modeling of the cooling capacity is necessary for flood and jet cooling systems. Overhardening of the piece is a recurrent phenomena that needs to be avoided in cutting metals. Dimensional deviation due to very low temperature must be predicted. A general rise in cutting forces and power and energy consumption due to cryogenic fluxes

are main drawbacks of this method, suitable for limited materials, [2, 3, 4, Yildiz 2008, Shokrani 2013, Deshpande 2018].

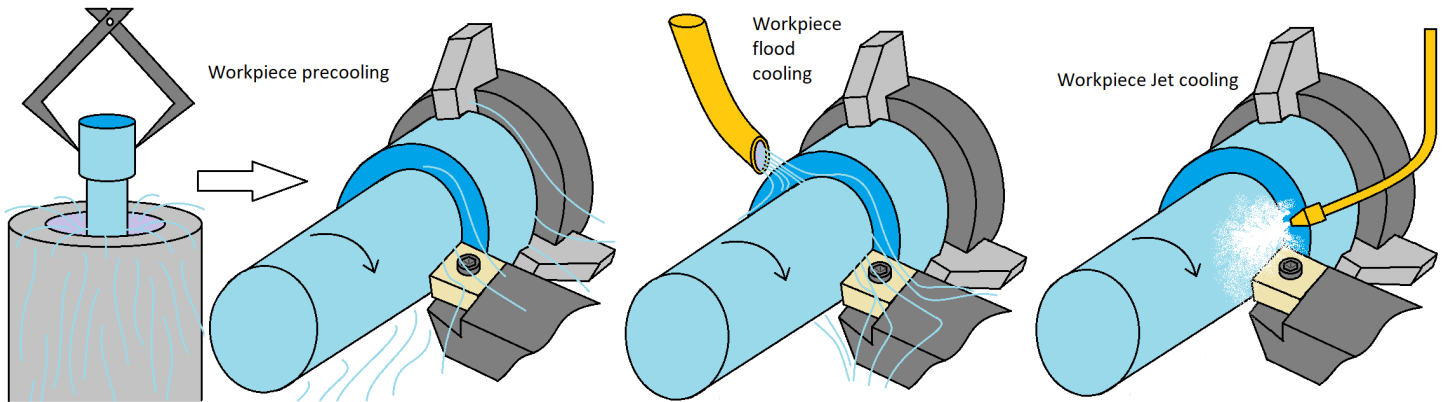


Figure 2.2.1: Different strategies for workpiece cooling

## 2.2.2 Indirect Cooling

Indirect cooling technique refers to the cooling of the insert only. Also known as Cryogenic Tool Back Cooling or Conductive Remote Cooling, [2, Yildiz 2008]. This technique is highly dependent onto tool thermal conductivity properties. The cryogenic fluid can be recirculated into the machine. Tested applications apply the cryogenic fluxes to the rake and rear face of tools by means of external covers. Thus, the tool being set in a sandwich of cryogenic flux. This method is very interesting from a modeling point of view as its benefits will refer only to the material properties achieved at lower cutting temperature (to be measured) and not to unclear and incoherent interpretation of cryogenic fluxes lubrication effects.

The effectiveness of this approach, dependent on the thermal properties of the insert, proves less with insulating materials like ceramics. Moreover, the cooling effect is more effective as cryogenic fluxes are provided in the liquid form (LN<sub>2</sub>, LCO<sub>2</sub>) having higher heat transfer capacity. Effective cooling depends as well on the position of the highest temperature point. The larger the contact area, the larger the cooling capacity, [2, Yildiz 2008]. One of the advantages of this method is that overhardening of the workpiece is prevented, being the cooling action localized to the insert, [15, Wang 2000]. Moreover, increase in the heat conductivity is reported at low temperatures, [16, Dhar 2001].

The cooling system schematically consists of evaporation, adiabatic and condensation zones. By conduction, heat is extracted from the cutting zone and evaporate the fluid, which is sent through an adiabatic delivery to the condensation unit to be re-liquefied, [3, Shokrani 2013]. Excellent example describing promising results have been already published in the nineties, [17, 15, Wang 1996, Wang 2000] and will be treated in the Performance chapter, Chapter 4.

## 2.2.3 Pressure jet cooling

This is one of the most promising alternatives. The jet is highly controlled and delivered where it is needed, cooling locally the rake, the flank or the bending chip. Cryogenic

consumption is minimized and optimized for the required function: cooling the wanted target, avoiding workpiece material alterations, [12, 3, 4, Yasa 2012, Shokrani 2013, Deshpande 2018]. Nozzles can be externally added to the machining apparatus, thus lowering the implementation effort of cryogenics. However, this could cause cooling of unwanted areas promoting overhardening of the piece. A smarter implementation to avoid this is combining the design of the tool with micro-nozzles that minimize the cryogenic flow rate maximizing the cooling effect by precision toward the cooling targets [2, Yildiz 2008]. Various researchers implemented integrated nozzles designs, including chip breakers, cooling rake and/or flank faces, detailed presentation will be held in the next chapter, Chapter 3.

Heat transfer properties are strictly dependent on the dynamics of the flow, which in turns depend on the flow condition. Flow is localized when directed at the rake-chip interface or at the bending chip. Flow is free when directed to the flank or impinging on the insert, [1, Jawahir 2016].

**Free flow and confined flow properties**

Regarding LN2, a jet impinging on a surface (free flow) is characterized by the dense jet core, the stagnation region at the contact with the surface and the wall jet region, where it spreads radially and the speed becomes parallel to the surface. The formation of a liquid wall jet region with vortices entertaining fluid strongly influence the heat transfer properties of the jet. The length of the liquid like jet can last up to 10 diameters, therefore the cooling target should be closer. At 40 diameters from the exit, 50% of LN2 is gaseous, with astounding increase in volume (1 : 694) that has a good chip evacuating effect, [1, Jawahir 2016]. In the article, several other sources are reported regarding heat transfer capacity of jets. Along the centre of the cores lies the highest heat extraction ability (up to  $50 kW/m^2k$ ) while in the wall region it reduces drastically ( $\approx 1500 W/m^2K$ ).

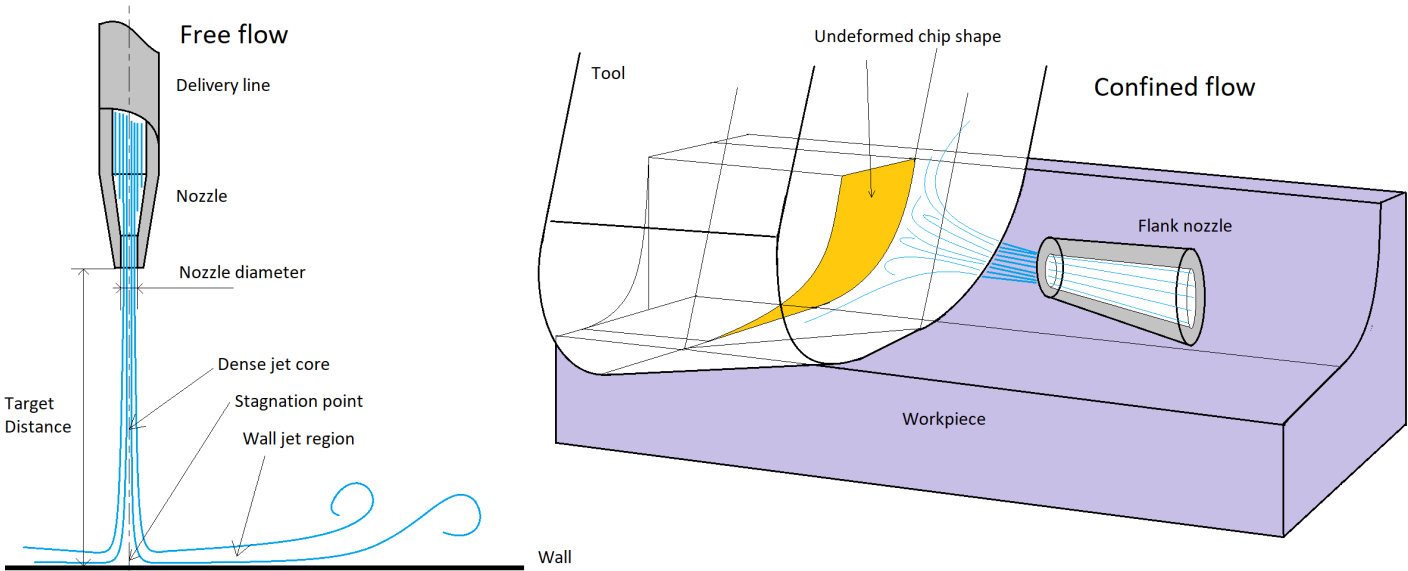


Figure 2.2.2: Free flow and confined flow

However, regarding the cutting process, the flow is generally confined in the crevice between tool flank and workpiece, or tool rake and chip. Heat transfer mechanisms are there governed by strong mixing momentum transfer. Heat transfer capacity is influenced by geometry and by surface overheat temperature.

### Heat transfer determination

Heat Transfer Coefficient (HTC) determination is really important for the determination of the cooling capabilities of the flux. However, it remains an issue to be addressed, due to the high number of parameters that influence the problem. It is clear that boundary vapour film is to be suppressed due to poor HTC properties, jet velocity, pressure and orientation of the nozzle can help, forced convection boiling, should be achieved for enhancing the HTC [1, Jawahir 2016].

The geometry of the crevice formed by tool-chip and tool-surface of the piece needs to be considered, as the stagnation point of jets is not on a flat plate but at some depth of the crevice. HTC should be calculated for this geometries (crevice like gap, nozzle diameter and distance), for variable pressure and related jet speed (nozzle diameter link), fluid quality. In general the HTC would be dependent on the surface temperature as well, depending on heat generation zones during cutting.

Moreover, for jet speed much higher than workpiece or tool peripheral speed, the relative movement can be neglected. However, due to the opposite motion of jets and chip or work surface, the ratio is in terms of  $2\frac{v_{chip/surf}}{v_{jet}}$ , which has to be small in order to model the sliding surfaces: back chip or workmaterial machined layer, as standing still. Furthermore, when the gap between tool and chip/work surfaces reduces, evaporation and high expansion rates would generate turbulence and slow down the average jet speed. The fluid/vapour flow would then be dragged out of the crevice due to tool-workpiece relative movement. At the author knowledge, the fluid-dynamic nature of jet-material interaction have never been studied with this level of detail, however, HTC values depending on surface overheat and cutting geometry can be found. Detailed analysis will be given in Chapter 5, Modeling.

### 2.2.4 Hybrid Cooling

To exploit the benefits of multiple cooling strategies, one can achieve indirect and direct jet cooling contemporarily. With this method, before the jets exit from the nozzle toward the heat generation zones, it would pass in contact with the insert. This could create in the bulk of the tool a heat sink capable of extracting heat more rapidly from the skin in contact with the piece, added to the usual external action of jets promoting interface cooling or work material surface enhanced properties. However, at the author knowledge there are no example of this technique present in the literature.

Another example of Hybrid cooling technique would be the use of both the hot and cold streams of a RHVT (Ranque-Hilsch vortex tube) cooled compressed air. The hot stream targeting the shearing zone, the cold on passing through or on the tool so to keep it cold.



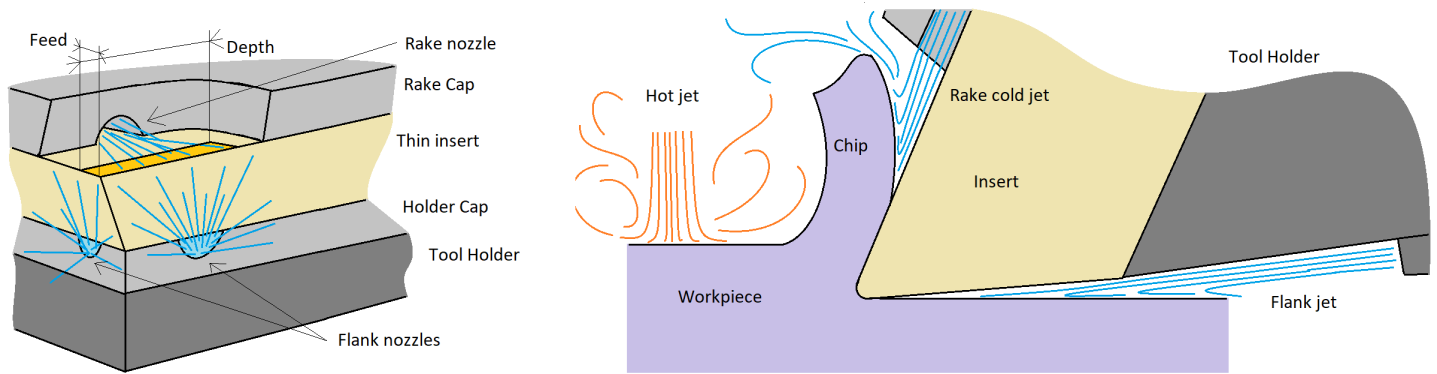


Figure 2.2.3: Hybrid cooling strategies

## 2.3 Tribology and chip morphology

Tribology deals with the determination of contact properties derived by the interaction of materials in relative motion. CoF (Coefficient of Friction), lubrication and wear are some important concepts in tribology. This study area plays a role in determining frictional components of the cutting forces in machining. Friction behaviour at rake and flank depends on chip induced pressure, sliding velocity, material sliding couple, temperature. Friction at flank, other than flank wear, promote heat build up, higher forces, tensile residual stresses and possible phase transformation or metallurgical alteration of the machined surface.

### 2.3.1 Cutting forces

Cutting forces represent macroscopic quantities, affected by several phenomena, often addressed as the most important variables of a cutting process. They are used for process stability analysis, tool wear evolution, power prediction. They depend on cutting insert geometries, material pair, process parameters, chip characteristics, overhardening of the workpiece by wrong cooling, alteration of CoF by lubro-coolants as a function of speed, [12, Yasa 2012]. It is clear how carefully cutting forces should be analysed, and comprehensible is the scatter in result obtained by researchers regarding their difference between cooling strategies, therefore no general conclusion can be drawn, [18, Haron 2018]. [3, Shokrani 2013] and others, in their review, draw a complete comparison on studies and findings on cutting forces underlying the incompatibility among results. Various results of cutting forces comparison between lubro-coolant types, strategies and implementation will be given in the cryogenic performance chapter, Chapter 4.

Generally cutting forces increase with feed (higher chip load) and decrease with speed (reduced shearing deformation area) being the material unable to express his all ductility (brittleness induced by high strain rates) or, in contrary, being the material softer because more ductile at higher temperature. BUE tendency increase forces by modifying the sharpness of the tool and increasing the friction at flank, therefore both thrust and feed forces can be influenced.

What is clear is that an indiscriminate cryogenic application in the cutting zone is capable of overhardening the piece, thus motivating the results of overall higher cut-

ting forces found in literature, [2, Yildiz 2008]. Even considering precise micro-nozzle applications, hypotizing little penetration of cryogenic fluid in the tool-chip interface and considering the lifting action due to liquid-gas expansion ratio, at low speed the material just ahead the tool could have time for overharden. The shearing stresses will grow thus determining higher forces. At high speed less time would be given to the material to harden, whereas less time would be given to remove heat. The cutting zone will be hotter and the material sheering almost unaffected, besides the tool could still be relatively colder and the obtained forces could be lower, [4, Deshpande 2018]. Cutting forces are often used in experiments for the determination of the inserts wear rate. By looking at the variation (raising) of cutting forces as the cut proceed the consumption of the tool is guessed, [12, Yasa 2012]. In cryogenics, improved wear resistance properties of tools coming from the controlled cutting zone temperature translates into stabler cutting forces for longer cuts.

### 2.3.2 Coefficient of Friction

In principle, it is not easy to separate the cutting forces into shearing force, friction at rake, friction at flank, bending of chip. So CoF estimated by overall cutting force measurement can lead to misleading evaluations as the way to relate overall forces to friction forces is purely geometrical. This includes, in the calculation of friction, other effects such as shearing strength of the material. The very concept of a single friction coefficient to represent a complex contact phenomena is also matter of discussion. Another method to determine the CoF could be by reconstructing the frictional behaviour in laboratory, putting into sliding contact two surfaces under pressure. Devices that tries to reproduce frictional behaviour of sliding pairs are called Tribometers.

It is however clear that for decades the adoption of lubricant as cutting fluids has preserved the tool, lowering the CoF between chip and inserts. The effect of CCF (Conventional Cutting Fluids) has proven to be effective at low speeds (relative between workpiece and tool), the fact explained by the formation of a lubricating film in the tool-chip interface. Due to the very high pressures between rake and chip this has been argued, in the same manner regarding the hypothesis of lubricating vaporized film of cryogenic fluid in the interface, [2, 3, 7, Yildiz 2008, Shokrani 2013, Hong 2001d]. Adhesion takes place and any fluid in between the surfaces will be ejected. The effectiveness of conventional lubro-coolant fluids are likely to be addressed to a partial penetration of lubricating liquid, a reduction in tool chip contact length (especially for high pressure cooling), heat removal maintaining the bulk tool colder, so harder and less sticky, and finally a colder workpiece surface which induce lower ductility and more definite tearing.

Cryogenic fluxes certainly help to avoid heat build up at high speed, especially for hard to cut materials. On the other hand, the lubrication effect of cryogenic fluids is not clear. For sure the lower temperature alter properties of materials and increase surface hardness, [4, Deshpande 2018]. What is not clear is if the reduced friction depends on the hardening, compactness, avoided thermal softening of tool only, or on some lubricating mechanism of cryogenic flux infiltrating and expanding in micro-gaps between tool and chip, or both the two mechanisms.

It has also been determined that tool properties are more relevant than material properties in describing frictional behaviour. Coatings designed for dry cutting may induce

lubrication at high temperature and will result in failures or higher forces when applied in cryogenics. On the other hand if cryogenic machining application is inaccurate it would result to a simil-dry cut and the coating effect would be activated, [2, 12, 3, Yildiz 2008, Yasa 2012, Shokrani 2013].

Misleading and conflicting effect in literature on CoF reduction/increase should be due to process/cryogenic parameters interaction. In [7, Hong 2001d], by measuring cutting, feed and thrust forces and consequent 3D decomposition, they obtained frictional coefficients for various cutting speeds for dry and cryogenic (LN2) cutting with rake, flank or both cooling nozzles activation. They found lower friction coefficient for rake cooling and combined flank and rake cooling, despite cutting and thrust forces increase. They also underlined metallurgical evidence of reduced friction by much thinner SDZ layer on the chip (see following section). Reduced friction was attributed mostly to compactness and decreased stickiness of the tool kept cold, added to the chip-breaker lifting action, promoting lower contact length and increasing fluid penetration.

Some researchers performed tribological studies with pin-on-disk or pin on bar techniques: a roller corresponding to the piece was pushed against a surface (tool) while rotating, then several lubro-coolant environments where applied to study the variation of the CoF. Some others related experimental tribological trials to FEM analysis for better understanding the nature of heat exchange and friction stresses shared between the sliding bodies, details will be given in the Modeling chapter, Chapter 5.

What becomes clear by these studies is that the CoF strongly depends on the shape of the tool and on the way lubro-coolant is provided to the cutting zone. Some argued as well that with tribometers, achievable pressure are much lower than real cutting pressures. In some cases even the delivery of fluids does not resemble the cutting process, easing their penetration into the interface of the bodies in relative motion.

Another factor which can influence the friction behaviour is that, for LN2, the nitrogen vapour isolate with inert environment the cutting zone, thus avoiding welding phenomena and reaction with atmospheric Oxygen (excellent isolation for Magnesium alloys cutting).

Material pairs also influence the CoF. For example, cutting Titanium alloy Ti-6Al-4V, [19, Courbon 2013] found that LN2 could not alter neither friction not adhesion. On the other hand, during cutting of Inconel they noted that CoF was reduced as well as adhesion.

### 2.3.3 Chip morphology

Produced chips during machining are more than scraps. Chip morphology and metallurgy analysis can explain tool wear modes, removal process dynamics and performance. Chip morphology include analysis on the shape, thickness, continuity, fragmentation, saw teeth presence, metallurgy (grain size and orientation), colour of obtained chips. By looking at those features one can extract process variables that are impossible to be noted during the process because of limited visibility. Generally ductile material produce continuous chips, whereas brittle ones produce discontinuous chips. Chip thickness increases with feed and reduces with speed at equal feed because of reduced shearing area.

With respect to dry or CCF cutting, cryogenic machining produces thinner chips. Colder chip will translate in a decreased deformed chip thickness, and consequent in-

crease in the shearing angle, [18, Haron 2018]. Consistent results have been presented by [20, Dhananchezian 2010] and colleagues. Chip thickness and shearing angles were reduced for all cutting parameters combinations, details in Chapter 4. Higher shearing angles allow for lower shearing stress limits. By the way, this effect is often negatively balanced by overhardening of the workpiece, thus an increment in forces can be seen. Reduced chip thickness could release some pressure on tool rake face, thus reducing rake wear. Finally by looking at the side of the chip that scratched with the rake face of the tool, thicker secondary deformation bands are index of higher friction and associated wear rates of tools, [18, Haron 2018].

The secondary deformation zone induce recrystallization in the lower layer of the chip, generating a long tail with longitudinally oriented grains, whereas in the upper part, grains are transverse in the shearing direction. The long tail reduce chip breakability. Cryogenic machining help in decreasing adhesion, welding and therefore recrystallization phenomena. Lower thickness of SDZ was found for cryo-turning of Ti-6Al-4V. This was taken as a proof of reduced friction coefficient between rake and chip, [7, Hong 2001d].

Excellent images were obtained through SEM (Scanning Electron Microscopy) and EBSD (Electron Back Scatter Diffraction) by [21, Courbon 2013a] and colleagues. It shows how temperature build up due to deformation can cause recrystallization in both primary and secondary zones. Careful analysis of chip metallurgical features can give evidence of material deformation history, which in turns could help in understanding differences between cooling strategies.

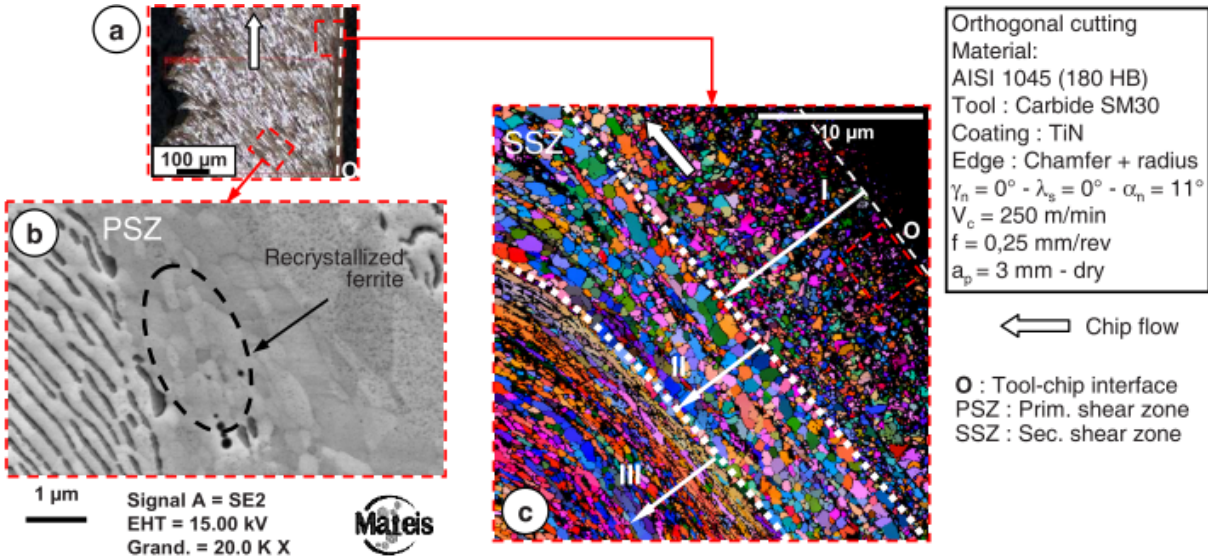


Figure 2.3.1: Chip morphology and metallurgy characteristics for AISI 1045, obtained with SEM and Electron Back Scattering Diffraction, EBSD, [21, Courbon 2013a]

### Shear banding

*Shear bands formation represents still a research topic, its motivations deepening in material science. Since shear banding is not the main topic of this work, we will report what is needed with the help of one of the most complete reviews on the topic.*

Shear banding, shear localization, shear band deformation are all same names regarding

the tendency of a material to yield along preferential, narrow, well defined paths. We know that the main deformation mode of materials is shearing: even in tensile tests, metals finally yield with inclined surfaces, evidence of catastrophic shearing. In shear banding, shear deformation begin to localize in narrow bands. Going on with the strain, the bands progressively define and carry the deformation of the material, which outside the band remain almost undeformed.

[22, Xu 2008] et al. organized the work of many other researchers. They listed the main characteristics of shear banding:

- Shear band formation start at a critical strain, in turns depending on the strain rate:  $\varepsilon_{cr} = f(\dot{\varepsilon}_{cr})$  ;
- It is a progressive process during which shear deformation become gradually localized;
- High strains can be achieved quasistatically avoiding shear bands, therefore strain rate has a great importance in shear banding. High deformation rates and low thermal conductivity cause inelastic heat generated to promote thermal softening and consequent shear localization;
- Temperature in the shear band could reach  $440 \div 550^{\circ}C$ , enough for  $Ti_3X$  small particles to form, particles likely to be sheared by dislocations;
- Materials prone to SB (shear banding) exhibit low specific heat/conductivity, high thermal softening and low strain hardening (which logically will restrain shear localization);

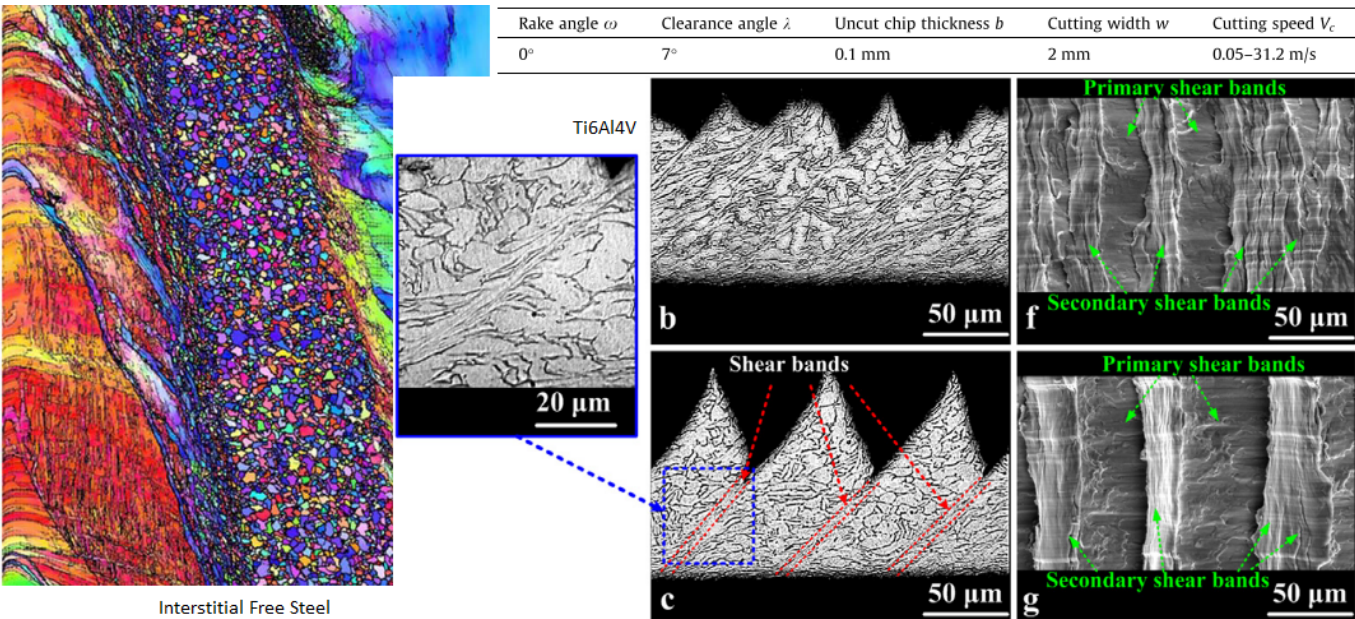


Figure 2.3.2: Shear bands in Interstitial Free Steel (left, [22, Xu 2008]) and Ti6Al4V shear banding at b) 30m/min, c) 300m/min, f), g) superior face of the chip, [23, Ye 2013]

- High temperature and strains levels reached in shear bands promote recrystallization. Dynamic recrystallization (DRX) is originated by the reorganization of dislocations in cells, forming new boundaries and equiaxed grains
- Deformation mechanisms of small, nanometer, grains is different from normal metal matrix grains, dislocations generate at GBs and annihilate at the opposite side promoting grain rotation;
- Coalescence and growth of microvoids and microcracks in the shear band lead to ductile fracture inside the band while it is still hot;
- Shear banding spacing is described well by a Weibull distribution, dependent on strain.

Studying shear bands is, as expected, not trivial. It is difficult to obtain them in a controllable way, extremely complicate to look at their evolution, they are hard to be seen clearly due to the nanometer size and the evolution of phase transformation that can hinder their deformation history. [24, Cotterell 2008] and colleagues analysed the evolution of shear bands in orthogonal cutting of Ti6Al4V as a function of feed and speed. With a sophisticate microscope and strobed copper-vapour laser illumination system they captured at 24000 *frames/s* the evolution of shear bands. Then with the aid of analytical formulas approximating strain in the shear bands they described their geometry at the variation of cutting parameters. Interesting to note that the shear band frequency increases with speed and reduces with feed. [25, Molinari 2013] and coworkers undergo an exhaustive analysis on shear band evolution for Ti6Al4V as a function of cutting parameters.

Serrated chip morphology is characterized by segment heights (peak to valley  $h$  and peak to bottom  $H$ ) and pitch (distance between two peaks  $p$ ). Serration degree and pitch frequency are also recurrent quantities, being respectively expressed as  $\chi_s = \frac{h}{H}$ ,  $f_s = \frac{V \cdot f}{p(H-h/2)}$ , being  $V, f$  speed and feed (uncut chip thickness).

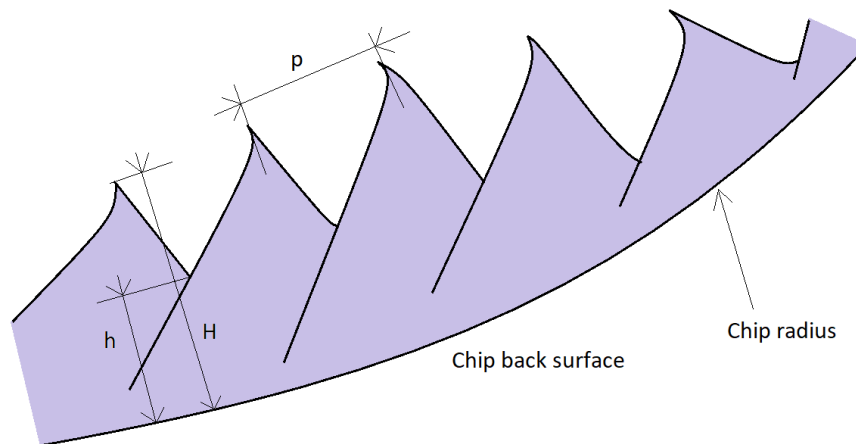


Figure 2.3.3: Segmented Chip Morphology

[26, Krishnamurthy 2017] studied deeply the chip morphology during Dry and Cryogenic bathed Ti-6Al-4V with PCD. The segmented chip formation was described by

points: i) the tool generate a concave crack in the material, ii) crack initiation along the shear plane, iii) stable propagation of the crack along the localized shear band, iv) unstable crack propagation till the workpiece surface or slightly below.

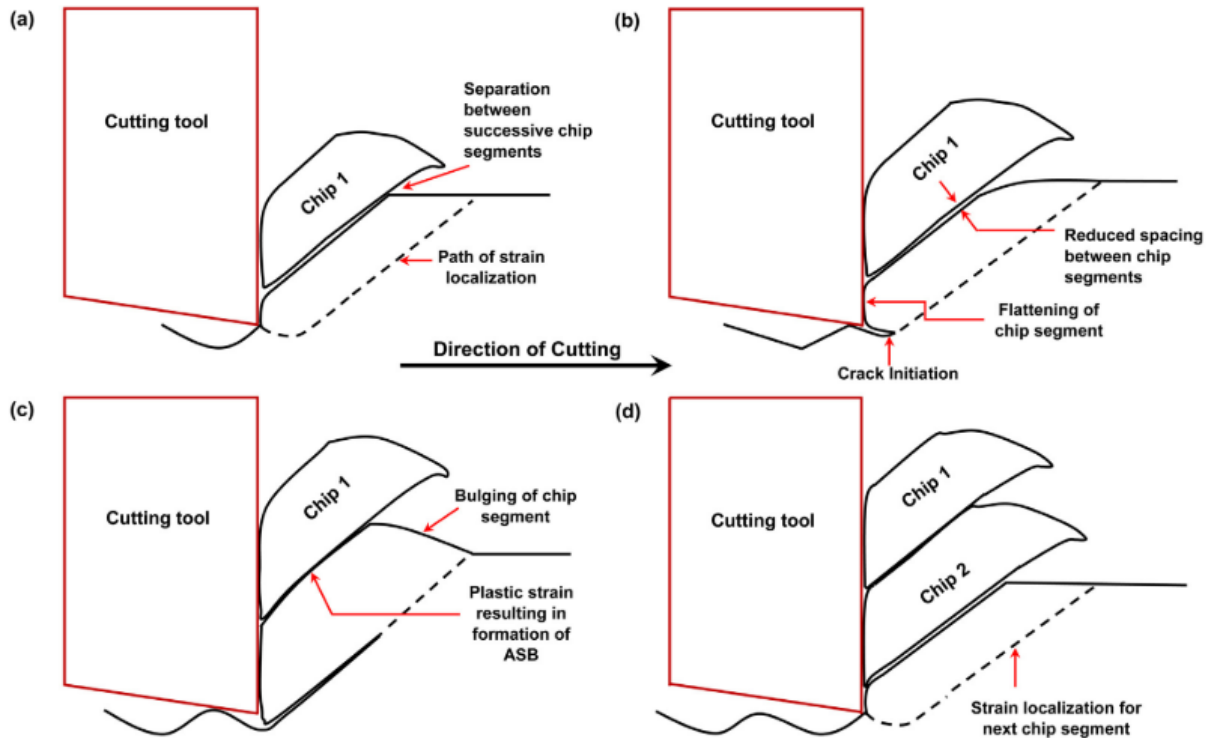


Figure 2.3.4: [26, Krishnamurthy 2017], chip formation procedure in Ti-6Al-4V

Whether or not shear bands are modeled with cracks or material softening, obtaining this particular material behaviour in cutting simulations require considerable effort. Shear bands are neatly obtained in orthogonal cutting models, but reconstructing the stress state of the material is difficult due to the interaction of other phenomena, like friction. Therefore, material models needs to be developed extrapolating data coming from other kind of test (in which material behaviour is simpler to be described) like Split Hopkinson Pressure Bar, SHPB. This introduces material models which are theoretical forecasts of material behaviour, based on experimental evaluations or dislocation behaviour (the more sophisticated and difficult to implement). Exhaustive details will be presented in the Modeling chapter, Chapter 5.

## 2.4 Productivity

During machining of difficult to cut materials, such as the high strength alloys cited above, the build up of high temperatures, promote intense wear rates on tools. Dry cutting exhibit generally the highest wear rate. MQL become ineffective in removing heat from the cutting zone. Cryogenic coolants or high pressure flood cooling help in a significant reduction of heat and could preserve the cutting inserts for longer time. A longer lasting tool means lower MT stops, lower number of insert used, continuous production, machine stand by energy spread over longer cutting period meaning less

energy for unit volume material removed. The result of a longer life tool translates in higher productivity at lower cost, both considering energy and time, which translates in higher flexibility.

### **2.4.1 Tool wear, wear rate, life and failures**

The majority of researchers found cryogenic fluids (LN<sub>2</sub>, LCO<sub>2</sub>, Chilled Air) to prolong the wear resistance of tools in comparison with dry cutting, [18, Haron 2018]. More variability is found considering the comparison with other lubro-cooling techniques such as Flood or MQL. It is clear that the life benefits depend on the particular insert-workpiece couple. A lot of studies describe the improvements with cryogenic fluids as cutting speed dependent. Cryogenics will be therefore meaningful for high performance cutting, high speed cutting of hard to cut materials, so where it is really necessary to remove heat from the cutting zone.

Mechanisms responsible for tool life enhancement under cryogenic conditions regard decreased wear rates due to higher hardness, compactness, strength. Reduced softening, stickiness, chemical activity, diffusion wear process, adhesion and welding phenomena, BUE formation. Another important aspect concerning specifically LN<sub>2</sub> strategies is the inert environment generation, which exacerbate oxidation and corrosion phenomena.

Tool wear analysis has been performed by monitoring cutting forces or by stopping the cutting process to look at the insert with a microscope, [18, Haron 2018]. When the tool flank and rake wears out, surface friction increase and chip flow is more difficult, therefore forces are higher. Force monitoring allow for continuous cutting without interruptions. Interrupted cutting could cause additional thermal cycling in the cutters, so each stop a new tool should be used. This is more demanding from an experimental point of view because of number of inserts needed, but wear determination is more precise.

Until now, few studies tried to describe and determine the optimal cooling capacity of cryogenic flux to the cutting zone as a function of cutting parameters, material properties, cryogenic fluid properties. In literature, conflicting results have pointed out the necessity of further investigation in the topic. Some researchers found better results with indirect cooling than applying direct jets, and attributed the fact to overhardening of the workpiece in the second configuration. From a material point of view, a lack of studies investigate the effect of cryogenics with expensive and modern ceramic or PCD tools. The great portion of studies concentrate on Carbides, for economics and ability to retain toughness at low temperature. Lack on comparisons with cheap tools & Cryogenics versus more expensive high performance inserts and conventional lubro-cooling strategies is also found, [3, Shokrani 2013].

In the Performance chapter, Chapter 4, tool life and wear characteristics of inserts related to cryogenic machining will be presented.

### **2.4.2 Product quality and performances**

[1, Jawahir 2016] suggest that among all possible benefits coming from the application of cryogenics in machining, one of the most relevant is the enhancement of surface properties. With respect to dry conditions, deterioration of the tool (tool wear rate) was decreased for the majority of performed tests in the literature, resulting in better



surface finishing for longer cutting time. This proved to be wrong for large grained workpieces overhardened by the coolant. Researchers pointed out as well the reduction in chemical activity of piece and tool. Cryogenics can induce beneficial phase transformation, promote severe plastic deformation layers (SPD), high dislocation density and grain refinement, enhanced microhardness. Furthermore, it has been showed how the effect of low temperatures on the machined surface can induce improved compressive residual stresses, heightening fatigue life, stress corrosion resistance and pitting corrosion resistance. Performance characteristics include surface oxidation resistance and chemical reactivity, surface polarization and biological parameters such as cell attachment and proliferation.

*As already mentioned, we will not directly focus on surface integrity-quality analysis. However, its analysis is not separate from the subject we are dealing with: comparing different lubro-cooling strategies, surface integrity must be considered, and we will do it, where it will be important to point out, in brief. Moreover, a lack on studies about surface integrity has been observed in the literature, especially in accordance with normatives and legislation in the aerospace field. Study and Analysis in this field will help in allowing cryogenic machining applications in high performance fields, where it offers the more benefits.*

## **Topology: Geometric and Natural Finish**

In the cutting process, parameters like feed, depths, tool radius and edge angles, define the geometric finish. The natural finish, obtained by fact, in the machined surface is different. What causes the difference are vibrations, tool wear, BUE, chemical activity, effectiveness of lubro-coolant fluxes etc. Dimensional deviation is the difference between the designed final dimension and the achieved one. It depends mostly on workpiece strength, MT stiffness, flank wear, dimensional stability of tool assembly and workpiece. BUE and material ductility can also affect the natural finish by material deposition and burr formation. Lower feed and higher speed decrease surface roughness by reducing geometric finish as well as the plasticity of ductile metals.

The benefits of cryogenic machining can be noted observing a better natural finish. It has been pointed out that one of the major factor responsible for that is the decreased tool wear, promoted by the higher resistance of cutting edge materials at lower cutting temperature (higer hardness, dimensional stability, wear resistance, reduced thermal softening, stickiness and adhesion), [2, Yildiz 2008]. Cryogenics can also avoid BUE deposition on tools, therefore reducing forces and increasing surface quality, [27, Kane 2016]. On the other side, the low temperature can reduce the ductility of work materials. Thus the removed material can exhibit uneven tearing and the surface characteristics can worsen. Cryogenic temperatures also poses problems regarding the dimensional stability of MT organs and workpiece.

[28, Isakson 2018] and his team tried to get rid of the difference in tool flank wear so to understand whereas cryogenic fluxes had an influence on surface quality which was not directly dependent on reduction in tool wear. Using preworn inserts they found that both surface roughness and residual stresses improved, with respect to flood cooling (6bar) even if cutting forces were found slightly increased.

## Surface Metallurgy

Conventional machining is characterized by high temperature generation in the tertiary deformation zone. This can cause several metallurgical alteration on the machined surface. Depending on the heat affected zone size, alloy depletion, carbide coarsening and decarburization, phase transformation can occur. This phenomena changes skin properties in the workpiece that can lead to decreased performances in field.

Cryogenic machining help in reducing surface temperature, reducing flank friction, keeping it sharp for longer. This obstacle temperature rise, lowering the possibility of thermal alteration in the material. Furthermore, cryogenic machining promotes grain refinement (high dislocation density and dynamic recrystallization) and could induce beneficial phase transformation, such as lowering RA content in steels promoting hard martensite phases. The insulating nature of Nitrogen or CO<sub>2</sub> could help in avoiding interaction and reactivity with the environment.

## Surface Mechanics

Cryogenic temperatures enhance hardness and micro-hardness of workpiece surface. Also the depth of the hardened affected layer is found to be higher [29, Nimel 2019]. It is proven how high temperature lead to tensile stresses while low temperatures promote residual compressive stress states. Conventional machining of hard to cut materials exhibit high tool wear rates, consequent force rise and heat build up at flank. Tensile residual stresses are detrimental for fatigue life and corrosion resistance performances in service. Cryogenics offers to be a valid machining approach to improve service performances of machined pieces.

## Chemistry

Corrosion resistance in stainless steels can be deteriorated due to the high temperatures reached during cutting. Cryogenic machining could help in reducing the maximum temperature, preserving Chromium content in the metal matrix. Further thermal cycles to restore corrosion resistance could be avoided, [30, Bertolini 2019a].

## 2.5 Economics and ecologics

One of the most important aspects, often underlined, for cryogenic machining stands in its need to be of superior economic and ecologic with respect to conventional machining. By prolonging tool life, cryogenic fluids allow for more performant machining, less time consuming, high quality producing, which turns out in less energy demanding processes. On the other side, looking at CCF substitution, cryogenic fluxes limit or totally eliminate disposal issues, cleaning workpiece and chip, filtration of lubro-coolants, existence of CCF recirculation systems (pumps etc.). Regarding Health Hazards, cryogenic fluids also eliminate the threat of CCF in polluting the environment if non correctly disposed, and partly eliminates human health danger produced by mists.

It is to be underlined that the economical benefits of cryogenics over conventional strategies must be analysed considering both productivity and cutting fluid consumption and treatments, concerning energy and time consumed. It becomes evident that

the benefits of cryogenic fluxes is as high as their use is smart, optimizing flow rates to maximize their effect, being their production on of their principal cost, [31, Supekar 2020]. Determining the correct amount of cryogenic flux is again addressed as one of the primary issues to be further investigated. Economics of cryogenic machining is for sure affected by the initial investment cost for the MT adaptation and the price of non-reusable cryogenic fluxes, [12, Yasa 2012].

Many researchers found cryogenic machining to be performant at high speeds compared to CFL or MQL techniques. [4, Deshpande 2018] and others underline how, economically, cryogenics is the cheapest option at high speed, and should be implemented with the perspective of improving productivity, [32, Strano 2013].

[33, Pusavec 2011] and teammates developed a life cycle assessment of conventional machining versus cryogenic LN2 assisted turning of Inconel 718. They deeply analyse the effect of CFL production costs and impacts, health related issues, machining costs (initial costs, depreciation, maintenance, labour), waste associated costs and production costs. It turned out that cryogenic machining is economic at higher cutting speed, but lower cutting speed for economics of conventional machining are not optimal, therefore cryogenic is to be used where higher production rates are achievable.

The key factor for cryogenic machining performance is tool life improvement. It leads to lower tooling costs, downtime and machining cost spread over parts. Therefore improving tool life is seen as the major factor influencing cryogenics economics. Absence of post cleaning and swarf treatments are also influencing. These pros balance the drawbacks of higher initial costs, labour and maintenance costs and LN2 energy production costs.

Regarding Sustainability of Cryogenic machining with respect to high pressure emulsion cooling, the author strongly suggest the reading of a previous project-work, developed with a thesis mate and the aid of MUSP lab. The document will be available in the additional information.

### **2.5.1 Cutting fluids consumption and impact**

Many companies are not enough aware of the cost proportion that CCFs have in the manufacturing process [5, Pusavec 2009]. Cryogenic Machining emphasise those cost to highlight the benecial effects of its implementation. The effective cost and impact of CCF in manufacturing processes in terms of maintenance, cleaning of chips, part, machine and disposal, pollution and health hazard is high. [2, 5, Yildiz 2008, Pusavec 2009] and others pointed out, looking at the astounding and threatening consumption of CCF in the machining sector, that is necessary to adopt environmentally acceptable coolants. The global lubricant consumption for the machining sector is estimated to reach the 2000000tons in 2022. Large portion of machining lubricants are mineral based and provide lubrication, heat extraction, tool-workpiece and MT protection from corrosion, removing also metal particles, prolonging tool life and allowing for higher cutting speed and surface quality. However their effectiveness in performing this actions lowers with increasing cutting speed, [34, Benedicto 2017].

Purchase, workpiece and chip cleaning, water consumption (for cleaning and fluids content), energy, replacement, storage, supply and maintenance, filtration and disposal cost affect cutting fluids. Additional costs come from realization of safe and healthy environments for workers, [34, 5, Benedicto 2017, Pusavec 2009].

## CCFs

Conventional Cutting Fluids are straight/neat oils (mineral, animal or vegetable, poor cooling capacity but excellent lubrication, effective at low cutting speed) or water soluble (increased cooling effectiveness). Water soluble CCFs are emulsions (Oil content  $> 40\%$ ), semisynthetic fluids ( $< 40\%$ ) or synthetic (only cooling capacity, Oil free). CFLs are generally applied as floods and need: pumping, circulation, filtering, recovering, storage systems. Moreover, they require to be re-added of components that may be consumed in the process. They can be also provided in mists, pressurized toward the cutting zone. The carcinogenic nature of those mists has been underlined by various researchers, [34, Benedicto 2017]. They represent a threat for environment due to disposal energy, water and detergent demands and disposal in their turn. The threat of ecosystems pollution becomes reality if indiscriminately released in the environment. Several techniques develop different solution to limit or avoid the usage of CFLs. Among this Dry, MQL, Vegetable Oils, Cryogenic, Solid lubricants, Nanofluids are studied. We will report in brief the excellent work of [34, Benedicto 2017] and colleagues.

Problems linked to CFLs disposal concerns Oil-Water separation, debris separation. During usage microbial growth and additives depletion, fluid drag out in chip and material cavities and consequent cleaning, atomization and evaporation of oil due to impacts and high temperature generating hazardous mists.

## Dry

Dry machining tries to avoid completely the usage of cutting fluids and related issues by exploiting superior high temperature strength, hardness, lubrication, thermal fatigue and corrosion/chemical resistance of engineered coatings. Disadvantages of this technique are in the heat affection of both tool and workpiece generating welding and adhesion phenomena added to poor machined surface properties. Dry machining could provide longer tool life in intermittent cutting processes due to less thermal shocks with respect to other more aggressive cooling strategies.

This strategy eliminates all consumption and pollution threats related to CCFs. The only drawback is the lower productivity performance achieved. High consumption of tools with higher energy history must also be considered.

## MQL

To reduce the amount of CFLs used, a mist made by droplets of Oil and pressurized air is fed to the cutting zone. It combines the chilling effect of air with the lubrication effect of oil with a precise application of flux so to optimize fluid consumption.

Economic advantages of this technique come from the lower fluid consumption, absence of chip and piece cleaning due to the almost total absorption of oil in the process. Also recirculating system and maintenance are avoided. Anyway those oil have to go somewhere, therefore fumes extraction and caged environments is compulsory, given the carcinogenic nature of oil mists.

## **Solid Lubrication**

The lubrication effect of Graphite, Molybdenum Disulphide or Titanium Disulphide is addressed to the layered atomic structure with weak Van Der Waals bonds in between layers. They provide stable lubrication at high temperature and pressure and have excellent thermal conductivity properties. Application in the cutting zone is however difficult due to the solid nature.

## **Gaseous lubricants**

Generally air or chilled air is used. Due to its poor lubricating capacity it can be added by oil mists. Alternatively, gaseous Nitrogen can be used, losing the latent heat thermal extraction capacity but preserving the cooling action.

## **Sustainable Fluids**

Biodegradable vegetable or synthetic oils have been produced to replace petroleum derived oils. They have low cooling effect and oxidation protection but excellent lubricity and low volatility. However, their cost, almost double than conventional oils, is a limit on the diffusion. Finally, their ecologic superiority is achieved only if smart consumption is adopted, [35, Clarens 2008].

## **Nanofluids**

Nanofluids exploit the synergy of solid lubricant nanoparticles and compressed fluids or gases so to increase penetration in the cutting region. They promote thermal conductivity and lubrication. A drawback is increased viscosity in the cutting fluid and difficulties in maintaining homogeneous dispersion of particles in the fluid.

The high cost is one of the major drawback limiting the diffusion of this method. Moreover, studies have to go deeper in understanding where these microparticles would go during the cutting process and their threat for human and environment.

# Chapter 3

## Application of Cryogenics

Cryogenic cooling strategies have been extensively adopted in turning operations. The fixed nature of tool and holder allowed for easy conversion of conventional lathes into cryogenic machines. Cryogenic fluxes have been directly applied through nozzles. In other cases more complex apparatus have been adopted, delivering the cryogenic flux through the holder and/or through small holes in the insert itself or using a properly shaped chip breaker and insert holder. Less immediate is the integration of the cooling flux through the spindle of a milling machine [2, 3, Yildiz 2008, Shokrani 2013]. Therefore, many researches opted for external nozzles. In a milling machine, the interrupted nature of cutting, lead at first to problems of sudden and brittle failure of inserts, probably due to thermal shocks (heating during engagement and freezing in idle phase). This problem could have been enhanced by the use of external nozzles which allow for low precision in targeting the heat generating zones, cooling too much the WP and the inserts, but unable to reach the rake and flank face during cutting. Other researchers made use of internal nozzles, carved into the spindle and holders, exiting directly at inserts. This allowed for high control of cooling media.

[3, Shokrani 2013] and others observed a lack of application of cryogenic machining in industrial environments. They pointed out how cryogenic application has been restricted to turning operation with LN<sub>2</sub> only. The consumption of LN<sub>2</sub> is another issue that requires precise flow tailoring. Exact targeting by cryo-nozzles must be achieved. Orientating studies on more widespread materials instead of exotic alloys and toward milling and drilling operations could attract the interest on this performant and possibly environmentally friendly technology.

### 3.1 Tool design

#### 3.1.1 Turning and Milling angles

It is important to introduce the way to describe insert orientation in turning and milling. An insert in space is characterized by three rotation axis, therefore three angles can describe its position relative to the workpiece. Added to this rotations, there are other angles that refer to the original geometry of the insert. To compute interaction angles with the workpiece the insert shape has to be considered.

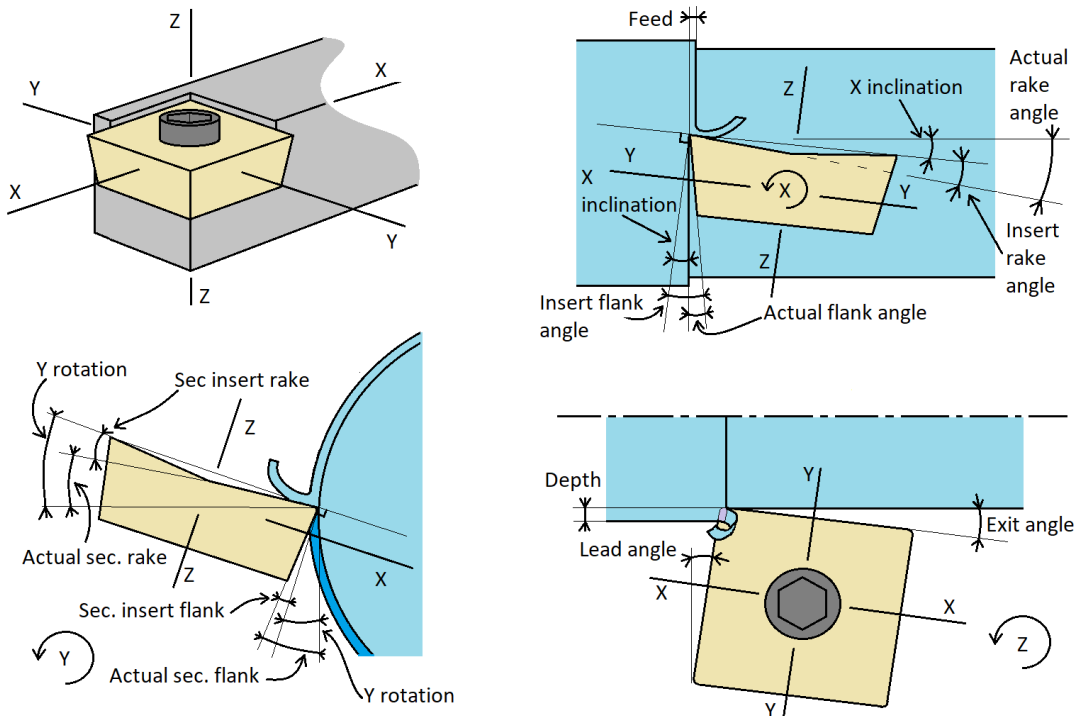


Figure 3.1.1: Angles in turning

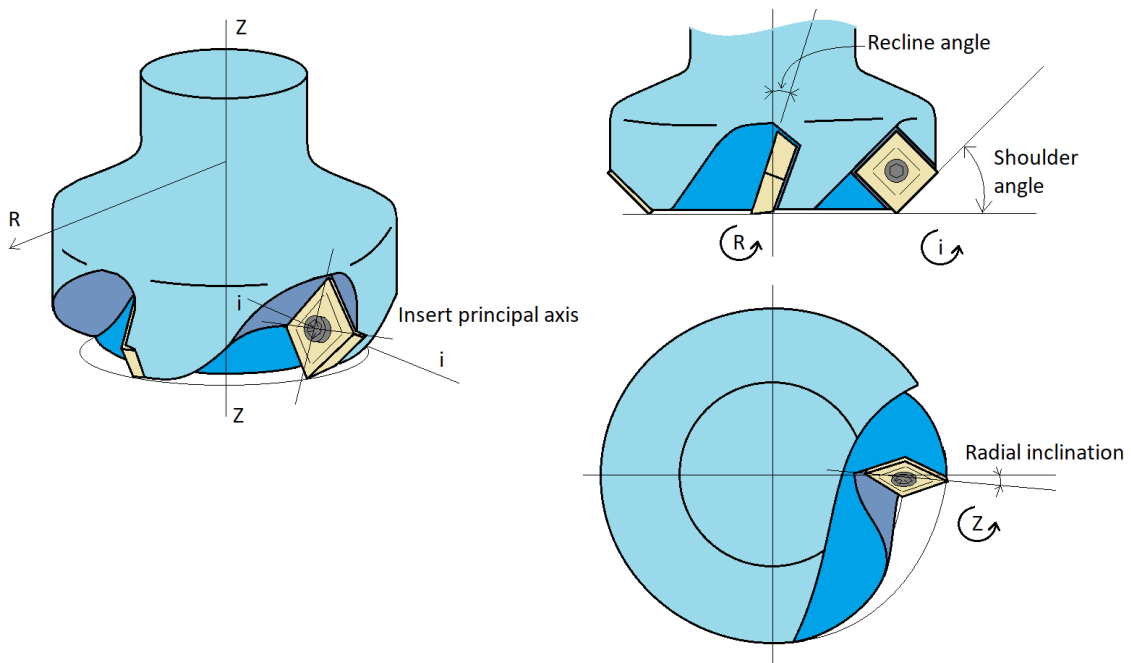


Figure 3.1.2: Angles in Milling with indexable mills

### 3.1.2 Cryogenic Tool design

With respect to the tool, inserts have started to be designed specifically for cryogenic applications, an aspect which have never been given the correct attention. In turning, tool life achievements with cryogenic machining have reached levels that researchers are hardly capable of reproducing in Milling. This is to be linked to the complex interrupted nature of the process, the delivery difficulties and tool design variations. Turning tools are very bulky. Flank angles can be small as the roundness of the workpiece can compensate, avoiding the flank face to rub the workpiece surface. In Milling, higher flank angles are needed. Especially for solid mills, the reduced space and tolerances push in designing light geometries with sharper angles. Regarding this aspect, is important to point out some recent findings.

It has been made hypothesis (consequently to experimental findings at MUSP lab, Piacenza, Politecnico Milano) on how large positive rake angles are detrimental for cryogenic milling: it means we need to strengthen the tool. This can be due to excessive overhardening of WP, leading to higher forces. Another explanation possible is the excessive cooling of the tool, raising its hardness but lowering too much its toughness. Another important aspect underlined by failures in experimental trials is the mechanical load experienced by inserts as a combination of insert shape and milling strategy adopted. Square shoulder inserts with small or null recline angles in wall milling are subjected to intense hammering action when approaching the cut. The whole insert edge is engaged at one time, the engagement is sudden and not gradual. Moreover the square shoulder concentrate the chip load on a small bulky rake area. This rapid and cyclic mechanical load could be the explanation of the poor results obtained with square shoulder mills, especially with cryogenic cooling ([36, Tapoglou 2017]), as the workpiece can be overhanded, the tool slightly embrittled, the thermal cycles could be enhanced or a little reduced ([37, Augspurger 2019]) and little lubrication and damping action can be obtained from the cryogenic fluid, whereas it is offered by emulsion.[38, Fernandez 2019] and teammates, comparing cryo CO<sub>2</sub> and emulsion cooled cutting of Inconel 718, Gamma Ti-Al and EA1N grade Steel adopted 45° shoulder angled mills instead of 90° and obtained fair results. [39, 40, Sadik 2016-2017] adopted round shaped high feed inserts that would provide a gradual engagement while approaching the workpiece: they obtained excellent results with LCO<sub>2</sub> cooling.

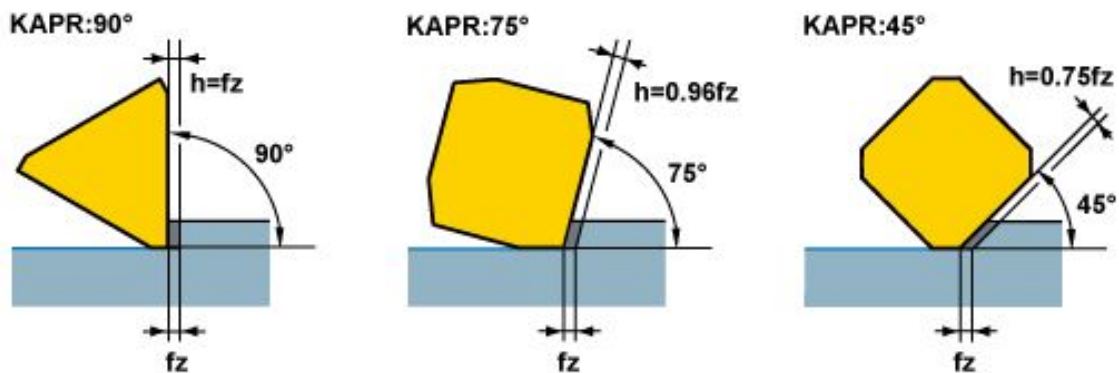


Figure 3.1.3: Shoulder angle variation in Milling



In drilling is difficult to reach the cutting zone. Limitation of the external nozzle approach is pointed out as it decrease the reachability of nasty features. An internal nozzle system is fundamental. This pose the challenge of making small holes into HSS or Carbide drills, generally by EDM.

### 3.2 Cutting parameters and approach

Cutting speed and feed will be given much attention in the next chapter, Chapter 4. Here we consider the process design, which is linked to the geometry of the part we want to achieve, governing the choice of depth of cut and percentage engagement of the mill in Milling.

#### 3.2.1 Natural process parameters

##### Turning

The depth of cut is generally governed by practical issues such as layers to be removed or stability of the process (Stability Lobes Diagrams). Increasing depth in turning with the same feed increase the edge portion under load. Decreasing the feed while increasing depth raise the mechanical loading of the insert edge, which is the weakest part of it. Low depth and high feed, on the contrary, generates localized thermal and mechanical load on the insert, which is difficult to be reached by the coolant.

The author believes handy to refer to a new process variable we called Chip Ratio, CR:

$$CR = \frac{\text{depth of cut [mm]}}{\text{feed [mm/rev \setminus mm/tooth]}} \quad [-]$$

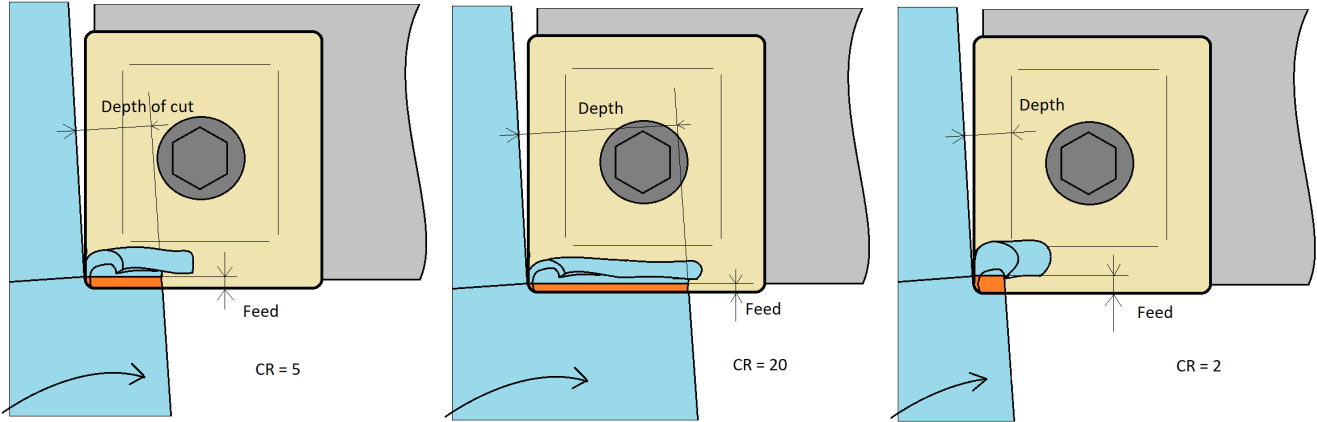


Figure 3.2.1: Angles in Milling with indexable mills

The belief is that there is an optimal Chip ratio that allows for good reachability of the heat affected zone by the coolant and fair sharing of mechanical load on the edge, not being localized in one spot and not concentrated on the outer brim of the weak edge. The optimal CR for longer tool life depend on the characteristics of the cutting fluid. Emulsion has confirmed higher bulk cooling capacity, [41, Pusavec 2019], LN2

has not because it tends to evaporate suddenly in contact with hot surfaces. LCO2 has higher bulk cooling capacity, [42, Kirsch 2018]. Bulky Chip Ratios can be effectively cooled with emulsion but are detrimental for Liquid Nitrogen. On the other side, huge CR means it is difficult for a fluid to spread on a so large area, if its delivery is highly localized.

This reasoning is a mere consequence of logic and reason, we will deepen into it, with examples that confirm or debate it in Chapter 4. Moreover, the Chip Ratio is a useful criteria considering alternatives at the same MRR, so with the same Chip Section area, CS (at constant cutting speed):

$$CS = \text{depth of cut [mm]} \cdot \text{feed [mm/rev \setminus mm/tooth]} \quad [\text{mm}^2]$$

**Milling**

For what concerns milling operations, the depth of cut is governed by the same reasoning of turning. Depth of cut and feed can be regulate so to vary the Chip Ratio and ease or not the reachability of the cutting edge by the cutting fluid, optimizing the load on the cutting edge. However, the feed varies along the cutting arc so that, depending on the chosen engagement, we can regulate only the average CR along the arc. When the tool leaves the workpiece the feed would be very low (down milling). The shoulder angle can regulate the CR for shoulder milling operations, by regulating the contact area size between tool and chip. The recline angle and variable shoulder angle could ease the approach of the cutting edge with the material.

The chosen engagement is often due to workpiece final geometry, process stability or tool producer specifications. However, for roughing operations it can often been optimized. Few studies have concentrated on thermal and mechanical cycling of Milling inserts as a function of mill engagement. It has been found that thermal cycles in dry cutting are characterized by higher maximum, average temperature and amplitudes of thermal oscillations, raising the engagement from wall milling toward slot milling ([43, 44, Jiang 2013, Karaguzel 2016], see Chapter 5). However, a lower engagement produce lower MRR and consequent increase in the number of needed passes.

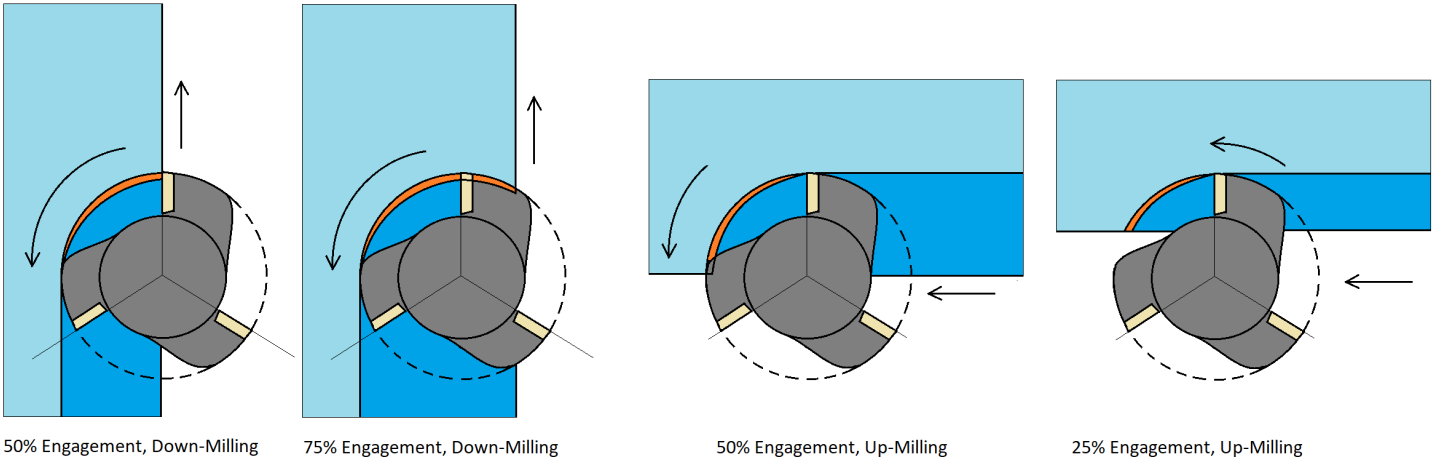


Figure 3.2.2: Milling engagement, Up and Down milling strategies

The milling strategy can influence the thermal and mechanical load felt by the insert. Regarding thermal cycles, in dry cutting, thermal loading is steeper for up milling, while it is more gradual for down milling ([45, Sato 2011], Chapter 5). On the contrary, up milling generates smoother mechanical loads, due to the gradual increase of chip thickness from zero, while down milling generates impacts when the cut is engaged.

*In what way this would help for cryogenic machining? We don't want to increase the thermal cycling on the inserts, therefore accurate analysis of engagement and strategies must be done. In the particular case of Ti6Al4V, up milling is not recommended as the alloy has a strong tendency to refuse the cut, due to its strength and low elastic modulus. On the other hand, it is needed more research aiming at the understanding of the variation of thermal cycles on insert due to cryogenic actions in relation with the engagement.*

## 3.2.2 Cryogenic parameters

### Cryogenic Flow Rate and Pressure

Average values for cryogenic flow rates can be found in literature, but not all studies are correlated with the necessary information regarding flow rates. For LN2, [46, Madhukar 2016] and colleagues report  $0.5 \div 3.5 \text{ Kg/min}$  at a pressure ranging in between  $1.4 \div 24 \text{ bar}$ , and the most common combination to be  $1 \text{ kg/min}$  at around  $7.5 \div 15 \text{ bar}$ . No relation with materials and nozzle apparatus was given. Slightly higher values were applied in milling ( $4.5 \text{ kg/min}$ ). For LCO2 even scarcer information are found. [47, Venugopal 2007a] and colleagues justify qualitatively the applied flow rate of Nitrogen by achieving stable flow and avoiding OH of the workpiece. However, after seeing the reduced effectiveness of cryogenic at higher cutting speed for turning Ti-6Al-4V, they stated that low cooling capacity or little penetration of cryo in the cutting region was imputable. Therefore cryogenic flow rate must be adapted in parallel with other process parameters during cutting. More detailed information regarding flow rates can be found in the following chapter, Chapter 4, where cryogenic machining trials for Ti6Al4V would be carefully analysed.

In general, fluid-dynamic flow properties such as pressure and flow rate are fundamental parameters that characterize cryogenic machining. The absence of indications of that nature in an experimental trial are not only a tremendous lack, but a complete misdefinition of prerequisites, which turns the whole study shaky from the beginning. The cryogenic flow pressure determines the entity of the jet speed while approaching the target. The jet speed is a measure of the capacity in breaking the vapour bubbles formed in the contact with the hot target. This is for sure influenced by the nozzle size, but in general each nozzle design fixes the spot diameters to similar values. The flow rate primarily influences the fluid consumption which has a great importance regarding the sustainability of the cryogenic alternative.

### Cryogenic fluid quality

Regarding Liquid Nitrogen, since the article of [48, Pusavec 2016] and colleagues, measuring the flow quality at the nozzle has become crucial. When applying cryogenic machining, it is necessary to prefer having full fluid title at the exit of the final nozzle

as its conductivity is much higher than the vapour phase and we could exploit the latent heat of vaporization. In fact, gas layers are considered of insulating nature.

Nitrogen Phase Properties					
	$T - [^{\circ}C]$	$\rho - [kg/m^3]$	$c_p - [kJ/kg^{\circ}K]$	$\mu - [Pa \cdot s]$	$\lambda - [W/m^{\circ}K]$
LN2	$-196^{\circ}C$	803.6	2.046	$1.463 \cdot 10^{-4}$	0.132
GN2	$-196^{\circ}C$	4.979	1.351	$0.05331 \cdot 10^{-4}$	0.0077

Figure 3.2.3: Properties of Liquid and Gaseous Nitrogen, [48, Pusavec 2016]

The nature of the fluid state at the exit of the nozzle can be understood by the continuity of the flow. Unstable flow is characterized by intermittent portion of gas phase in the delivery tubes. The design of the delivery line in relation with the delivery pressure is fundamental to avoid unnecessary losses and stable liquid flow.

For LCO2 there are less problems related to evaporation but increased danger due to high pressure fluids. There are few studies concerning the LCO2 phases in relation with the properties of the jet such as vicinity of the nozzles or over pressurization.

### 3.3 Cryogenic systems

#### 3.3.1 Cryogenic production units

Liquid Nitrogen is generally purchased and delivered with Dewars, vacuum insulated stainless steel tanks containing up to 500 kg of fluid, kept at a constant pressure thanks to a valve that releases the evaporated fraction in the ambient air. The full content of the Dewar, due to heat leaks of the tank, can evaporate in 3 days and it is therefore to be used instantly.

The most widespread production route for obtaining LN2 is from air liquefaction, in a process called Cryogenic Distillation. From the process, high purity medical liquid oxygen can also be obtained. Other processes make use of selective membranes to isolate nitrogen before liquefaction. Production units for LN2 can be purchased with maintenance contracts from the cryogenic supplier, for more information we suggest to look at a previous Author's work available in the additional information.

Liquid Carbon Dioxide is purchased in pressurized bottles, also grouped in pallets as the single bottle can hardly contain more than 50 kg. This also raises the importance of a smart and low consumption of cryogen. Generally, high purity CO2 is available at high pressure in the liquid state for the food and beverage industries. However, its cost is in most of the cases prohibitive for machining operations with the actual flow rates ( $> 1\text{€}/kg$ ). There is, in general, lack of studies indicating its purchase and application cost. Several alternatives are available for LCO2 production. As a natural component of crude Oil wells, where it occupies the top layer, CO2 can be kept rather than released into the environment when extracting the Oil. CO2 is a by product of many chemical routes, for example during Ammonia production, Hydrogen refinement and Bio-Ethanol production. Another interesting alternative is represented by CO2 capture, however being still a research topic.

Chilled air is in general obtained with Ranque-Hilsch Vortex Tubes, starting from pressurized air. For temperatures lower than  $-50^{\circ}\text{C}$  vapour compression cycles can be used. For very low air temperatures, coils where air flows are set into cryogenic LN2 dewars. The lower the temperature, obviously, the higher the cost for the refrigerating systems. The interesting aspect of RHVT is the need of compressed air only as an input (generally available in shop floor) and the output of both a hot and a cold stream. The hot stream could be oriented toward the back of the chip so to soften the material, while the cold stream toward (or inside) the tool so to cool it down. However, to the author knowledge, no study has been presented considering this. Probably the temperatures are too low and the HTC of air too small to influence the materials behaviour at the rate (cutting speed versus heat transfer speed) of the chip removal process.

### 3.3.2 Cryogenic delivering system and issues

For delivering the cryogenic LN2 flux toward the cutting zone, and keeping it in the liquid state, vacuum jacket tubes have often been adopted. They are characterized by an inner flow of high pressure liquid nitrogen, an outer flow of low pressure evaporated LN2 (coming from gas separators, later described), an insulating vacuum tube and reflecting materials outside, [46, Madhukar 2016]. Avoiding any heat penetration in the tubes is fundamental to avoid vaporization, consequent gas separation and energy wasting due to vain production of liquid LN2 which then vaporizes.

Problems are underlined for the achievement of very low flow rates, [8, Hong 2001b]. Of great importance is the delivery line design and the delivery pressure. Cavitation is seen as one of the most important phenomena (more than heat leaks) regulating the evaporation of LN2, in presence of valves and bends of the tubing system, [49, Tahmasebi 2019].

Another important aspect of delivery lines for LN2 is that they necessitate some time, depending on the line design, to be cooled down and achieve stable flow. Regarding this aspect, it is crucial to provide an reliable industrial design that minimize heat leaks and cavitation effects, so to provide flexibility, readiness and low wastes. However, gas evaporators are often needed, but sub coolers could be preferred so to avoid the loss of Nitrogen, unless increasing energy consumption.

LCO2 delivery systems pose much less problems, they necessitate high pressure pipings and do not thermally affect the machine tool organs. In the next sections we will deal with the literature implementation of final cryogen application to the cutting zone.

#### Indirect cooling applications

[17, 15, Wang 1996, Wang 2000] and colleagues developed a system for indirectly cool the tool in turning applications. It consisted of a copper cap in which LN2 was recirculated. The inlet of the cryogenic fluid was on the side nearer to the tool tip (cutting zone), figure 3.3.1. During cutting they provided temperature measurements through termocouples. Even if the measured temperature was not linked with the cutting zone (due to distance of the termocouple), it was significantly reduced if compared to dry or emulsion assisted machining. Examples were provided for RBSN, Ti and Ni alloys and Tantalum. They demonstrate the significant improvement in tool life achieved by exploiting the cooling of the insert only, which maintained its cold properties avoiding

thermal softening.

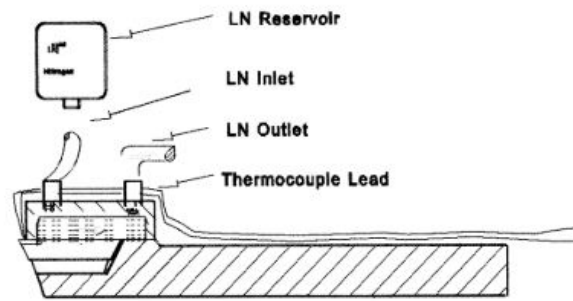


Figure 3.3.1: Tool back cooling application scheme, [17, 15, Wang 1996, Wang 2000]

[50, Minton 2013] and teammates studied the effects of diamond nanocrystalline layer and internal cooling for improving wear resistance of inserts in cutting Grade 2 CP Titanium. In order to control the high cutting zone temperature, highly conductive diamond layer, micro chamber for automotive engine coolant and very thin WC insert were used. The coolant was supplied by a reciprocating pump at ambient temperature. Issue linked to the pump was the unsteady flow of refrigerant. The approach managed to avoid hot spots by spreading heat over the insert with the coating and cool the heat generation zones. Tool wear mechanisms (crater and flank) were retarded and life increased by 40% with respect to uncoated uncooled, coated uncooled, and uncoated cooled. This also means that diamond coating are even detrimental in cutting Titanium due to their graphitisation above  $400^{\circ}C$ , temperature likely to be reached in short time. Also cooling WC insert indirectly is not very effective given the poor conductivity of the WC material. However, WC conductivity is enhanced at cryogenic temperature, so a trial with LN2 could be performed to compare coating and cooling to cryogenic indirect cooling.

[51, 52, Park 2015, Suhaimi 2018] made use of an internally cooled mill for wall operations at high depth of cut and small engagements. The strategy failed to prologue tool life, with LN2 worsening it. However, in cooperation with external MQL it provided the longest life.

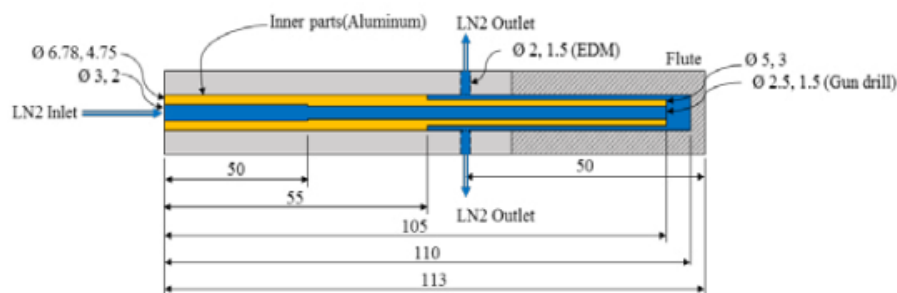


Figure 3.3.2: [51, 52, Park 2015, Suhaimi 2018] internally cooled wall mill

### Direct spraying

[53, Zurecki 2004] and others provided a scheme for double phase Nitrogen spraying with external nozzle on the tool rake face, figure 3.3.3. They didn't provide comparison on

forces between conventional and cryogenic approach, but concentrated on tool duration and surface hardness and roughness. Tool life and surface hardness properties improved while roughness improved only for soft PM steels.

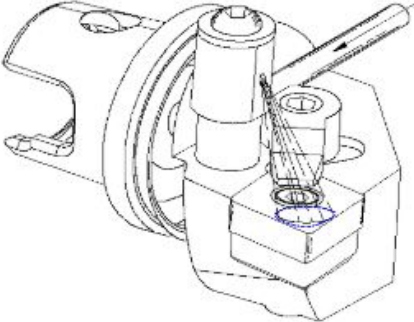


Figure 3.3.3: External nozzle spraying system scheme, [53, Zurecki 2004]

[54, Shokrani 2012c] and his team failed to prolong Tool life and improve surface roughness milling Inconel 718 with external nozzle. [55, Bermingham 2011] et al. applied LN2 to rake and flank by a system of tool cap and copper nozzles, 3.3.4. Same strategy of nozzled cap was applied by [56, Machai2011] for LCO2 delivery on the rake face.

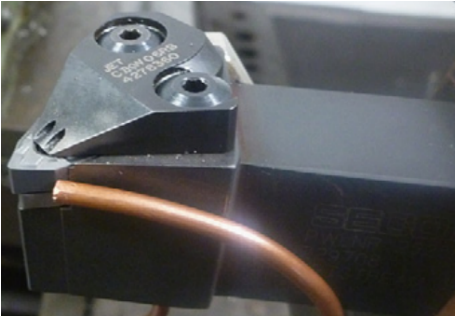


Figure 3.3.4: [55, Bermingham 2011] LN2 delivery nozzle apparatus

In a following study, [57, Bermingham 2012] and his team compared High Pressure emulsion cooling with LN2 varying nozzles layouts. They demonstrate the higher influence of nozzle position on tool life with respect to cooling approach adopted. The tested nozzle layouts are shown in figure, 3.3.5. Best performances where achieved with design 3 for cryo and design 3 and 4 for HP. In those cases the nozzles orientation where parallel but opposite to chip flow on insert rake and nose. This means nozzle position and orientation must be carefully optimized looking at chip flow.

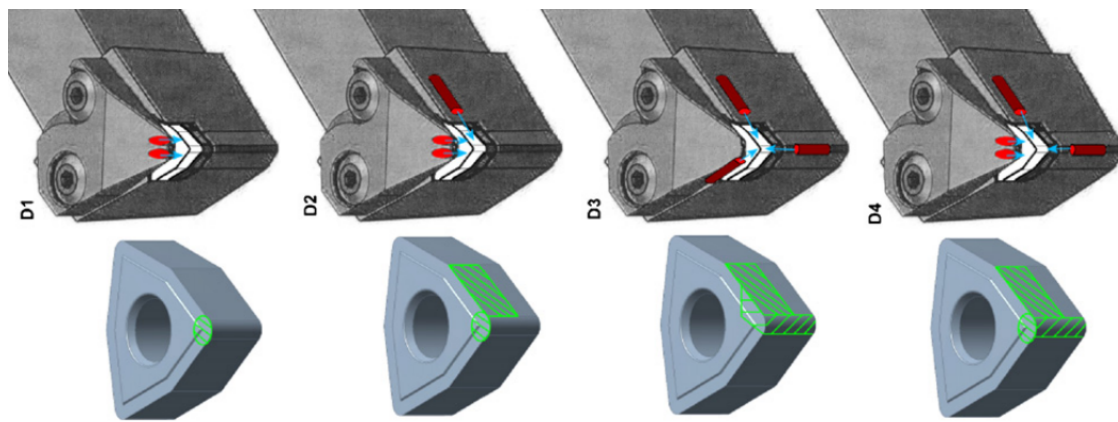


Figure 3.3.5: [57, Bermingham 2012] tested nozzle designs

[58, Klocke 2013] and colleagues applied several cooling media with an insert cap nozzle. They stated that best improvements in finishing Gamma Ti-Al in terms of tool life and roughness were achievable by cryogenic LN2 cooling.

[32, Strano 2013] and colleagues applied LN2 by modified holder to the rake and flank faces.

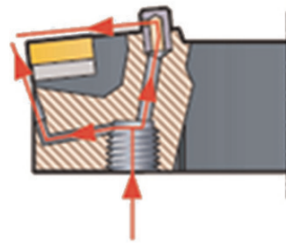


Figure 3.3.6: [32, Strano 2013] LN2 nozzle delivery through holder

[59, Kaynak 2014] applied LN2 on flank face in cutting Inconel 718 achieving longer tool life. He also tested rake&flank cooling configuration which proved inefficient because of complex grooving of the insert, that inhibited LN2 reaching the tool-chip interface. Cutting edge grooved geometry can impair effectiveness of cryogenic machining.

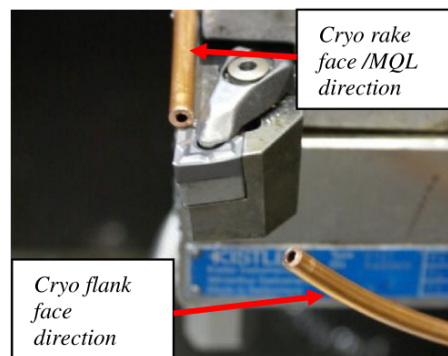


Figure 3.3.7: [59, Kaynak 2014] nozzle configuration



[60, 61, Shokrani 2016a, Shokrani 2016] provided a static ring nozzle design for LN<sub>2</sub> application on tools and cutting zone in milling Ti-6Al-4V. Unless the fact that the system is quite bulky and could work only for face milling applications, it has proven to increase tool life.

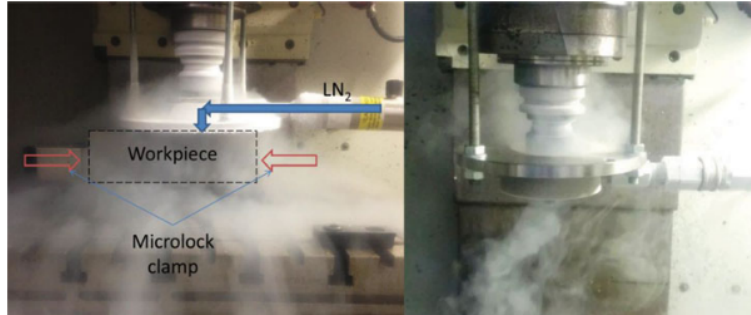


Figure 3.3.8: [61, Shokrani 2016a] ring LN<sub>2</sub> nozzle delivery picture

[29, Nimel 2019] successfully prolong tool life by applying LCO<sub>2</sub> with an external nozzle in a slot milling process of Ti-6Al-4V.

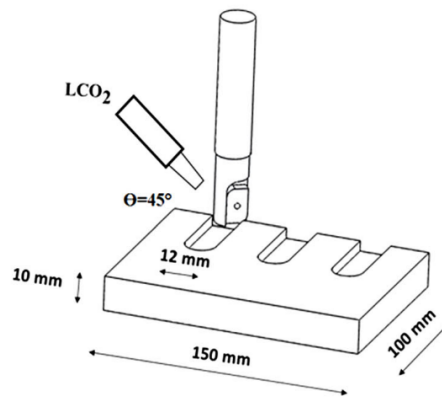


Figure 3.3.9: [29, Nimel 2019] external nozzle set up

### Direct localized spraying

[13, 8, Hong 2001c&2001b] patented, already in the nineties, a very precise LN<sub>2</sub> delivery system using a chipbreaker. The flux was delivered by micro channels made by EDM on the breaker and exit from small holed just at the level of the rake face, 3.3.10. The system was also designed for flank cooling delivery. Several practical implementation regarding holes on the breaker, micro grooves on the rake, flank delivery switching (on-off) and nozzle orientation on rake face were provided.

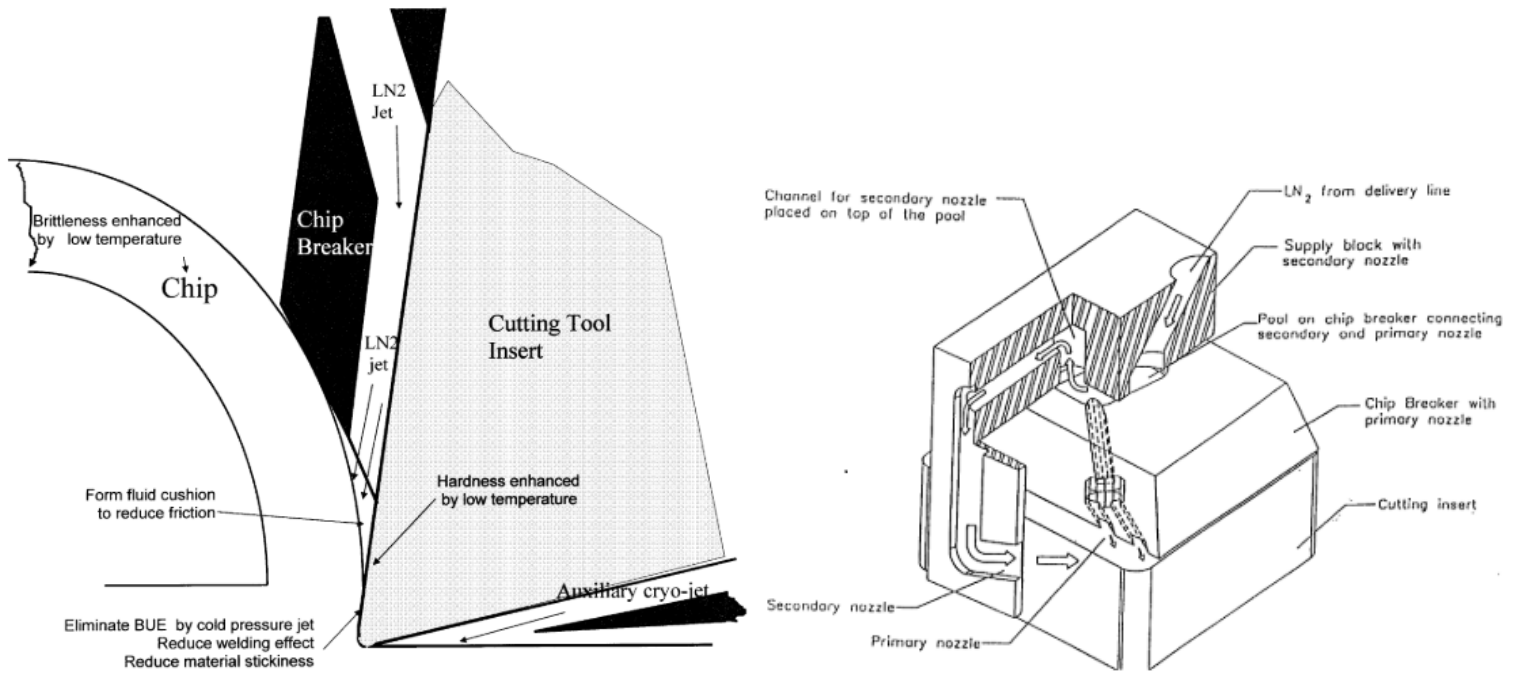


Figure 3.3.10: [13, 8, Hong 2001c&2001b], chipbreaker and flank micronozzle scheme

The nozzle scheme aimed at cooling the highest temperature affected zone in the tool, proven to be at the location in the rake face where crater wear generates, approximately at a distance from the tip equal to the undeformed chip thickness. The chip breaker helps in lifting the chip and allow the cryogenic flux to reach the higher heat affected cutting zone. Expansion ratio of liquid to gas Nitrogen can help in reducing the more the friction, wear and heat build up. Chip breaker distance from the cutting tip was optimized cutting Ti-6Al-4V which resulted in almost double tool life for both flank and rake nozzles activation. In the text, promising result of tool life improvement were also reported for some Steels, Tool Steels and another Ti-alloy. Since the patent is of the nineties, it seems awkward that other researcher, even decades after, had tried for external nozzles or flood cryo-delivering systems, when avoiding OH and precise tool-heat-affected-areas cooling was marked as fundamental. A reason could be the difficulty in handling the chipbreaker from a flexibility point of view. Hong didn't considered the raise of set up time for tool change, moreover varying depth of cut, the position of the breaker is to be varied, introducing delays for trials or modeling. Anyway, weighting drawbacks, the strategy already answers to research remarks that have been made decades after.

[62, Hong 2000] and Broomer developed an Aluminium nozzle cap delivering LN2 by means of two grooves, making little tubes when sealed with the insert, to provide LN2 cooling in machining AISI 304 Stainless Steel with minimum amount of LN2 and grooved tool. The nozzle, described as Z, provided best performances compared to the others, both in terms of LN2 consumption and life improvements.

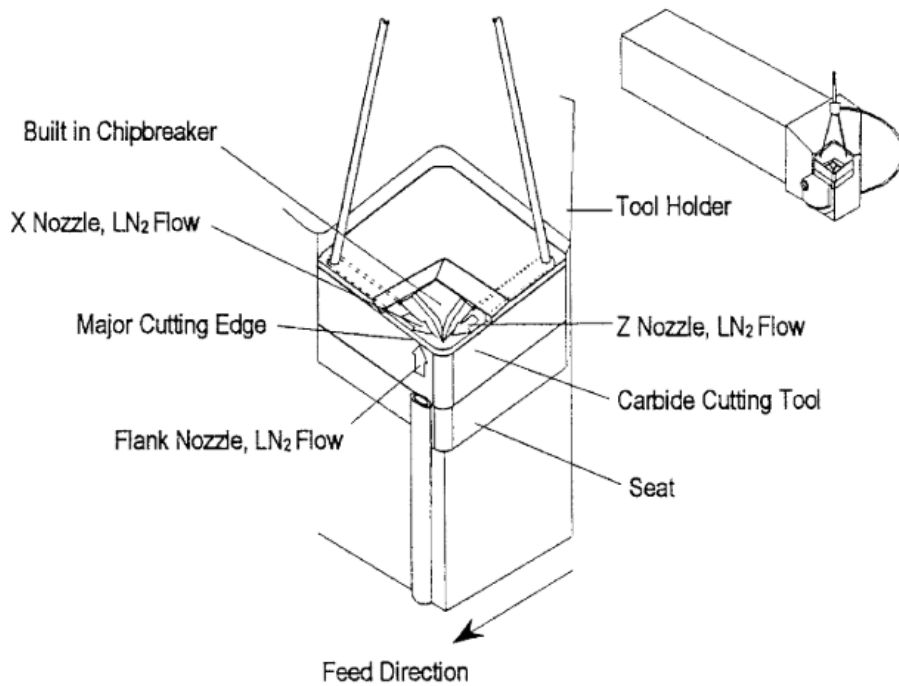


Figure 3.3.11: [62, Hong 2000] Al nozzle cap delivery system

Those historical articles might be old, but point out solutions to errors that have been committed far afterwards. Nozzle direction must be opposite to chip flow, nozzles must be positioned as near as possible to their targets to achieve maximum effectiveness. [63, Dhananchezian 2011] and colleagues, by EDM machining holes into the insert on rake, primary and secondary flank, 3.3.12. LN2 at 3 bar was directed toward the rake hole, the major portion splashing on the rake face and the rest ejected through the flank nozzles. The system proved to be good for cooling the insert and the cutting zone, avoiding OH of the workpiece at all speed thus achieving lower forces, decreasing flank and rake wear. The system represent the first rough application of hybrid direct-indirect cooling of insert and cutting zone by ejecting the cryogenic fluid after having passed into the insert. The hybrid technique could benefit in extensive cutting tool thermal evacuation and cutting zone temperature control.

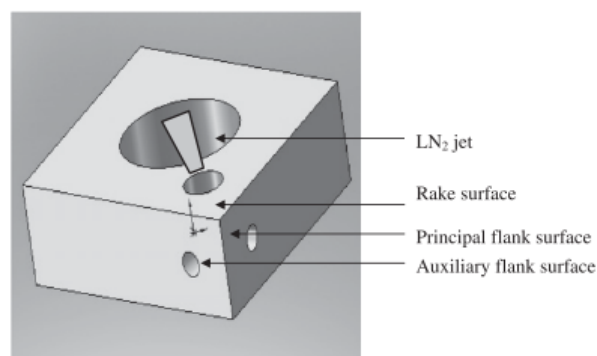


Figure 3.3.12: [63, Dhananchezian 2011] holed insert scheme

[51, Park 2015] and his team developed an internal LN2 delivery system for end

milling Ti-alloys. LN2 was fed through the tool holder and ejected by small holes toward the tool-chip interface, 3.3.13. The system proved to be good with an indexable mill and low axial depth of cut. However it wasn't effective in wall milling, with high axial depth of cut and small radial engagement, due to the long tool-chip contact area which was hardly reachable by LN2. In this case in fact, the mill exhibit severe adhesion. Higher pressure MQL proved to be more effective.

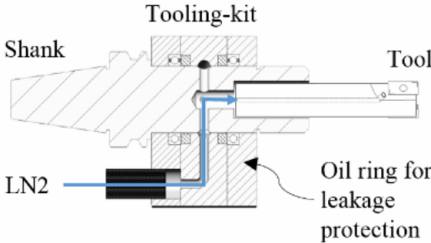


Figure 3.3.13: [51, Park 2015] through holder LN2 delivery system

[39, Sadik 2016] and team applied LCO2 through channels in the tool holder provided by Sandvik (CoroMill 600-040Q16-12H) with four spherical inserts at a pressure of 50bar and variable flow rates of 0,15/0,19/0,64 Kg/min. Excellent results were achieved, discussed in the next chapter.

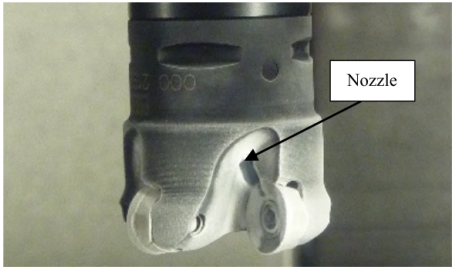


Figure 3.3.14: [39, Sadik 2016] through holder LCO2 delivery

[38, Fernandez 2019] and colleagues developed an internal CO2 delivering system for local spraying on inserts during cutting of difficult to machine alloys in milling. The system is interesting as it consisted in modification of the tool holder only, without interfering with the interior of the spindle system. The layout is capable of delivering LCO2 at 50bar to 4 inserts.

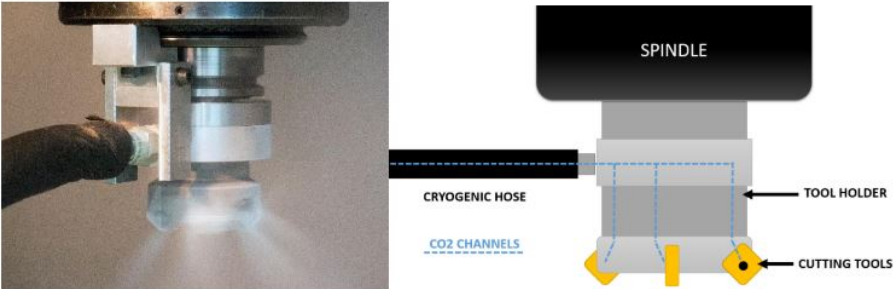


Figure 3.3.15: [38, Fernandez 2019] internal CO2 delivery system

[64, Mia 2019] and colleagues applied rake and flank cooling as effective lubro-coolant strategy lowering forces, temperatures and roughness profiles versus dry cutting in turning Ti-6Al-4V.

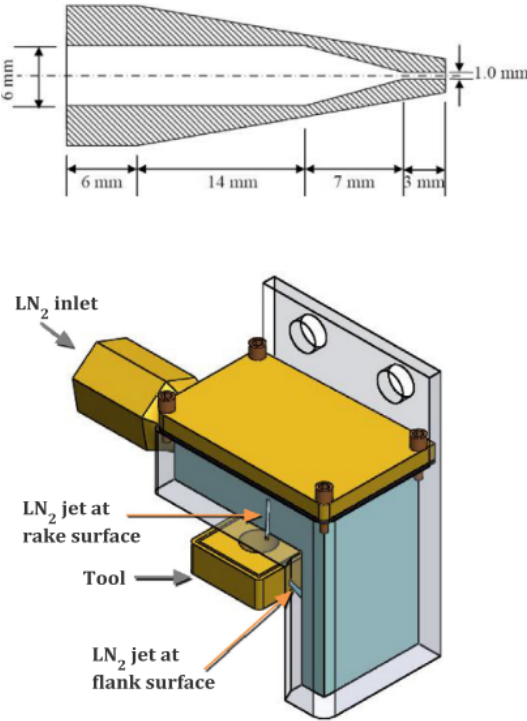


Figure 3.3.16: [64, Mia 2019] rake&flank nozzle scheme

**Pulsed jet**

Providing the cryogen only during the active cutting phase of the milling insert could lead to lower fluid consumption, unless its effects on thermal cycles should be experimented. Since it is not clear if the temperature build up in the insert is decreased, for cryogenic machining, due to its precooling in the non cutting phase, cooling in the active cutting phase or both, a phase shift of the pulsed jet could be tailored to achieve optimal tool life. Higher frequency pulsed jets, switching on and off during a single cutting phase, could also brake the Leidenfrost effect and increase the heat transfer, [1, Jawahir 2016]. However, to the Author knowledge, no study refers to pulsating cryogenic fluid delivery.

# Chapter 4

## Cryogenic machining performance

### 4.1 Workpiece material: cryogenic machining of Ti-6Al-4V

*Cryogenic machining has been applied to several materials: from soft polymers, Aluminium and low Carbon steels to strong Nickel, Titanium alloys and brittle composites or technical ceramics. It proved excessively demanding for this work to investigate cryogenic performance onto such a huge variety of materials with the level of detail needed to provide worthy information. Therefore, it was decided to concentrate on the Titanium alloy Ti-6Al-4V. Much of the cryogenic studies focused on the machinability of this alloy as almost 50% of the Titanium produced correspond to this  $\alpha - \beta$  mixture, mechanical properties are readily achievable, material models are quite developed. On the other side there have been researchers who underlined the necessity to move from expensive high performance alloys to softer Aluminium or other lower grade materials for easing the spread of cryogenic machining. However, stronger and nobler materials such as Inconel 718 pose more problems and need increased attention. Eventually, as we will perform numerical simulation of T6Al4V milling process, it is found straightforward to concentrate on the cryogenic cutting performances of this alloy.*

Literature reviews of cryogenic machining have sometimes paragraphs referring to different materials, with useful tables summarizing articles of experimental trials. However only qualitative comparison are drawn, resulting in a great amount of information lost between words. What is the most applied cooling media? With which technique? What cutting tools are most used? What is the range of flow rate applied? What is the average increment of tool life depending on cutting parameters? All those question have not an easy answer: there aren't two articles which results can be compared due to the variation of some factors: cryogenic media, nozzle configuration, flow rate, flow state, cutting parameters, cutting approach and more. However, it is considered worthy to draw a quantitative numerical comparison of experimental cryogenic trials concerning cutting Ti6Al4V, hoping it would provide useful insight for next studies and induce to do the same for other materials.

During a literature research, lasted three months during Covid-19 lockdown, were found many cryogenic machining (liquid LN2, LCO2) articles containing a comparison with other cooling technique (Dry, Emulsion-Flood, High-Pressure-Emulsion, MQL, Cryo-MQL) in terms of performances (tool life, quality, productivity). The articles were initially sorted by materials. For what concerns materials different from Ti64, the

number of articles is lower than reality, because the research was not oriented in that direction. The priority was given to tool-life studies, however, a fair number of tool life articles contained surface quality analysis, while other had a sequel entirely specified on quality investigations. This were not considered, therefore, to avoid give partial pictures to problems, we will not present surface quality related issues if not some indications regarding surface roughness.

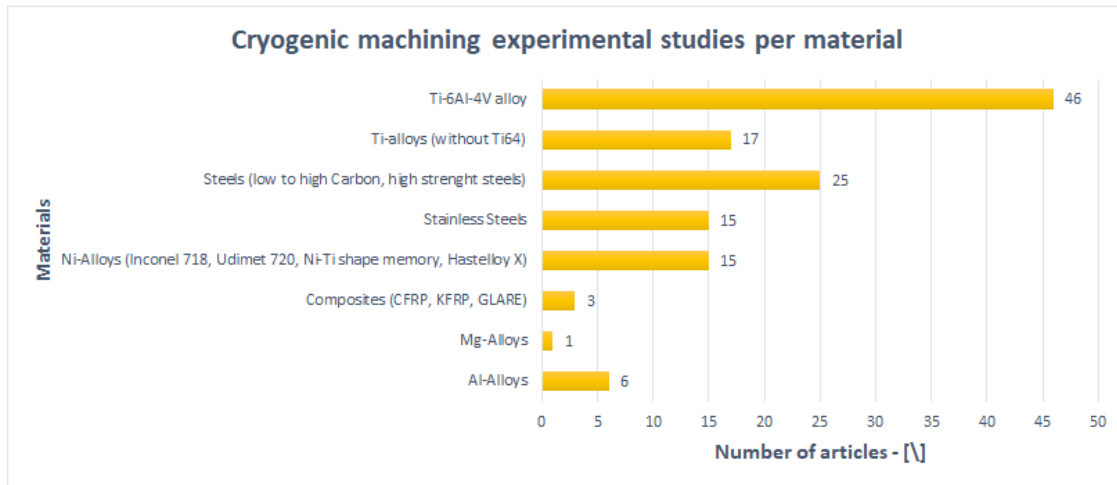


Figure 4.1.1: Materials articles span

Analysed articles firstly gave information regarding the approach followed for the experimental performance comparison:

**Cutting approach:** most of the articles referred to turning operations, less to milling and no article was found dealing with cryogenic drilling of Ti6Al4V (unless there could be). Other articles refer to the useful application of cryogenic fluid in drilling of hard alloys;

**Cooling media:** the cryogen applied, either LN2, LCO2 or both. We can see how LN2 is generally preferred than LCO2. As we will see after, this is not due to the achieved performances but a choice considering drawbacks and advantages of both strategies;

**Comparative environment:** the “base” cutting strategy to which cryogenic machining was compared in terms of performances: dry cutting, emulsion cooling (wet) or MQL. A lot of articles compare cryogenic cutting to dry cutting, which is justified only for particular applications in which dry cutting is the industrial practice: final aerospace Oil-free operations and biomedical applications (using oil would require expensive additional cleaning). For all other applications, cryogenic alternative should be compared to the industrial practice of flood cooling, from low to middle pressure ( $2 \div 50 \text{ bar}$ );

**Delivery design:** the system adopted to send the cryogenic liquid in the proximity of the cutting zone: Flooding (low pressure, high flow rate), localized-R&F (rake and flank dedicated nozzles), Rake-Cap (particular nozzle configuration pointed to the tool tip), Micro-R&F (dedicated rake and flank nozzles placed very carefully near the cutting edge), External-Spray (external nozzles placed more than  $10 \text{ mm}$  far from the cutter), Indirect (tool back or rake face cooling), Through-Holder (localized delivery passing in the holder), Mill-Channels (internal milling cutter channels). The great variety of delivery techniques make impossible a direct comparison between results obtained with

two different strategies;

**Life indication:** if tool life is indicated in the article and how: a wear distribution in time or a proper tool life as a function of process parameters and end-of-life criteria. Being a tool life analysis time and cost demanding it would be advised to expose the result in a handy and clear way, but that is not often done. Where it was possible (enough wear data), tool life was fitted on wear values with linear, quadratic or cubic functions and a tool life limit of  $0.3\text{mm}$  was chosen as the most adopted. Anyway, tool life data are to be intended as a general trend;

**Tool type:** all articles made use of carbide tools, due to economics and retained strength at low temperature, the only difference was in terms of adopted coatings. Many different types of coating were adopted, it is not clear whether they have a beneficial effect;

**Sustainability:** some articles presented economic and or environmental analyses. Unless being, in most cases, heavily approximated, this performance aspect is fundamental after tool life and surface quality analyses. Also in this case we find some articles entirely referred to sustainable (economic, ecologic, social) performance of alternative cooling strategies for Inconel 718.

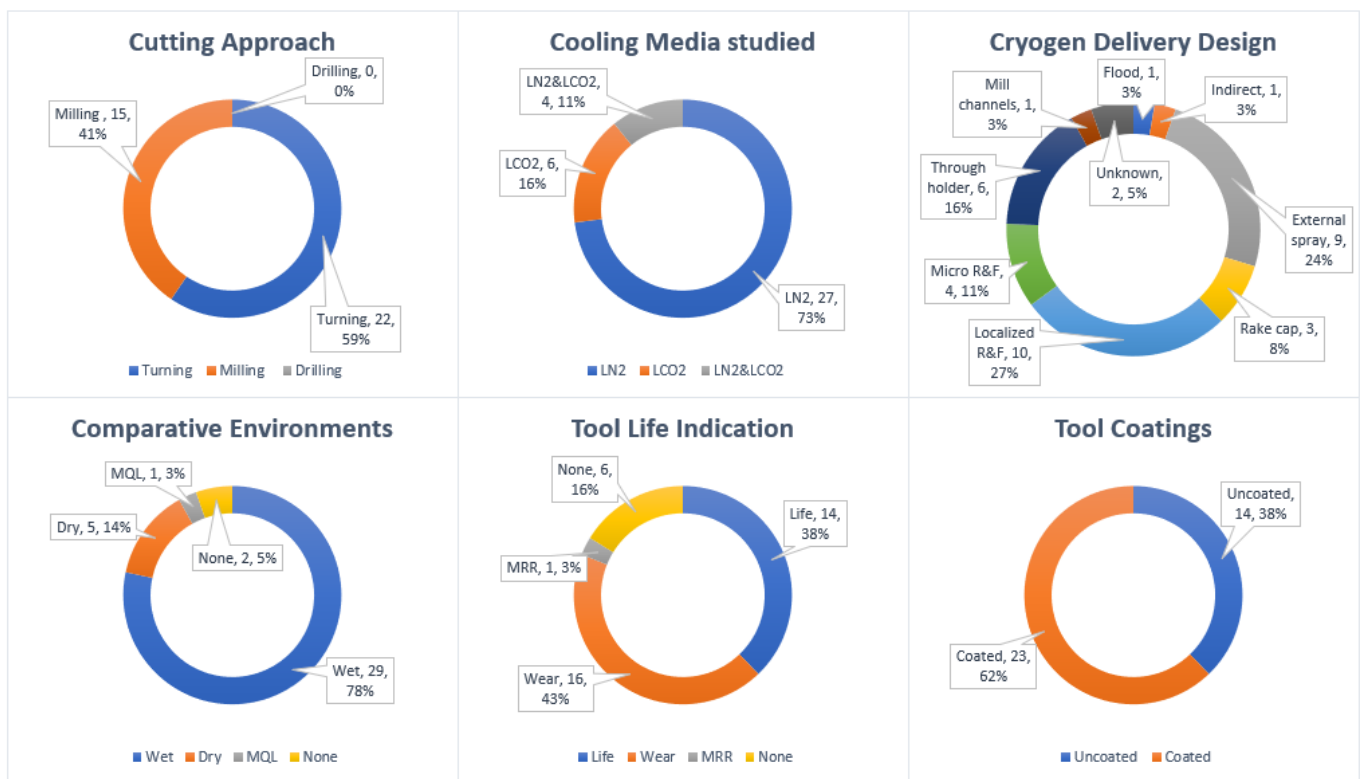


Figure 4.1.2: Data analysis from experimental cryogenic machining cutting trials articles

The second part of the analyses dealt with quantitative analyses of results from the articles. In this part, only articles comparing cryogenic to emulsion were considered. This because emulsion cooling is the widespread industrial practice and is difficult for cryogenic to surpass its performances, while results are positively influenced if cryogenic cutting is compared to dry cutting.



### 4.1.1 Turning approach

LN2 was far more studied than LCO2, localized rake and flank nozzles were widely applied, wet environment was the most frequent used for comparisons. However tool life was vastly indicated as wear profiles in time or single wear measurements which made impossible a comparison with other studies.

Looking at reviews, there is a general confusion regarding cutting forces and friction behaviour in cryogenic machining. Half of the studies regarding Turning showed a reduction in cutting force, a quarter an increase and the last quarter didn't observe any variation. Friction between rake and chip exhibit the same uncertainties of cutting forces (being often calculated through them). For what concerns the articles analysed, surface roughness was lower or equal to the base cases. Remarkable is the lack of flow rate and pressure data regarding cryogenic and emulsion fluxes, it means the comparison is not clear from the beginning, and results are hardly reproducible.

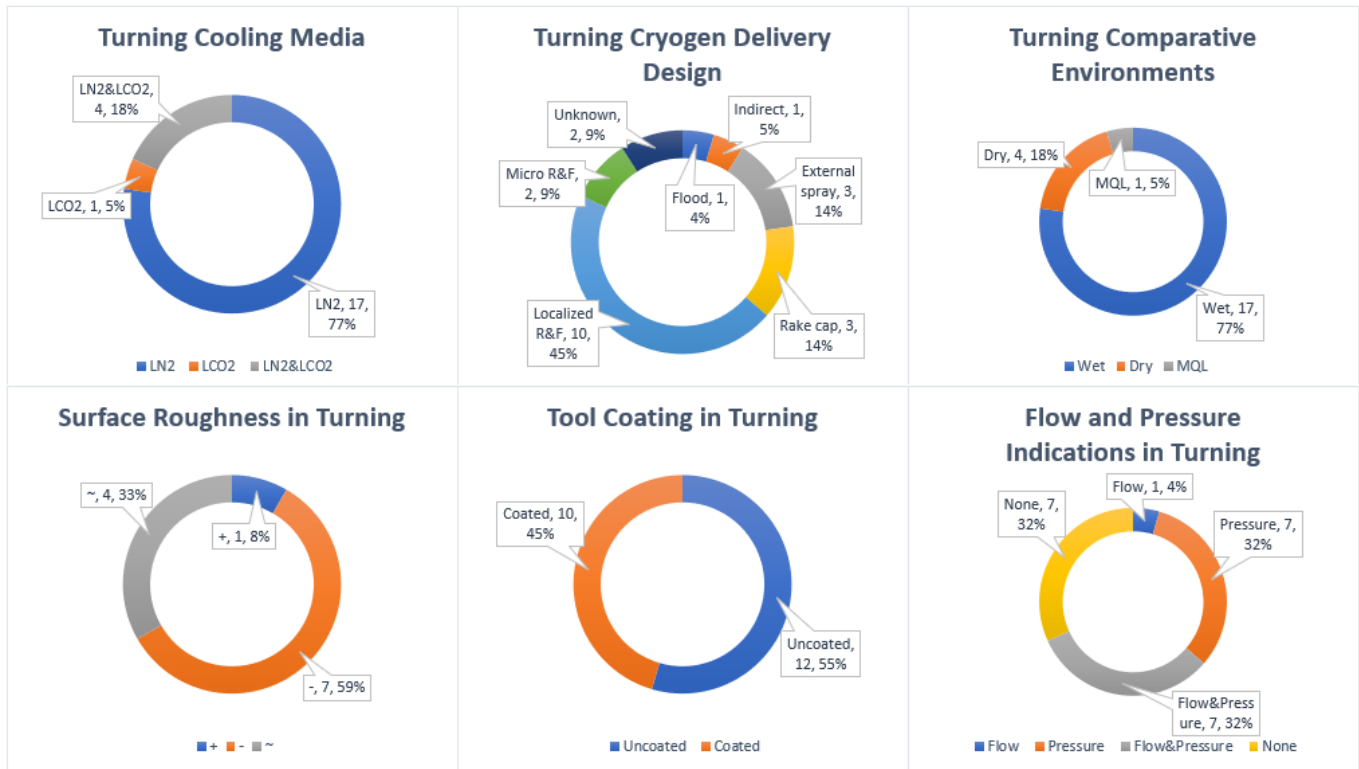


Figure 4.1.3: Data analysis from experimental cryogenic Turning cutting trials articles

### Tool life

Tool life was found to increase in the majority of studies, therefore, it is necessary to concentrate on the ones in which it doesn't:

[12, Yasa 2012] and colleagues compared dry, CCF and Cryogenics in machining of Ti-6Al-4V with vertical axis turning machine and LN2 apparatus. The coolant was applied by flooding but no precise explanation or scheme of the flow delivery to the tool was depicted. Cryogenic technique proved valid over dry cutting, but no advantage could be discerned in comparison with conventional flood cooling. They addressed the

problem to the overhardening of the workpiece, being surrounded by cryogenic mist. Overhardening of the workpiece is generally due to excessive cooling capacity due to a missed matching with process generated heat (too high flow rate, too low MRR, wrong targeting). Also, excessive amount of LN2 cause Health risks and high energy consumption.

[57, Bermingham 2012] and his team extensively studied tool wear mechanisms and chip morphology during turning, comparing LN2 with High Pressure cooling with water based emulsion coolants. They focused as well on nozzle delivery systems, varying nozzle positions. Tool life showed slightly better improvements for HP than cryo, over dry machining. What they clearly pointed out is that tool life is influenced more by nozzle positions than coolant applied. Higher effectiveness in HP cooling was addressed to a greater heat extraction ability of Oil. This seems a paradox but emulsion was delivered at 100bar against LN2 at 8bar, higher specific gravity of oil then favour higher momentum transfer and so higher heat removal. Interface length and chip thickness were lower for HP, underlying higher chip lifting, penetration and cooling ability. Moreover a previous study ([55, Bermingham 2011]) underlined the impossibility of the LN2 jet to reach the heat affected cutting zone, further confirmed by the presence of same wear features of dry cutting, even if retarded. This is even more understandable by considering that emulsion remain liquid and keep the contact with the piece, whereas LN2 vaporized immediately. Nitrogen vapours have less heat extraction capability than liquid emulsion.

[65, 66, Deiab 2014, Raza 2014] and teammates compared Dry, MQL vegetable oil, MQL vegetable oil with refrigerated air, flood emulsion, cooled air only and cryogenic LN2 environments in turning with uncoated carbides. From their findings in terms of flank wear, roughness and energy consumption they concluded that MQL with vegetable Oil was the best choice, followed by MQCL (C for chilled) and Cryo. However, MQCL performed worse than Cryo from what they reported, therefore their conclusion is contradictory. Moreover, nothing has been said for cryogenic nozzle design, which is pointed out by others to be crucial for effectiveness of the method. Moreover, the variation of tool wear and roughness are very small between environments. Finally, the cutting parameters are highly below the threshold for economics of cryogenic apparatus (high MRR, later explained).

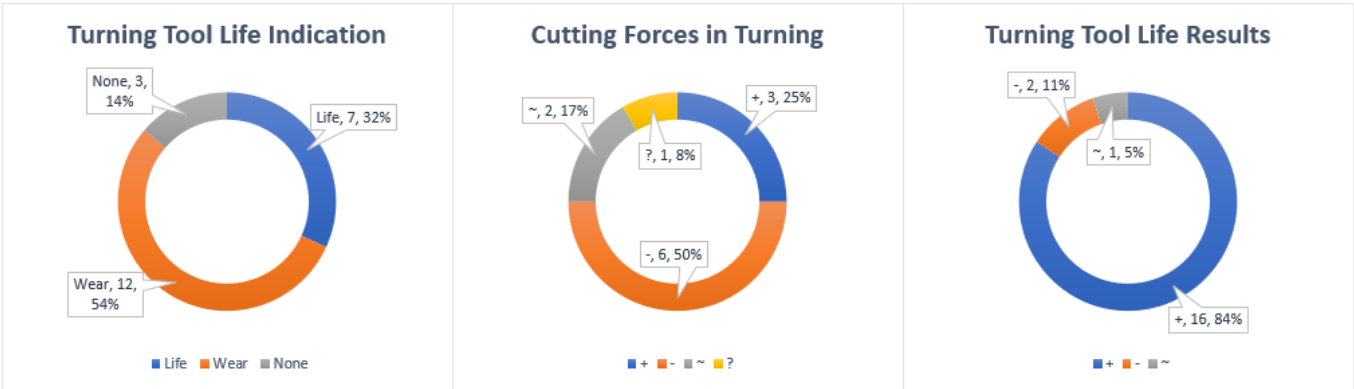


Figure 4.1.4: Data analysis from experimental cryogenic Turning cutting trials articles

Trying to draw general trends from such a diversity of methods, parameters, tool

angles, flow types, different end-of-life criteria and general lack of complete data is practically impossible. Only case studies comparing cryogenic to emulsion cooling were considered. Cutting edge geometry while cutting was considered of no influence as there are hardly two studies that uses the same configuration. The considered parameters were: cutting speed  $V_c - [m/min]$ , feed rate  $f - [mm/rev]$ , depth of cut  $DOC - [mm]$ , material removal rate  $MRR - [cm^3/min]$ , cryogenic flow pressure  $p_{cryo} - [bar]$ , cryogenic flow rate  $m_{cryo} - [kg/min]$  and cryogenic delivery design. Tool life increment has been chosen as the target variable, as it highlights the variation of tool life with respect to wet cutting with the same process parameters set:

$$\Gamma_{\%} = \frac{\Gamma_{cryo} - \Gamma_{wet}}{\Gamma_{wet}} \cdot 100$$

When necessary, the absolute tool life will also be displayed. The complexity of the problem is remarkable even by eliminating variation sources such as tool geometry and coatings, as can be seen while trying to plot tool life increment as a function of process parameters. A slight general increasing trend in the MRR confirms the statements of [32, Strano 2013] and teammates. They studied the influence of cryogenic LN2 cooling on cutting forces, friction and Tool life pointing out that cryogenic effectiveness in improving life is more evident at higher MRR whereas LN2 cooling effect is more effective at low MRR, which gives time for heat dissipation. [67, Tirelli 2015] and his team analysed the performance of cryogenic machining for roughing Ti6Al4V. They observed higher increment of tool life with the highest cutting parameters (feed and speed respectively  $0.2mm/rev$  and  $70m/min$ ). [68, Sun 2010] and his team studied extensively the machinability in turning aided by compressed air (CA) and cryogenic compressed air (CCA, a LN2 Dewar with copper coil to cool air down to  $-196^{\circ}C$ , then supplied to rake and flank at  $7bar$ ). They observed better cooling effect with lower feed and decrease in cooling capacity at higher speed. This because the heat removal rate depends on the fluid temperature and HTC, but absolute heat evacuated depends on interaction time, which is low at high speed. In [9, Sun 2015a], proposed process parameters were of interest for roughing and semi-roughing.

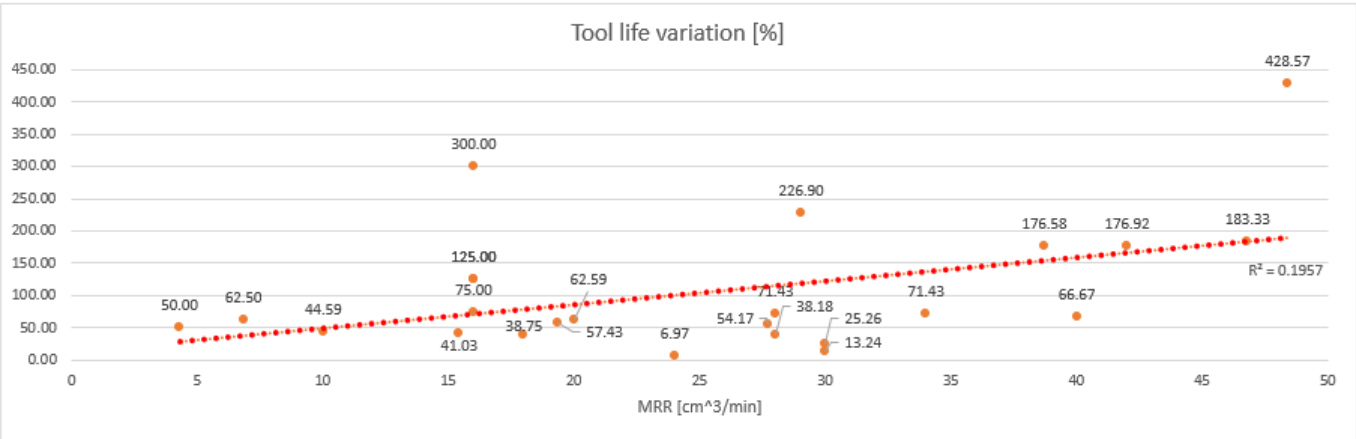


Figure 4.1.5: Tool life analysis from experimental cryogenic turning cutting trials articles, comparison with low-middle pressure emulsion cooling as industrial practice

Process improvements are strictly dependent on process parameters. [55, Bermingham 2011] and colleagues reported a detailed study on the effect of feed and depth of cut during turning Ti-6Al-4V under dry and cryogenic LN2 cooling. Cryogen was delivered at rake and primary flank face at a pressure of 8,27bar. Speed and depth were varied so to keep MRR at  $49\text{ cm}^3$  at a speed of  $125\text{ m/min}$ . Higher feed rate increased the cutting zone temperature, this intuitively by increasing the chip contact length with the tool. Best improvements were found for high feed and low depth, where heat has more need to be carried away, but longer tool life was achieved for low feed. They concluded that preventing heat generation is better than remove generated heat with cryogenics. This is in line with the difficulty of LN2 to reach the cutting zone with high feeds, therefore low feeds, high depth are preferable.

Low feed high depth means low chip thickness and lower chip pressure, this could enable interface penetration. Larger portion of primary edge is interested, it can cause uniform thermal distribution and so less stress concentration on insert. This for sure has a limit since it loads the extreme portion of the edge by going on with very low feed and high depth. On the other side high feed and low depth cause asymmetric stress on tool, higher chip pressure and wear, cryogenic fluids can help by promoting tool hardening and heat removal. However, the thermal and mechanical load developed are so high that absolute tool life is reduced.

The great variability of results is due to the different flow rates, pressure, combination of feed, speed and depth even at the same MRR and nozzle delivery design. Even if 22 different articles were analysed, due to lack of information and differences in the high number of parameters, there aren't enough data to extract reliable information regarding the trend of tool life increment in speed, feed or depth of cut.

Thanks to the articles of [69, Ayed 2017] and other articles specifying pressures and flow rates, better tool life can be obtained with higher flow rate and pressure. However, Ayed concentrates on flow rate keeping same speed, feed and depth of cut, therefore finding only the suitable match of flow rate and pressure to the given process parameters. Moreover there would likely be a threshold of pressure and flow rate which starts to be detrimental for tool life, also not considering the sustainability point of view.

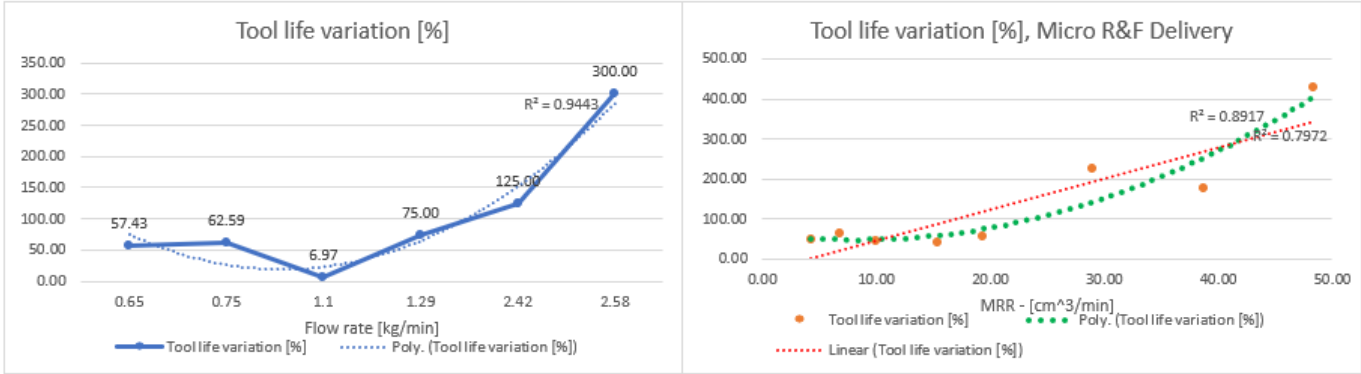


Figure 4.1.6: Tool life analysis from experimental cryogenic Turning cutting trials, focus on micro R&F delivery and flux sensitivity

Trends get better when the same delivery technique is considered (micro delivery, very precise), following the works published in [70, 13, Hong 2001a&zc] and [63,

Dhananchezian 2011]. Hong and his team work is renown. They demonstrate how precise and tailored delivery of cryogenic flow is needed for economical and effective tool life improvement, avoiding Titanium overhardening at low temperature. Dhananchenzian and Kumar analysed the effect of LN2 applied by small holes EDM machined on rake, primary and secondary flank.

Multiple effects must be considered to highlight relevant trends. The following page include graphs in which data coming from the same articles are elaborated to provide alternative visualization hopefully explaining trends and clarifying issues. Bar charts are added by a table so to easily associate to the height of the bar a numerical value. The table, therefore, contains values reported on the y coordinate of the charts. In the x axis cutting speed is always reported. In the depth, CR, MRR, or feed are set. The effect of depth of cut can be showed by representing depth and feed condensed in the CR. Being the feed always between  $0.15 \div 0.3 \text{ mm/rev}$  while the depth between  $1 \div 2 \text{ mm}$ , is the DOC that most influence the amount of edge engaged in the cut. Larger CR, due to large depth, are difficult to cool down homogeneously, while too short depth and high feed (low CR) promote hot spots concentrates on tool tips which are hardly reachable by the cooling media. All this given same chip section area ( $f \cdot \text{DOC} - [\text{mm}^2]$ ), so the same MRR at the same speed.

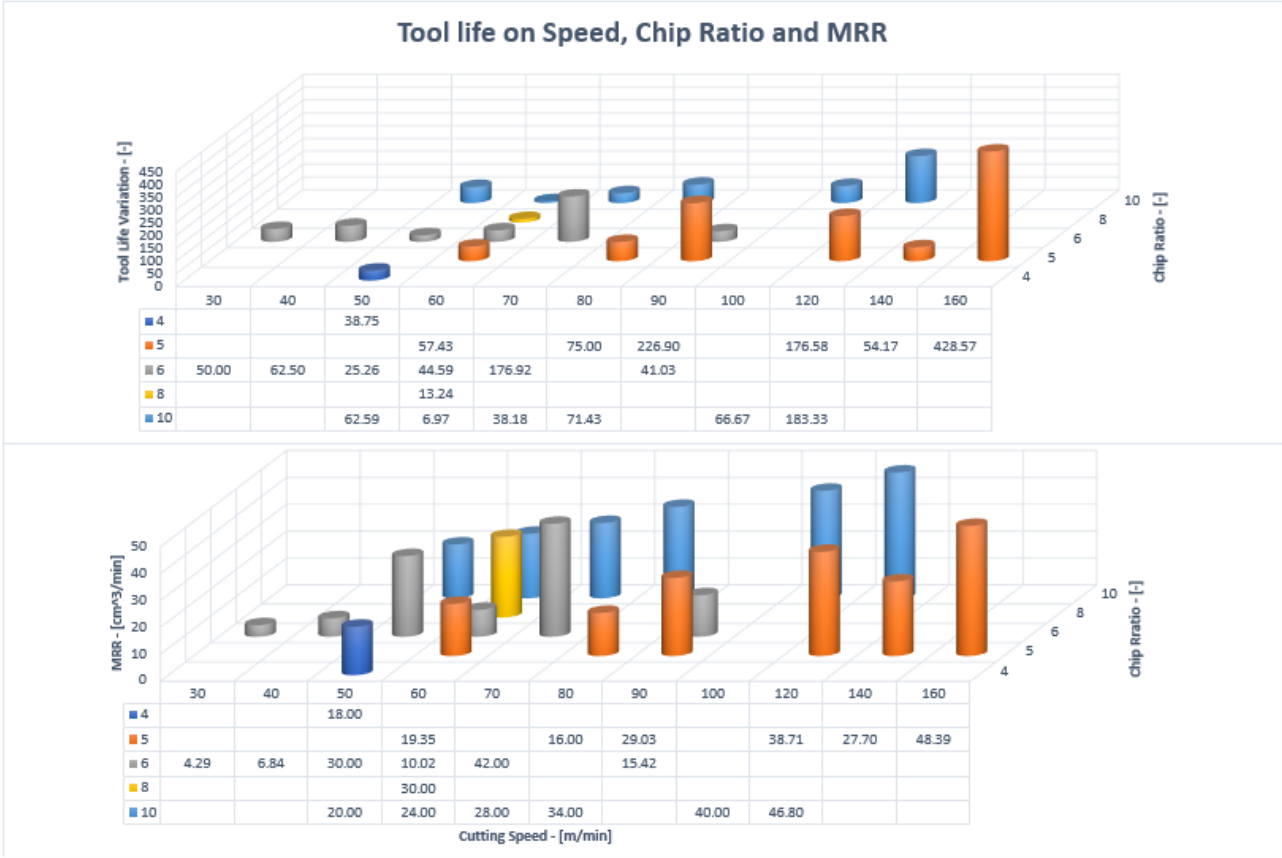


Figure 4.1.7: Tool life dependence on multiple parameters

This effects, however, we failed to highlight, as can be seen in the first two graphs. Process complexity is high and it is hard to find sets of parameters, within different

studies, in which only one quantity changes so that its only effect can be seen. Anyway we reported our efforts.

Being feed and DOC not very variable, variation of cutting speed reflect the variation of MRR, therefore higher cutting speed generate averagely better tool life improvements, however the absolute tool life lowers. It is confirmed the general trend of increase in performances given by cryogenic machining. It provides higher tool life in extreme cutting conditions. The last three graphs reports this findings.

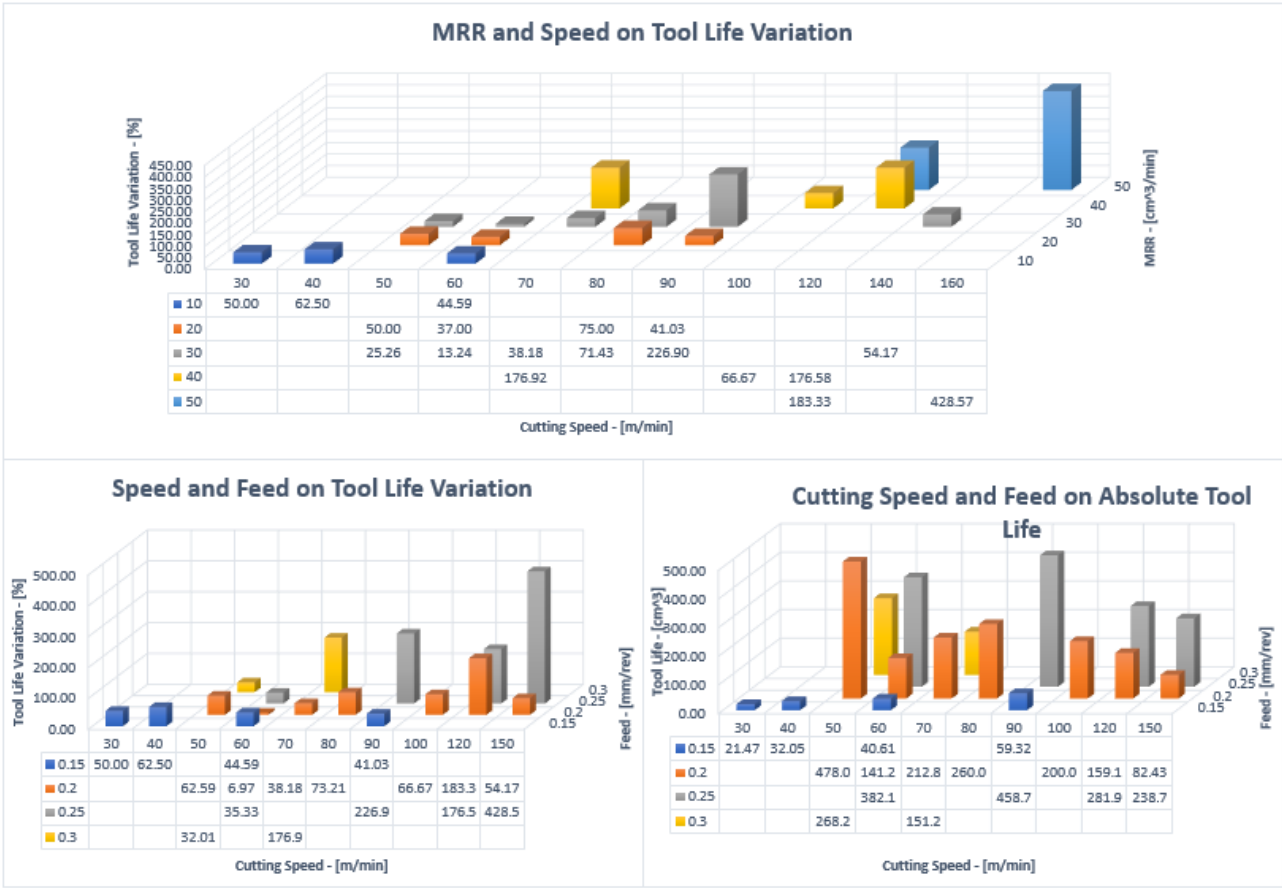


Figure 4.1.8: Tool life dependence on multiple parameters

**Cutting forces**

*Cutting force behaviour is influenced by two main phenomena: material softening while increasing the cutting speed (and cutting temperatures), material overhardening due to a mismatch in the cooling potential offered by cryogenic machining and process heat generation, or wrong localization of cold spots, targeting the material to cut instead of the heat affected zone in the tool. Said so, it is difficult to give a measure for the heat generation in the process and its localization so to understand the correct flow rate and pressure for the cryogen and the correct direction for the jets. Overhardening has been always addressed as a motivation to bad performance of cryogenic fluid experiments, however it has never been proved.*

In [55, Bermingham 2011], cutting force decreased with cryo (LN2) and with combination of higher feed and lower depth of cut. However, cryogenics increased thus force, justified by higher rake friction or due to stronger chip and presence of chip breaker.

What they pointed out is that force variation is a result of competing factors: OH of chip and increased friction or chipbreaker bending action, and flank friction decrease due to tool hardening, lower surface springback and hypothetical VN2 cushion. So they removed flank cooling and demonstrate the increase of cutting forces compared to Dry cutting when only rake cooling is active, due to OH of chip. Therefore the reduction of forces for rake and flank cooling is a positive balance between OH and flank friction decrease.

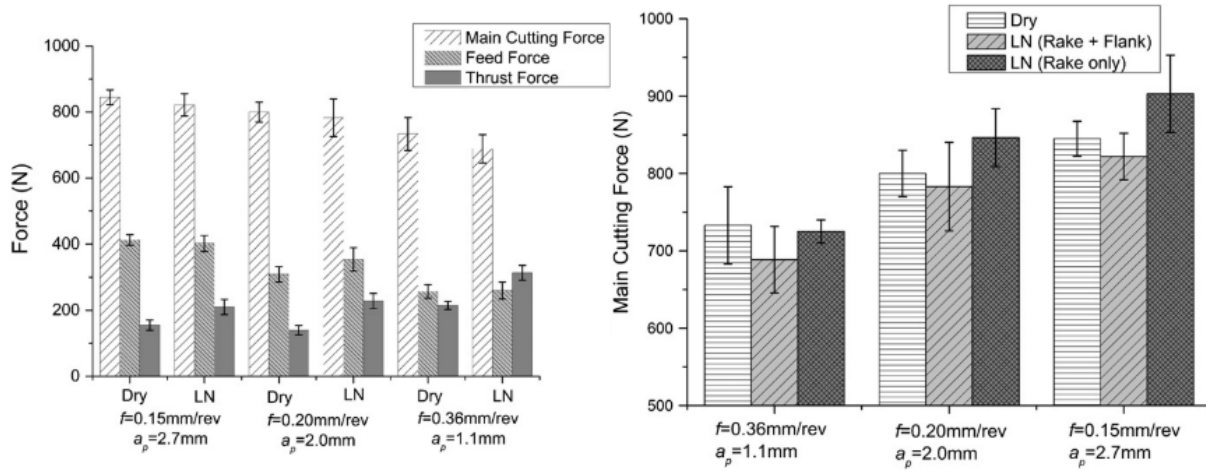


Figure 4.1.9: [55, Bermingham 2011] cutting force analysis

[7, Hong 2001d] and research mates found higher forces in turning Ti-6Al-4V even adopting a very precise micronozzle delivering system. Due to the lower temperature in the shearing zone, cutting and thrust forces increased. Other articles report variation of cutting forces, in some an increase is seen, in others a decrease. Results are dependent on a lot of different parameters and great inconsistency among results is found.

## Chip morphology

*Different cutting fluids result in different cutting performances and cutting behaviours. Chip formation process can be influenced by the lower temperatures achieved with cryogenic fluxes. In particular, for Titanium alloys, chip morphology can change in serration characteristics. Secondary deformation layer depth can help in defining friction behaviour,* [71, Melkote 2017] [55, Bermingham 2011] and colleagues found that during dry cutting, shear band thickness, secondary shear zone thickness and chip thickness increase with feed, while shear band angle decrease. Metallurgical analysis in chips stated that temperature remained below  $1000^{\circ}\text{C}$ . Cryogenic machining (LN2) reduced chip contact length, probably due to LN2 chip lifting action, decreased shear band angle and chip thickness. In a following article, [57, Bermingham 2012], regarding chip morphology: distance between serrations increased, chip thickness decreased, curl radius proved to decrease and shear band angle remained statistically the same from dry to cryo (large scatter was noted and statistical analysis was performed). [72, Jerold 2013] and [73, Kumar 2013] observed lower distance between serrations and lower shear band thickness with SEM micrographs for cryogenic machining (LN2 and LCO2). [74, Bordin 2017] and colleagues investigate the effect of LN2 in finish turning of AM Ti6Al4V. Chip thickness lowered and distance

between serrations increased in case of cryogenic machining. [75, Bordin 2015a] and his team saw how cryogenic machining reduced chip contact length. More effective reduction is found at high speed high feed. Chips curling was found higher for cryo. Therefore, it is clear that cryogenic machining reduce chip thickness and tool-chip contact length. Curl radius variation seems to be dependent on the position of cooling jets and tool geometry. Shear band angle seems to decrease while distance between serrations (pitch) seems to increase.

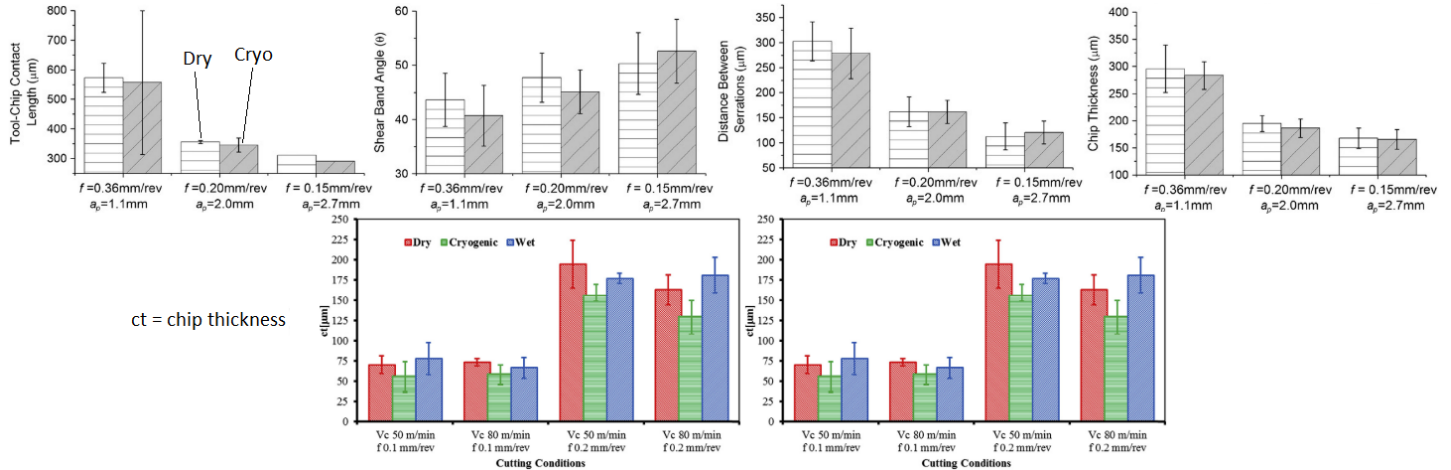


Figure 4.1.10: [55, Bermingham 2011] (up) and [74, Bordin 2017] (down) chip morphology results

## Tool wear mechanisms

*Tool wear with Titanium alloys exhibit peculiar features. Crater wear is formed due to adhesion dissolution phenomena, and it is concentrated on a narrow region near the edge, it can meet flank wear promoting edge recession.*

[10, Venugopal 2007], [47, Venugopal 2007a] and collaborators studied the effect of cryogenics (LN2) on tool wear versus dry and wet machining in turning with uncoated Tungsten Carbide. Due to high temperature, chemical activity in cutting Ti alloys is enhanced, BUL forms and by adhesion, dissolution and diffusion, tool material move into the adhered Ti layer. The layer, growing, become unstable, it detaches and carries away tool portions, resulting in crater wear. Crater is nearer to the cutting edge, unlike steels, and it meets flank wear. Crater width is short: on the outer edge Ti is adhered, on the other flaking is observed. Flaking on the inner crater edge does not happen for dry cutting at low speed, whereas occurs at high speed and at all speed for wet and cryo. Flaking is attributed to thermal shocks felt by the insert due to highly unstable dynamic forces caused by chip segmentation (due to the segmented chip, tool-chip contact length is variable, and the crater edge in the tool interior feel variable mechanical and thermal loads, causing fatigue cracks and flaking). Flank wear was characterized by abrasion marks. Flank, nose wear and edge depression lowered for wet and cryo at all speed. Cryo effectiveness reduced with speed, due to probably lower cooling capacity with respect to heat generation. [63, Dhananchezian 2011] stated that crater wear and flaking of insert decreased for cryo.

[55, Bermingham 2011] and colleagues reported that all inserts, irrespectful of cutting



environment (LN<sub>2</sub>, dry), failed by extensive flank wear, crater and flaking due to adhesion and diffusion. Cryogenic environment helped in delaying the wear rate, achieving 40% higher tool life. Diffusion of Co matrix into Ti and exposure of brittle WC carbides to the abrasion action was depicted as the crater formation mechanism. Flank wear generates by abrasion of both WP material or WC carbides torn out of flank. Cryogenic was able to lower flank wear rate but unable to reach the nose.

[56, Machai 2011] and colleagues reported that flank wear decreased (LCO<sub>2</sub>) due to lower temperature and consequent springback of the surface and material uncut pushed by the rounded tip. However, rake crater (adhesion-dissolution phenomena) was present for both environment, meaning that cryogenic flux was not able to cool the interface (temperature was not reduced enough to limit Ti chemical activity). Both the environments failed in maintaining the coating upon the insert. Remarkable was the absence of notch wear with cryo, probably due to tool compactness-hardness retention at lower temperatures.

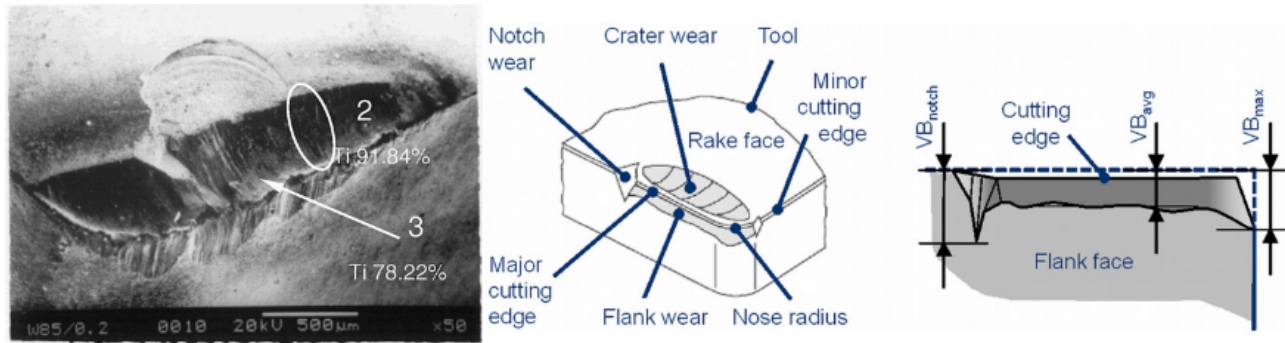


Figure 4.1.11: [10, Venugopal 2007] experimental worn tool features and [56, Machai 2011] worn features scheme

[57, Bermingham 2012] and his team extensively studied tool wear mechanisms and chip morphology during turning, comparing LN<sub>2</sub> with High Pressure cooling with water based emulsion coolants. They compared the two approaches using the same nozzle delivery systems, varying nozzle positions, (look chapter 4). Tool life showed slightly better improvements for HP than cryo, over dry machining. However, wear patterns were only retarded by the cooling approach, which means the coolants failed in decreasing temperature below diffusion-dissolution threshold. All insert exhibit flank wear, adhesion-dissolution crater and flaking, BUE and BUL on insert surfaces was observed. [32, Strano 2013] and his team observed as tool wear was characterized by S shaped profiles, with initial wear growth, then plateau and increase toward failure. Cryogenic cooled insert exhibit a larger plateau, which translates also in robustness in cutting performances.

[9, Sun 2015a] and colleagues studied tool wear in turning under cryogenic LN<sub>2</sub> cooled air versus dry machining. They made sections parallel to the rake&flank plane observing the cutting edge profile variations in terms of flank wear, crater depth, edge depression and chip contact length. At 150 *m/min* the main failure mechanisms where flank and crater wear, both decreasing with application of cryogenic air. Tool life for Cryo improved by 37%, flank wear exhibit less steep and longer plateau. At 220 *m/min* dry cutting tool failed for plastic deformation being bent upward and backward, while

Cryo exhibited accelerate wear rates with previous mechanisms and still the plateau. 104% increase in Tool life was reported at high speed. In the plateau, flank wear and rake recession were observed to be linked by linear relation: by decreasing edge depression flank wear can be lowered as well. This meant, by the authors, that flank wear can be retarded even by a precise rake cooling only.

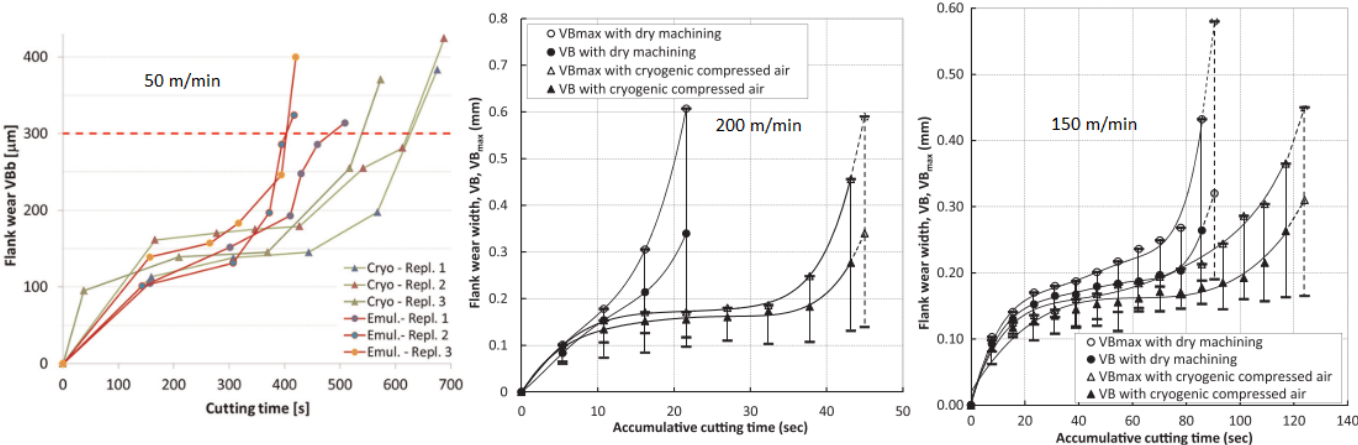


Figure 4.1.12: [32, Strano 2013] and [9, Sun 2015a] wear evolution of cutting edges

[75, Bordin 2015a] and colleagues analysed LN2 turning in comparison with dry cutting for AM Ti64. The choice of comparison with dry cutting was justified by the absence of cleaning needed for the production of biomedical implants. Similar wear modes but different wear rates are found: abrasion chipping and adhesion for the flank and crater BUL and BUE for the rake. Lower quantities of Ti Al and V were found for cryo, so it limits adhesion. Rake 3D and 2D profiles were done to study the BUL thickness and crater wear. By limiting the amount of WP BUL, LN2 limited detaching and induced chipping. Tool wear proved to be around 20% lower for all cutting parameters combinations.

[76, Bruschi 2016] and teammates undergo a detailed study on wear and friction coefficient for dry and LN2 turning of wrought and AM Ti6Al4V. Tool wear was described as cratering and edge depression followed by chipping and cracking generated by the variable forces characteristic of segmented chip formation. Both cryogenic and wet cutting were affected by edge flaking as a results of thermal cycles.

[42, Kirsch 2018] and coworkers analysed tool life in case of LCO2 and LN2 cooling against wet machining and polyhidric alcohols blended in water. With respect to wet machining, LN2 (1.1 kg/min, 2 bar) and LCO2 (1.65 kg/min, 60 bar) performed almost in the same manner and slightly better than emulsion (11 kg/min, 12 bar). Tool life criterion dealt with the ratio between crater wear depth and its center distance from the cutting edge.

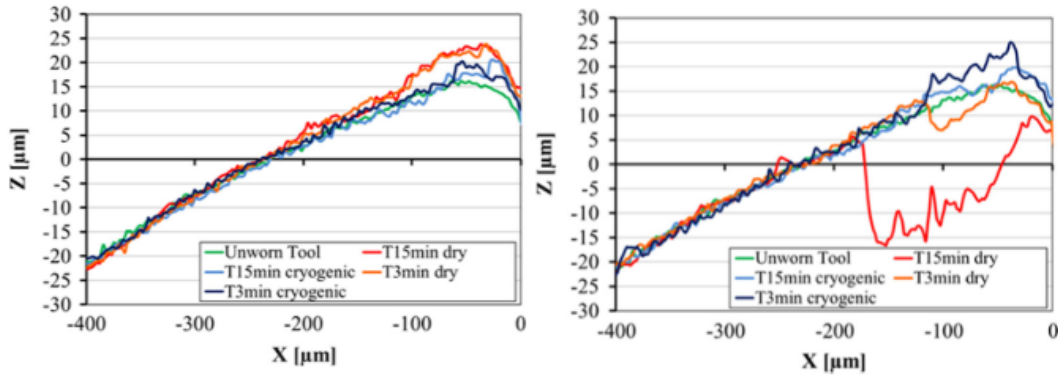


Figure 4.1.13: [75, Bordin 2015a] crater wear evolution, dry and LN2

It becomes clear that cryogenic fluids tool life enhancement come from a retarding effect with respect to dry and wet wear rates. The retardation can be obtained if the process parameters are tuned on heat generation rates and fluxes concentrated on heat generation zones. Flaking due to alternate mechanical and thermal loads can be reduced with cryogenics thanks to correct targeting of the interested areas (inner edge of crater). Often, rake&flank cooling cause too high cooling action and detrimental effects by increasing the hardness of the workpiece material, but in general, no tailoring of flow rates or pressure is performed, nor variation in nozzle design to promote more precise targeting. Some studies underlined how cryogenic machining promotes a larger and less steep plateau for the tool wear profile, with a gain in robustness of the cutting process.

## 4.1.2 Milling operations

For what concerns milling operations, 15 articles were found containing a comparison between cryogenic and other cutting strategies. Here, LCO2 has been given wider attention. Delivery configuration are essentially divided into through-holder and external delivery. In general, it is more difficult to provide the cryogenic flux in a highly localized and precise manner due to the rotating tool. However, when localized delivery is performed, results are generally better. Cutting tool life is found to increase in half of the articles, while it decrease or remain constant for the other half. The general lack of information on flow rate, pressure and diversity of tool life indication is always present.

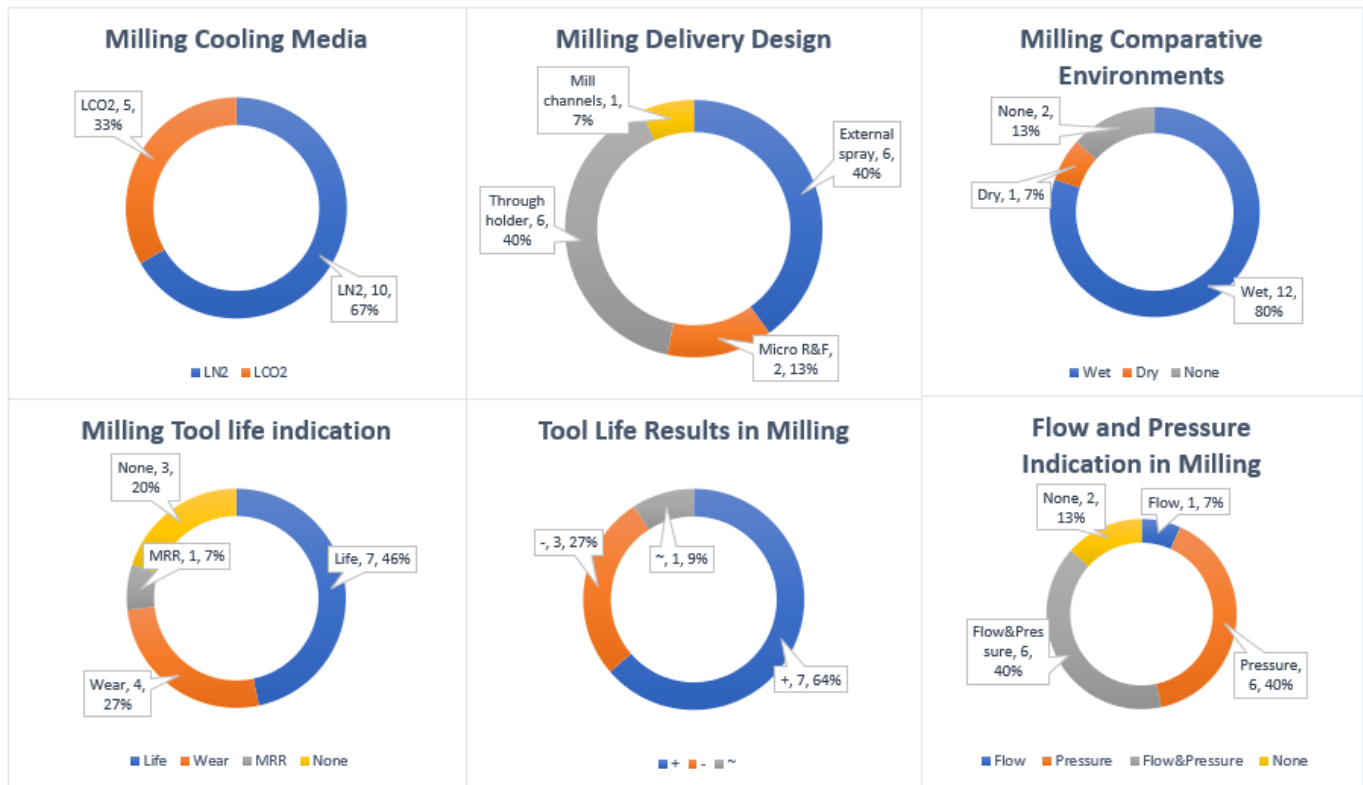


Figure 4.1.14: Data analysis from experimental cryogenic Milling cutting trials articles

A distinction can here be done on cryogenic milling with LN2 and LCO2. The former have simply too few published studies, and the ones containing reliable information come from the same Authors. The convenience of cryogenic machining for high performance cutting parameters and the necessary tailoring with the cooling power (pressure and flow rate) holds also for milling.

## Liquid Nitrogen, LN2

Rigorous application of LN2 to the Milling process has substantially been carried out by the same author. Shokrani and his group focused on low MRR and solid carbide mill Ti-Al-N coated. In [77, Shokrani 2015] they studied the effect of process parameters in milling with solid carbide TiAlN coated mill and three different LN2 flow rates applied externally to the cutting zone. They developed a ring supplying LN2 with precision in the cutting area, and found that an intermediate flow of LN2 was effective for optimizing tool life, roughness, power and specific cutting energy. Extended tool life requires low feed, high depth and speed, probably due more uniform heat generation along the cutting edge. In a following study [60, 61, Shokrani 2016a, Shokrani 2016] and coworkers studied in detail the effect of cryogenic LN2 cooling on tool life, surface roughness, micro-hardness, integrity, cutting power and specific cutting energy ( $J/mm^3$ ). They performed experiments with variable feed, depth, speed comparing LN2 cooling to Dry and Wet flood cooling in end milling with TiN-TiAlN coated carbide tool. Statistical analysis was performed on results. Cryogenic cooling, applied at 1,5bar and 0,4l/min proved to increase tool life by 70 and 230% versus Dry and Flood respectively. However, it is not clear if this improvement is an average over all studied parameters range or at

a particular feed and speed combination. Signal to noise ratio was used to understand if a variation of a parameter resulted in a better or worse output. Then ANOVA analysis of variance was performed to understand the significance level of parameters on the output and their percentage influence: major influence on tool life was given for speed by 40%, feed by 30%, cutting environment by 20% if measured in cutting length, whereas influence of 30% for cutting environment, feed and depth was stated if life was measured in MRR. From the cryogenic signal to noise ratio and the ANOVA results it was deduced that LN2 can increase the tool life, but a direct comparison at the same parameters was not performed. An L9 orthogonal array was used to investigate the effect of 4 different parameters (speed, feed, depth and environment) with the result that no environment had been tested with the same parameters set for a direct comparison.

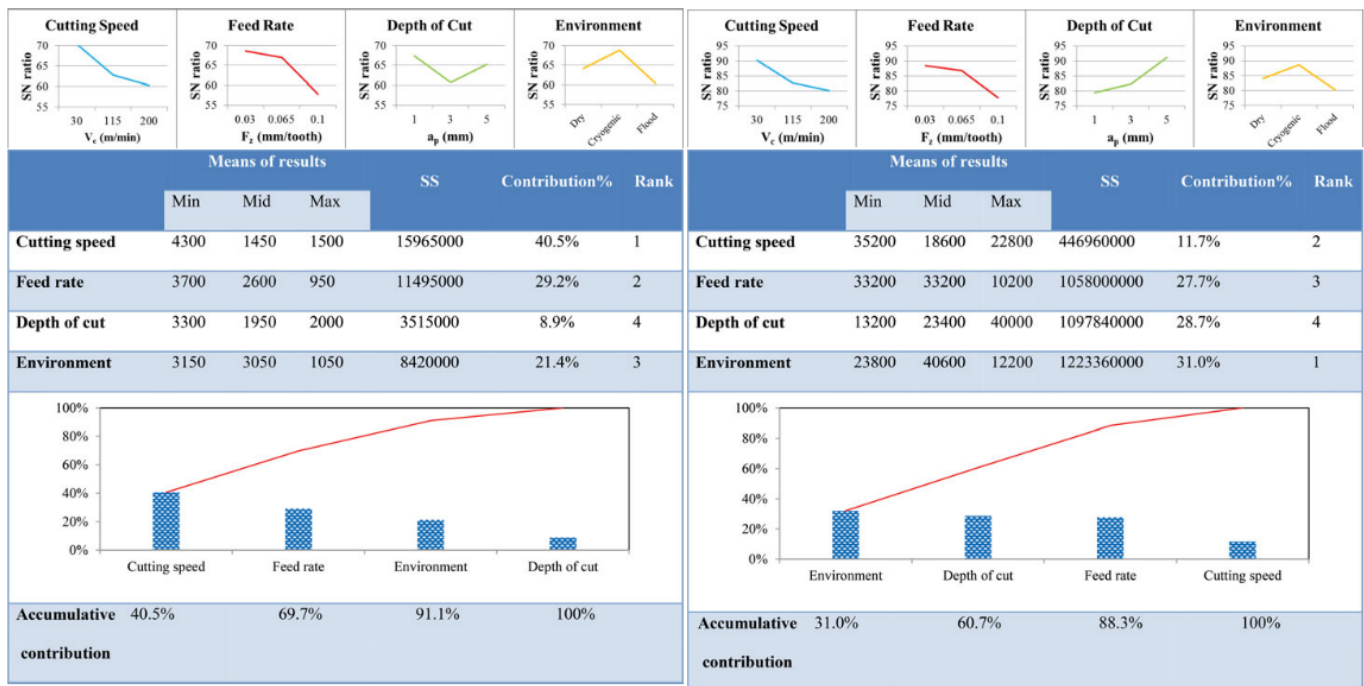


Figure 4.1.15: [61, Shokrani 2016a] ANOVA and signal to noise ratio Pareto charts related to cutting tool life, MRR base

**Cutting power:** cutting environment was most influential in machining power, because cryogenic and dry environment could get rid of the flood coolant pump. However, it is not clear if energy for LN2 production has been taken into account. The specific energy was strongly biased by the high idle MT consumption, so high feed, speed and depth are to be chosen for maximizing the MRR and spread the idle consumption over higher amount of removed material. **Wear modes:** no problem of thermal fatigue on tool was underlined by the authors regarding cryogenic cooling in this study. Cryogenic coolant helped in reduce thermal induced crater wear and exhibit uniform flank wear. [78, Shokrani 2018] and colleagues performed LN2 cooling tool life comparison with wet and dry machining and solid carbide mill for cutting Ti6Al4V. Abrasion and chipping are found frequent at low speed and feed, while at higher levels we have crater and adhesion. Tool life slightly improved for the range of parameters chosen whereas it

had an astounding peak for LN2 cooling at  $200\text{ m/min}$  with  $0.03\text{ mm/tooth}$  feed and  $5\text{ mm}$  depth (huge chip ratio CR, meaning a chip spread over wide portion of the edge). At the same speed, with lower chip ratios tool life did not reach that improvement. However, neither was it investigated why only at that precise combination of parameters tool life increased so much, nor was any hypothesis even mentioned in the article. [79, Shokrani 2019] and Newman investigate the optimal geometry of tool edges for a solid carbide mill in cutting Ti64 with LN2 cooling. Adhesion and dissolution crater formation weakened the rake face and promoted chipping of the edge, BUL and BUE decreased with large edge angles but rake over  $16^\circ$  and flank over  $10^\circ$  caused edge weakening.  $14^\circ$  for the rake and  $10^\circ$  for the flank was the best option. Tool life tests were than performed with the chosen optimized angle layout but no comparison with any other cooling technique was presented.

Another interesting example is given by the study of [51, 52, Park 2015, Suhaimi 2018]. The team compared cryogenic LN2 cooling to MQL with nanoparticles in wall milling. They also analysed external and tool holder internal LN2 delivery. Remarkable is the failure of the solid mill in case of cryogenic cooling: cutting forces raised exponentially until catastrophic failure before completing the task, while MQL, flood, MQL + internal LN2 delivery all exhibit quite stable forces in cutting length and achieved all the designed cutting passes. This has been imputed to the high axial depth of  $24,5\text{ mm}$  of wall milling: LN2 could not spread over the whole helix portion in contact with the chip, therefore high adhesion wear was observed. In a previous study, [?, Park 2015b] and colleagues demonstrates the effectiveness for tool holder LN2 delivery in end milling with indexable mill and low depth of cut. Lack of studies in deep pocketing and wall milling with LN2 is underlined, particularly the way to spread LN2 to larger surfaces. Additionally, looking at thrust forces they observed increased fluctuations over a raising mean value, due to wear of edges and rubbing action on the workpiece surface which dropped the cutting force to zero. A possible alternative regarding the cooling technique would be to apply LCO2, thanks to its higher pressure versus LN2 it could spread over larger contact surfaces.

## Liquid Carbon Dioxide, LCO2

Interesting performance results have been found for milling with LCO2. However, even if different authors have studied the problem with different delivery configurations, data regarding tool life as a function of cutting and flow parameters are influenced by the remarkable results of Sadik and coworkers so that their parameters turns out to be the more interesting regarding tool life enhancement.

[39, Sadik 2016] and his team looked at flow rate variation for LCO2 and emulsion cutting in influencing tool life and wear mechanisms with indexable end mill. They observed three fold improvement versus wet machining for low flux ( $0,15\text{ Kg/min}$ ) and 4,5 times increase in cutting life for the highest flow rate ( $0,64\text{ Kg/min}$ ). LCO2 was applied through channels in holder and delivered near the cutting insert. They identified the end of life responsible as the notch wear. While flank wear was uniform and not particularly influenced by the cutting environment, notch wear proved to diminish with cryogenic application. SEM observations found that cryogenic environment could lower the lateral thermal fatigue crack propagation, decreasing notch chipping. Possible explanation for this can be the lower thermal amplitude excitation due to LCO2 cutting

zone cooling. In a following study, [40, Sadik 2017] and Isakson compared uncoated and TiAlN coated inserts in LCO<sub>2</sub> and emulsion environments, both at 50 *bar*. Tool life results were exposed as Taylor expressions in variable feed and speed. The PVD coating didn't provide much increment in tool life with respect to the uncoated tool. LCO<sub>2</sub> machining proved to be effective in prolonging tool life but, raising speed and feed, its effectiveness lowered. This could be explained by a flow rate-heat generation matching at the lowest speed and feed, however flow rate was not stated. They explained how the low temperatures obtained with LCO<sub>2</sub> decrease the propagation rate of longitudinal cracks (parallel to the cutting edge). This cracks are responsible for the chipping of the insert when meet perpendicular cracks moving toward the interior of the tool.

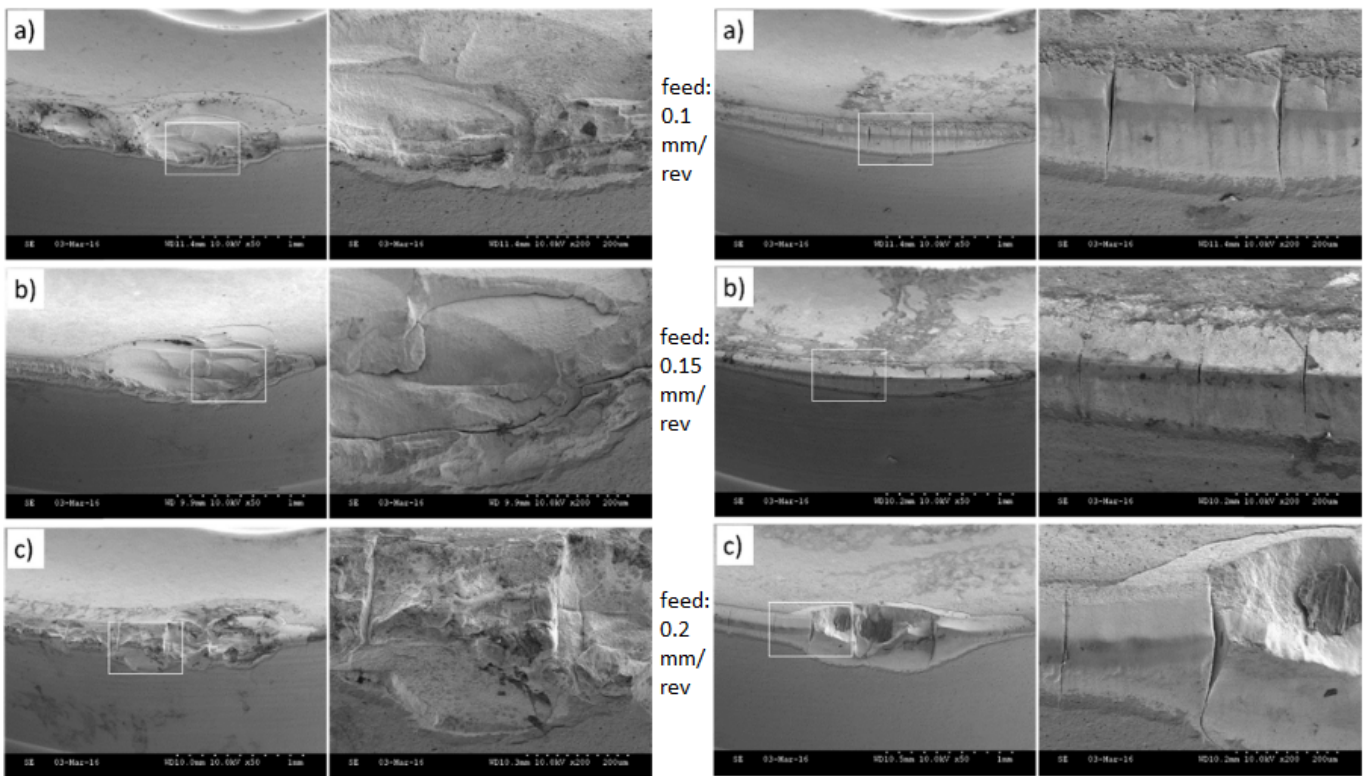


Figure 4.1.16: [40, Sadik 2017] SEM images of worn insert, 80 m/min, PVD TiAlN coated insert

[36, Tapoglou 2017] and coworkers analysed tool life in case of flood, MQL, MQL with LCO<sub>2</sub>, LCO<sub>2</sub> only and dry machining. They used insert with positive angles at high feed ( $0.45 \text{ mm/tooth}$ ) but very low radial engagement and high depth of cut (respectively  $1 \text{ mm}, 6 \text{ mm}$ ). Tool life in case of pure cryogenic application (LCO<sub>2</sub> only) was one tenth with respect to flood lubrication. The answer to the poor result could be addressed to the lack in need of a strong coolant in a process in which the insert cuts for a very short time. Moreover, the portion of the edge interested by the cutting action is quite large, due to the high depth of cut, so that it is difficult to be homogeneously cooled or even wetted by volatile fluids like cryogenes.

[80, Pittala 2018] applied LCO<sub>2</sub> through channels in the milling cutter while machining Ti6Al4V. Two nozzle diameters and positions were tested. LCO<sub>2</sub> and emulsion cooling were compared both at 50 *bar*. Wall milling was performed: the depth of cut was quite

high (8mm) with respect to the feed chosen ( $< 0.15\text{ mm/tooth}$ ). Cutting tool life results in this case goes proportionally with chip ratios. For high chip ratios (thin chip spread over wide insert areas) LCO2 perform worse than emulsion, for low chip ratios (bulky chip) LCO2 perform better. This can be due to the reduced spreading of LCO2 over the cutting edge and to a matched MRR-flow rate-delivery technique combination. The best position for the exit holes in the milling cutter was to cool the flank of the previous insert.

This final statement raises a doubt: in turning, tool life are strictly dependent on whether or not flank cooling is adopted. Rake cooling cannot prologue tool life as flank cooling does. Flank cooling allows to cool and harden the tool portion unto which wear measurements are done. In milling there is hardly an example where flank cooling is performed as it is very difficult to apply this. However it would be very interesting to propose a cutting insert design suitable for flank cooling in milling and investigate its effect in comparison to through holder cooling alone.

The positive results of Sadik and colleagues are characterized by the use of a high feed tool used at moderate feed and speed. Round and tough inserts are adopted. There is hardly an example of the use of high feed tools for LN2 cooling.

### 4.1.3 Conclusion

Having said so we can conclude that a complete performance comparison between cutting strategies must follow a structured scheme. For a cooling strategy to be performant, tool life has to be evaluated against the industrial practice, which can vary depending on the chosen case study. Being one of the most influencing aspects, delivery techniques must be optimized, moreover, flow rate and fluid quality must be clearly stated. In general, delivery options have to be studied for the particular case, this is the real limitation of cryogenic machining. Finally, tool life has to be reported preferably with Taylor law so that economic and ecologic studies can be performed. The life analysis, if successful, should be followed by a surface quality analysis and a sustainable (economic, ecologic, social) performance case study.

## 4.2 Insert materials

*With respect to cutting inserts material the vast majority of researchers opted for Tungsten Carbides. Research focused on the evaluation of different coatings. There is hardly an example of cryogenic machining using using other tool material than carbides.*

### 4.2.1 High Speed Steels, HSS

HSS coated cutters are generally applied for drilling applications. However, no article came to the Author attention regarding this aspect. Also, the difference with respect to milling and turning and the aim of simulating the Milling process, moved the research far from drilling applications.



## 4.2.2 Carbides

Everyone uses carbides unless without specifying why, probably due to the high performance/price properties. From the excellent work of Hong and colleagues, [11, Hong 1999], it seems that Carbides have been chosen blindly by any research dealing with cryogenic machining. Recently, tool failures especially regarding milling cutters, could shift the attention toward different materials.

[81, Safari 2014] compared WC uncoated and Ti-Al-N plus Ti-N coated inserts, with same geometry and manufacturer, in cryogenic air assisted high speed end milling of Ti-6Al-4V. The coated tool produced higher forces and slightly higher surface roughness compared to the uncoated counterpart. The author imputed the change to the increase of edge radius due to the coating. Higher forces meant higher vibrations and roughness.

Several other authors compared various coatings (Ti-Al-N in primis) applied with different techniques: PVD, CVD. None of the coatings seems to give noticeable increment of performances in cryogenic machining. The main problem being the thermal expansion match between coating and substrate, especially in the inner crater edge, experiencing variable mechanical and thermal loads. Moreover, in many studies the coating was torn away in minutes either by cryogenic or conventional lubricating coolant strategies, [82, Venugopal 2003]. Another key point noted was the increase in the edge radius, growing the more the higher the number of coating layers (multiple coatings have been tested). Titanium cutting is very sensible to edge radius, being a strong material with low elastic modulus, it tends to refuse the cut and move under the cutting edge. Therefore some researchers preferred to adopt uncoated inserts with edge preparation rather than larger radius coatings.

## 4.2.3 Ceramics, CBN, PCD

Expensive tool materials are generally avoided from cutting wear trials, being a lot of inserts necessary to complete a reliable study. However, it could be interesting to investigate the eventual increase in expensive cutters life with cryogenic machining. The problems of ceramic tools is the brittle nature at low temperature and the reduced resistance to blows.

Polycrystalline Diamond tools are generally avoided due to the graphitization tendency and consequent loss of properties. Interesting is the use of Polycrystalline Cubic Boron Nitride and Binderless Cubic Boron Nitride which guarantees higher conductivity with respect to Carbides, therefore thermal fields could be smoothed and heat extraction improved.

## 4.3 Cooling media

The most used cryogenic fluxes are LN<sub>2</sub> and LCO<sub>2</sub>, added by Chilled Air (analogous findings in line with cryo performances can be done for cryo cooled air). Often authors doesn't justify the cooling media selection, unless some address their choice to cons related to the alternative. LCO<sub>2</sub> is reported to pose higher difficulty due to ice formation and nozzle clogging. The main problem related to LCO<sub>2</sub> nowadays is the price (never investigated by authors), the handling of large quantities (*1 kg/min* flow rate requires

up to 500 kg/shift LCO2 supply to each MT) high pressure gases, and the ventilation systems required for operator safety. LN2, on the other side, is much more difficult to be handled due to the low temperature (LCO2 can be stored at high pressure and ambient temperature), affecting all machine tools parts nearby its passage (spindle units, tool holder), causing contraction and dimensional deviation.

Regarding the cooling capacity LCO2 has higher static cooling potential, considered the latent vaporization and sublimation heat from a target hot temperature:

$$q = c_p(T) \cdot (T_{surf} - T_{fluid}) + \chi_l \cdot h_{l-v} + \chi_s \cdot h_{s-v} \quad [J/mol]$$

where  $c_p$  is the specific heat,  $\chi_l$  and  $\chi_s$  are liquid and solid fractions for the impinging jet,  $h_{l-v}$  and  $h_{s-v}$  are the evaporation and sublimation enthalpies. This because a portion of liquid LCO2, due to the sudden expansion, transforms into vapour at the exit of the nozzle while a fraction of the jet solidifies. Therefore an LCO2 impinging jet is found to be formed by vapour, solid and remaining liquid particles. LN2 exploit generally only heat extraction due to temperature difference and vaporization enthalpy. Chilled Air, C.A. exploit the cooling effect of gases only.

	LN2	LCO2	C.A-30°C	C.A-180°C
T_JET - [°K]	77	195	243	93
T_JET - [°C]	-196	-78	-30	-180
DT_400 - [°K]	596	478	430	580
H_L-V - [KJ/MOL]	6	16.5	0	0
H_S-V - [KJ/MOL]	-	26	0	0
CHI_V	0	0.6	0	0
CHI_S	0	0.4	0	0
CHI_L	1	0	0	0
MM - [KG/MOL]	0.028	0.044	0.029	0.029
CP - [KJ/MOL*K]	0.029	0.037	0.030	0.030
CP - [KJ/KG*K]	1.036	0.841	1.04	1.04
Q_DT - [KJ/MOL]	17.284	17.686	12.9688	17.4928
Q_H - [KJ/MOL]	6	10.4	0	0
Q - [KJ/MOL]	23.284	28.086	12.9688	17.4928
Q - [KJ/KG]	831.57	638.32	447.20	603.20

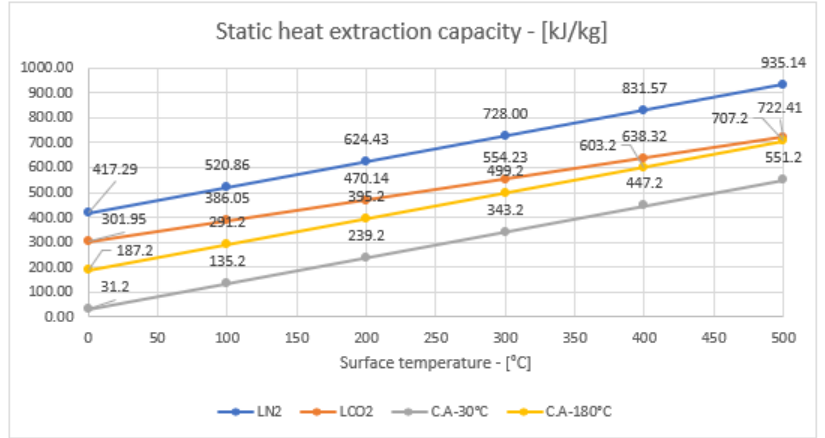


Figure 4.3.1: Static cooling capacity, cooling media properties (NIST) and cooling power for variable surface temperature

The real cooling capacity of cryogenic fluxes, however, is time dependent. Fluid and thermo-dynamic phenomena are fundamental to determine the Heat Transfer Coefficient for surfaces in contact with the flux:

$$q'' = h_{cryo} \cdot (T_{surf} - T_{fluid}) \quad [W/m^2], \quad h_{cryo} = f(p_{cryo}, v_{jet}, \chi_i, T_{surf}, geometry, media)$$

The HTC is not of easy determination, it is generally inversely deduced from CFD simulation or experiments. Analytical relations for the HTC in case of LN2 have been developed (chapter 5 Modelling). However, nothing has been published for HTC in machining environment for Chilled Air and LCO2 (there is something for supercritical CO2,  $p > 72 bar$ ,  $T > 31 °C$ ). Due to variation in jet phase and properties, it was believed that using the relation for LN2 was inaccurate, therefore no analysis of HTC between different media is done here.

[83, Kramer 2014] and his team demonstrate how cooling capacity of cryogenics is much more dependent on pressure than flow rate, because pressure influence the velocity out of the nozzle with the ability to break the vapour bubbles formed on the hot targets by Leidenfrost effect. In [49, Tahmasebi 2019], CFD simulations showed that too high pressure and consequent jet speed caused flushing of fluid away from the tool at a too high rate, so that cooling extraction was impaired by short contact duration. [72, Jerold 2013] and [73, Kumar 2013] compared LN2 and LCO2 versus wet and dry turning of Ti-6Al-4V with uncoated Carbide inserts. Remarkable results were reported for cutting forces reduction, surface roughness, chip thickness and tool life in terms of reduced crater and flank wear. In the order, the approaches performed from worse to best, Dry-Wet-LN2-LCO2. LN2 experiences slightly higher forces than LCO2, due to claimed higher hardening effect on the WP. Lower forces with respect to Wet and Dry were addressed to tool hardness and slippery properties retention and absence of BUE. Doubts arise on how they managed to achieve force reduction with a  $2\text{mm}$  nozzle at  $50\text{mm}$  from the cutting zone, but they didn't provide any flow data to make reproducible the obtained results. The better performance of LCO2 are likely to be attributed to higher delivery pressure than LN2. Similarly to [57, Bermingham 2012], in which HP coolant had higher momentum transfer, surpassing the cooling capacity of LN2, here LCO2 might surpass the cooling effectiveness of LN2. This underlines the importance of delivery conditions of lubro-coolants fluids. [83, Kramer 2014] and colleagues found that LN2 performed better than LCO2 against emulsion cooling turning with cemented Carbide at  $150\text{m}/\text{min}$ ,  $0.13\text{mm}/\text{rev}$ ,  $0.3\text{mm}$  depth. However, very scarce information on fluxes and nozzle delivery was given. In [42, Kirsch 2018] et al. similar and slight improvements in tool life with respect to emulsion cooling were found for both LN2 and LCO2. A thermocouple was put in contact with the tool back surface and measured the bulk cooling effect of fluids: LN2 has the lowest bulk cooling capability due to the instantaneous evaporation. LCO2 performed better than emulsion for what concerns cooling action. [84, Iqbal 2019] and his team obtained lower tool wear by using LN2 instead of LCO2 while face turning Ti64. In [41, Pusavec 2019] a higher absolute heat extraction was found for emulsion coolant. While LCO2 and LN2 failed to keep in contact with the hot target for enough time, emulsion wetted a much wider surface dragging heat removal.

### 4.3.1 Liquid Nitrogen, LN2

LN2 advantages, with respect to other low temperature boiling gases, are to be abundant in atmosphere, colourless, odourless, totally inert, with strong cooling capacity. Another advantage deriving by the use of Nitrogen is the generation of an inert environment surrounding the cutting zone. It obstacle Oxygen penetration, avoiding chip burning in HSM or cutting magnesium, [85, KE 2009]. It is toxicless as it does not cause problems if breathed, being it the most part of our atmosphere, but that is not an advantage (claimed by many) since other gases are toxicless in that sense, CO2 as well. The problem is not related to the toxicity but to the Oxygen depletion if Nitrogen content in the atmosphere surpass 80%.

The main drawbacks are the energy and water demand necessary to produce it, [31, Supekar 2020], and the fact that all the LN2 used is then lost in atmosphere (and lost in gas separators), although the lack of recirculating system can be an advantage as well,

[12, Yasa 2012]. For certain the insulation and delivering system represent a challenge: keeping LN2 properly liquid until the nozzle is very difficult. Viscous friction and heat penetration in the vacuum jacket pipes initiates boiling, therefore is necessary to cool or pressurize LN2 over the critic point (posing problems of storage). Cavitation cause the more bubbles that can block the flow in tubes, thus promoting unstable flow at the nozzle, [49, Tahmasebi 2019]. Gas separator are often needed to keep high liquid percentage in tubes. Mass flow rate is of complicate measurements given the double phase, so researchers use to monitor the weigh of the LN2 tank. Another issue is the warming up (or more intuitively: the cooling down) of the MT elements associated with the delivery of LN2: it can require half an hour to achieve stable liquid flow, depending on the delivery system adopted, meanwhile watching the precious LN2 evaporating.

### 4.3.2 Liquid Carbon Dioxide, LCO<sub>2</sub>

The advantage of LCO<sub>2</sub> over LN<sub>2</sub> is that can be stored and delivered at ambient temperature and relative easily achievable pressure of around 60bar. Therefore, no thermal insulation is required and the MT is not thermally affected by the circulating LCO<sub>2</sub>. Delivery system design, tool and spindle or holder modification are simpler. When it exits the nozzles, finding a much lower pressure, it evaporates extracting heat from the cutting zone. The sudden evaporation needs heat, which is taken from the cutting process, however some portion of the CO<sub>2</sub> can become solid. The impinging jet is therefore composed by gaseous and solid CO<sub>2</sub>, which can cool down to  $-78^{\circ}C$ , [1, Jawahir 2016], by Joule-Thomson effect.

[38, Fernandez 2019] and colleagues found improvements in tool life by internal CO<sub>2</sub> delivery and localized insert application in milling Gamma Ti-Al and EA1N grade Steel. [56, Machai 2011] and his team applied successfully LCO<sub>2</sub> on rake in cutting Ti-6Al-4V increasing Tool life. LCO<sub>2</sub> didn't need insulating pipes as it could be stored at 57bar, 20°C. Measured flow rate during cutting was 2,72 Kg/min. Out of the nozzle it was stated that 60% of CO<sub>2</sub> was in vapour phase and 40% in solid phase. The solid phase sublimates in contact with the hot tool and WP surfaces thereafter. At the end of cutting operation the workpiece was cooled down to  $-36,9^{\circ}C$ . An extraction system was reminded to be used for CO<sub>2</sub> extraction.

In Putz et al. as reported in [1, Jawahir 2016], they stated that a lower distance between nozzle and target and lower diameter was more effective in cooling than higher diameter and flow rate. High collimation, lower distance from target are to be addressed for optimal cooling and consumption of coolant.

### 4.3.3 Chilled Air

Chilled Air has been used as a coolant media for machining applications at a temperature not lower than  $-50^{\circ}C$ . As we have told before we will treat it as well, even if it does not answer properly to the term Cryogenics, because some features like cooling capacity matching with process heat generation are the same. Chilled air cooling is often adopted in synergy with MQL, compensating the almost null lubrication capacity of air. Application of this cooling media have been implemented cutting Titanium alloys, Aluminium alloys, Cast Irons, Stainless Steels. Stated advantages are in line with the one obtained with cryogenic fluxes. Chilled compressed air by the way is easier and

cheaper to produce, by traditional vapour compression systems or adiabatic expansion, [86, Rubio 2015]. With respect to this, RHVTs (Ranque-Hilsch Vortex Tube) represent a cheap way (500 ÷ 1000 €) to produce chilled and warm gases out of a compressed flow. However, the efficiency of this cheap systems is low.

Major drawbacks in using chilled air as a cutting fluid is the poor heat extraction capacity and almost null lubrication action. The first is compensated by high pressures and lower temperatures. The second cannot be improved. Contrary to liquefied gases like LN<sub>2</sub> and LCO<sub>2</sub>, chilled air cannot benefit on liquid to gas expansion ratio, therefore even the low possibility of penetrating the Tool-chip interface offered by cryogenic fluxes is hardly achievable.

Chilled air cooling was found to be more effective in comparison to CCF or MQL at high speed and low feed, [86, Rubio 2015]. In this range of parameters, efficiency of CCF is proved to be low. Therefore chilled air would excel over conventional approaches for higher cooling capacity. High speed low feed means low forces and torques but increased MRR. It is needed a fluid capable of removing not so much heat, but rapidly and in this air cooling seems to perform well, at least better than CCF. Readiness in removing heat by the cooling mean must also be considered as a discriminant property. It should deal with cooling media pressure, velocity, wetting and very important sudden evacuation out of the cutting zone. Maybe low boiling point gases have low readiness due to this phenomena: time to exploit the latent heat, however, no one ever tried to compare different cooling media at different heat generation rates (different MRR or cutting speed).

[68, Sun 2010] and his team found enhanced tool wear resistance using cryogenic LN<sub>2</sub> cooled compressed air, however they lack of a comparison with CFL.

[87, Yuan 2011] and colleagues proved the effectiveness of refrigerated air at different temperatures, combined with MQL, in end milling of Ti-6Al-4V. Lower cutting forces, roughness, flank wear rates, were observed versus Dry, Wet and MQL with room temperature air.

# Chapter 5

## Modeling Machining Processes

In recent years, advances in computational resources have made available numerical evaluation of models regarding cutting processes. With respect to cryogenics, also thermal analysis, modeling the heat generation of a cutting process, have become important. CFD analysis of jets helps in defining the correct nozzle design. Hybrid thermodynamic-CFD simulation are needed to forecast Heat Transfer Coefficients of fluxes so to predict characteristics of the flow to be delivered at the cutting zone. Recently, models have also been developed to predict surface properties after machining such as metallurgical structures, stress states, roughness.

Modeling cryogenic assisted processes is fundamental to decrease the number of process variables. Added to the classic process parameters of feed, speed, depth of cut, Tool angles, number of teeth, strategy etc, cryogenic processes also need to determine flow rates, pressure, nozzle position, orientation, diameter, number, cooling flux nature, cooling strategy. Modeling become fundamental with super alloys like Ti, Ni, Co, Mg, Al alloys, stainless steels, tool-steels, reducing the number of necessary cutting experiments and help in understanding critical issues, [4, Deshpande 2018].

Regression Modeling, Response Surface Methodology, Artificial Neural Networks, Genetic Algorithms have been applied to cryogenic machining for evaluating performances like tool life and surface finish. FEM simulations with huge variety of material models for chip formation have been implemented for the study of stress-strain states, temperature, forces and power.

FEM analysis of cutting process aims at the prediction of:

- Cutting forces: which at their turn influence power, energy consumption and machine tool dynamics;
- Chip morphology: mainly it has been used as a check with experiments to validate the goodness of a material/contact model, but can be used to understand stress, strains, strain rates in the material, tool-chip interactions fundamental for wear prediction;
- Tool wear prediction: temperature and mechanical loading on the chip-tool interface are needed for prediction of the evolution of cutting edge wear. It would be an outstanding result to be able to reproduce a cutting tool life test, so to forecast tool life without long and expensive experimental campaigns, however FEM models can only simulate milliseconds of cutting, therefore other methods are needed to aim at this goal;

- Surface quality: grain size, hardness, phase changes, roughness, deformation layers, residual stresses are quantities that can already be forecasted by tuning the models with experiments and by the modification of material constitutive models.

Running a FEM simulation of a cutting process is not at all an easy task. For instance the material properties are needed. In the table we report the material properties used for Titanium alloy Ti6Al4V:

Material properties for FEM simulations				Ti-6Al-4V	WC-Co
Family	Property	Symbol	Units SI, mm-s-N	Value	
Mechanical	Density	$\rho$	$kg/m^3, tonn/mm^3$	4429 ÷ 4512	$15250, 1.525 \cdot 10^{-8}$
	Thermal expansion	$\alpha$	$1/K$	$9 \cdot 10^{-6}$	–
	Poisson module	$\nu$	–	0.31 ÷ 0.37	0.22
	Young module	$E$	$GPa$	104 ÷ 113	600
Thermal	Thermal conductivity	$\lambda$	$W/m \cdot K, mW/mm \cdot K$	6.7@20°C	44
	Specific heat	$c_p$	$J/Kg \cdot K, mJ/tonn \cdot K$	$526, 5.26 \cdot 10^8$	$188, 1.88 \cdot 10^8$
	Melting point	$T_m$	°C	> 1600@p = 1 atm	–
	Inelastic heat fraction	$\theta$	–	0.9	–

Table 5.0.1: Material properties needed for FEM simulation of cutting process, values for Ti6Al4V and Carbide tool

Other than material properties, interaction properties are needed: contact and thermal interaction properties. Finally a good material model, able to represent with accuracy the strain, strain rate and thermal effect on the stress flow is necessary for reliable results.

The computational burden of chip forming FEM simulation is very high, a simple orthogonal cutting simulation can take some hours (2 ÷ 10) before convergence on performing workstations, while a single tooth arc pass in 3D milling can take more than a week. Therefore analytical models are still needed and useful to:

- Predict the order of magnitude of results and apply them as boundaries to ease the convergence of simulations;
- Proceed with the calculation at a larger time scale than the one that can be reached with simulations. For example, thermal and stress loading of an insert out of a single tooth pass simulation can be fed to an analytical wear model to calculate the tool material erosion rate at repeated engagements.

In this chapter, modeling of cutting process with particular attention to cryogenic machining will be presented. The analysis of the literature articles will answer also to the collection of data needed for the simulation of the cryogenic milling process.

## 5.1 Thermal models

Analytical models, correlated by experimental coefficients, have been developed to predict temperature in the cutting region. Accurate thermal predictions are useful for understanding possible outcomes in the cutting process, especially metallurgical features. Generally only average values can be predicted by handy formulations which give an order of magnitude of the real cutting process temperature. [88, Benabid 2014] et al. reported a synthetic analytical formula for the prediction of the order of magnitude of temperature in the shearing region:

$$T = 0.4 \frac{U}{\rho c} \left( \frac{v \cdot t_0}{K} \right)^{1/3}$$

where  $U$  is the specific cutting energy,  $\rho$  the density,  $c$  the specific heat,  $v$  the cutting speed,  $t_0$  the feed,  $K$  the conductivity of the workpiece. This approximated values would be useful for example in order to tune the cooling capacity of the cutting fluid flow. Material pair fixed, the temperature build up in the cutting insert would be proportional to the cutting power, cutting parameters (speed and reachability of the cutting zone), workpiece geometry. Optimal pressure, flow rate and velocity of cutting fluids could then be designed in order to reach a maximum temperature in the cutting zone.

For what concerns cryogenic machining, the thermal prediction in the cutting zone, added to a precise forecast of cooling jet properties would allow for a first estimation of cryogen flow rate. Flow pressure can be obtained due to the optimization of the delivery line for minimum discharge ([49, Tahmasebi 2019]) and can be changed iteratively over small ranges. However, a good correlation between cutting jet HTC and mass flow rate, pressure, velocity and flow quality (vapour and liquid phase) is needed.

### 5.1.1 Temperature measurements

[89, Ay 1998] et al. observed with thermocouples the temperature evolution in the cutting insert being first order exponential. They also concluded that the maximum temperature region along the rake face of the insert is shifted from the tip. This is a consequence of chip drag, which carries away the heat generated in the shear zone, and by friction. How this distance is related to the chip thickness (feed) or material properties is not mentioned. [90, Dhar 2002a] et al. stated that the shift of the maximum tool temperature is due to the friction heat build up, when friction changes from sticking to sliding the heat generated lowers and can be easily dragged away by the chip.

Several techniques were adopted to obtain reliable temperature measurements. It becomes evident that a meaningful temperature measurement must include accurate data regarding the tool-chip interface temperature. The principal problem stays in the limited physical space available. Thinking of an orthogonal cutting scheme, the chip thickness is in general in the order of hundred of microns. The finest sheathed thermocouple in the market nowadays is  $150 \mu m$  in diameter, which is comparable with the width of the interface in the highest temperature region. Researchers then developed other techniques in order to capture the finest temperature measurements, [91, O'Sullivan 2001]:



- Workpiece-tool thermocouples: need isolation of the piece and tool, they measure an average of the interface temperature and the calibration must be accurate, [92, Bacci da Silva 1999];
- Thermocouple wires: a wire of different material than the workpiece is embedded in it and a thermocouple is made when it comes in contact with the tool. The piece must be isolated. The contact develop in very short time, [92, Bacci da Silva 1999]. It would be better to place the wires on the insert, but that is more challenging from a practical point of view. Careful calibration and preparation are necessary, [93, Yang 2014];
- Thermocouples sheets: embedded in the workpiece as “slices”, when cut by the insert give a continuous measurement. The problem is that the measurement is an average over the contact between the sheet and the tool;
- Infrared pyrometers: [94, Ng 1999] et al. used an optical fiber pyrometer, with a response faster than thermocouples, so are suitable for milling measurements. Also the very thin optical fiber can be installed right in the interface. The main problem is that the view of the fiber must not be obstructed by deposited material on tool face;
- Thermocameras: cameras capable of detecting infrared rays. They need to be very sensible and calibrated over the particular workpiece emissivity. They cannot penetrate the interface, but give only average values regarding the exiting chip. However they're the easier way to compare two temperature measurements;
- Metallurgical alterations: temperature experienced by the workpiece can be evaluated by a metallurgical evaluation. Transformation temperatures are used as thermal history detectors. This method only helps in defining temperature ranges, while the skin transformation is also influenced by strain and strain rates.

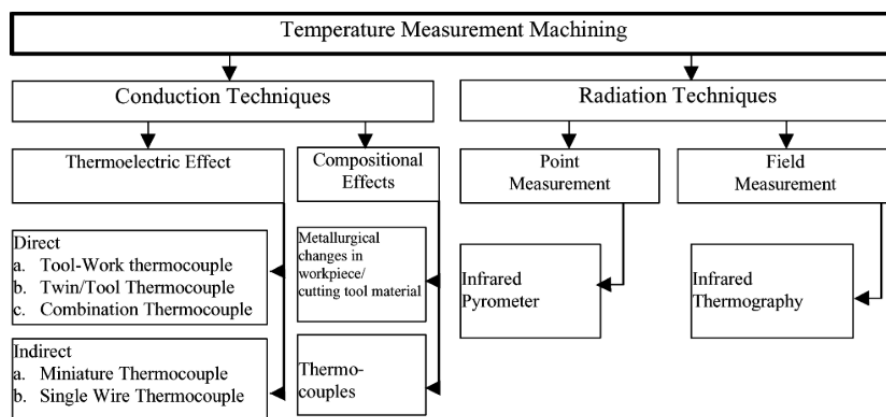


Figure 5.1.1: [91, O’Sullivan 2001] temperature measurement strategies

A complete review on temperature measurements in cutting process can be found in [95, Davies 2007]. For what concerns milling, of importance becomes the readiness of instruments, being a single insert passage in the order of some milliseconds.

### 5.1.2 Pure Thermal Models

[96, Komanduri 2000] et al. made a very detailed study divided along three articles aiming at the analytical identification of the thermal fields in cutting inserts. The model is rather complex and nowadays thermomechanical FEM models would be used, [97, Majumdar 2005]. However, having the necessary coefficients the model could be suitable for the prediction of the thermal field in the insert to be placed as boundaries in the FEM models and speed up their convergence. They also underlined how the friction heat source is preponderant for cutting temperature rise.

[8, Hong 2001b] and colleagues made a complete study analyzing the capacity of various cooling techniques in the temperature manipulation during turning Ti-6Al-4V. Dry cutting, emulsion, LN2 precooling, tool back cooling, rake, flank, rake&flank jet cooling by micro chip breaker assisted nozzles were modeled and experimentally validated. By applying a depth of cut much higher than feed and neglecting flank friction they hypotized 2D steady state heat transfer on the rake face. The model included portion of the workpiece, tool, holder, chip and atmospheric air. Boundary conditions were set with average convective heat transfer coefficients either from literature or calculated through experiments and analytical relations. LN2 jets of  $7,5 \cdot 10^{-6} m^3/s$  produced a HTC of  $2,327 \cdot 10^4 \div 4,675 \cdot 10^4 W/m^2K$ . From measured cutting forces, heat sources were determined. Shear angle, interface contact length and deformed chip thickness were obtained by chip and tool wear analysis and used to determine model geometries. Simulations were validated by placing a  $0,3mm$  thermocouple in the chip contact surface. Measured temperatures proved to differ of 22% maximum with respect to the model.

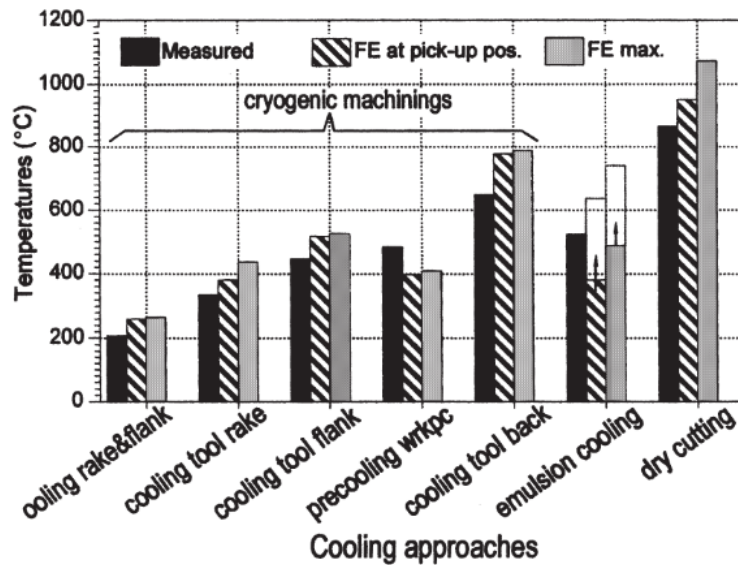


Figure 5.1.2: [8, Hong 2001b] numerical and experimental cutting zone temperature comparison

For cutting speed of  $90m/s$ , dry cutting proved to reach around  $1000^{\circ}C$ , tool back cooling only reduced temperature around  $700^{\circ}C$  while emulsion cooling, rake, flank and workpiece precooling achieved temperatures in the order of  $500^{\circ}C$ . Simultaneous tool rake and flank cooling guaranteed maximum cutting temperatures on rake face of around  $250^{\circ}C$ , 5.1.2. For increasing cutting speed, simultaneous rake and flank cooling

proved to guarantee the best cooling effect. As diffusivity in Ti alloys is supposed to start above  $500^{\circ}C$ , a proper choice of cooling approach could prevent adhesion-dissolution dependent wear. The rake and flank nozzle delivery they used in the study is very precise in targeting the cutting zone, therefore same results are hardly achieved by using external nozzles. Moreover, the tool back cooling strategy they chose is the less effective approach among the indirect cooling strategies, and they would have obtained better result by applying the LN2 chamber on the rake face instead then on the back, as did [17, 15, Wang 1996, Wang 2000].

[6, Abukhshim 2006] et al. defines the heat generated in the cutting zone as:

- Primary zone heat generation:  $Q_{PDZ} = F_c v$ ,  $F_c$  cutting force,  $v$  cutting speed;
- Secondary zone heat generation:  $Q_{SDZ} = \frac{f_{\mu} v}{\lambda_h}$ ,  $f_{\mu}$  friction force,  $\lambda_h$  chip ratio,  $f_{\mu} = F_c \sin \alpha + F_f \cos \alpha$ ,  $\alpha$  rake angle,  $F_f$  feed force.

Further assumptions need to be carried out for determining the heat partition coefficient and the heat source distribution:

- The heat partition coefficient is a factor defined a priori which describes the proportion of heat flowing into chip and tool. A first guess is then refined looking at results of the simulations. The physical behaviours should be studied in order to get rid of this uncertainty. The proportion of heat flowing in the tool depend on the properties of materials, velocity of the chip, contact conductance;
- The heat source distribution accounts for the geometry of the cutting process: the primary heat source is reasonably shifted toward the tool tip while the secondary depends on the contact conditions. It is reasonable to depend on the sticking sliding nature of the contact, rising in the sticking region and decreasing the sliding region.

[98, Liu 2007] et al. create a 3D thermal model for tool and holder and 2D model for chip, to determine cutting temperatures in tool-chip interface during cutting of A390 Al-alloy. The model consisted in heat sources for primary and secondary deformation zones, sharing a the heat  $q$  through the partition coefficient  $\beta$  to be determined iteratively as a function of process parameters, comparing interface temperature match in the two sub-models of tool and chip side. The cooling air effect was introduced as a HTC boundary condition. The HTC was obtained by both impinging jet empirical evaluations and experiments. Values in case of room temperature and chilled air where respectively  $200 \div 240 W/m^2 K$  and  $750 \div 1100$ . They experimentally tuned the model and used to predict trends over process parameters variation. However, temperature predictions were in contrast with experimental results.

### 5.1.3 Temperature prediction in Milling

[99, Kitagawa 1997] and colleagues used thermocouple wires sintered within the tool and then exposed through grinding of the insert. When in contact with the workpiece they realized a thermocouple and temperature measurements were deduced. They compared continuous cutting with HSM and proved that with interrupted cutting absolute

maximum temperature is lower but the thermal loading is stronger due to thermal oscillations.

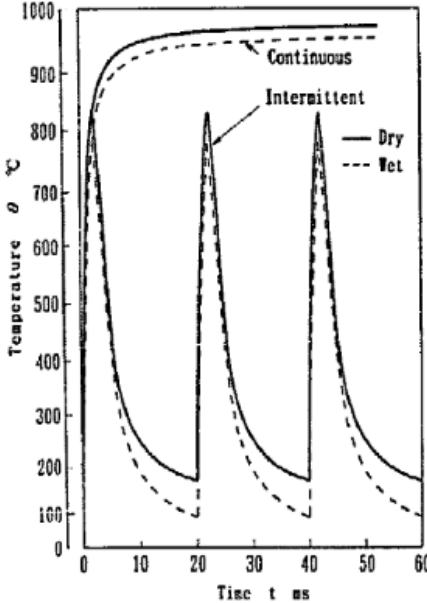


Figure 5.1.3: [99, Kitagawa 1997] continuous and interrupted cutting temperature profiles, *Ti6Al4V2Sn*,  $100m/min$ ,  $0.1mm/rev/tooth$

From the graph is clear how thermal steady state for continuous cutting can be achieved after almost  $20ms$  while for interrupted cutting also the first engagement is representative of the steady state situation, until tool wear affect the behaviour. Moreover, wet cutting helps by a little in shifting the whole curve downward.

[93, Yang 2014] and colleagues obtained good agreement between measured and simulated temperatures, milling *Ti6Al4V* with a solid mill. For the experimental temperature measurements over the whole cutting arc they used a Constantan Band as a thermocouple. Calibrated with the workpiece, the termocouple was placed as a sandwich within the piece, then it was cut by the tool and made contact with the workpiece, so a voltage proportional to temperature was measured. Good correlation with simulated temperatures was found.

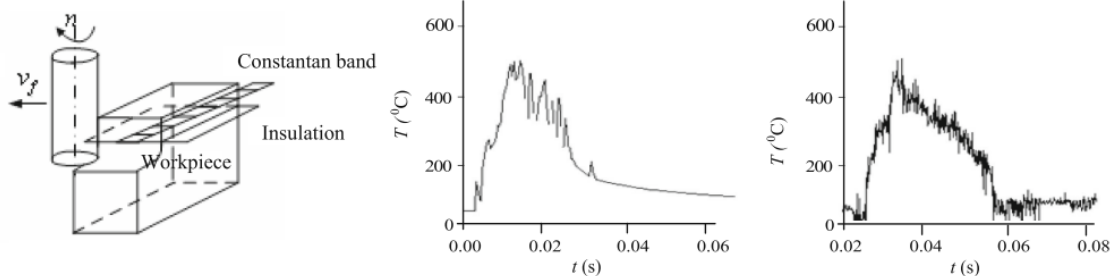


Figure 5.1.4: [93, Yang 2014] comparison of simulated and measured temperatures, milling *Ti6Al4V*

[45, Sato 2011] et al. used an optical fibre set into the insert and linked to a pyrometer for detecting the evolution of temperature in the cutting arc while cutting

Ti-6Al-4V. They modeled the 3D transient heat transfer problem with the help of Green functions, assuming a pulsating heat source as a plane with the dimensions of the feed and the depth of cut. If the material properties are constant and radiation is neglected, the equations describing the thermal field in the semi-infinite insert representing a quarter of the cartesian space are:

$$\frac{\partial^2 T}{\partial x^2} + \frac{\partial^2 T}{\partial y^2} + \frac{\partial^2 T}{\partial z^2} = \frac{1}{\alpha} \frac{\partial T}{\partial t}$$

$$-K \frac{\partial T}{\partial z} = \dot{q}''(x, y, t) = \dot{q}''(t) \quad 0 < x < L_x, 0 < y < L_y, z = 0$$

where, in the order, it is described the time dependent spacial heat transfer equation and boundary conditions in the heat generation zone. The Green function describing the temperature solution due to an instantaneous point source at time  $t$  situated in  $x = x_p, y = y_p, z = 0$  is:

$$\Theta_G(x, y, z, x_p, y_p, z = 0, D) = \frac{2}{\sqrt{\pi D}} e^{-\frac{z^2}{D^2}} \cdot \left\{ e^{-\frac{(x+x_p)^2}{D^2}} + e^{-\frac{(x-x_p)^2}{D^2}} \right\} \cdot \left\{ e^{-\frac{(y+y_p)^2}{D^2}} + e^{-\frac{(y-y_p)^2}{D^2}} \right\}$$

$$T(x, y, z, t) = \frac{\alpha}{K} \int_0^t \int_0^{L_x} \int_0^{L_y} \Theta_G(x, y, z, x_p, y_p, 0, D) \cdot \dot{q}''(x_p, y_p, \tau) dx_p dy_p d\tau$$

if the heat source is uniform the green function can be simplified:

$$\Theta_{GR}(x, y, z, L_x, L_y, D) = \int_0^{L_x} \int_0^{L_y} \Theta_G(x, y, z, x_p, y_p, 0, D) dx_p dy_p = \frac{1}{2\sqrt{\pi D}} e^{-\frac{z^2}{D^2}} \Theta_{GU}(x, L_x, D) \cdot \Theta_{GU}(y, L_y, D)$$

$$\Theta_{GU}(u, L, D) = \text{erf}\left(\frac{L+u}{D}\right) + \text{erf}\left(\frac{L-u}{D}\right), \quad D = 2 \cdot \sqrt{a(t-\tau)}$$

where  $D$  is a characteristic dimension,  $K$  the thermal conductivity and  $\alpha$  the thermal diffusivity. The Green function  $\Theta_{GR}$  represent the solution to a spacial uniform heat source with an instantaneous heat impulse. Depending on the chosen strategy (Up or Down milling) the width of the heat sources varies during the cutting arc:

$$L_x(\tau) = \frac{l_c}{h} f \sin \left\{ \left( \frac{\tau}{\tau_1} \right) \eta \right\} \quad \text{Up Milling}$$

$$L_x(\tau) = \frac{l_c}{h} f \sin \left\{ \left( 1 - \frac{\tau}{\tau_1} \right) \eta \right\} \quad \text{Down Milling}$$

where  $\tau_1$  is the cutting time and  $\tau$  the time elapsed in one cutting,  $f$  the feed,  $\eta$  the arc engagement angle. They approximated the heat source with a uniform distribution of the cutting power and the partition coefficient from experiments was set at 12%. The Up-Milling strategy promoted higher thermal gradients in the insert, even if gradual engagement is achieved. The Down-Milling strategy exhibited smoother profiles. Therefore Down-Milling is preferable for what concerns thermal loading of the insert.

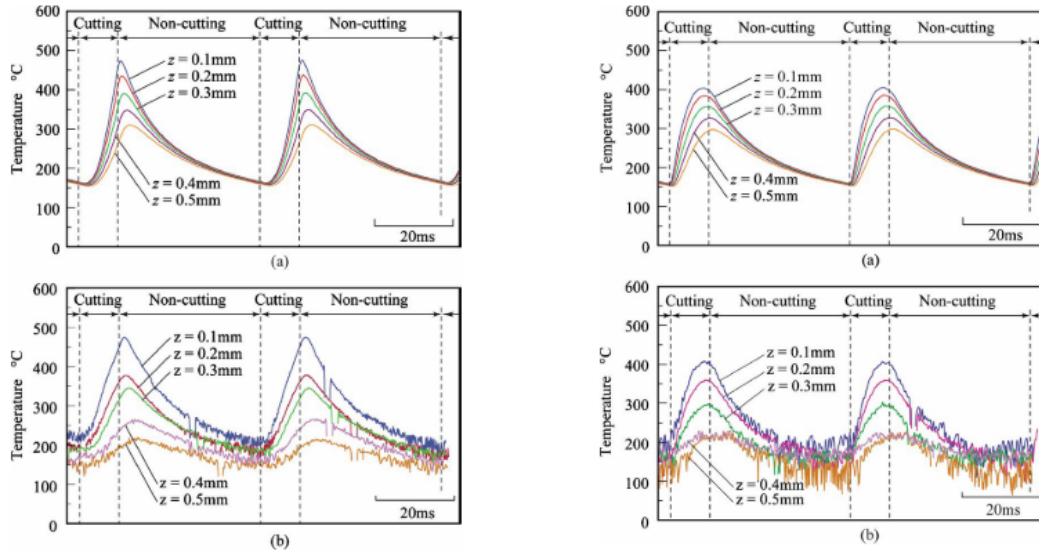


Figure 5.1.5: [45, Sato 2011] comparison of simulated and experimental thermal profiles (a) predicted, (b) experimental, left: Up-Milling)

Very good agreement is found for temperatures in the bulk body of the insert, however the temperature profiles in the skin depend much more on the heat source distribution, so on the contact nature.

[43, Jiang 2013] and colleagues studied the thermal problem in the milling insert with the same solution as in [45, Sato 2011] but with a varying heat intensity. The heat flux varied from a minimum toward a maximum depending on the uncut chip thickness. They varied the engagement and reported the variation of the relative temperature profiles in the tool. They also modeled the temperature distribution in the workpiece. From the figure is evident how the larger the engagement the higher the thermal loading of the insert body, but for what concerns the tool skin nothing can be said.

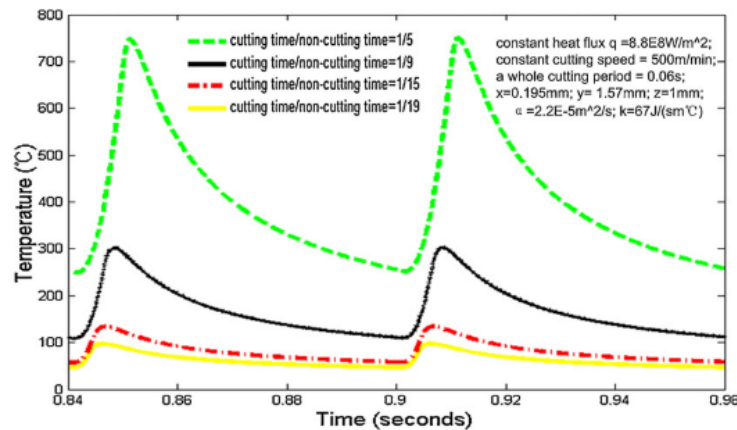


Figure 5.1.6: [43, Jiang 2013] variable engagement tool temperature profiles

[44, Karaguzel 2016] et al. still made use of Green functions to calculate the transient thermal fields in the milling cutter. They modeled the heat source intensity as  $Q =$

$F_{Res}v_c$  which is not properly the cutting power. They observed that lowering the engagement both reduced the maximum and average temperature of thermal cycle for the insert. Higher cutting speed reduces the oscillations of temperature but increase the average temperature of the cycle. For what concerns the boundary conditions, a detectable difference in the results is noted only for a heat convection toward the environment larger than  $100 W/m^2K$ .

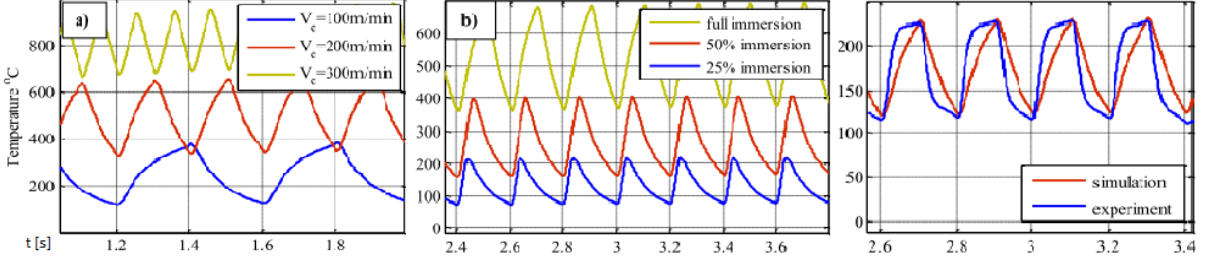


Figure 5.1.7: [44, Karaguzel 2016] temperature profile variation in speed, engagement and experimental results (*AISI 1050, 75 m/min, 0.15 mm/rev, 1 mm depth*)

[100, Baohai 2016] et al. modeled with Green function the transient thermal problem while cutting Inconel 718. They considered a heat source distribution depending on the contact conditions:

$$Q(x, y, z, t) = q_1(x)q_2(\tau)$$

$$q_1(x) = \begin{cases} 1 & 0 < x < \delta L_x \\ \frac{L_x - x}{L_x} \frac{1}{1 - \delta} & \delta L_x < x < L_x \end{cases}$$

where  $\delta$  describes the proportion between sticking and sliding zone. Due to the difference in the heat source the solution for the temperature field changes as follows:

$$T(x, y, z, t) = \frac{\alpha}{K} \int_0^t \Theta_{GR}(x, y, z, \delta, L_x, L_y, D) \cdot q(\tau) d\tau \quad + \quad \dots$$

$$\dots \quad + \quad \frac{\alpha}{K} \int_0^t \frac{1}{2\sqrt{\pi D}} e^{-\frac{z^2}{D^2}} \Theta_{GL}(x, L_x, \delta, D) \cdot \Theta_{GU}(y, L_y, D) \cdot q(\tau) d\tau$$

$$\Theta_{GL}(x, L_x, \delta, D) = \frac{L_x - x}{L_x} \frac{1}{1 - \delta} \cdot [\Theta_{GU}(x, L_x, D) - \Theta_{GU}(x, L_x, \delta, D)]$$

For the cooling phase during non cutting, they approximated the problem with a infinite plate in convection with air. The heat partition coefficient into the tool was assumed by the formula:

$$\beta = \frac{\sqrt{K_t \rho_t c_t}}{\sqrt{K_t \rho_t c_t} + \sqrt{K_w \rho_w c_w}}$$

A set of FEM cutting simulations were developed in order to fit the relationship between feed and speed with the generated heat and tool-chip contact length. Simulated temperatures were compared to experimental values obtained by workpiece embedded thermocouple. Found values were in accordance with the experimental ones, however

the location of the maximum temperature is unknown. Also the determination of the heat partition is purely static as doesn't take into account the dynamics of the chip. Nevertheless, after all the approximations needed for simulations, the results are accurate, thanks to good model tuning. Moreover, this article prove that it is possible to reduce the number of experiments by performing simulations.

[37, Augspurger 2019] and his colleagues investigated the transient temperature in the milling inserts while cutting Ti-6Al-4V. The time history of pulses were chosen as a simple square wave. They found the heating and cooling power intensities by iteration referencing to measures obtained with thermocouples. The study compared the thermal cycles obtained for MQL and MQL plus LCO2 cooling. They proved that LCO2 is able to shift the temperature cycles down by  $50^{\circ}\text{C}$  while imperceptibly rising the amplitude of cycles.

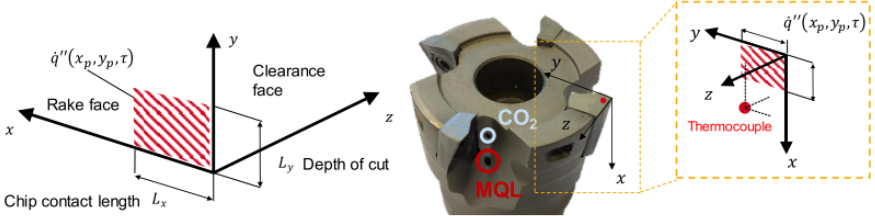


Figure 5.1.8: [37, Augspurger 2019] heat source scheme

In a following study, [101, Augspurger 2020], the team used the same analytical model to match the temperature measurement at the thermocouple cutting AISI 1050. In this case however they fixed the heat source as a portion of the cutting power  $P_c = F_c v \cdot \beta$  and iterate for  $\beta$ . They saw that rising speed the portion of heat transmitted to the tool lowered, the partition coefficient decreased. This was explained by the higher chip dragging action, which carried away most of the heat produced in the cutting zone. Tool temperature predictions are quite accurate for transient and steady state at low speed, while become less and less accurate rising the speed, tool wear accounted as responsible for that.

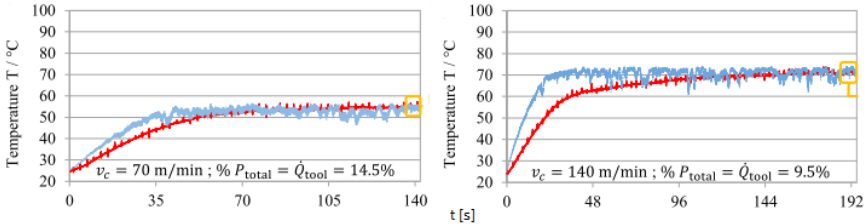


Figure 5.1.9: [101, Augspurger 2020] low and high speed simulated and measured tool temperature comparison

### 5.1.4 Thermal behaviour in chip removal simulations

Generally a chip removal simulation require lot of calculations: the mesh is highly refined in the deformation zones, remeshing (ALE) is necessary to avoid excessive distortion of elements, the thermal problem is coupled with the mechanical one, the contact



problem require additional iterations. Generally cutting simulations, in case of continuous operations, are stopped at the convergence of the cutting forces but that is not enough for the convergence of the thermal fields in the insert. To overcome this problem, larger conductance coefficients are placed at the tool-chip interface ( $> 10 kW/m^2k$ ). This is like hypotising perfect contact of a super conductive layer glued to chip and tool interface. Likely it would represent in short time what needs seconds to evolve. The temperature fields obtained are logically accurate only for the high pressure portion of the interface in which we can approximate perfect contact. The actual heat transfer coefficient can be obtained by applying the nodal temperatures of the interface as boundaries for a 3D pure thermal heat transfer problem, checking for the prediction of temperature inside the tool. What is found with this procedure however is the average conductance that allow the convergence of a suitable interface temperature distribution in the short time simulation so to reach the measured temperature inside the tool. [102, Umbrello 2007] et al. underline how the conductance at the interface and the contact conditions highly influence the thermal behaviour of a cutting simulation. Through an iterative process, the interface temperature generated by a short time duration simulation were applied to a 3D thermal simulation, then the temperature at thermocouples point were compared and the conductance at the interface updated. The conductance value which promoted agreement with the thermocouple measurements was  $1000 kW/m^2K$ . This value is really high, and is influenced by the short duration time of the simulations. With a physical conductance value the simulations should last seconds to reproduce the real case. Nevertheless, short simulations with modified conductance and 3D pure thermal calculations are able to reproduce the thermal field in the insert at steady state. However, this strategy is completely non physical, research should be oriented in studying the physics of the interaction.

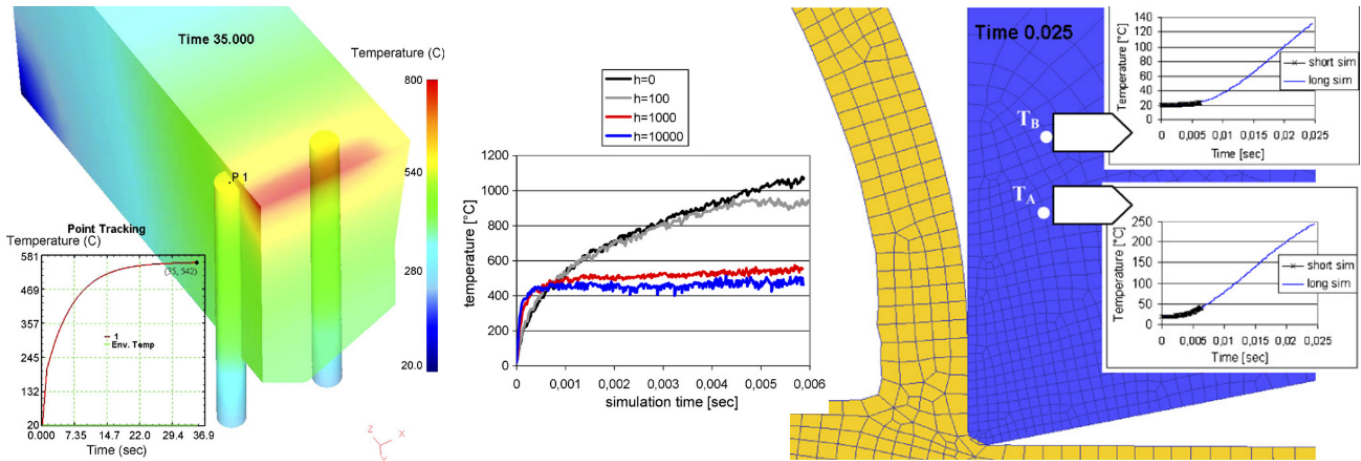


Figure 5.1.10: [102, Umbrello 2007] conductance dependence on tool temperature

[103, Ceretti 2007] and colleagues studied the variation of the numerical conductance cutting AISI 1045 with carbide insert. The authors simulated cutting with Coulomb-Tresca friction model, defining the heat transferring into the tool as the sum of the friction heat and the heat due to difference in temperature:

- Heat generation by friction:  $Q_{\mu} = \tau_{\mu} v_{sl} \beta$ ,  $\tau_{\mu}$  shear friction,  $v_{sl}$  sliding velocity,  $\beta$  heat partition coefficient;

- Heat flow due to difference in temperature:  $Q_{SDZ} = h(T_w - T_{chip})$ .

They simulated chip formation without considering the thermal interface problem, setting the conductance equal to zero. Then they applied the heat generated using the velocity and friction fields to the 3D problem, iterating for the conductance value. Different values of conductance were found for various feeds and speeds. They explained the variation looking at the average pressure and temperature on the rake face:

- Higher speed means higher temperature and pressure on the rake face, as the cutting forces decrease a bit, but the contact length reduces by a higher extent. Therefore the conductance increase;
- Higher feeds means higher temperature build up, however the increase in force does not challenge the longer contact length leading to lower average pressures. Therefore the conductance exhibit a minimum.

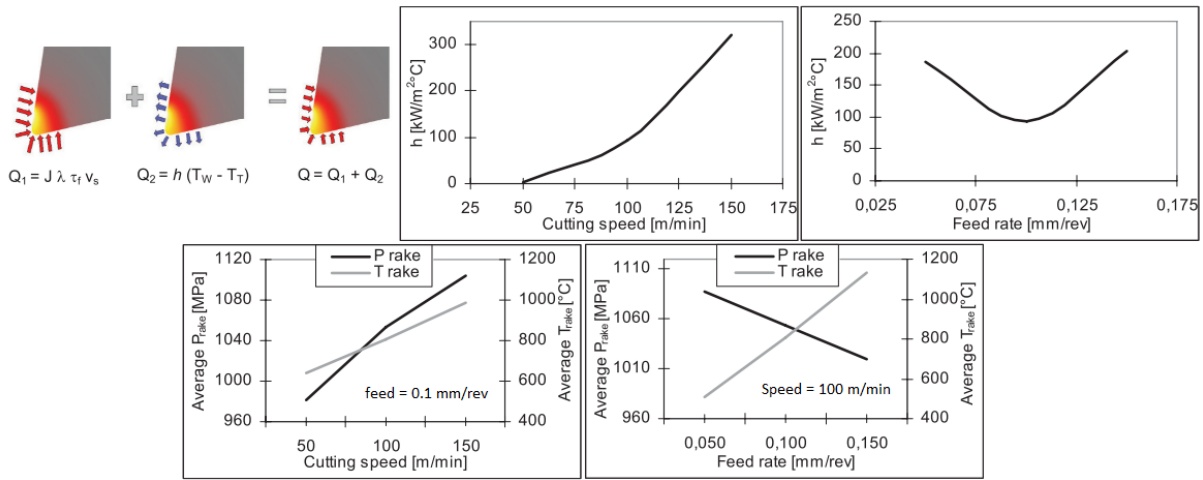


Figure 5.1.11: [103, Ceretti 2007] variation of tool-chip conductance in feed and speed, *AISI 1045, WC*

By the way, applying zero conductance to the initial simulation (providing stress and velocity fields) raises the temperature in the chip to higher values than the real case, probably causing softening in the material.

Modern FEM software require partition coefficient of heat toward the tool, and conductance values. The first is better be obtained by experiments, a first guess being the ratios of workpiece and tool effusivities. Conductance value needs to be physical to reproduce accurate temperature distributions at the interface. In milling is no sense in raising the conductance to non-physical values, being the process unsteady by nature.

## 5.2 Tribology

With tribology is generally indicated the science of interacting surfaces in relative motion involving phenomena like friction, wear and lubrication. For cutting processes simulations, detailed material models have been developed, while reduced attention

have been given to contact models. The material model influences cutting forces and chip morphology for the most, the contact nature influences temperature and tool wear. In the past decades, material models have struggled to fill the gap left by the impossibility to experimentally reproduce very high strains and strain rates. However, we still refer to simple sticking-sliding models for what concerns friction.

More sophisticated contact formulations have been developed unless not providing the coveted improvement of results. The main problem is that a simulation has to deal with two great uncertainties: the material model and the contact model. If it was possible to prove the accuracy of a material model in the whole range of strains and strain rates, then it would be possible to see the effect on results of the contact model alone. Being that impossible, the results of a simulation are affected by the two approximations.

Tool-chip contact length is still difficult to reproduce, simulation give much lower values than measured ones. Therefore, the logic pushes us to think it is neither a problem of the simulation nor of the researchers, simply what we are measuring is not the same thing we want to reproduce. The experimental tool-chip contact length is the result of some seconds of cutting, in which the chip is subject to its weight and other inertia forces that pushes it toward the tool face. During some milliseconds of simulation the chip hardly reaches the millimeter in length, therefore it would hardly scratch the surface of the tool as it does in reality, and it is not a matter of scratches measurement precision.

When it comes to simulate the difference between two cutting fluids some difficulties arise. Lubrication and friction are often misunderstood terms:

- Lubrication is an action aiming at the reduction of friction and wear between two sliding bodies. Lubricating strategies exploit, by different techniques, the separation of the two sliding bodies by a layer (the lubricating layer) with which the two bodies exhibit low friction;
- Friction is a physical reaction between matter in relative motion. In most of the cases it refers to the dry/solid friction between two rigid bodies. Viscous friction develops between deformable objects or fluids, because it is influenced by the viscosity of matter.

In the next sections we will deal with contact model types, implementation and experimental coefficients extraction.

## 5.2.1 Contact models for cutting simulations

### Coulomb-Tresca contact model

Solid friction is often modeled as Coulomb friction. Between two bodies in contact there develops a force proportional to the normal reaction between them:  $F_f = \mu \cdot F_n$ . This however is not the case in which two bodies in contact deform, so that they're more represented by viscous bodies. In that case the Tresca friction model is used:  $\tau_f = m \cdot \tau_{lim}$ , where  $\tau_{lim}$  is the shear stress limit and  $m$  a coefficient. The combination of this two models is the sticking-sliding contact model already implemented in the most FEM software:

$$\tau_f = \begin{cases} \mu \cdot \sigma_n & \mu \cdot \sigma_n < m \cdot \tau_{lim} \\ m \cdot \tau_{lim} & \mu \cdot \sigma_n > m \cdot \tau_{lim} \end{cases}$$

which limit the possibility of the coulomb friction to overcome the shear stress limit of the material. The factor report the normal stress to the shear stress limit, which in normal conditions in case of Von Mises stress is  $\sqrt{3}$ . It can be lower or higher depending on the local pressure, temperature and velocity fields. More sophisticated models considers the flow stress of the material for determining  $\tau_{lim} = \sigma_{fl}(\varepsilon, \dot{\varepsilon}, T) / \sqrt{3}$ . In this case  $m$  is an additional softening value which generally covers for unknown effects, mostly used to tune simulations on experimental results.

[104, Moufki 1998] and colleagues modeled the contact behaviour between tool and chip as temperature dependent. For cutting speed over  $1\text{ m/s}$  they assumed friction to be described by the average temperature of the interface. Pressure and sliding speed affect friction by their effect in modifying temperature. They approximated and solved analytically for the heat transfer problem due to friction at the interface, obtaining the mean interface temperature with iterations. For the expression of friction coefficient depending on temperature  $\mu = \mu(\bar{T}_{int})$ , they run experiments and fitted the experimental curve obtained. Unless the model considers an average interface temperature, the analytical model return a temperature distribution, and profiles of temperature along the rake face can be obtained varying the exponent of the pressure distribution. A part from a little shift at high feed, the model can accurately estimate feed  $F_q$  and cutting  $F_p$  forces.

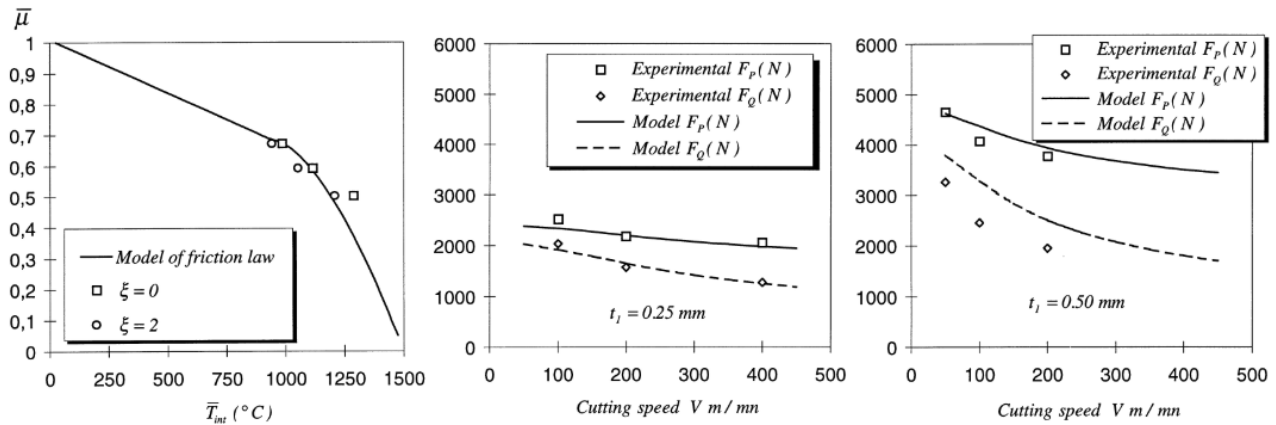


Figure 5.2.1: [104, Moufki 1998] temperature dependent friction coefficient results

After having validated the model, the authors undergo an extensive study on speed-feed sensitivity. The main findings relate the increase in speed and feed to the increase of temperature and the reduction of the friction coefficient, while positive rake angles determine lower temperatures and higher friction coefficients, but reduced forces and contact lengths.

[105, Childs 2006] analysed the contact behaviour between tool and chip at variable cutting speed. He reported valuable insight from tool-split techniques. In the tool split technique the insert is cut at different levels and variation on friction and normal forces are evaluated. Proportionality between shear and normal stress is found for low normal stress values, high normal stress values induces preponderant sticking and activate the shear stress limit of the material.

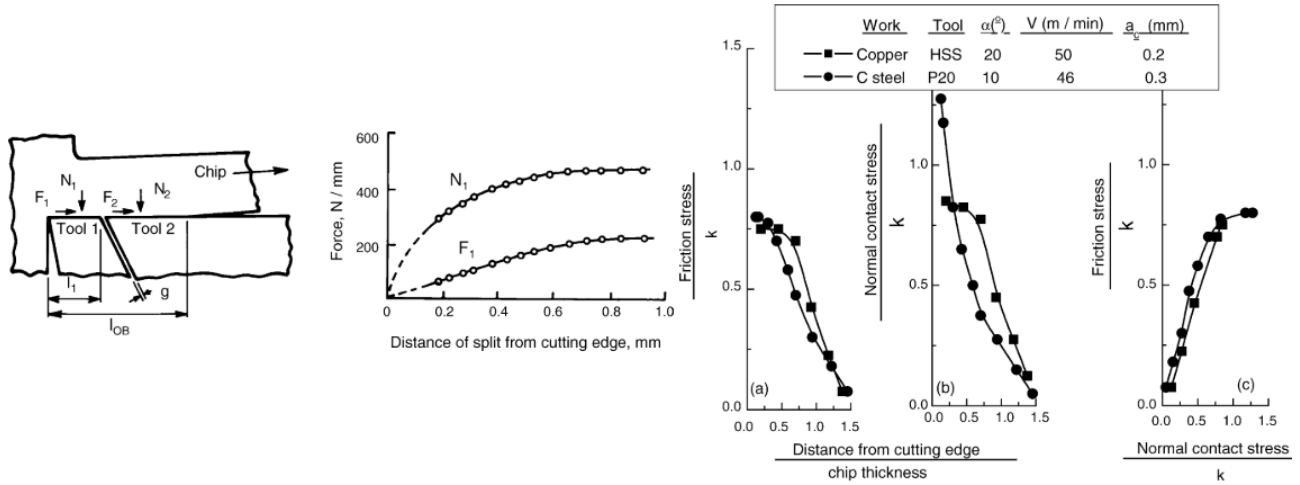


Figure 5.2.2: [105, Childs 2006] tool-split technique

[106, Ozel 2006] analysed the influence of friction models on cutting simulations outcomes of low carbon free cutting steel. They underline as the best way to describe the contact behaviour of the tool-chip couple is to directly measure the stresses, for example by split tool techniques. The best situation would be to consider the actual shear stress limit depending on the material flow stress  $\bar{\tau} = \bar{\sigma}/\sqrt{3}$ . Other models were developed to overcome sharp variations between the two laws: the Shirakashi friction model:

$$\tau_f = k \left( 1 - e^{-\frac{\mu \sigma_n}{k}} \right), \quad k \text{ material limit shear stress } (\bar{\tau})$$

and the Dirikolu friction model:

$$\tau_f = m \cdot k \left( 1 - e^{-\left(\frac{\mu \sigma_n}{m \cdot k}\right)^n} \right)^{1/n}, \quad 0 < m < 1, n \text{ coefficients}$$

Constant shear friction (1), constant shear and friction regions (Coulomb-Tresca) (2), variable shear friction as Dirikolu (3), variable friction depending on normal stress from split tool techniques (4) and variable shear plus variable friction with given predetermined lengths (5) were compared with orthogonal cutting simulations.

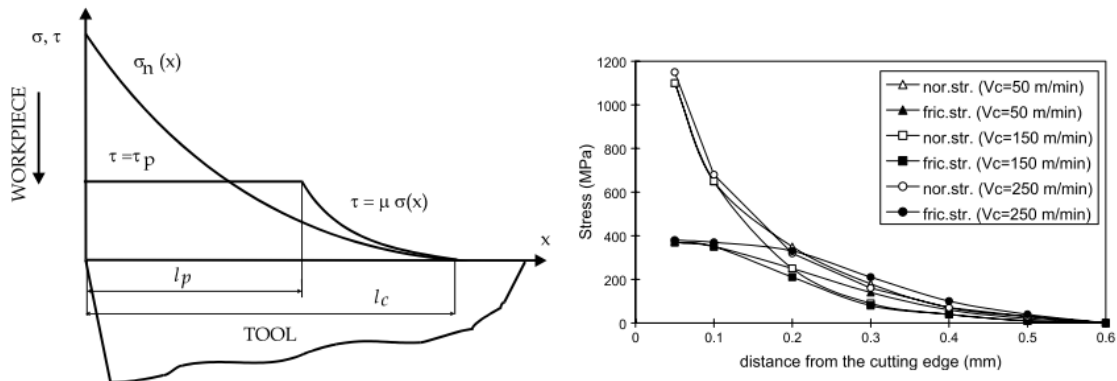


Figure 5.2.3: [106, Ozel 2006] normal and shear stress on tool rake face, left: idealized scheme, right: tool split test

Model (3) and (4) gave the best prediction of feed force, temperature and shear plane angle at 50,150,250m/min. However, cutting force was much overestimated apparently due to a low accuracy in the material model in describing thermal softening effects.

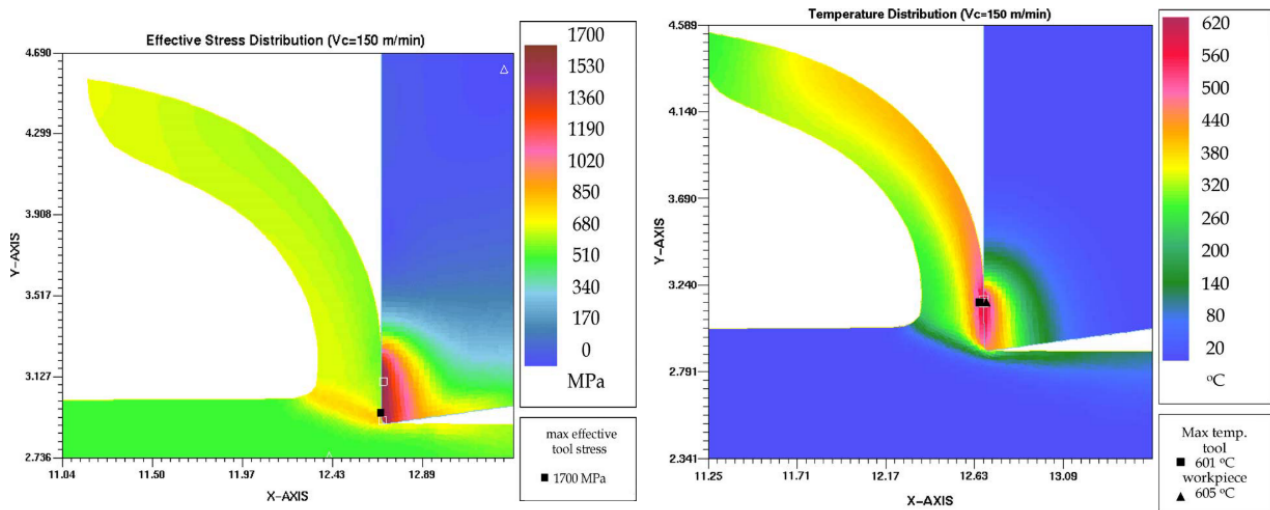


Figure 5.2.4: [106, Ozel 2006] Model 3 results

[107, Filice 2007] and colleagues critically analysed the performance of different friction models in cutting simulations. Constant shear friction, constant Coulomb friction, Coulomb-Tresca mixed model with constant coefficients (with and without predefined sticking length) and Dirikolu’s model. Feed force and chip thickness were underestimated, shear angle was overestimated. As no friction model influenced much the results, it leads to think that either the presented material model was inaccurate or the variation of the coefficient for some of the models was incomplete. Tool temperatures were compared by setting an initial conductance value, waiting for temperature convergence to a constant value in the 2D thermomechanical simulation, moving the boundaries to a 3D problem, calculating the thermal field in the insert and comparing it to the experiments. If the field did not match the simulation was run again with another conductance value.

Experimental results	Best results for each friction model						Predicted temperature in the tool				
	Models	$F_c$ (N)	$F_t$ (N)	$l_c$ (mm)	$t$ (mm)	$\phi$ (deg)	Models	$h$ (kW/m <sup>2</sup> K)	$T_{FEM}$ (°C)	$e$ (%)	
Cutting force $F_c$ (N)	745	I ( $m = 0.82$ )	780	462	0.25	0.20	26	I ( $m = 0.82$ )	1000	560	3.32
Thrust force $F_t$ (N)	600	II ( $\mu = 0.4$ )	761	430	0.26	0.20	27	II ( $\mu = 0.4$ )	10 000	551	1.67
Contact length $l_c$ (mm)	0.5	III ( $m = 0.5; \mu = 0.3$ )	749	425	0.34	0.19	27	III ( $m = 0.5; \mu = 0.3$ )	1 000 000	324	40.22
Chip thickness $t$ (mm)	0.29	IV ( $\mu = 0.2$ )	731	387	0.26	0.20	28	IV ( $\mu = 0.2$ )	10 000	443	18.27
Shear angle $\phi$ (deg)	19	IV ( $\mu = 0.4$ )	766	432	0.23	0.20	26	IV ( $\mu = 0.4$ )	10 000	551	1.67
Measured temperature (°C)	542	V	755	432	0.22	0.20	27	V	100	545	0.55

Figure 5.2.5: [107, Filice 2007] friction models comparison results

This lead to the average conductance value which guarantee the same thermal field in the insert, and couldn’t give results to discriminate for the goodness of the models. Indeed some of the models couldn’t converge at all. The authors claimed for the necessity of new friction and conductance model for the tool-chip interface. Moreover,

the article underlines the importance of starting with a good material model with low uncertainties, to fit a good friction model.

Another analysis for the performance of different cutting models was performed by [108, Haglund 2008] and teammates. They underline how previous studies found the friction stress to be almost constant for half of the tool-chip contact length, then decreasing to zero. The shear friction limit depending on the material flow stress. AISI 4140 was simulated with predefined chip free to evolve to the final shape. This allowed for convergence in  $1.6ms$ . Constant Coulomb model, two zone constant Coulomb friction, shear limit and Coulomb friction and three new temperature dependent friction models were implemented:

- Temperature dependent friction model: 
$$\mu(T) = \begin{cases} 1 & T < T_1 = 625^\circ C \\ 1 - \frac{T-T_1}{T_m-T_1} & T_1 < T < T_m \end{cases}$$
- Temperature dependent shear stress limit, depending on yield, plus constant friction coefficient: 
$$\tau_{lim}(T) = \sigma_y(T), \quad \tau_f = \begin{cases} \mu\sigma_n & \mu\sigma_n < \tau_{lim}(T) \\ \tau_{lim}(T) & \mu\sigma_n > \tau_{lim}(T) \end{cases}$$
- Temperature dependent friction coefficient plus constant shear limit: 
$$f(T), \quad \tau_f = \begin{cases} \mu(T)\sigma_n & \mu(T)\sigma_n < \tau_{lim} \\ \tau_{lim} & \mu(T)\sigma_n > \tau_{lim} \end{cases}$$

Cutting forces and feed forces were best estimated by the double Coulomb model, the temperature dependent Coulomb friction model and the limited shear stress at  $400MPa$ . Chip thickness was guessed by all models. This confirms the findings of [107, Filice 2007] that the chip thickness depends more on the material model than the friction conditions. The best model proved to be the thermal dependent friction coefficient, however the model is non-physical, as the friction coefficient for small normal pressure and temperatures approaches 1.

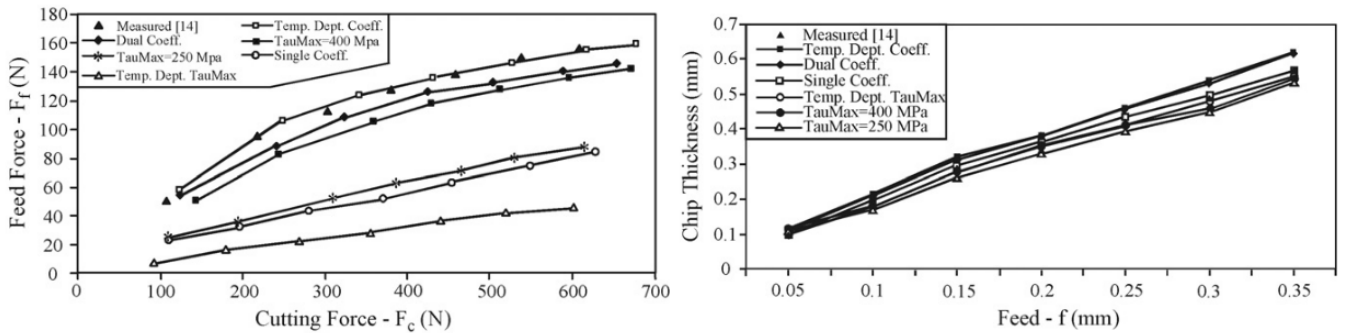


Figure 5.2.6: [108, Haglund 2008] friction models results

[109, Shi 2009] and Attia carefully analysed the contact phenomena between tool and chip, considering friction and thermal aspects. It is standard procedure to set a nonphysical large value to the interface conductance so to promote fast thermal convergence, however the conductance depend on contact nature and influence the thermal profile of the interface. A complex micro-mechanical friction model was implemented

to predict the interface conductance. For the friction coefficient they adopted a normal pressure distribution and the Shirakashi model. However the model performed almost like a constant Tresca model with  $m = 0.9$ . The article proves how is possible to gain marginal improvements with intricate contact models, at the price of strong efforts.

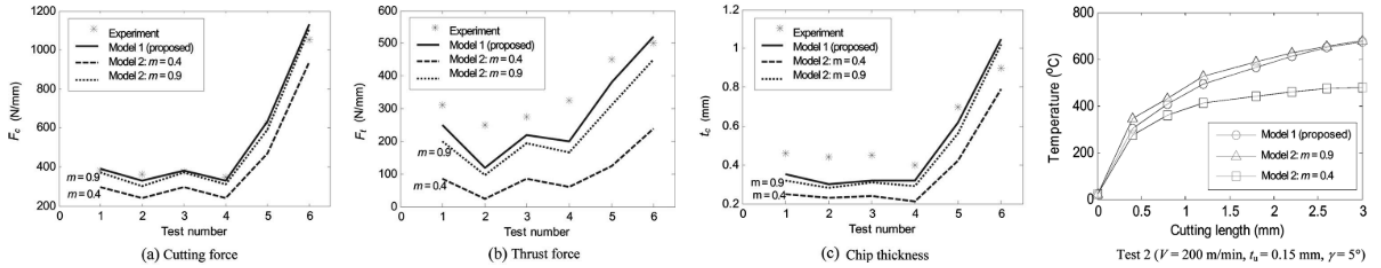


Figure 5.2.7: [109, Shi 2009] friction model results

[110, Arrazola 2010] and Ozel evaluated the performance of different friction models in cutting simulations. They varied the shear limit stress of the Tresca shear friction model from 200 to 700 MPa modeling orthogonal cutting of AISI 4340. For the sliding region  $\mu = 0.48$  was considered, when the shear stress reaches the limit it become then constant, being illogically for it to go beyond the strength of the material. Larger shear limit factors resulted in better force predictions. The normal pressure to the rake was similarly predicted by all models. The authors suggested also that the limit shear stress could also be calculated with the material model, depending on temperature, strain and strain rates. By calculating the limit shear stress with  $T = 1000^{\circ}C, \varepsilon = 4, \dot{\varepsilon} = 10^5$  they obtained a shear stress flow limit of 400 MPa which agreed with the limit flow stress for good prediction of forces.

Test no.	FE modeling technique		Simulated							Experimental		
	Limit shear stress ( $\tau_{limit}$ )	Model boundaries	$T_{tool}$ (K)	$T_{chip}$ (K)	$\sigma_n$ (MPa)	$\tau$ (MPa)	$F_c$ (N/mm)	$F_t$ (N/mm)	$t_c$ (mm)	$F_c$ (N)	$F_t$ (N)	$t_c$ (mm)
1	Unlimited	Eulerian	1503	1543	2720	1005	500	204	0.39	514	204	0.33
2	200	Eulerian	1200	1222	2727	222	455	133	0.37			
3	300	Eulerian	1399	1429	2703	373	473	165	0.38			
4	400	Eulerian	1501	1543	2551	476	491	197	0.38			
5	500	Eulerian	1504	1545	2481	500	497	209	0.39			
6	600	Eulerian	1504	1544	2396	601	499	207	0.39			
7	700	Eulerian	1503	1543	2514	766	500	205	0.39			
8	Unlimited	Lagrangian	1579	1608	1880	211	529	178	0.24			
9	200	Lagrangian	1381	1437	1533	210	455	122	0.27			
10	300	Lagrangian	1561	1617	1619	210	507	176	0.28			
11	400	Lagrangian	1534	1595	1574	227	514	174	0.27			
12	500	Lagrangian	1572	1633	2272	226	525	210	0.29			
13	600	Lagrangian	1501	1574	1920	220	532	192	0.30			
14	700	Lagrangian	1527	1583	1679	213	584	200	0.31			

Figure 5.2.8: [110, Arrazola 2010], simulation results for different shear limit values and mesh strategies

The article proves how stick and slip models are more accurate, but the shear limit must depend on the material model.

[111, 112, Molinari 2011, Molinari 2012] and coworkers analysed extensively the contact



characteristics for orthogonal metal cutting. With the aid of simulations and analytical models they shown how friction become gradually sticking with increasing cutting speed due to the decrease of material flow stress at high temperature. The decrease in the mean friction coefficient on the rake face is evident only if sticking is present, as temperature decrease the flow stress. Thermal softening influence is also studied in term of inelastic heat fraction coefficient variation. In the latter study they concentrated on tool stresses. Sticking contact is promoted by larger friction coefficients, for low friction coefficients the shear stress is not higher than the shear flow stress of the material, so sticking is not activated. Temperature rise in the sticking region, reaches a peak in the transition region and lowers in the sliding region, as a result of the mutual effect of deformation heat, friction heat and chip drag.

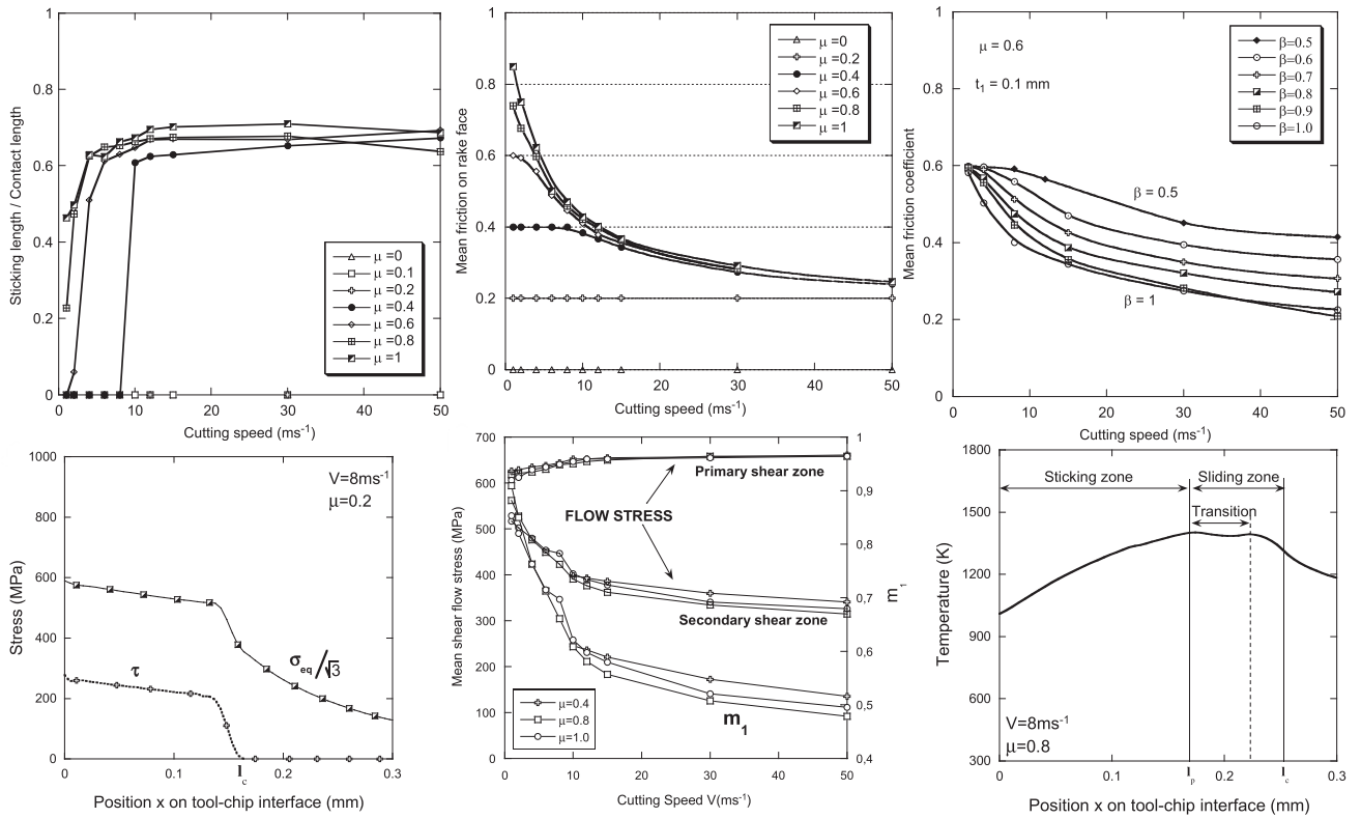


Figure 5.2.9: [111, 112, Molinari 2011, Molinari 2012] synthetic findings for friction behaviour

The articles are an example on how to combine analytic and numeric methods to understand complex phenomena. However, they are at the same time exhaustive and exhausting to be read. Moreover their range of speed is extremely out of industrial practice ( $1 \div 50 \text{ m/s} \Rightarrow 60 \div 3000 \text{ m/min}$ ).

[113, Ulutan 2013] and Ozel undergo an extensive analysis on the contact conditions between workpiece, tool and chip during cutting processes. Insert rounded edges and flank wear were considered, complete stress analytic evolution along tool interface were built. Also flank wear and change in the geometry of the tool was taken into account. For the complete mathematical expression the Author suggest to look directly at the source.

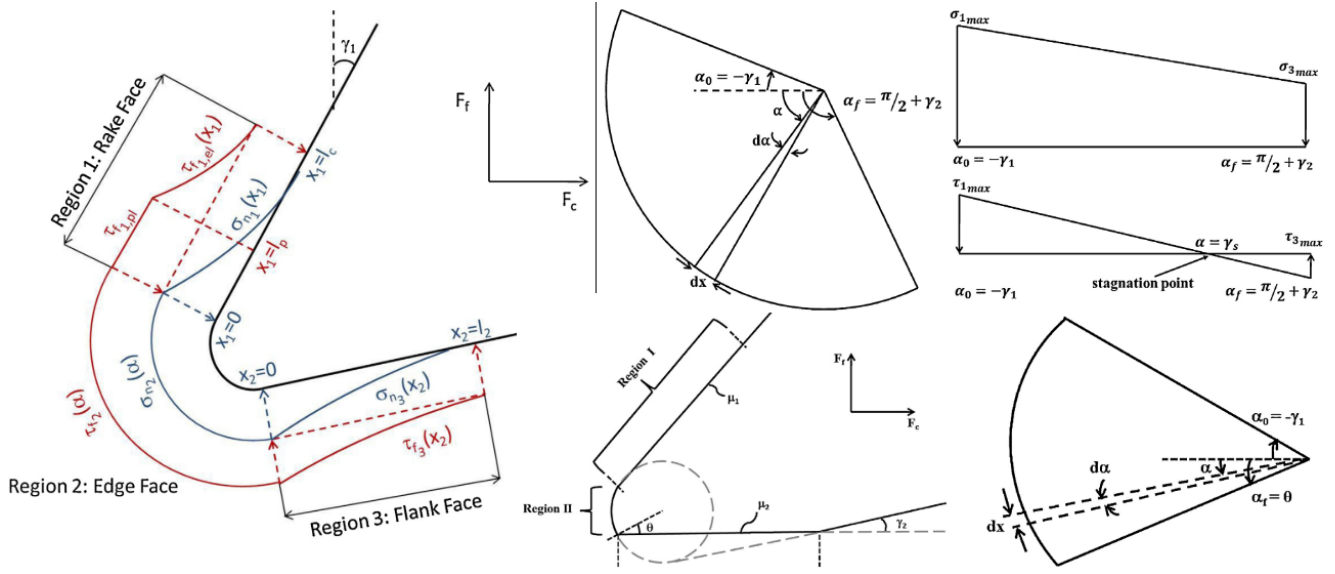


Figure 5.2.10: [113, Ulutan 2013] model scheme

- Along the rake face:  $0 < x < l_{rake}$

$$\sigma(x) = \sigma_{max,rake} \left(1 - \frac{x}{l_{rake}}\right)^n, \quad \tau(x) = \begin{cases} \mu_{rake} \cdot \sigma(x) & \mu_{rake} \cdot \sigma(x) < m \cdot \tau_{lim} \\ m \cdot \tau_{lim} & \mu_{rake} \cdot \sigma(x) > m \cdot \tau_{lim} \end{cases}$$

- For the tool tip:  $-\gamma_{rake} < \alpha < \pi/2 + \gamma_{flank}$

$$\sigma(\alpha) = \frac{(\sigma_{max,flank} - \sigma_{max,rake})\alpha + [\gamma_{rake} \cdot \sigma_{max,flank} + (\pi/2 + \gamma_{flank})\sigma_{max,rake}]}{\pi/2 + \gamma_{rake} + \gamma_{flank}}$$

$$\tau(x) = \frac{(\tau_{max,flank} - \tau_{max,rake})\alpha + [\gamma_{rake} \cdot \tau_{max,flank} + (\pi/2 + \gamma_{flank})\tau_{max,rake}]}{\pi/2 + \gamma_{rake} + \gamma_{flank}}$$

The stagnation angle given by:  $\alpha_s = \frac{(\pi/2 + \gamma_{flank})\tau_{max,rake} - \gamma_{rake} \cdot \tau_{max,flank}}{\tau_{max,rake} - \tau_{max,flank}}$ . When tool wear is present the final angle changes, and so the stresses at the border:

$$\theta = \gamma_{flank} + \arcsin\left(1 - \frac{VB \sin \gamma_{flank}}{r_{edge}}\right), \quad \alpha_s = \frac{\theta \tau_{max,flank} - \gamma_{rake} \tau_{edge}}{\tau_{max,flank} - \tau_{edge}}$$

$$\vec{\sigma}_{edge} + \vec{\tau}_{edge} = \vec{\sigma}_{max,flank} + \vec{\tau}_{max,flank} \implies \begin{cases} \sigma_{edge} = \sigma_{max,flank} (\mu_{flank} \sin \theta - \cos \theta) \\ \tau_{edge} = \tau_{max,flank} (\mu_{flank} \cos \theta - \sin \theta) \end{cases}$$

$$\sigma(\alpha) = \left(\frac{\sigma_{edge} - \sigma_{max,rake}}{\gamma_{rake} + \theta}\right) (\alpha + \gamma_{rake}) - \sigma_{max,rake}, \quad \tau(\alpha) = \left(\frac{\tau_{edge} - \tau_{max,rake}}{\gamma_{rake} + \theta}\right) (\alpha + \gamma_{rake}) - \tau_{max,rake}$$

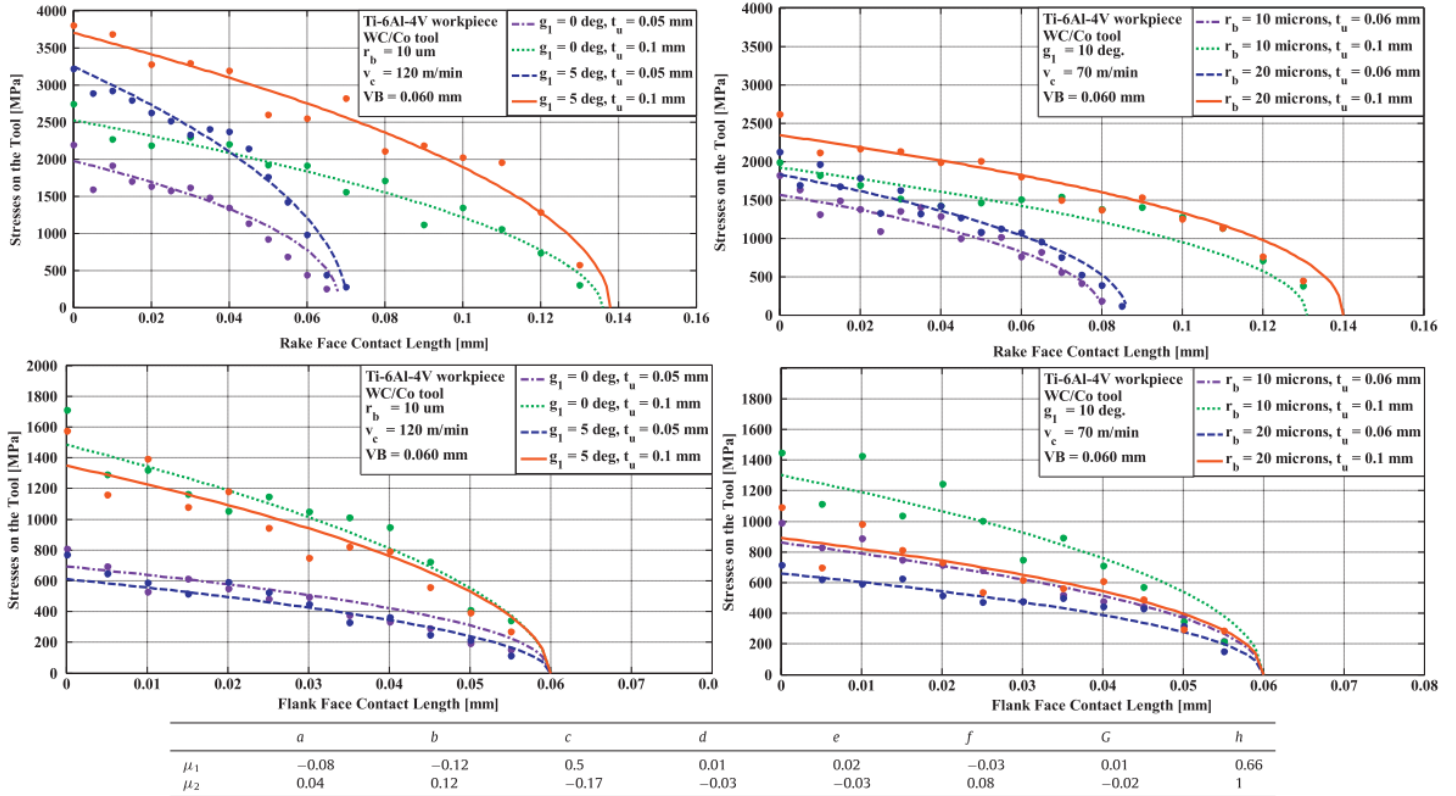
with the constraints:  $2 \sin(\gamma_{flank}) < \frac{VB}{r_{edge}} < 1 + \frac{1}{\sin(\gamma_{flank})}$  to be able to calculate  $\theta$ , and  $\mu_{flank} < \frac{1}{\tan \theta}$  for the stagnation point to be on the edge;

- For the flank face, spring back is neglected, the contact length is equal to the flank wear:  $0 < x < VB$

$$\sigma(x) = \sigma_{max,flank} \left(1 - \frac{x}{VB}\right)^m, \quad \tau(x) = \begin{cases} \mu_{flank} \cdot \sigma(x) & \mu_{flank} \cdot \sigma(x) < m \cdot \tau_{lim} \\ m \cdot \tau_{lim} & \mu_{flank} \cdot \sigma(x) > m \cdot \tau_{lim} \end{cases}$$

All geometrical quantities are known but for the tool-chip contact length on the rake  $l_{rake}$ , normal pressure distribution must be guessed  $\sigma_{max,i,n,m}$ , the friction coefficients  $\mu_{rake}, \mu_{flank}$  must be determined. From experiments, forces and wear are deduced, then  $l_{rake}, \sigma_{max,flank}, \sigma_{max,rake}, \mu_{rake}, \mu_{flank}, n, m$  are guessed and iteratively updated to obtain the cutting forces. This is only the first part a larger iteration cycle, as then the friction coefficients are fed to a FEM simulation, stress distributions are extracted and  $\sigma_{max,flank}, \sigma_{max,rake}, n, m$  are used for the next iteration to find  $\mu_{rake}, \mu_{flank}$ .

Alloy	A [MPa]	B [MPa]	n	C	$\dot{\epsilon}_0$	m	D	p	R	s
Ti-6Al-4V	1000	625	0.55	0.029	$10^{-5}$	0.995	0.48	0	1.2	2.7
IN-100	1350	1750	0.65	0.017	$10^{-3}$	1.3	0.6	0	1.0	5.0



$$\mu_1 = a_1 v_c + b_1 t_u + c_1 r_\beta + d_1 v_c t_u + e_1 v_c r_\beta + f_1 t_u r_\beta + g_1 v_c t_u r_\beta + h_1$$

$$\mu_2 = a_2 v_c + b_2 t_u + c_2 r_\beta + d_2 v_c t_u + e_2 v_c r_\beta + f_2 t_u r_\beta + g_2 v_c t_u r_\beta + h_2$$

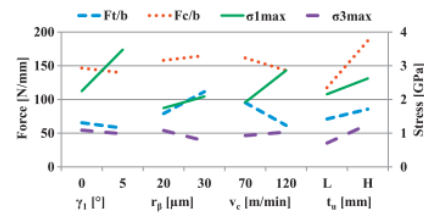


Figure 5.2.11: [113, Ulutan 2013] tool stress and friction model results

A Calamaz-modified JC model was adopted for Inconel 100 and Ti6Al4V. The tool

was considered rigid until chip formation ( $1 \div 1.5 \text{ ms}$ ) and then changed to deformable until internal stresses convergence ( $0.1 \text{ ms}$ ). Two edge radii, rake angles and variable speeds were simulated. Finally a fitting formula for the friction coefficient as a function of speed, uncut chip thickness and edge radii was given.

Rake maximum stress is higher at larger speed, feed, edge radii and rake angle. For the flank normal stress the speed is almost insignificant, while higher feed increases the stress but both raise in the rake angle and edge radius reduce tool solicitation. The article is an excellent example of synergy between analytic and FEM models which provide reliable data for future speculations.

[114, Atlati 2014a] and coworkers developed a new modeling technique for tool-material interface in cutting simulations. The heat partition between tool and chip is overcome by considering the conductance, depending on pressure, temperature and sliding speed. The heat generated by plastic deformation through the inelastic heat fraction coefficient is transferred to the tool depending on the local conductance:

$$q_{plastic} = \eta_{pl} \int \bar{\sigma} \cdot \dot{\varepsilon} d\varepsilon, \quad q_{pl-tool} = k(T_{wp} - T_{tool})$$

The heat generated by friction at the interface needs to be partitioned:

$$q_{friction} = \eta_{fric} \cdot \tau_f \cdot v_{sl}, \quad q_{fric-tool} = \alpha(\sigma_n, T_{int}, v_{sl}, \alpha_{theo}) \cdot q_{friction}$$

Heat partition coefficient was obtained through cutting tests, depending on sliding speed, conductance was iteratively guessed. However, no experimental temperature measurement was compared with the numerical results.

## 5.2.2 Friction determination for cutting simulations

For what concerns lubricating action of cutting fluids, the situation is even more confused. Generally cutting forces are used to deduce friction forces, so determining a better-or-worse friction performance. We have already explained as this can be misleading. Other researchers prefer using tribometers.

Tribometers are devices able to reproduce contact conditions between sliding bodies getting rid of disturbs. To be suitable for a cutting simulation, friction evaluation must be carried out on a tribometer able to reproduce the average pressures ( $> 1 \text{ GPa}$ ), temperatures ( $> 700^\circ \text{C}$  for dry cutting) and sliding velocities ( $0 \rightarrow V_{cut}$ ) developing in a real cutting process. Moreover, the work material surface must be fresh or refreshed. A problem related to high pressures stays in the impossibility to avoid the deformation of bodies. Therefore, the friction coefficients will be the result of sticking, sliding and work material deformation. With tribometers, only macroscopic friction coefficients can be obtained.

[7, Hong 2001d] and colleagues used a 3D force decomposition model in turning for the determination of the friction coefficient during cutting a Ti-alloy. The model consisted in the projection of the cutting, feed and thrust forces over the chip flow direction. By consequent projections and measurement of the chip flow inclination angle  $\beta$  looking at insert wear after machining (dependent on the influence of nose radius), they could determine the friction coefficient by a ratio between normal and tangential force on the rake surface, . The model however neglected flank friction, a simplification that was said to be applicable for unworn inserts.

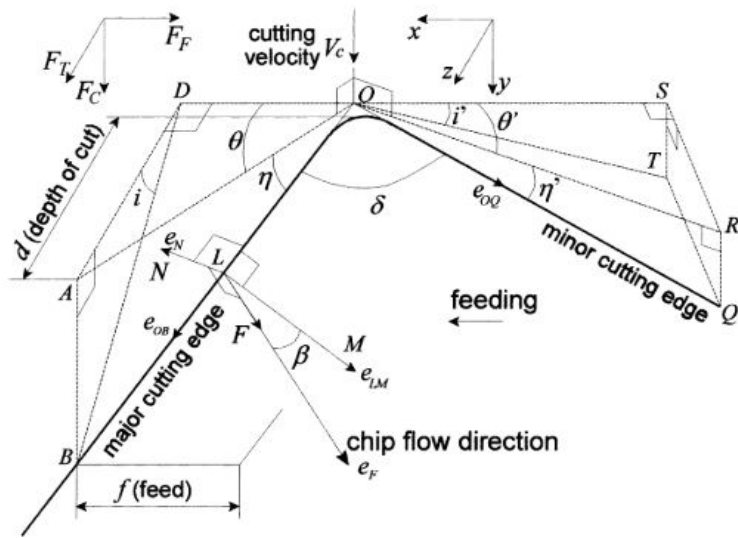


Figure 5.2.12: Friction model used to determine friction from overall cutting forces, [7, Hong 2001d]

[115, Hong 2002] et al. reported that the friction coefficient in case of cryogenic cooling decreased also thanks to the possibility of vapour expanding in the gaps in between the bodies. They developed a tribometer that could be mounted on a lathe capable of providing the same average contact pressure of the cutting process. For AISI 1018 they found that the average friction coefficient can be lowered at low normal load with an high pressure liquid nitrogen jet (24bar), but at high load it almost resemble dry cutting. For Ti6Al4V LN2 high pressure jets still presented the same trend (more effective at low load, less at high load) but its performance was better than emulsion and dry cutting, for the ability of removing heat and reducing adhesion and build up edges. Low pressure jet (6.5bar) performs like dry cutting.

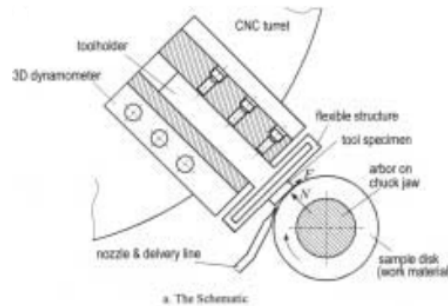


Figure 5.2.13: [115, Hong 2002] tribometer

Some problems regarding the tribometer are the non-refreshed surface and the wrong positioning of the LN2 nozzle: there is not a real cutting process in which the cutting fluid is dragged toward the cutting zone. The geometrical and dynamic resistance developing in the rake-chip and work-flank crevices are here in favour of the fluid action while in cutting they are against its spreading in the affected zones.

[116, Jun 2005] and colleagues proved with vector manipulation, force projection and geometrical relations that friction coefficient in case of cryogenic cooling with rake&flank

microdelivery ([70, 13, Hong 2001a&c]) was lower than emulsion and dry cutting. The problem of using macroscopic cutting forces is that we cannot separate the material property variation and the friction variation. It is however clear that cryogenic cooling has a friction reduction effect, which is hardly due to a lubrication property, since for a high volatile fluid in contact with hot surface it will be unlikely to form a lubricating film, but is probably due to material property alteration.

[117, Hong 2006] et al. wanted to analyze if cryogenic Nitrogen improved friction was due to an alteration of physical properties of materials or the result of a lubricating action. Probably to separate the material property alteration from the study, the normal forces were reduced, the heat build up due to friction was therefore limited, the sliding speed was reduced as well. Several tribometers were built in order to study the effect of tool back cooling, workpiece cooling and jet cooling. The jet was positioned (wrongly) still at ease of penetration thanks to the rotation of the disk. Still the tribometers do not supply fresh surfaces to the friction zone. What is investigated here is the low load friction coefficient in case of hydrodynamic induced lubrication of LN2, which is completely not what happens in cutting, unless by the very last portion of chip detaching from the rake. The interesting discovery is that coated tools may exhibit worse behaviours with LN2. However, no conclusion can be extrapolated for cutting conditions.

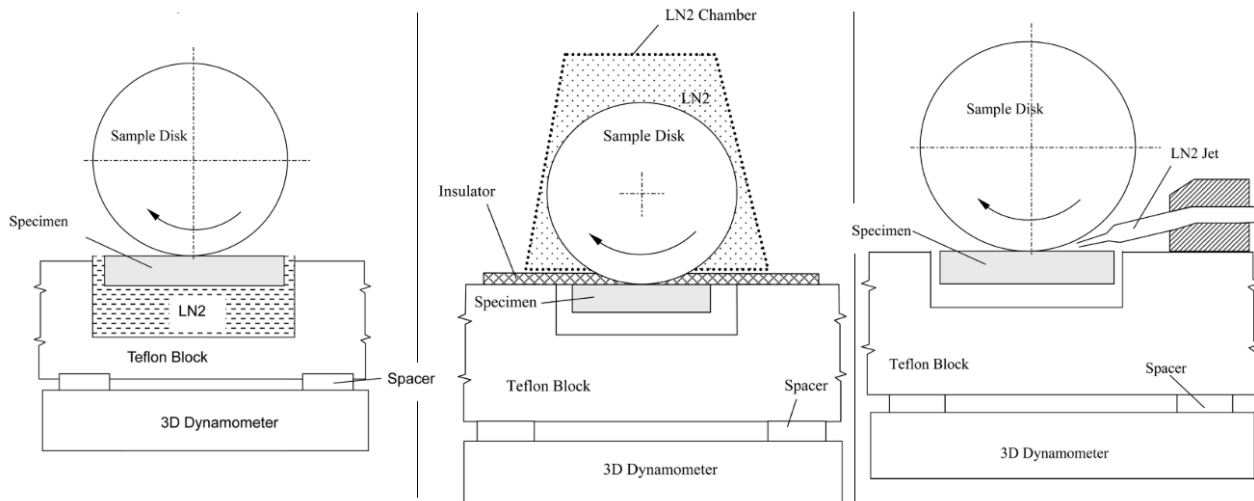


Figure 5.2.14: [117, Hong 2006] tribometers

[118, El-Tayeb 2009] and colleagues made an exhaustive evaluation of the friction coefficient for Ti6Al4V and Ti5Al4V against WC in dry and cryogenic jet conditions. They studied the dependence on speed, load and sliding time:  $\mu = f(v, N, t)$  and their mutual effects. However, the loads were rather low, and no indications were given to arrive at the applied normal pressure, therefore the results are hardly applicable to a cutting environment. Cutting speeds were also limited to less than  $60\text{m}/\text{min}$  and the sliding surface was not refreshed on the work material side. Moreover, LN2 jet was dragged by the favourable rotation of the work material disc. Nevertheless, the article set the challenge for the determination of the friction coefficient based on local normal pressure, temperature and sliding velocity.

[119, Arrazola 2008] et al. investigated a new approach for deriving the average friction coefficient through orthogonal cutting tests. Merchant provided a simple relation for calculating the friction coefficient:

$$\mu = \operatorname{tg} \left[ \operatorname{tg}^{-1} \left( \frac{F_f}{F_t} \right) + \gamma \right], \quad \gamma \text{ rake angle}$$

Albrecht considered the linear portion of the feed and cutting force graph in variable undeformed chip thickness:

$$\mu = \operatorname{tg} \left[ \operatorname{tg}^{-1} \left( \frac{dF_f}{dF_t} \Big|_{\text{linear zone}} \right) + \gamma \right]$$

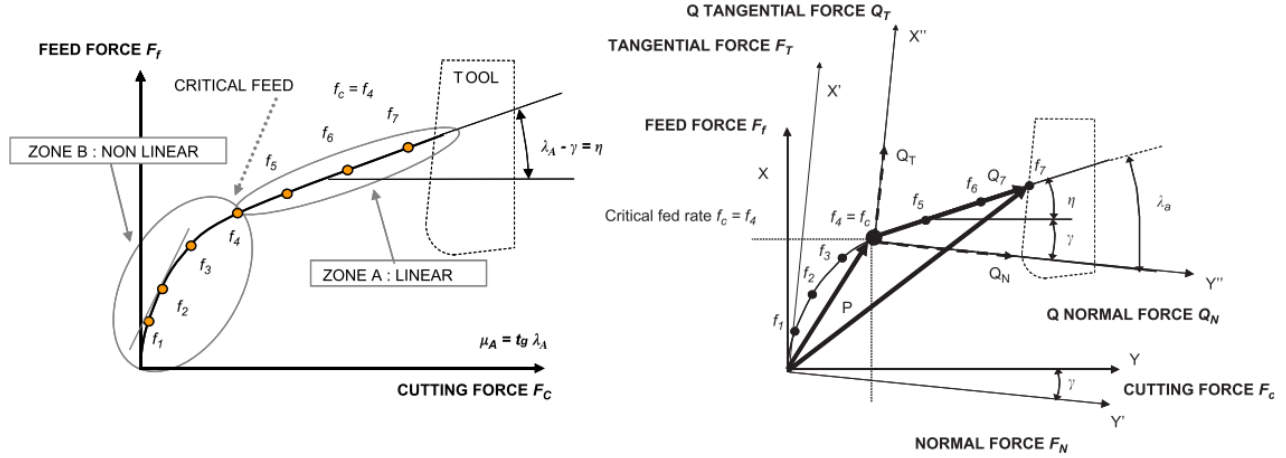


Figure 5.2.15: [119, Arrazola 2008] decomposition of forces for friction determination

The friction coefficient were then experimentally obtained for AISI 4140 steel. Simulations were carried out for variable feed and cutting, feed forces and chip thickness was evaluated. While chip thickness and cutting forces were very well predicted, feed force was lower. Trying to improve the results, two additional friction models were adopted. One considering variable friction coefficient until the linear zone, obtained deriving the expression also for the non linear zone. For the rest of the contact length, depending on the start of the linear zone, a constant friction coefficient obtained with the first method were adopted. The second model considered a variable friction coefficient calculated over the whole contact length with the same expression. Results with this two models concerning feed forces were improved.

The article proves that is possible to improve simulation results with a good material model and an experimentally based friction model, accounting for the friction variability along the nose and rake face.

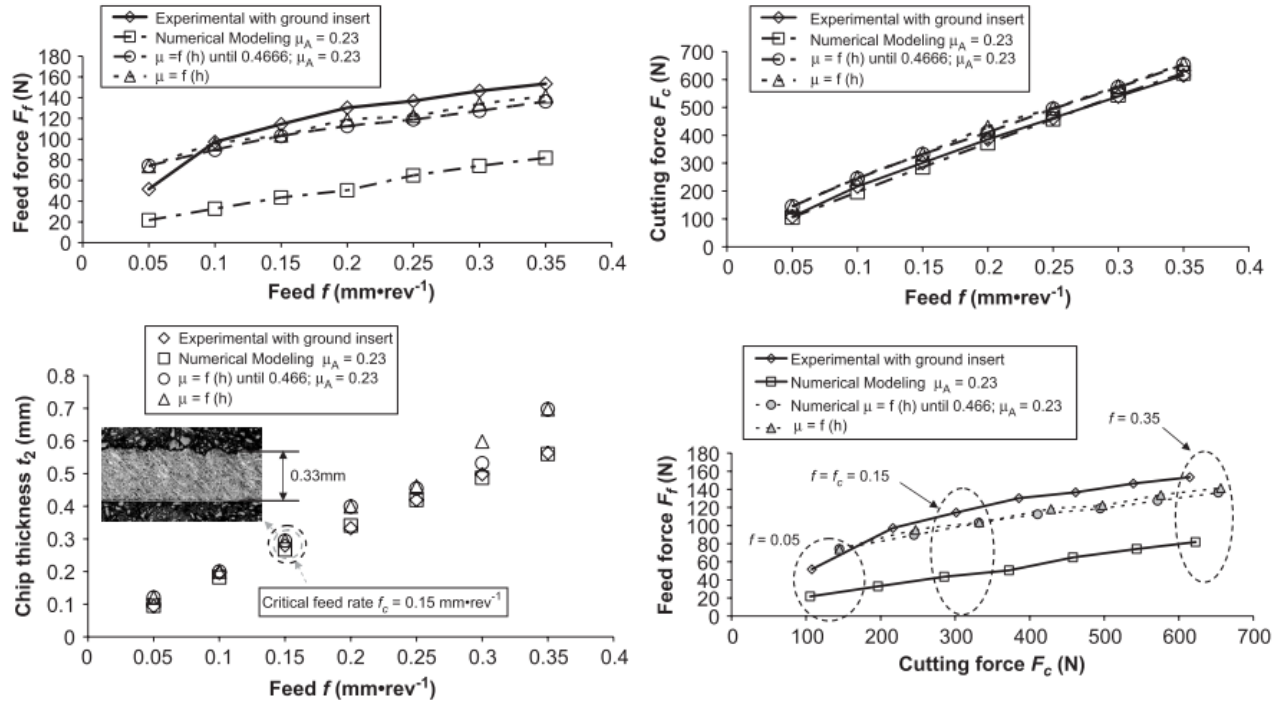


Figure 5.2.16: [119, Arrazola 2008] result of constant, semi-constant and variable friction coefficient models

[120, Bonnet 2008a] and colleagues studied friction behaviour of AISI 316 L steel against carbide tools with a pin on rod tribometer. Numerical FEM simulations were carried out to separate the adhesive friction coefficient from the plastic one, as the experiment give the macroscopic sum of the two effects:  $\mu_{app} = \mu_{adh} + \mu_{plast}$  with  $\tau_{friction} = \mu_{adh} \cdot \sigma_n$ . The heat coming from plastic deformation was one order of magnitude lower than the heat produced by friction and remained almost fully in the workpiece. The friction power toward the pin was measured and the experimental heat partition coefficient alpha was calculated:  $P_{pin} = \tau_{friction} \cdot v_{sl} \cdot \alpha$ . The experimental heat partition coefficient was found profoundly different than the theoretical one disregarding the chip speed:  $\alpha_{theo} = \frac{\sqrt{\rho_{pin} \cdot c_{pin} \cdot k_{pin}}}{\sqrt{\rho_w \cdot c_w \cdot k_w} + \sqrt{\rho_{pin} \cdot c_{pin} \cdot k_{pin}}}$ ,  $w$ : workpiece. The adhesive friction and heat partition coefficients were plotted as a function of the average local sliding speed found by the FEM, and as a function of the average interface temperature on the workpiece side, in his turn depending on the sliding speed. In [121, Bonnet 2008] they evaluate the performance of a sliding speed dependent friction coefficient in machining simulations of AISI 316L. The average friction coefficient was modified by the sliding speed:

$$\mu = r \cdot v_{sl} + \mu_{max}, \quad \mu_{max} = 0.4, r = -2 \cdot 10^{-3}$$

It is known that accurate prediction of friction coefficient does not influence much cutting forces, dependent mainly on the material model, but cutting interface temperature distributions. However, no comparison on temperature was done in the article.



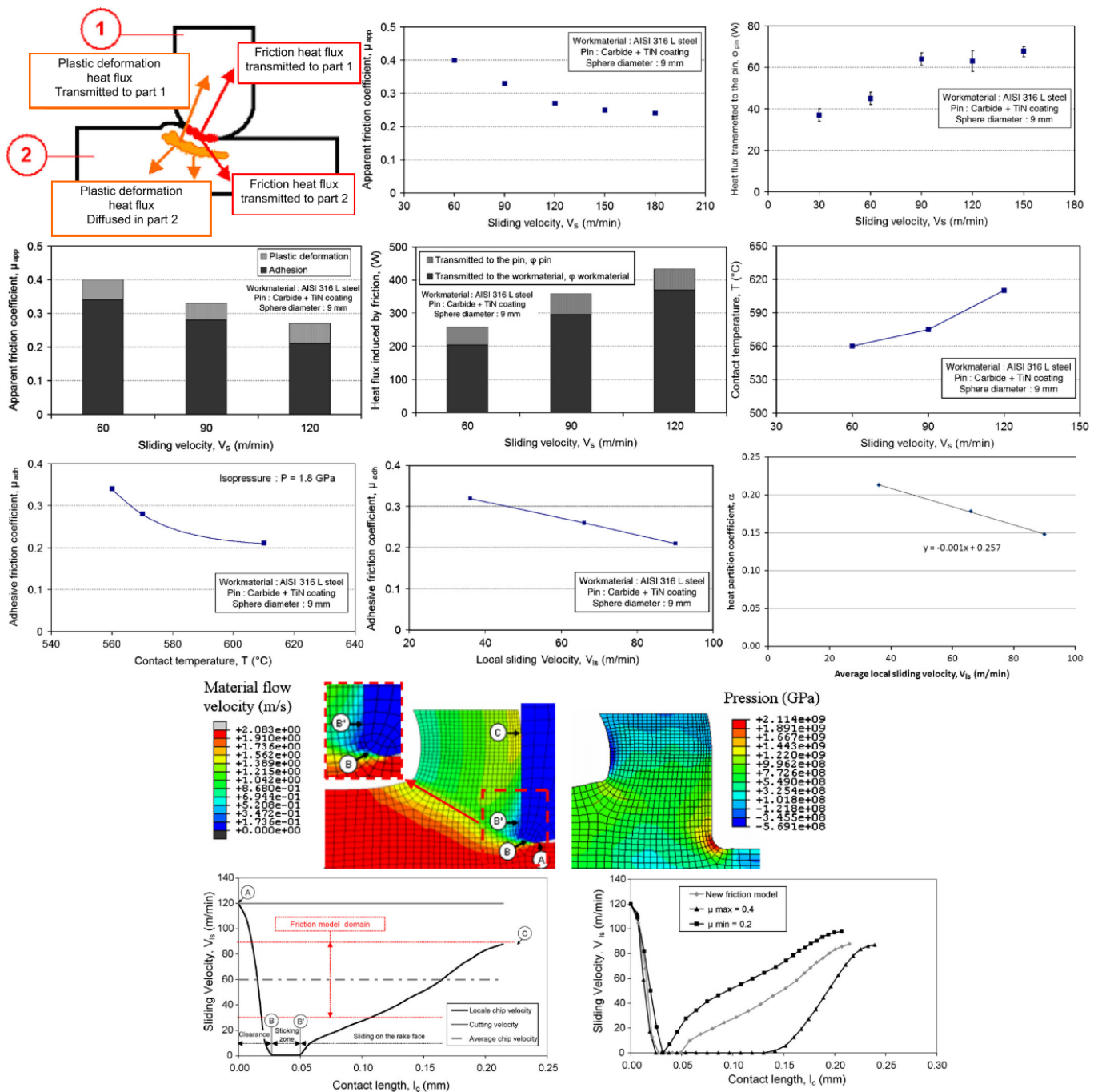


Figure 5.2.17: [121, 120, Bonnet 2008] friction models results

[122, Egana 2012] and teammates analysed the problem of the characterization of contact properties while cutting Ti6Al4V: friction and heat partition coefficients. The authors disapproves measuring the friction coefficient through cutting tests as they approximate the rake as flat, the tool as sharp and no contact on the flank. Moreover, as many authors said that the variation of the friction coefficient doesn't influence much the cutting forces, it is of no sense to calculate the coefficient from cutting forces. Material pair and lubrication fixed, contact properties depend on: sliding speed, temperature (depending on shear zone and sliding velocity) and pressure. Therefore a tribometer should be able to reproduce a wide range of speed and pressures. As roughness in-

fluence the problem, the sliding pair should be highly polished. They used a pin on rod technique, providing fresh surface to the friction region, with average pressures and temperatures similar to cutting processes. They also measured the heat transferred to the pin, then by considering the heat produced in the process as the total dissipated power:  $Q = F_f \cdot v$ , they calculated the partition coefficient toward the tool. Average pressures applied were in the range of 0.75, 1.3, 1.5 GPa.

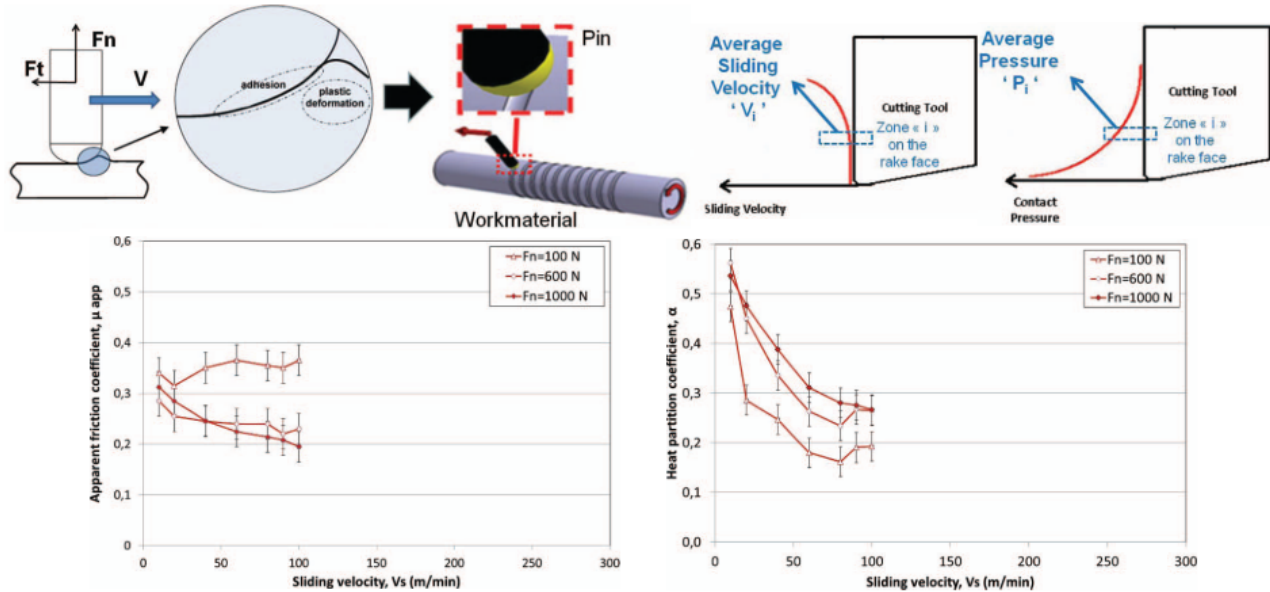


Figure 5.2.18: [122, Egana 2012] dry friction and heat partition coefficients for Ti6Al4V

The average friction coefficient is found to decrease with higher pressure, while the heat partition coefficient increases. Higher speed correspond to lower average friction and heat partition, for pressure high enough, while at low speed the coefficients are almost similar for every pressure. The authors suggest a threshold pressure and speed beyond which adhesion begun to be important, the low pressure friction being most representing sliding, the high pressure one also including sticking phenomena. With this data a variable average friction coefficient as a function of pressure and speed could be implemented in FEM simulations. Average friction was also seen to get little lower by the application of emulsion, but no further analysis in variable pressures have been done.

[123, Puls 2012] and colleagues presented a new tribometer design able to provide fresh surface and required pressure, velocity and temperature representative of the cutting process, being cheap and easy to implement on a lathe. It consisted of a grooving tool against a rotating disk, only pushing the material of the disc. However, just a portion of rotation can be performed, and high speed friction test need quick positioning and retracting devices. Moreover, no thermal steady state can be achieved. They obtained graphs with variable forces, temperature (thanks to a two color pyrometer) and calculated friction coefficient. Despite the variation of forces both temperature and friction coefficient remain almost constant. At low speed, AISI 1045 experience intense sticking phenomena.

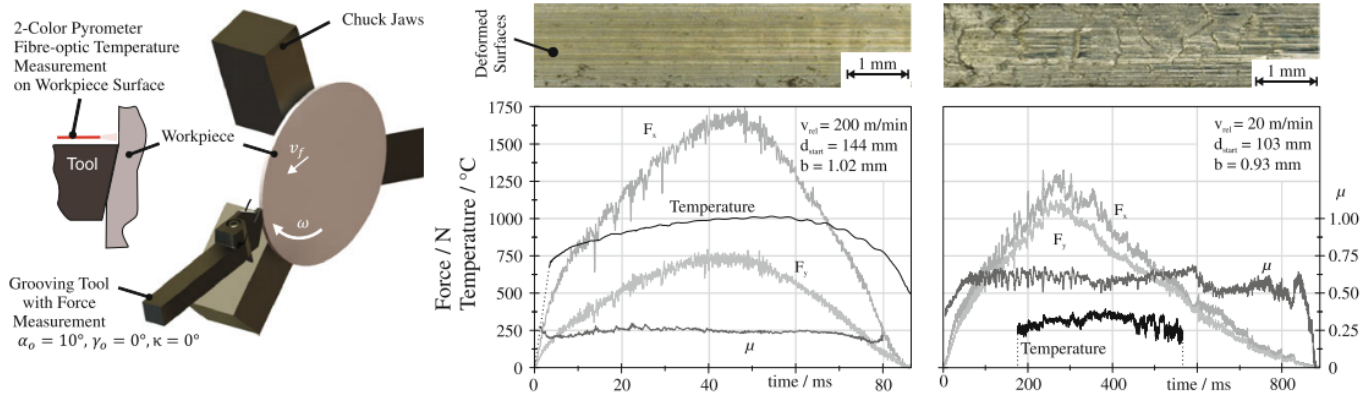


Figure 5.2.19: [123, Puls 2012] new tribometer design results

[19, Courbon 2013] and his team also analysed the variation of friction and heat partition coefficients as a function of speed, with dry and cryogenic machining. Ti6Al4V didn't exhibit a variation in the average friction coefficient from cryogenic to dry conditions, while the heat partition coefficient lowered for cryogenic. Inconel 718 proved a small reduction of average friction coefficient and the heat transmitted toward the tool was definitely smaller.

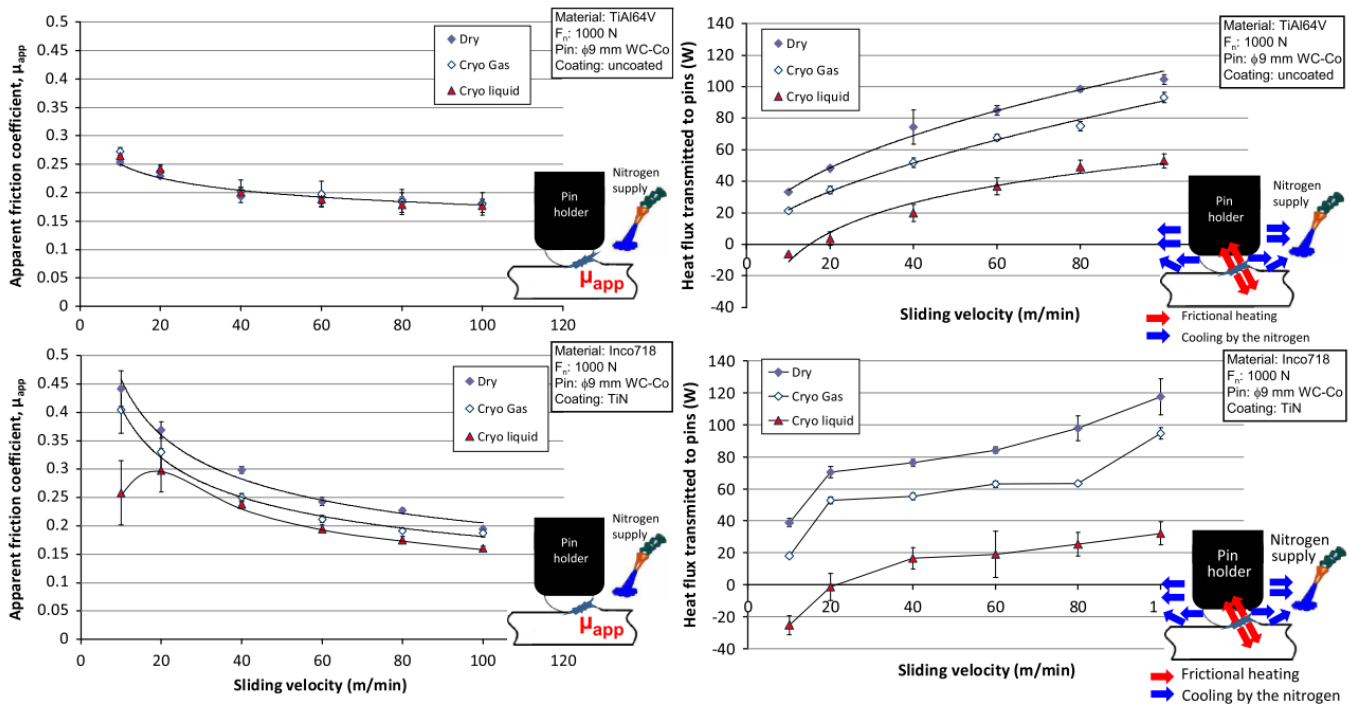


Figure 5.2.20: [19, Courbon 2013] friction and heat partition coefficients in variable cutting speed

[124, Rech 2013a] and colleagues analysed the heat partition and friction coefficient by means of a pin on rod open tribometer for different materials. Friction and heat partition coefficients were also fitted in cutting speed. Constant and speed-variable models were implemented in 2D orthogonal cutting simulation of AISI 1045 steel. The variable model giving much better results in particular regarding heat exchange.

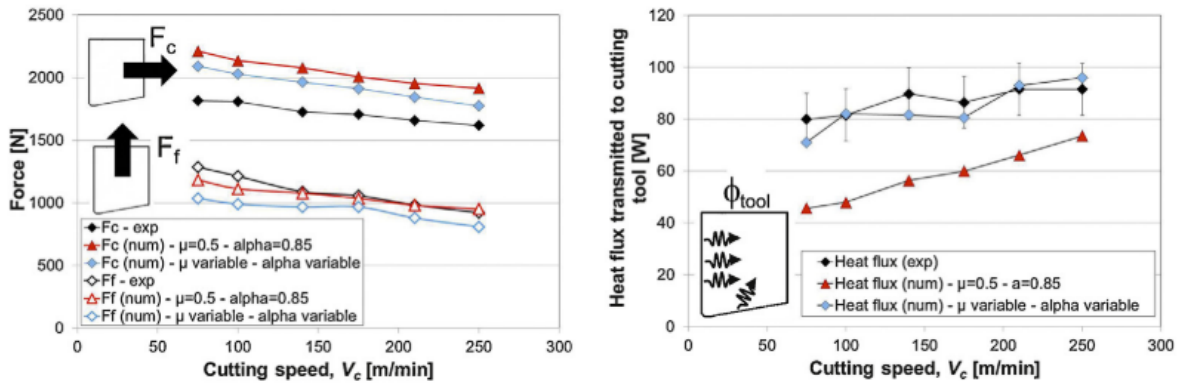
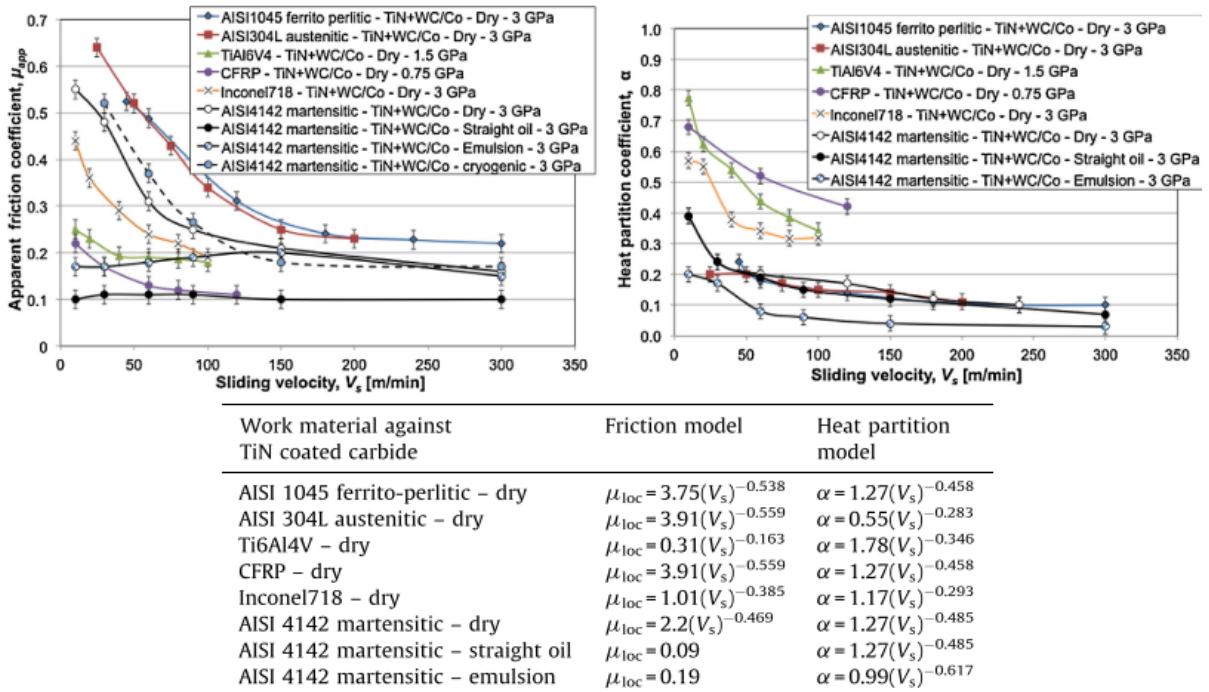


Figure 5.2.21: [124, Rech 2013a] friction and heat partition coefficients in variable cutting speed, simulation vs experimental results for constant and sliding-speed variable models

[125, Yousfi 2017] and his teammates experimentally determined the average friction coefficient in case of dry and cryogenic cooling of a carbide pin with a new CrN coating, against Ti6Al4V. They also simulated the experiment with FEM in order to calculate by inverse methodology the adhesion part of the coefficient. They found rugosity to be the most influential factor determining the average friction coefficient.

[126, Sterle 2019] and colleagues compared the performances of closed and open tribometers. They realized a tribometer by using the flat part of the cutting insert onto the side of the workpiece to cut. They examined the average friction coefficient of WC-Co inserts against Ti6Al4V and 42CrMo4. The system is very smart since it can easily be done without additional equipment on a lathe.

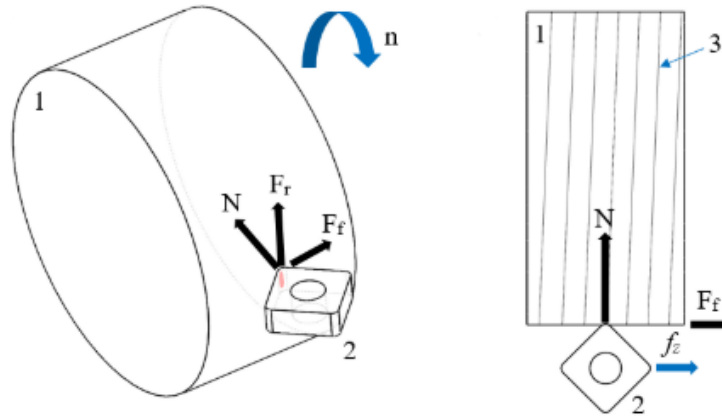


Figure 5.2.22: [126, Sterle 2019] tribometer

It only requires a modified tool holder capable of positioning the insert in the correct position to avoid cutting the work material. The contact pressure can be calculated with the Hertzian contact theory, considering two cylinders of different diameter. Lower maximum and average pressure can be achieved with the open tribometer compared to the classical pin on disc design. For 42CrMo4, the average friction coefficient calculated on the pin on disc tribometer was lower for emulsion and much lower in the case of LCO2 than the one calculated on the open device, while for dry condition they gave almost the same value. For Ti6Al4V the closed tribometer needed some sliding distance to achieve a stable measurement. The stable average friction coefficient's values were found lower for the closed system. While emulsion proved effective in lowering the average friction coefficient in case of 42CrMo4, for the Ti-alloy no cooling strategy proved so effective.

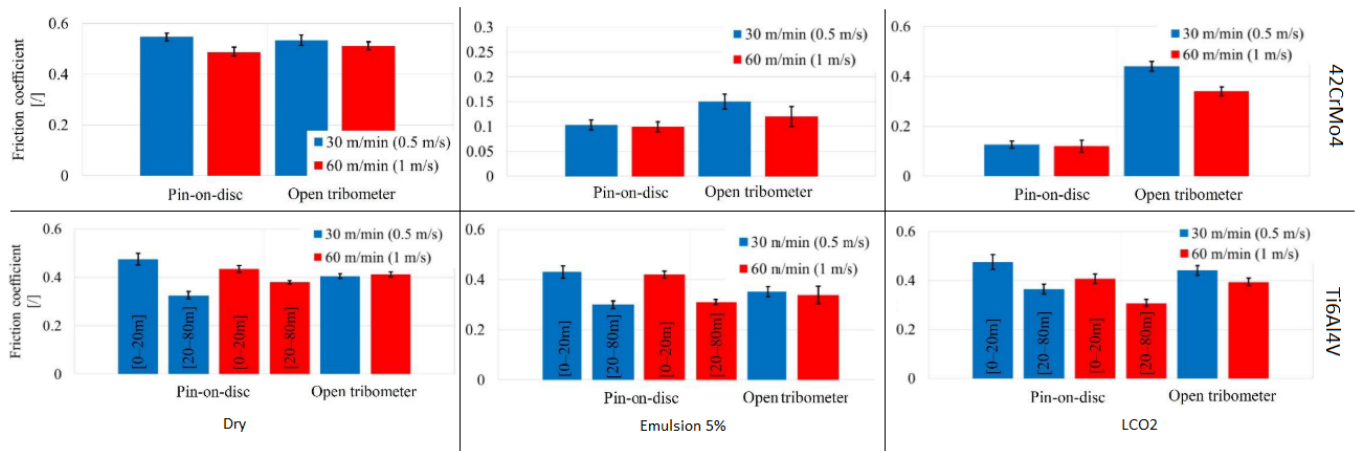


Figure 5.2.23: [126, Sterle 2019] average friction coefficient results

The article underlines how results obtained with closed tribometers can be inaccurate, especially for the cryogenic alternatives, due to ice residues onto the work material surface.

## 5.3 Material models

As we have previously underlined, modeling cutting processes need several ingredients, one of the most important being the work material behaviour. Many researchers tried different mathematical elaboration of achieved models for capturing particular strain, strain rate and temperature effects on the material flow stress. In parallel, others formulated new models, with more and more experimental coefficients. Others again, made efforts to extend the experimental reproducible range of strains and strain rates to obtain reliable data onto which base their models. Finally, some developed material models directly from cutting tests, or tuned model coefficients so to achieve the best prediction of experimental forces.

Either by adapting an analytical model to an experimental observation, or simply tuning its coefficients by iterations, or developing new models, making a choice for the best material representation for a cutting simulation is not an easy task.

For what concerns the material models, the Johnson-Cook is often applied due to its diffusion and low number of coefficients, widely available for a lot of materials. Other used models are the Zerilli-Armstrong, the simpler Power Law, while more intricate models looking at dislocation mechanics are the Baumann-Chiesa-Johnsons models, characterized by huge number of coefficients, set only for few materials since now.

We will not deepen into the way a FE model solve for the equation governing the elastic and plastic regime, strain-stress and strain-displacements fields relationships used to build the matrices and solve the great linear problem by minimizing potential energy. Nor we will look at the coupled solution of thermal fields and the numerical solution of contact problems. Those aspects are too wide for us to give anything else than a brief glimpse of it. For a quick flouring of the subject we suggest looking at the FORGE user guide (in the additional information), the software we will use for simulations.

There are two main alternatives for what concerns meshing strategy in cutting FEM simulations. In the Lagrangian analysis the mesh follows the deformation of the material, a remeshing technique is needed to avoid large mesh distortion, if not present, a good initial mesh geometry could prevent distortion and speed up time otherwise needed for remeshing. In the Eulerian analysis the mesh is a fixed grid and the material flows underneath it. A full Eulerian cutting simulation, however, require the chip to be already formed for the material grid to be placed. This a priori chip formation doesn't allow the evolution of the chip. Some solvers adopt an alternative solution in which both the strategies are used, the Arbitrary Lagrangian Eulerian analysis. In an ALE simulation the solver considers portion of the mesh as eulerian and some as Lagrangian, reducing the remeshing regions and consistently speeding up the calculations.

### Johnson-Cook material model

The JC model is one of the most diffused, due to the reduced number of coefficients, ease of their determination and implementation in most commercial FEM software. It separates the effect of strain, strain rate and temperature on the flow stress, without considering the possible mutual effects:

$$\bar{\sigma} = [A + B\varepsilon^n] \cdot \left[ 1 + C \ln \frac{\dot{\varepsilon}}{\dot{\varepsilon}_0} \right] \cdot \left[ 1 - \left( \frac{T - T_r}{T_m - T_r} \right)^m \right] = JC(\varepsilon) \cdot JC(\dot{\varepsilon}) \cdot JC(T)$$

the first term accounting for strain hardening, the second for strain rate, the third for thermal softening, [127, Johnson 1983].  $A, B, C, n, m$  are coefficient usually determined through Pressure Bar tests for a range of strains to 0.6, strain rates up to  $10^4 1/s$  and temperatures until  $1000^\circ C$ . However, during cutting achieved strains can reach  $3 \div 10$  in the secondary deformation zone and  $10^5 \div 10^6$  depending on the cutting speed. This lead to large extrapolation of experimental sets for the description of the material behaviour at high strains and strain rates.

### 5.3.1 Shear banding and damage models

Before deepening in the field of material modeling for Ti6Al4V we need to recall the peculiar shear banding effect the alloy exhibit at large strain rates. One of the frequent output of FEM models for machining, also used to confirm the validity of numerical results, is the chip morphology. A simulation that can correctly reproduce or predict chip morphology is more trustful that one which doesn't. We are interested here in material models that are able to reproduce the shear banding in cutting simulations. Several authors tried different description of material behaviour in order to capture this peculiar behaviour. Their efforts can be divided into two separate strategies:

- Addition of damage models to stress flow rheological models;
- Modification of rheological models without the addition of a damage model;

Damage models were ideated to numerically obtain material fracture in chip removal simulations. After a certain strain threshold, elements are labeled with a certain damage factor. When this factor reaches a critical value, the element is deleted so to give rise to a fracture. Frequently used damage models are the Johnson-Cook damage and the Latham-Cockroft damage models. Several other damage model are available in simulation software.

#### Johnson-Cook damage model

Frequently matched with the relative material model, it is implemented in most of FEM packages and the coefficients can be easily found in literature while their determination for new materials is standardized. It consists in the formulation of an equivalent strain to fracture, depending on the actual stress, strain rate, temperature, pressure conditions:

$$\varepsilon_{d,i} = \left[ D_1 + D_2 e^{D_3 \eta} \right] \cdot \left[ 1 + D_4 \ln \left( \frac{\dot{\varepsilon}}{\dot{\varepsilon}_0} \right) \right] \cdot \left[ 1 - D_5 \left( \frac{T - T_r}{T_m - T_r} \right)^m \right], \quad \eta = \frac{\sigma_1 + \sigma_2 + \sigma_3}{3 \cdot \sigma_{VM}}$$

where  $D_i$  are the five damage model constants, fitted with experimental tests, [128, Johnson 1985]. A cumulative damage variable represent the level of damage of each element:

$$D = \sum \frac{\Delta \varepsilon}{\varepsilon_{d,i}}, \quad D_i = \int \frac{1}{\varepsilon_{d,i}(\eta, \dot{\varepsilon}, T)} d\varepsilon = 1$$

being  $\Delta \varepsilon$  the strain accumulated in one integration cycle. When the damage variable  $D$  reaches one, the fracture occurs.

Some researchers, [129, 130, 114, Chen 2011, Wang 2014. Atlati2014], adopted the JC fracture model for describing fracture initiation, then, following the ductile fracture energy criteria, the damage evolved until rupture (JC damage evolution model):

$$G_f = \int_{\varepsilon_{d,i}}^{\varepsilon_{d,f}} L \cdot \sigma_y d\varepsilon = \int_0^{u_{d,f}} \sigma_y du$$

where the  $G_f$  represent the energy needed for a unit surface to yield completely, a first guess for it would be:

$$G_{f,I-II} = \left[ \frac{1-\nu^2}{E} \right] (K_c^2)_{I,II}, I : \text{opening}, II : \text{shearing modes}$$

The element stiffness is fully degraded when the displacement reaches  $u_{d,f}$ , meanwhile the flow stress is modified by the damage evolution.

$$D_{ev} = \begin{cases} \frac{L \cdot \varepsilon_{d,f}}{u_{d,f}} = \frac{u}{u_{d,f}} & \text{linear evolution} \\ 1 - e^{-\int^{u_p} \frac{\sigma}{G_f} du_p} & \text{exponential evolution} \end{cases}, \sigma = \sigma(1 - D_{ev})$$

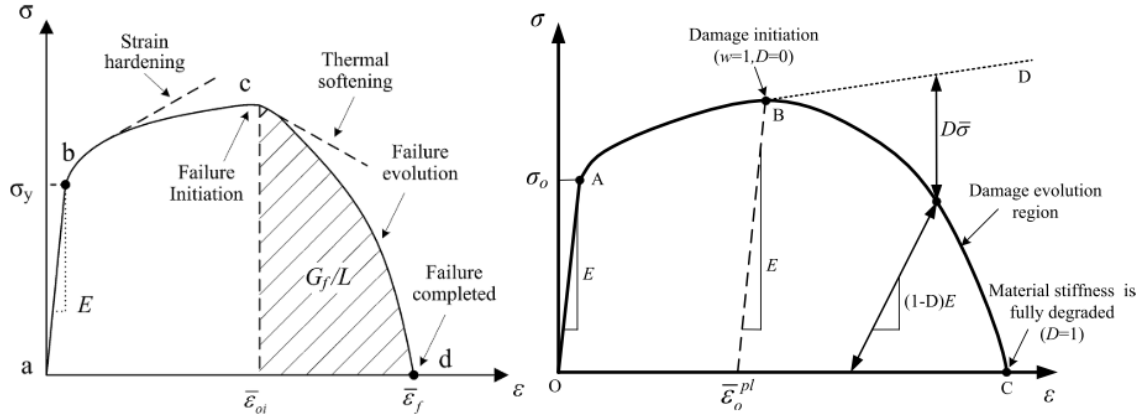


Figure 5.3.1: [129, 130, Chen 2011, Wang 2014] fractures evolution for the JC ductile damage model

### Latham-Cockcroft damage model

The Latham-Cockcroft model is widely diffused due to its compactness. The model evaluate the effect of the higher tensile component of the stress tensor along the effective strain path. When this quantity reaches a critical value, depending in primis on temperature and microstructure of the material, the material element is considered damaged and a crack is initiated. [131, Cockcroft 1968]:

$$\int_0^{\varepsilon_f} \sigma_1 d\varepsilon = D$$



The value of  $D$  in simulations is generally updated with iterations until the chip morphology is similar to the one obtained experimentally. Another version of the model is the Normalized LC:

$$\int_0^{\varepsilon_f} \frac{\sigma_1}{\bar{\sigma}} d\varepsilon = D_n$$

which is divided for the effective stress. This allow for the normalized constant  $D_n$  to assume values of  $0 \div 1$ . One of the drawbacks of the model is that the material never lacks of strength until sudden failure. Lack of stress bearing capability is determined by loss of elements in the model, leading to volume reduction.

### 5.3.2 Models application to Titanium cutting

In this section, the effectiveness of models applied to Titanium simulation cutting is analysed. Additionally, models applied to other materials but related to shear band formation are treated. Hopefully this would help in setting up our milling model. [132, Ozel 2006a] and Zeren tried to deduce model JC model coefficients and friction conditions using orthogonal cutting tests. They used the Oxley model for describing the strain and stress states in the cutting zone.

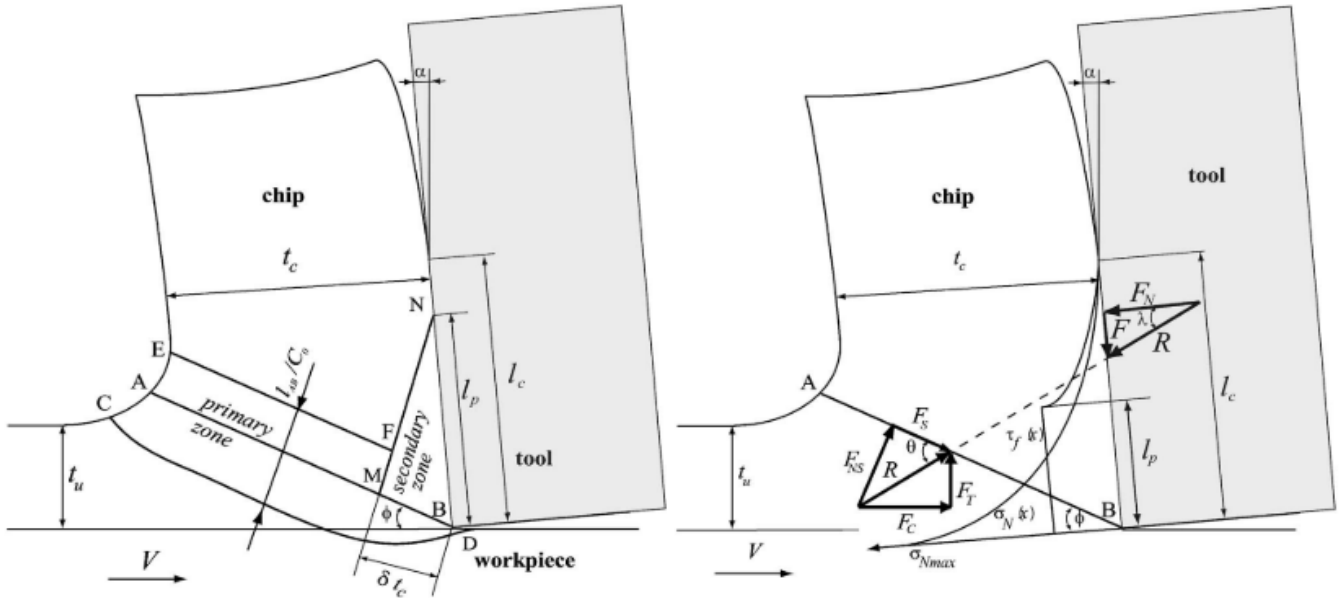


Figure 5.3.2: [132, Ozel 2006a] cutting zone model by Oxley

For a detailed description of the formulas used we advise looking directly at the article. By measurement of forces in various cutting conditions the average stress, strain and temperatures in the shear zone could be guessed. Several other analytical models were compared to the Oxley one, large scatter in terms of forces and temperatures were found. The friction model was derived by combining the Oxley model and integrating the stresses over the rake to find the feed and cutting forces. The procedure has been applied to several materials including Ti6Al4V.

Experimentally obtained JC model coefficients for Ti6Al4V							
$A$	$B$	$C$	$n$	$m$	$\varepsilon_{max}$	$\dot{\varepsilon}_{max}$	$T_{max}$
859.55	639.75	$2.215 \cdot 10^{-6}$	0.225	1.112	0.8	$8.5 \cdot 10^4$	$657^\circ C$

Table 5.3.1: [132, Ozel 2006a] Ti6Al4V JC model coefficients and strain ranges

The JC model constants were found through non-linear regression solution with Gauss-Newton algorithm and Levenberg-Marquardt modification for better convergence. In case of Ti6Al4V however, the cutting speed was limited due to chip segmentation, while the Oxley model is based on continuous chip.

[133, Guo 2006] and colleagues applied the Baumann-Chiesa-Johnson material model to AISI 52100 bearing steel. The model is dislocation based and can describe complex loading histories, recovery and microscopic effects. The price is a high number of experimental coefficients. We avoid reporting the set of expressions as this model will not be useful for our aim. The 20 coefficients were obtained with quasistatic and isothermal tests. Simulations were run with the aid of a cumulative damage criterion for chip separation. The contact conditions at the interface were set as maximum shear stress and Coulomb friction with  $\mu = 0.1$  for the sliding zone. The chip morphology was well predicted for maximum and minimum saw heights, however for saw pitch the prediction overestimates very much the real values. The efforts needed to determine the coefficients and the difficulties in the implementation of the model are a limit for its diffusion.

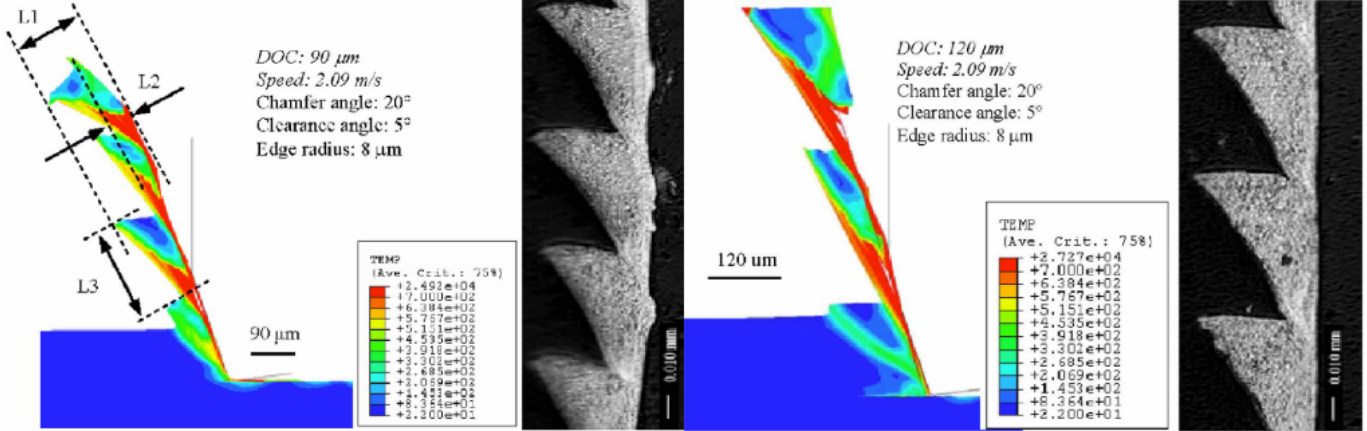


Figure 5.3.3: [133, Guo 2006] BCJ model results

[134, Anurag 2007] and Guo developed an internal state variable model to simulate complex loading histories happening in cutting simulations. They revised the available material models, including the Andrade-Meyers modified JC, the Usui-Shirakashi and the BCJ models:

$$\bar{\sigma} = [A + B\varepsilon^n] \left[ 1 + C \ln \frac{\dot{\varepsilon}}{\dot{\varepsilon}_0} \right] \cdot \left[ \frac{1}{1 - \left\{ 1 - \left[ \frac{(\sigma_f)_{rec}}{(\sigma_f)_{def}} \right] \right\} \cdot u(T)} \right], \quad u(T) \begin{cases} 0 & T < T_c \\ 1 & T > T_c \end{cases}$$

$$\sigma = \left[ \frac{A}{1000} \dot{\varepsilon} \right]^M \cdot \left[ \frac{e^{KT}}{1000} \dot{\varepsilon} \right] \cdot \left[ \int_{T, \dot{\varepsilon} \equiv h(\varepsilon)} e^{\frac{KT}{n}} \dot{\varepsilon}^{-\frac{m}{n}} d\varepsilon \right]^n \quad A, k, n, m \text{ constants}$$

where the first one is the Andrade-Meyers with  $T_c$  the recrystallization/recovery starting temperature. The model substantially varies the thermal softening function of a normal JC. The second one is the Usui-Shrakashi, consisting in a modified power law model in the strain rate with the integral part accounting for the strain rate history loading. The authors then set up their own dislocation based thermo-mechanical model. Higher temperature ease the dislocation movement while higher strain rate increase the pinning effect of solute atoms promoting dislocation entanglement. They divided the flow stress in a thermal and athermal part, the athermal part accounting for long range dislocation barriers such as GBs, dislocation forests and precipitates:

$$\sigma = \sigma_a + \sigma^*, \quad \sigma_a = a_0 + a_1 \cdot \varepsilon^n$$

The thermal part accounting for resistance of dislocation due to short range barriers: point defects, vacancies, interstitials, alloying elements, interacting dislocations and slip planes:

$$\sigma^* = \hat{\sigma}^* \cdot \left[ 1 - \left( -\frac{kT}{G_0} \cdot \ln \left( \frac{\dot{\varepsilon}}{\dot{\varepsilon}_0} \right) \right)^{1/q} \right]^{1/p}$$

$$\Delta G = G_0 \left[ 1 - \left( \frac{\sigma^*}{\hat{\sigma}^*} \right)^p \right]^q, \quad \dot{\varepsilon} = \dot{\varepsilon}_0 e^{\left( -\frac{\Delta G}{kT} \right)}, \quad \dot{\varepsilon}_0 = \rho_m b \bar{v}$$

where  $\Delta G$  is the energy barrier a dislocation has to overcome,  $G_0$  the energy needed for dislocation movement in case of null thermal stress,  $\hat{\sigma}^*$  the stress for the dislocation to overcome the barrier at  $0^\circ K$ ,  $\rho_m$  the average dislocation density,  $b$  the burger vector,  $\bar{v}$  the average dislocation velocity,  $k$  the Boltzmann constant ( $1.38 \cdot 10^{-23} J/^\circ K$ ). The material constants are found through SHPB compression tests, for Ti6Al4V they are showed in the following table:

Anurag-Guo material model constants for Ti6Al4V							
$a_0$	$a_1$	$n$	$\hat{\sigma}^* [MPa]$	$q$	$p$	$G_0 [eV]$	$\dot{\varepsilon}_0 [1/s]$
0	1215	0.062	601.2	5/4	4/3	0.9	$4.2 \cdot 10^8$

Table 5.3.2: [134, Anurag 2007] material model constants for Ti6Al4V

The model however hasn't been tested in a cutting simulation, nor there are, for the author knowledge, following articles using it.

[135, Calamaz 2008] et al. proposed a mathematical modification for the Johnson-Cook model to account for the formation of shear bands in Titanium alloys like Ti6Al4V:

$$\bar{\sigma} = \left[ A + B\varepsilon^n \cdot \left( \frac{1}{e^{\varepsilon^a}} \right) \right] \cdot \left[ 1 + C \ln \frac{\dot{\varepsilon}}{\dot{\varepsilon}_0} \right] \cdot \left[ 1 - \left( \frac{T - T_r}{T_m - T_r} \right)^m \right] \cdot \left[ D + (1 - D) \cdot \tanh \frac{1}{(\varepsilon + s)^c} \right]$$

$$D = 1 - \left( \frac{T}{T_m} \right)^d, \quad s = \left( \frac{T}{T_m} \right)^b$$

with  $a, b, c, d$  additional material constants to be determined. The parameter  $d$  controls the softening degree,  $a$  the level of the stress strain curve at high strains while  $c$  at low strains after the peak stress, which magnitude is set by  $b$ . Simulations were set up with a rigid tool,  $20\text{ kW/m}^2\text{K}$  for the tool-chip interface conductance, Coulomb-Tresca contact model:

$$\tau_f = \begin{cases} \mu \cdot \sigma_n & \mu \sigma_n < m \cdot \frac{\sigma_0}{\sqrt{3}} \\ m \cdot \frac{\sigma_0}{\sqrt{3}} & \mu \sigma_n > m \cdot \frac{\sigma_0}{\sqrt{3}} \end{cases}$$

The softening degree  $d$  varied between 1, 1.5,  $m$  between 1, 0.5 and  $\mu$  between 0.05, 0.3. Results show a correct prediction of shear bands at low speed ( $60\text{ m/min}$ ) for the Tanh model, while the chip for the unmodified JC model is continuous. Forces are well predicted for  $m = 1, d = 1.5, \mu = 0.3$ , however for  $d = 1.5$  shear band frequency is underestimated. In the simulated shear band strains reach 7, strain rates surpass  $10^5\text{ 1/s}$  and temperature near the tool tip reaches  $700^\circ\text{C}$ , while during the evolution of the shear band it can go up to  $600^\circ\text{C}$  for the highest speed. Adding a Latham-Cockroft damage criterion,  $D = 2400$ , the accuracy of the shear bands prediction was perfected.

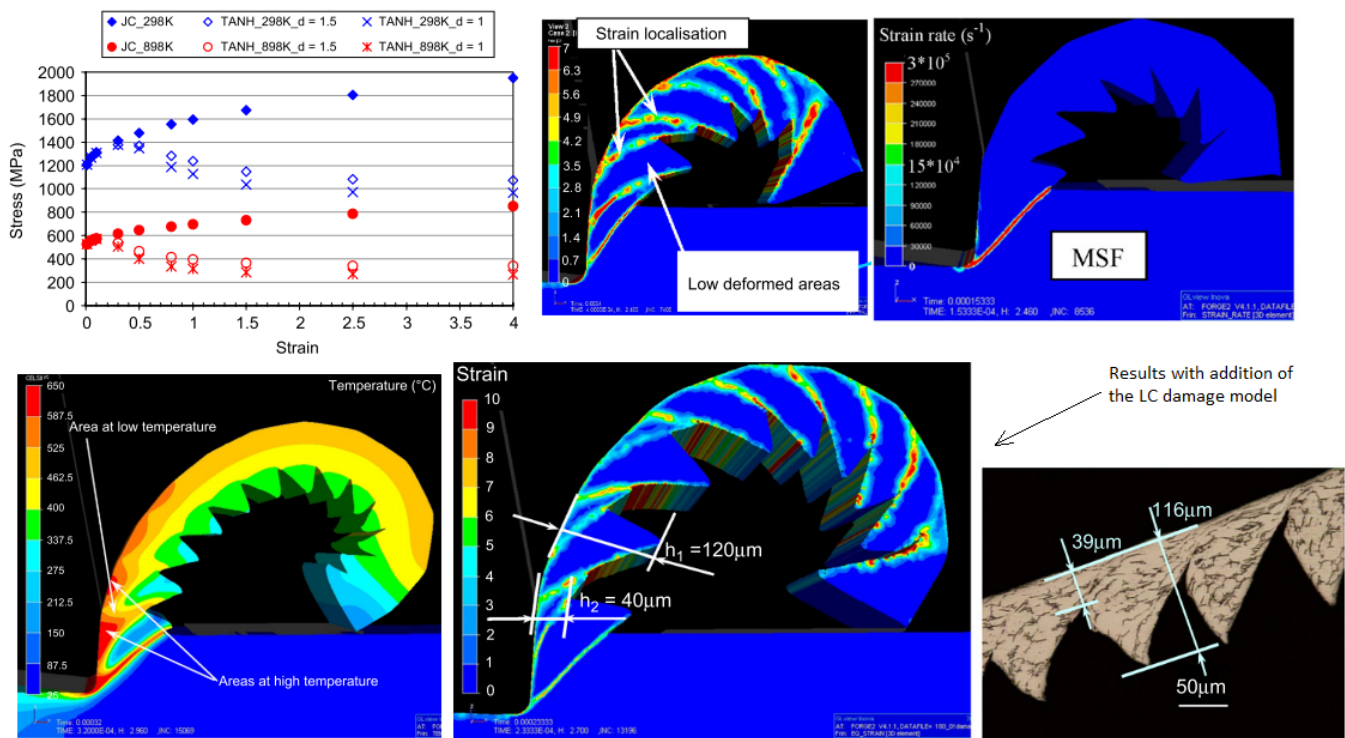


Figure 5.3.4: [135, Calamaz 2008] modified JC model results

In conclusion, the Tanh model offers an elegant representation of the material behaviour capable of reproducing shear bands where a simple JC fails. However, still a damage model need to be implemented to achieve better results, like what should be done with a simple JC.

An example of successful adoption of a Tanh model for machining is given in [136, Ozel 2011] for Inconel 718 turning. They compared the Tanh and simple JC models

in DEFORM-3D, modeling with a rigid tool, visco-elasto-plastic material and Coulomb contact model:

$$\bar{\sigma} = [A + B\varepsilon^n] \left[ 1 + C \ln \frac{\dot{\varepsilon}}{\dot{\varepsilon}_0} \right] \cdot \left[ 1 - \left( \frac{T - T_r}{T_m - T_r} \right)^m \right] \cdot \left[ D + (1 - D) \cdot \left( \tanh \frac{1}{(\varepsilon + S)^r} \right)^s \right]$$

The new model accounted for strain softening after a certain threshold. Through experimental tests, a comparison of forces showed how the Tanh model gave better results. Some iterations for the parameters is suggested for model fitting. The Tanh model also predicted lower temperatures with respect to the other models.

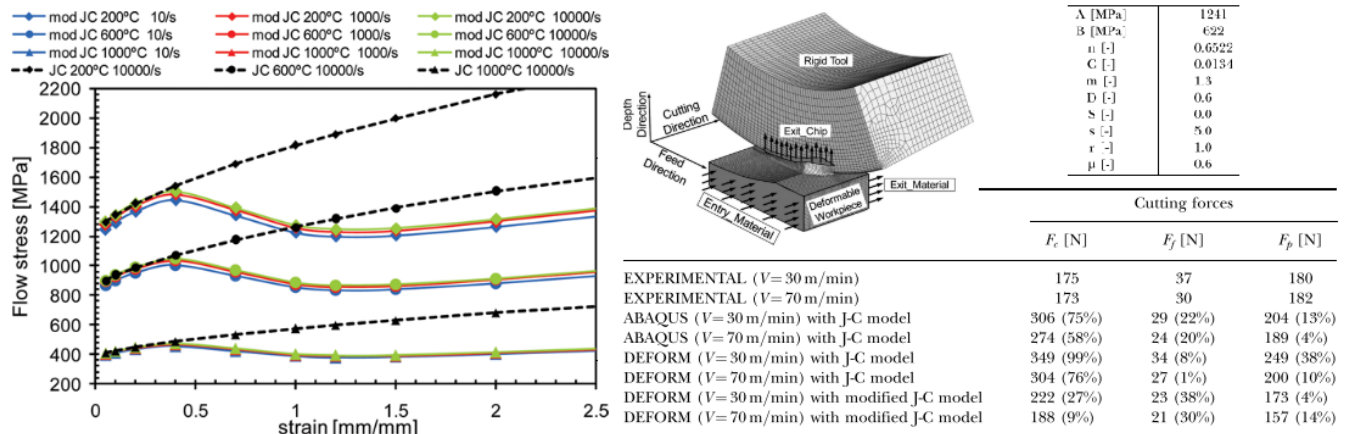


Figure 5.3.5: [136, Ozel 2011] Tanh model application to Inconel 718 turning, model parameters and results

[137, Umbrello 2008] underlined the importance of an accurate knowledge of the material behaviour previous FEM modeling for Ti6Al4V. Assuming a good material flow stress model as a starting point, damage model and friction coefficients need to be updated with iteration, respectively looking at chip morphology and cutting forces. They compared simulation results to cutting tests at low ( $120\text{ m/min}$ ) and ultra high speed ( $1200, 4800\text{ m/min}$ ) concluding that the model coefficients (JC) obtained by Lee and Lin was the most accurate, guaranteeing a good result after having found suitable damage and friction coefficients. Model coefficients obtained by cutting tests and cutting zone analytical stress theory by Dumitrescu showed poor performances.

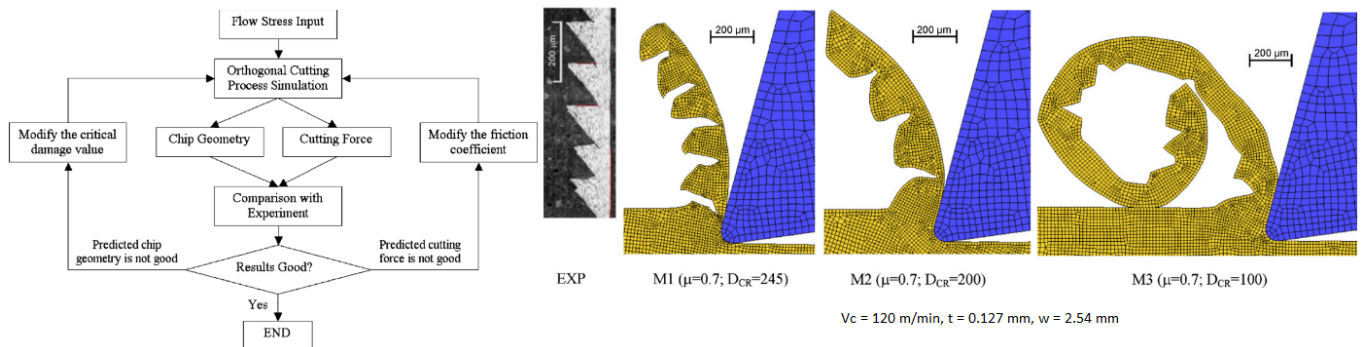


Figure 5.3.6: [137, Umbrello 2008]  $D$  and  $\mu$  iteration procedure, different models results

[138, Ozel 2009] and colleagues analysed the performance of different JC model coefficients in simulations of Ti6Al4V serrated chip with LC damage criterion. They showed as different model coefficient can influence chip morphology, cutting force and temperature fields.

The Lee and Lin and Meyer and Kelponis models were addressed as the most accurate.

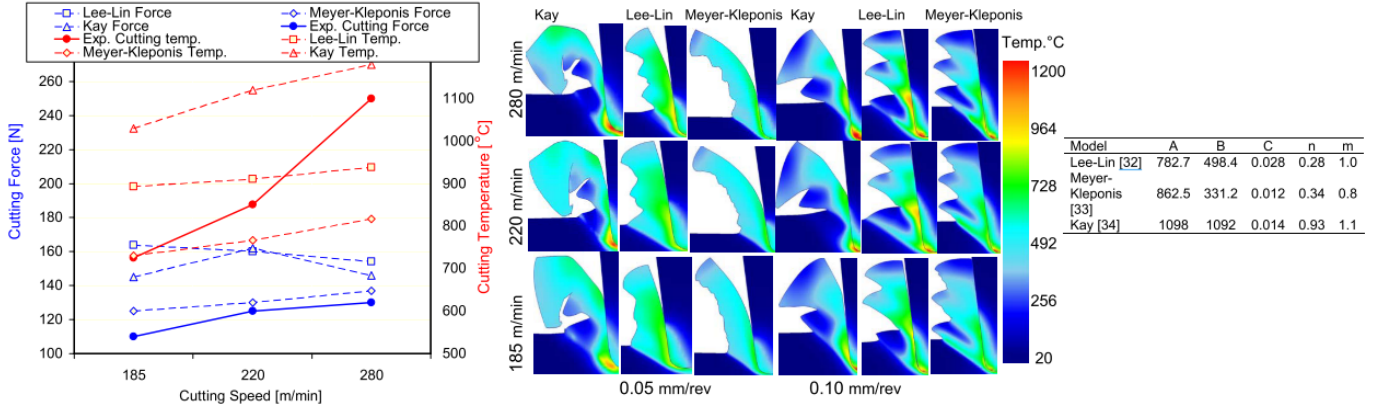


Figure 5.3.7: [138, Ozel 2009] different models results

[139, Sun 2009a] and Guo underlined how the reachable experimental ranges of strain and strain rates are much lower than their ranges in machining. A comparison with experimental data is impossible due to the limitation of the testing procedures. The authors tried to compare the JC model flow stress to analytical models for stresses and strains in the shearing zone. With the assumption of pure shear:

$$\bar{\sigma}_f = \sqrt{3} \frac{(F_c \sin \phi \cos \phi - F_t \sin^2 \phi)}{t \cdot w}, \quad \varepsilon = \frac{1}{2\sqrt{3}} \frac{\cos \alpha}{\sin \phi \cos(\phi - \alpha)}, \quad \dot{\varepsilon} = \frac{10}{\sqrt{3}} \frac{V \cdot \cos \alpha \sin \phi}{t \cdot \cos(\phi - \alpha)}$$

where  $t, w, \phi, \alpha, V$  are the uncut chip thickness, width of cut, shear angle, rake angle and cutting speed. The experimental derived flow stresses confirms the adiabatic JC model predictions (temperature build up due to deformation remains in the vicinity of the deformation, reasonable for metals with low conductivity).

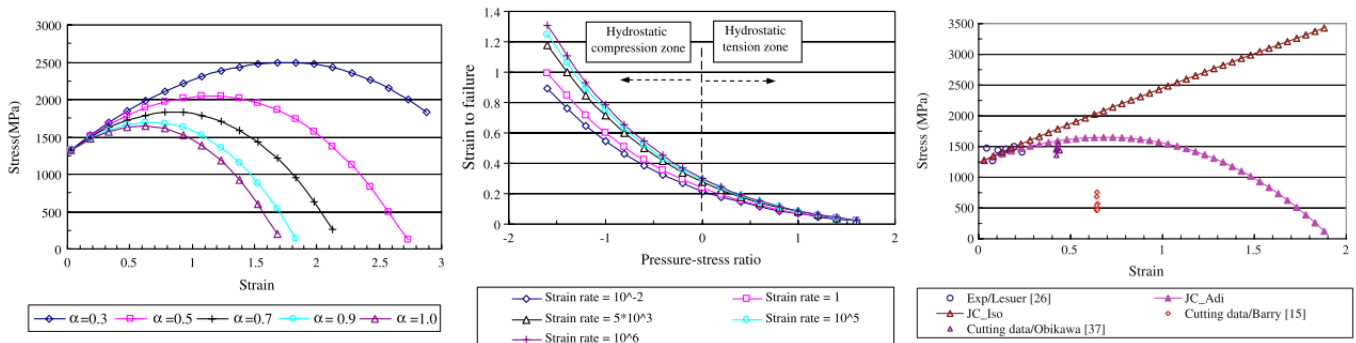


Figure 5.3.8: [139, Sun 2009a], flow stress sensitivity on heat fraction, fracture strain sensitivity on loading mode, cutting model flow stress comparison

Interestingly, they also underlined the effect of the inelastic heat fraction coefficient, responsible for thermal build up and material softening. Eventually, the stress state influences the fracture strain: while for tension it is similar for variable strain rates, for compression it varies and his value is much higher than in tension. Since shear compression is the main loading modality in cutting, torsion and compression tests for coefficient determination would be advisable.

[140, Shi 2010] and Attia remark how there could be more combinations of contact and material models giving same results in simulations. Since is difficult to reproduce strain, strain rates and temperatures encountered during cutting processes as well as to measure them during cutting process, predictive theories have been used. A computer program based on Oxley theory have been generally used, that tailored material model parameters to reproduce cutting forces, however the procedure was unable to deal with the higher temperatures of the secondary deformation zone and the final set of model coefficients was non unique. Through an improved Oxley model called DPZD (Distributed Primary Zone Deformation) model they evaluate the performance of the most used models and proposed improvements to match the DPZD stress, strains and temperature distributions in the shear zone. The Power law and Zerilli-Armstrong model proved to be more effective in reproducing the DPZD model predictions.

In a following study, published in two different articles ([141, 142, Shi 2010b, Shi 2010a]) the authors further reported the goodness of the DPZD model in comparison with FEM simulations. The model was able to predict FEM simulated temperature, stress, strain and strain rate for AISI 1045 steel under different feeds and rake angles.

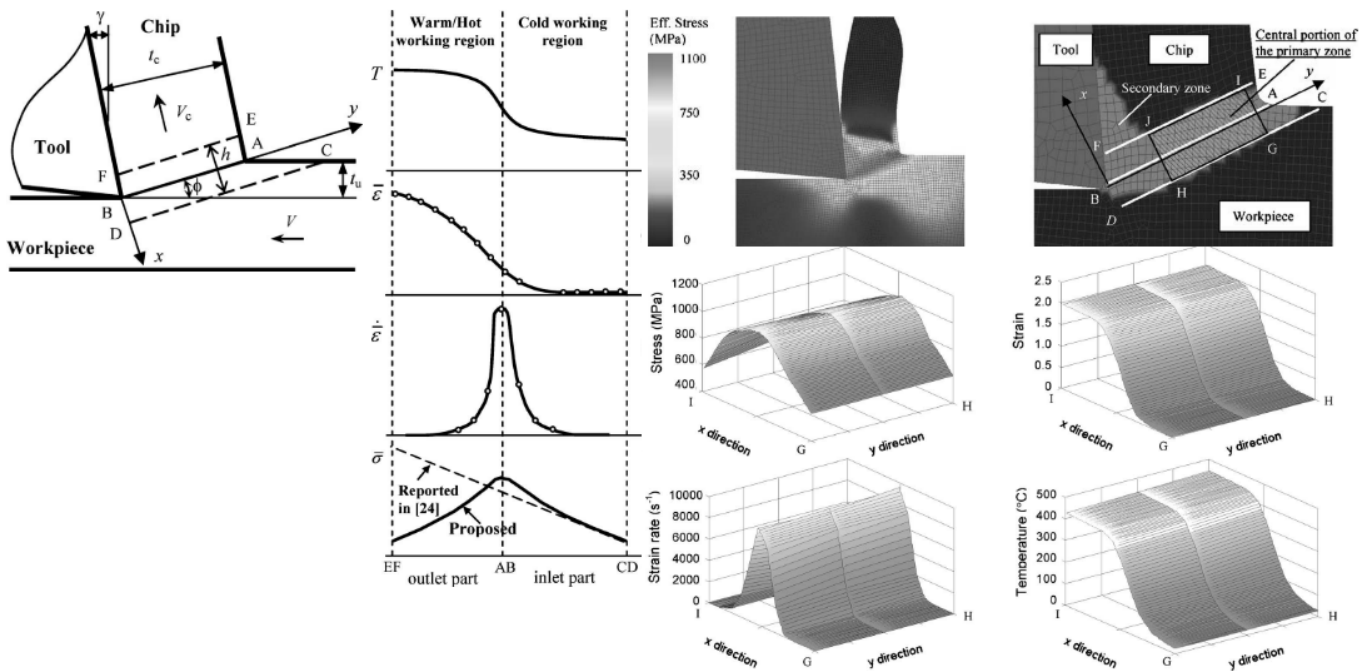


Figure 5.3.9: [140, Shi 2010] DPZD model field variable prediction

In the last part of the article, the authors presented experimental procedures to determine material constants, in synergy with the DPZD model, that would lead to more accurate FEM results. Quasi static indentation, room and high temperature cutting tests are needed:

- Quasi static indentation tests were used to determine yield stress as a function of temperature and strain hardening part of the constitutive law;
- Room temperature cutting tests and high temperature cutting tests were used to evaluate the strain rate and thermal dependence of the constitutive laws.

The procedure was able to identify JC parameters independently of the initial guess. SPHB tests confirmed the goodness of the model. However, speaking of orthogonal FEM models, cutting force prediction was bad.

[143, Sima 2010] and Ozel exhaustively analysed the newly Tanh model for Ti6Al4V cutting simulations. Firstly they presented three models accounting for flow softening and adiabatic shearing. The Tanh model, the Andrade-Meyers modified JC, the Nemat-Nasser micromechanical model:

$$\bar{\sigma} = \sigma_a + \sigma^*, \quad \begin{cases} \sigma_a = \sigma_0 \varepsilon^m \\ \sigma^* = f(T, \dot{\varepsilon}) = \hat{\sigma} = \left\{ 1 - \left[ -\frac{K}{G_0} T \cdot \ln \frac{\dot{\varepsilon}}{\dot{\varepsilon}_0} \right]^{1/p} \right\}^{1/q} \end{cases}$$

The equation refers to the Nemat-Nasser model, developed to describe the dynamic strain aging and  $K$  is Boltzmann constant and  $G_0$  is the total energy barrier,  $p$  and  $q$  are constants,  $0 < p < 1$  and  $1 < q < 2$ . All these models try to extrapolate from experiments the material behaviour at large strains and strain rates. As the material flow stress depend on three variables it is quite complicate to describe the effect of each one and the relation with the others. To facilitate this we look at the strain rate and temperature sensitivity:

$$S_{\dot{\varepsilon}} = \frac{\sigma_2 - \sigma_1}{\ln(\dot{\varepsilon}_2/\dot{\varepsilon}_1)}, \quad S_T = \frac{\ln(\sigma_2 - \sigma_1)}{\ln(T_2/T_1)}$$

Strain rate sensitivity decrease with increasing strain, while temperature sensitivity is almost constant, affecting all strain levels and overcoming strain hardening after a certain strain on (data coming from SHPB Lee and Lin's study). For simulating orthogonal cutting process, they chose the Tanh model with three different level of refinement:

- Temperature independent parameters, model 1:

$$\bar{\sigma} = [A + B\varepsilon^m] \left[ 1 + C \ln \frac{\dot{\varepsilon}}{\dot{\varepsilon}_0} \right] \cdot \left[ 1 - \left( \frac{T - T_r}{T_m - T_r} \right)^m \right] \cdot \left[ M + (1 - M) \cdot \tanh \left( \frac{1}{(\varepsilon + p)^r} \right)^s \right]$$

where  $M$  defines the strain passed which softening begins, however the softening effect is applied at all temperatures;

- Temperature dependent parameters, model 2:

$$\bar{\sigma} = [A + B\varepsilon^n] \left[ 1 + C \ln \frac{\dot{\varepsilon}}{\dot{\varepsilon}_0} \right] \cdot \left[ 1 - \left( \frac{T - T_r}{T_m - T_r} \right)^m \right] \cdot \left[ D + (1 - D) \cdot \tanh \left( \frac{1}{(\varepsilon + p)^r} \right)^s \right]$$

$$D = 1 - \left( \frac{T}{T_m} \right)^d, \quad p = \left( \frac{T}{T_m} \right)^b$$

where the exponents  $d, b$  control the softening effect;



- Strain softening effect, model 3:

$$\bar{\sigma} = \left[ A + B \varepsilon^n \cdot \left( \frac{1}{e^{\varepsilon^a}} \right) \right] \left[ 1 + C \ln \frac{\dot{\varepsilon}}{\dot{\varepsilon}_0} \right] \cdot \left[ 1 - \left( \frac{T - T_r}{T_m - T_r} \right)^m \right] \cdot \left[ D + (1 - D) \cdot \tanh \left( \frac{1}{(\varepsilon + p)^r} \right)^s \right]$$

$$D = 1 - \left( \frac{T}{T_m} \right)^d, \quad p = \left( \frac{T}{T_m} \right)^b$$

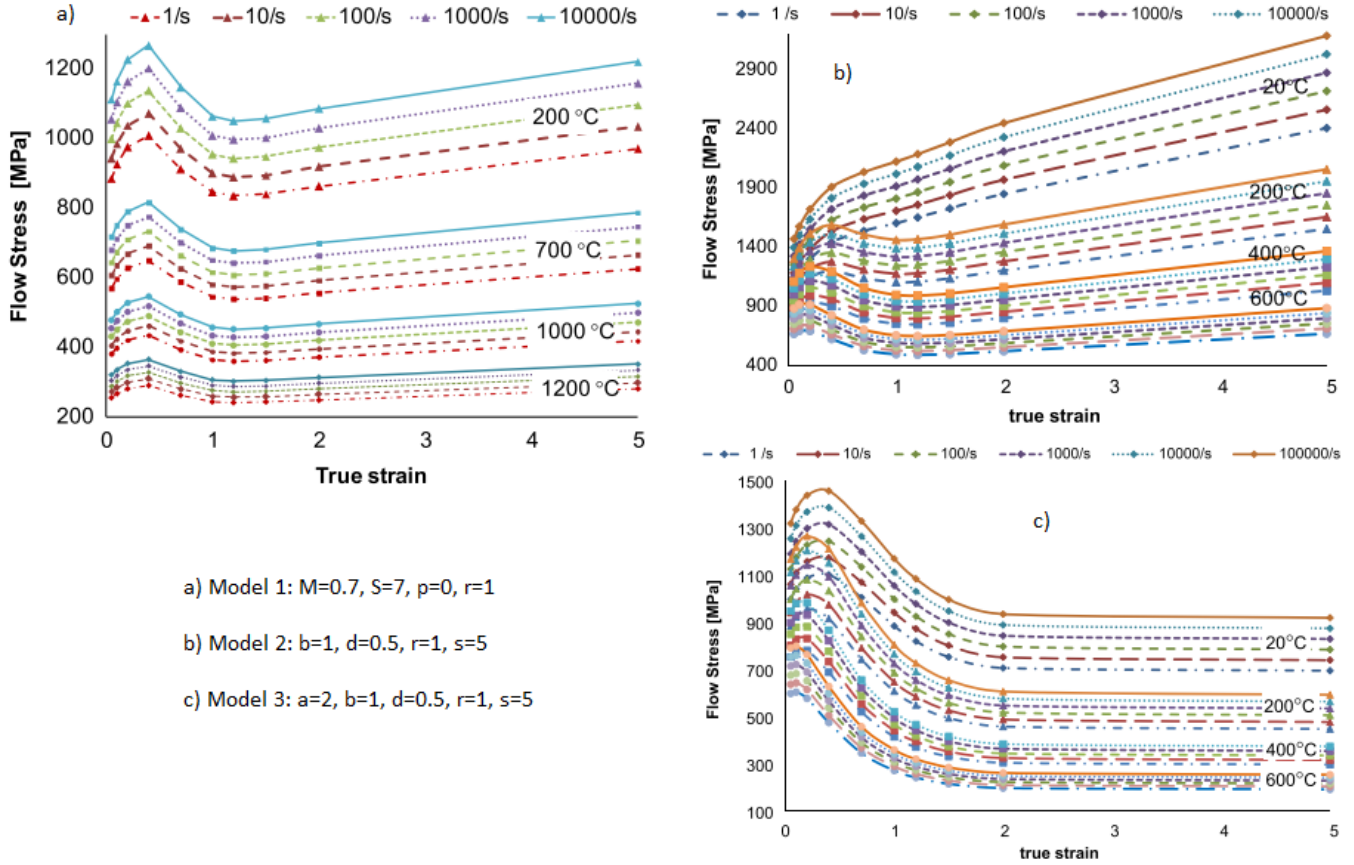


Figure 5.3.10: [143, Sima 2010] models 1, 2 and 3 visualization example

As can be seen from the example curves of the three models, the first one present a constant softening effect over the temperature ranges. Model 2 increase the softening effect at high temperature, while model 3 add strain softening, which at high strains contribute to the flattening of the curve. In model 3,  $a$  controls the strain at which strain softening starts,  $b$  control the position of the stress peak value,  $d$  the stress level at high strains,  $S$  the strain level at which softening starts.

A Deform-2D simulation with thermo-elasto-viscoplastic workmaterial and rigid tool was set up. Three regions of friction where defined: sticking with Tresca factor  $m = 1$  for the tool nose,  $m = 0.9$  for the rake sticking region and  $\mu = 0.5$  for the Coulombian sliding region. After some iterations for model calibration with experimental tests, Model 3 with  $[a, b, d, r, S] = [2, 5, 1, 1, 0.05]$  was found to perform better. Forces and chip morphology was quite in accordance with the experimental value, unless a clear error comparison was not presented.

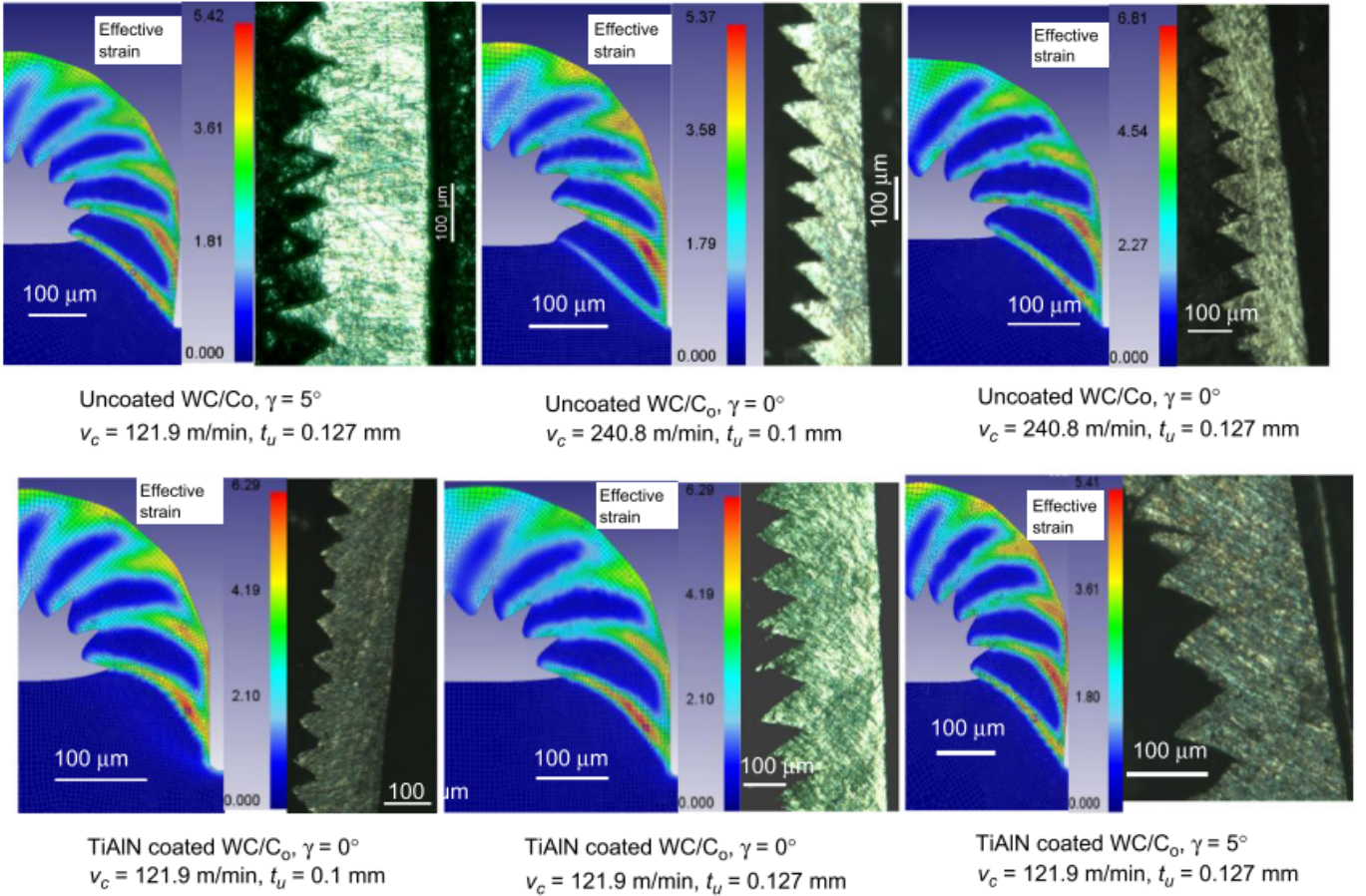


Figure 5.3.11: [143, Sima 2010] model 3 results

The article deeply investigate the problem related to material model extrapolation out of experimental data. Without new testing technique, capable of monitoring high strains and strain rates, it is necessary to iterate for the model coefficient to capture macroscopic variables observed in cutting simulations. Even remembering this is influenced by the contact problems as well.

[144, Calamaz 2010a] and colleagues modified their previous constitutive model to represent the strain softening of Ti6Al4V. The model become:

$$\bar{\sigma} = [A + B\varepsilon^n] \left[ 1 + C \ln \frac{\dot{\varepsilon}}{\dot{\varepsilon}_0} \right] \cdot \left[ 1 - \left( \frac{T - T_r}{T_m - T_r} \right)^m \right] \cdot \left[ D + (1 - D) \cdot \tanh \left( \frac{1}{(\varepsilon + \varepsilon_0)} \right) \right]$$

$$D = 1 - \left[ \frac{p \cdot \varepsilon}{1 + p \cdot \varepsilon} \cdot \tanh \left( \frac{T - T_r}{T_{soft} - T_r} \right)^q \right]$$

$\varepsilon_0$  regulate the strain corresponding to the peak stress and start of softening. The range of temperatures for the softening phenomena ( $q, T_{soft}$ ) and the shape of the curve during the softening ( $p$ ) is described by  $D(\varepsilon, T)$ . The new coefficients are found through cutting tests and inverse determination to match cutting forces and chip morphology. Contact conditions were assumed with a friction coefficient  $\mu = 0.3$  for all simulations. FORGE 2005 was used to set up the new model, a micro mesh of  $2\mu m$  was used near the tool tip to capture the small scale phenomena.

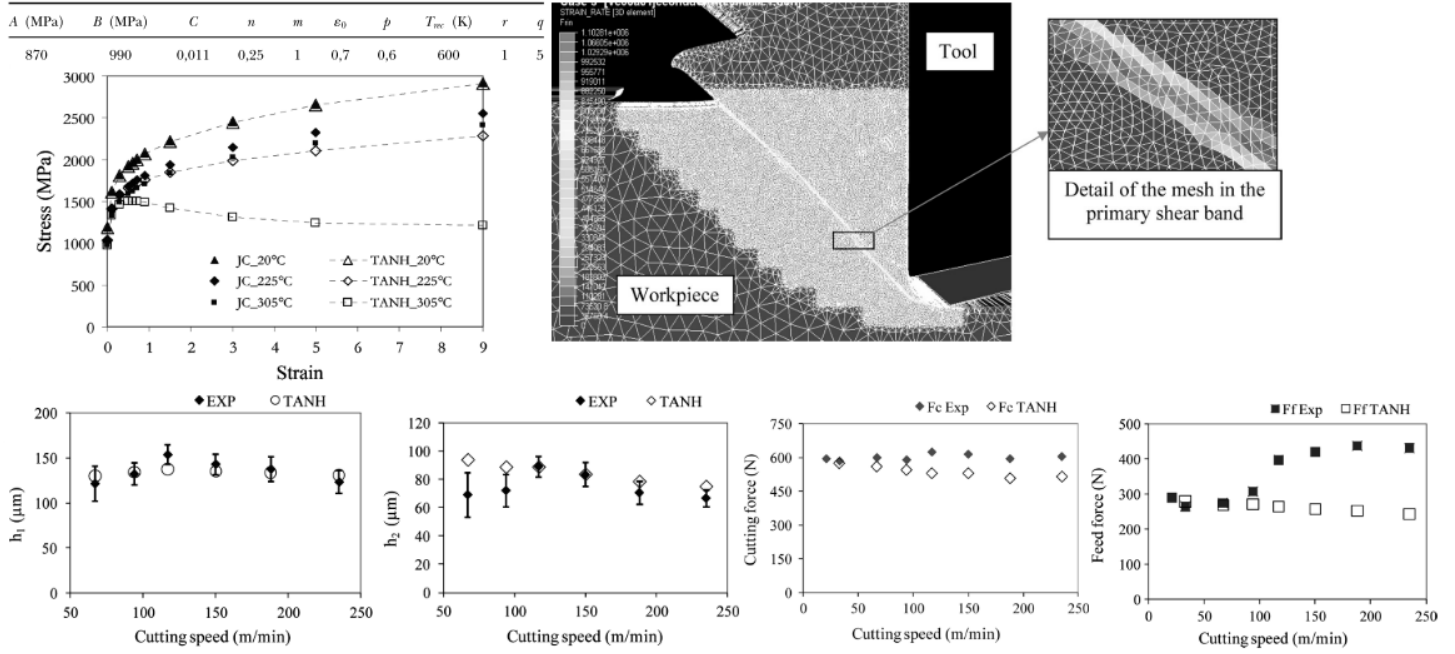


Figure 5.3.12: [144, Calamaz 2010a] material model coefficients and simulation results

Results were extremely good in terms of shear band and chip morphology. The material model predict the exact evolution and curvature of the band in the shear zone. Cutting forces diverged for high speed.

[145, Karpát 2011] developed a new model accounting for thermal softening of Ti6Al4V. The author underline the effect of dynamic recrystallization, occurring at a range of  $0.4 \div 0.5 T_m$  that can lower with increasing strain rate. Also phase transformation from  $\alpha$  to  $\beta$  and GBs sliding ease the generation of slip bands. Karpát included a softening effect in his previous model, resulting in the following:

$$\sigma(\varepsilon, \dot{\varepsilon}, T) = [ae^{n^*} + b] \cdot [cT^{*2} + dT^* + e] \cdot \left[ 1 - \left( 1 - \left( \frac{\ln \dot{\varepsilon}_0}{\ln \dot{\varepsilon}} \right)^q \right) \left( \frac{1}{l \cdot \tanh(\varepsilon + p)} \right) \right], \quad T^* = \frac{T}{T_r}$$

Three parameters are added to include the softening. After a certain  $\varepsilon_{cr}$  the softening begins, the steady state softened stress is determined by calculating the stress at the critical strain, multiplied by the S term, which is less than one if softening occurs. For the softening region the stress is reduced by a Tanh function for the relative strain distance to the critical strain.

$$\sigma_s = S \cdot \sigma(\varepsilon_{cr}, \dot{\varepsilon}, T), \quad S < 1$$

$$\sigma(\varepsilon, \dot{\varepsilon}, T) = \sigma - (\sigma - \sigma_s) \left( \tanh(k \cdot \varepsilon^*) \right)^r, \quad \varepsilon^* = \frac{\varepsilon - \varepsilon_{cr}}{\varepsilon_{cr}} u(\varepsilon), \quad u(\varepsilon) = \begin{cases} 0 & \varepsilon < \varepsilon_{cr} \\ 1 & \varepsilon \geq \varepsilon_{cr} \end{cases}$$

The critical strain value, however, has to be defined and would be dependent on strain rate and temperature in his turn. It finally needs 11 coefficients and to decide for this critical strain.

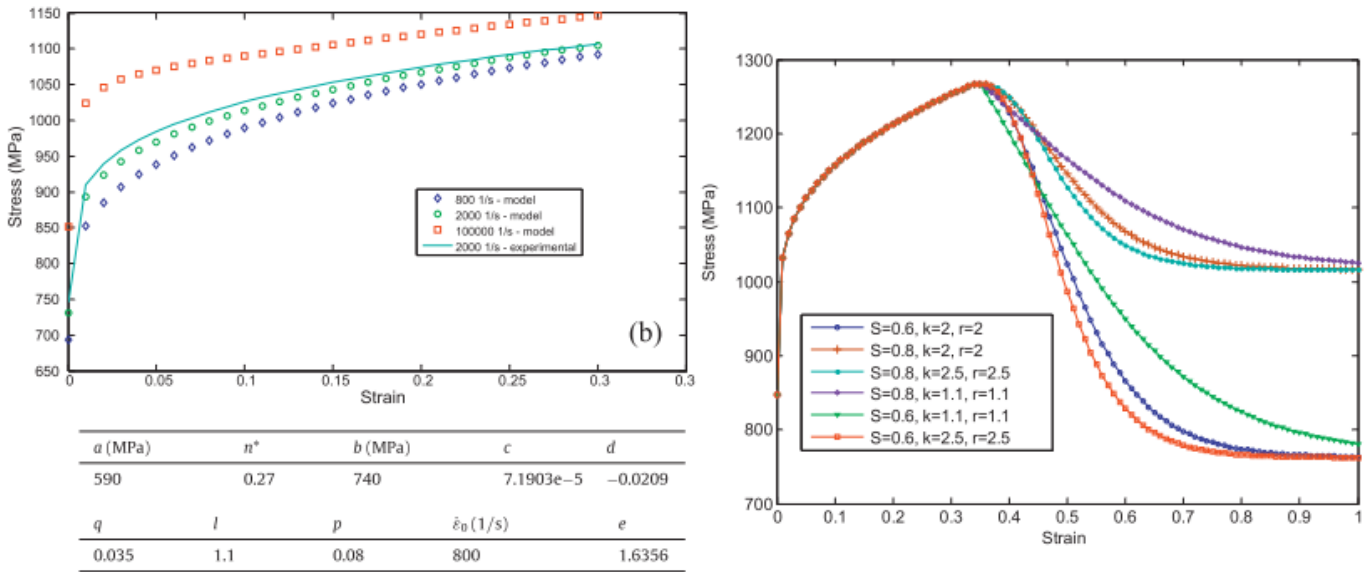


Figure 5.3.13: [145, Karpát 2011] model softening example

Several simulations are run varying the starting temperature for the softening. Friction modeling is achieved with a Coulomb-Tresca model,  $\mu$  20% higher than the experimental one, while a shear factor of one for a predefined length of 1/3 of the uncut chip thickness. Material properties were varied with temperature. They obtained excellent result for  $S = 0.6$  starting from  $350^\circ\text{C}$  with strain hardening from ambient temperature,  $k = r = 2, \epsilon_{cr} = 0.35$ . Results are good even considering two different experimental studies from two different authors with different tools. Finally they highlighted how shear band formation is influenced by mesh size in the shearing zone, larger the elements larger the shear band, lower the serration degree.

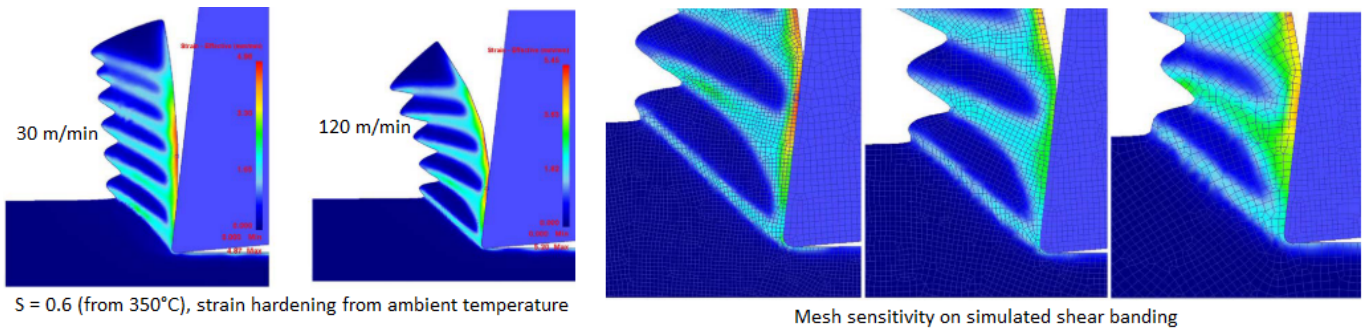


Figure 5.3.14: [145, Karpát 2011] model results

[129, Chen 2011] and teammates simulated HSM of Ti6Al4V with JC material and JC damage evolution models. They also added a shear damage criteria to ease chip separation from the workpiece and applied it to a narrow band of the workpiece at uncut chip thickness depth. This is done because no remeshing is performed, so to ease the plastic flow patterns. Experiments and simulations are performed at ultra high speed and high speed ( $170 \div 250 \text{ m/min}$ ). Average friction coefficient were implemented, cutting forces and chip morphology agreed with experimental results. The main drawback

of the adopted solutions is the necessity of a mesh “easing” the result, which sounds artificial and difficult to implement for difficult geometries.

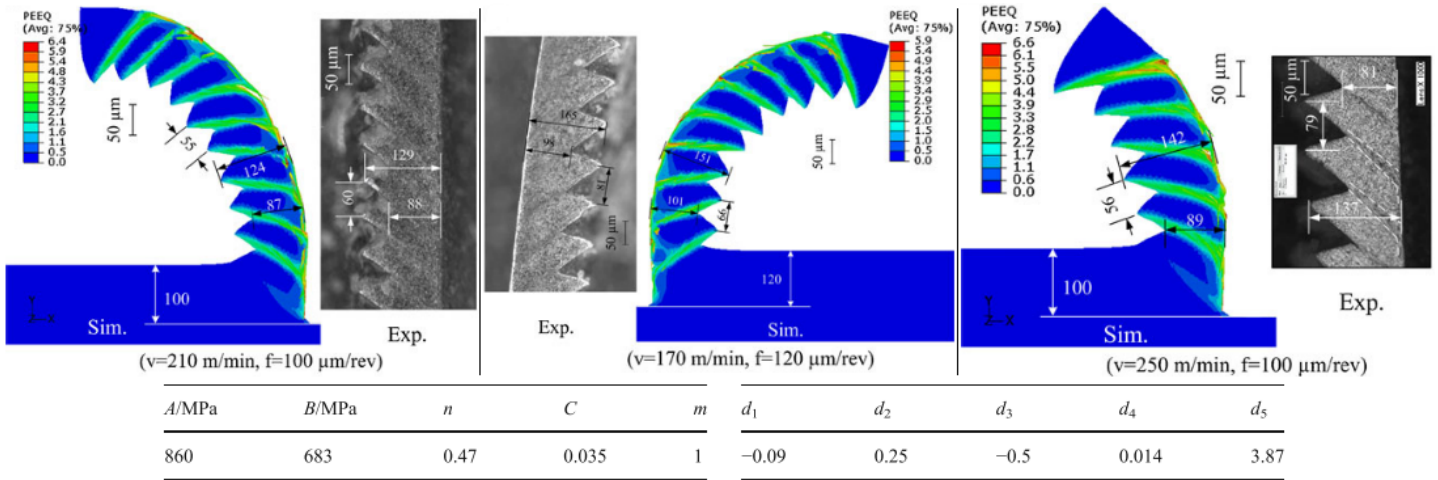


Figure 5.3.15: [129, Chen 2011] simulation with no remeshing, chip morphology results

[146, Calamaz 2011] and coworkers further modified their material model for capturing shear bands in Titanium machining. Their new modification to the JC model abandoned the Tanh function and the thermal softening, including more complex strain and strain rates dependencies:

$$\bar{\sigma} = \left[ A + B \left( \frac{1}{\dot{\epsilon}} \right) \cdot \epsilon^{[n-0.12(\epsilon \cdot \dot{\epsilon})^a]} \right] \left[ 1 + C \ln \frac{\dot{\epsilon}}{\dot{\epsilon}_0} \right] \cdot \left[ 1 - \left( \frac{T - T_r}{T_m - T_r} \right)^m \right]$$

Cutting forces and chip segmentation frequency was guessed with good accuracy over a fair range of speed and feeds for  $a = 0.11, \mu = 2$ . The choice of this high and non-physical friction coefficient was justified by the need to represent sticking with a coulomb friction law.

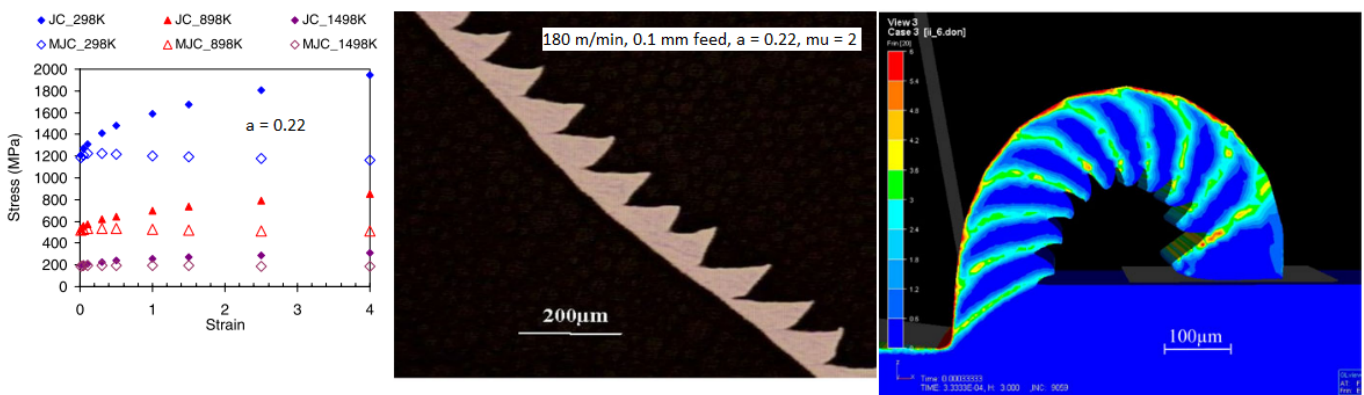


Figure 5.3.16: [146, Calamaz 2011] new model's results

However, this artificial sticking could have caused over heating in the secondary deformation zone increasing softening phenomena. Moreover, no result for what concern

feed force was presented. Eventually, no result analysis has been done on segment height and pitch: for instance, the comparison in the figure match perfectly the frequency, but misses totally the shape of the chip.

[147, Shrot 2012] and Baker underlined as there is no experimental procedure capable of achieving high strain, strain and strain rates to describe material behaviour. During cutting, strains in the secondary deformation zone can reach 10, while strain rates approach  $10^6$  1/s. The authors tried to obtain the JC coefficient for AISI 52100 bearing steel from inverse analysis, considering simulated cutting forces and chip morphology. Strong assumptions were made to simplify the model:

- No coupled temperature calculation, which can be a good approximation if high speed cutting of low conductivity materials;
- No clearance angle and null friction, null thermal transfer to the tool, this because the model needs to reproduce the material model, and the contact model must not influence it. The model parameters are updated looking at the error function obtained during a simulation with the original parameter set;
- No chip segmentation (however AISI 52100 is prone to shear banding);

Even by making these assumptions, depending on the starting set for the coefficient  $A, B, n$  (so only three coefficient), with the Levenberg-Marquardt Algorithm, different coefficients were found, leading to different material behaviours. Including the parameter  $m$ , the converged set resulted in a much different material behaviour. The article underline the difficulties in finding unique coefficient set for material models with inverse algorithms based on cutting simulations.

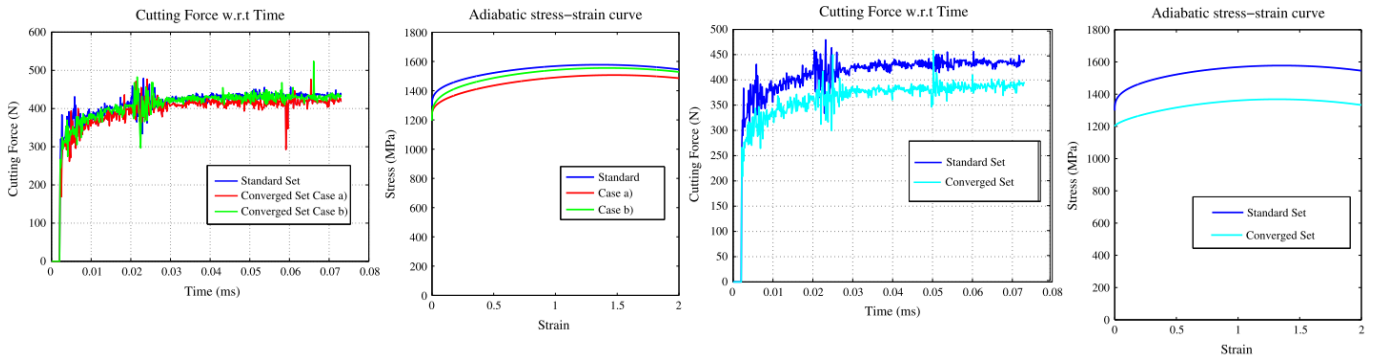


Figure 5.3.17: [147, Shrot 2012] difference in inversely determined JC model constants and original sets

[148, Liu 2013] and coworkers modified the Zerilli-Armstrong model to account for void nucleation and crack initiation during shear banding of Ti6Al4V. Shear bands are believed to be caused by both thermal softening effects (dynamic recrystallization and recovery) and void coalescence forming a crack:

$$\sigma = \sigma_a + B \cdot e^{-(\beta_0 - \beta_1 \ln \dot{\epsilon}) \cdot T} + B_0 \cdot \sqrt{\varepsilon_r \left(1 - e^{-\frac{\varepsilon}{\varepsilon_r}}\right)} \cdot e^{-(\alpha_0 - \alpha_1 \ln \dot{\epsilon}) \cdot T}$$

$$\sigma = \left[ \sigma_a + B \cdot e^{-(\beta_0 - \beta_1 \ln \dot{\epsilon}) \cdot T} + B_0 \cdot \sqrt{\varepsilon_r \left(1 - e^{-\frac{\varepsilon}{\varepsilon_r}}\right)} \cdot e^{-(\alpha_0 - \alpha_1 \ln \dot{\epsilon}) \cdot T} \right] \cdot \left[ H + (1 - H) \left( \tanh \frac{a}{\varepsilon} \right)^k \right]$$

The first equation is the Z-A accounting for the stress saturation at high strains, the second is the modification by the authors with a failure function which parameters are:

- Asymptotic stress factor, controlling the softening at high strains:

$$H = \begin{cases} 1 & \dot{\epsilon} < \dot{\epsilon}_0 \\ \left[ \frac{1}{\log_{10}(\dot{\epsilon})} \right] h_0 & \dot{\epsilon} \geq \dot{\epsilon}_0 \end{cases}, \quad \dot{\epsilon}_0 = 10 \frac{1}{s}$$

Its effect starting after a certain strain rate is achieved, before that heat conduction compete with temperature localization hindering shear banding;

- Critical strain, starting the softening:  $a = a_1 [\log_{10}(\dot{\epsilon}) - a_2]^2 + a_3$ ;
- Softening rate controller:  $[\log_{10}(\dot{\epsilon})]^{k_0}$ .

After the seven Z-A constants we need other five calibration constants:  $[h_0, a_1, a_2, a_3, k_0]$ . For what concerns the results, cutting forces are accurate, but more precision should have been addressed to the accuracy regarding the chip morphology prediction. Only the serration frequency is presented, which at high feed is a little overestimated.

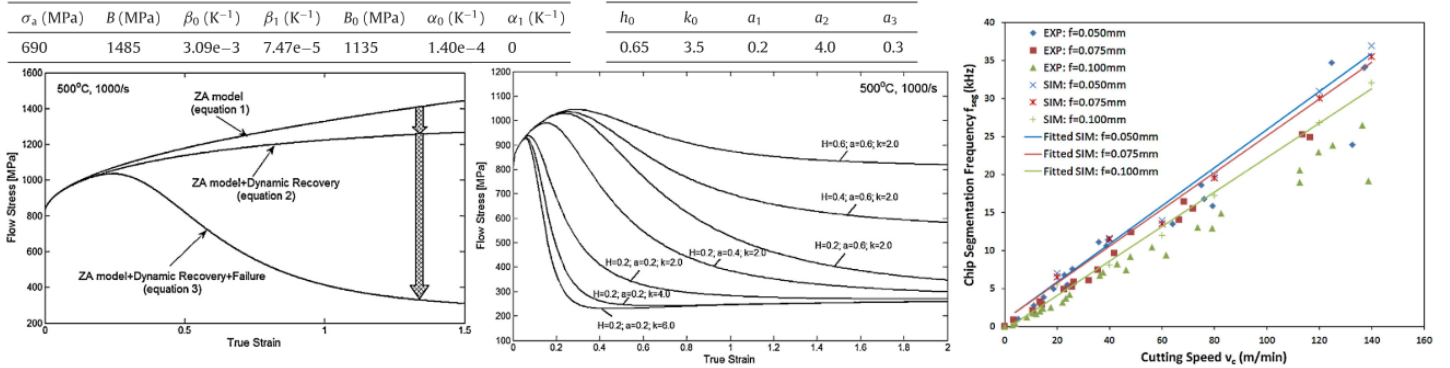


Figure 5.3.18: [148, Liu 2013] modified Z-A model results

[130, Wang 2014] and Liu implemented JC material and damage evolution models to simulate serrated chip formation in Ti6Al4V. They avoided remeshing by orienting the mesh appropriately for a width equal to the uncut chip thickness. Average Coulomb friction coefficient were adopted. The results show an outstanding accuracy in terms of chip morphology for a wide range of speed. Cutting forces are a bit underestimated at all speed, feed forces aren't investigated. Sensitivity on damage model parameters is also performed, calculated as the variation in the serration degree produced by the change in the relative damage coefficient:  $S = \frac{\chi_s^{var} - \chi_s^{original}}{\chi_s^{original}} \cdot 100$ . Damage constants  $D_1$  and  $D_2$  have the highest impact for what concerns shear banding, referring to the constant term and weight of the stress triaxiality factor  $\eta$ . The article represent a great success in modeling shear bands for Ti6Al4V, however being of difficult implementation of complex geometries.

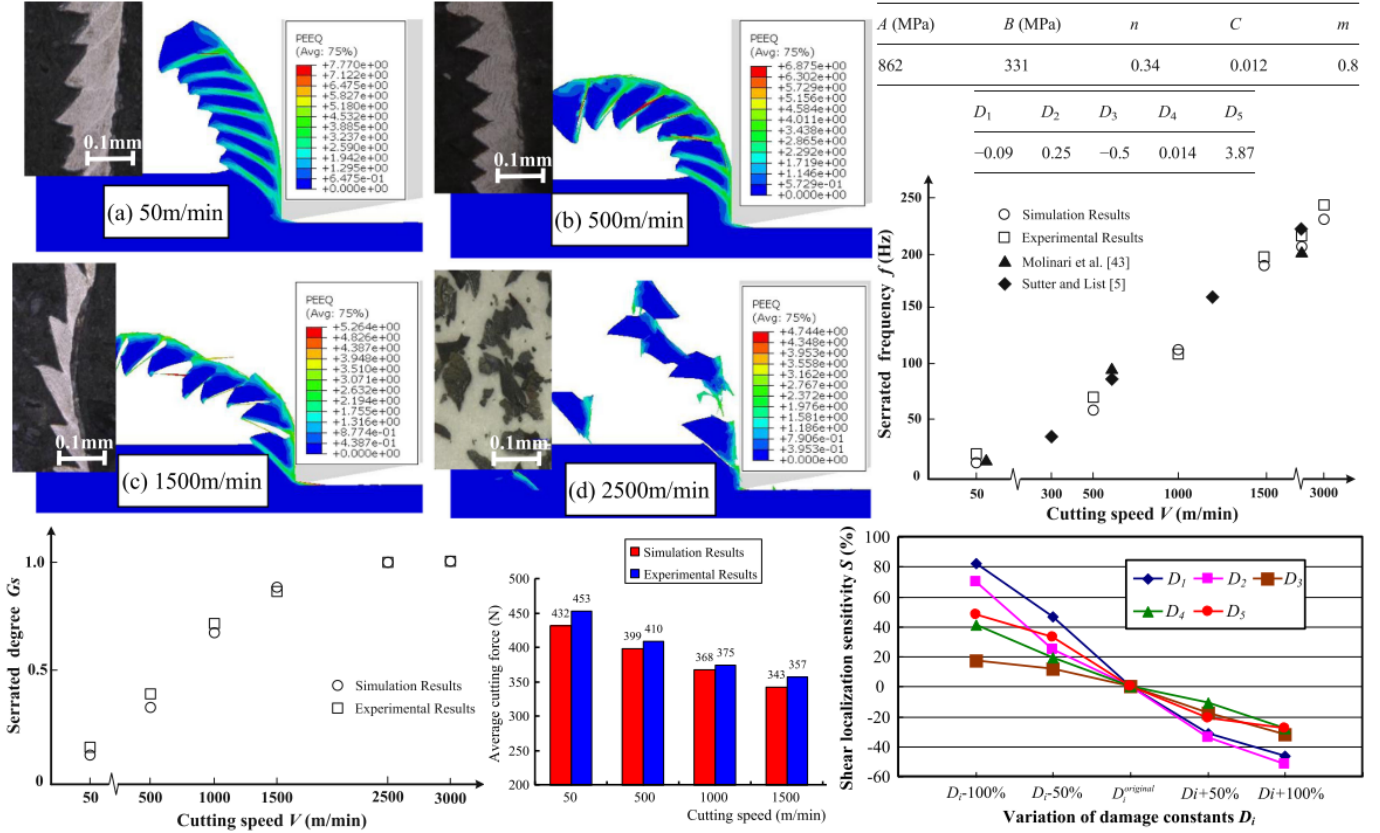


Figure 5.3.19: [130, Wang 2014] JC model coefficients and chip serration results, damage model sensitivity

[149, Cheng 2018] and colleagues investigate the realization of a more accurate material model for the simulation of cutting processes related to Ti6Al4V. They modified a JC model accounting for stress triaxiality:

$$\bar{\sigma} = \left[ A + m \varepsilon_p^n \right] \cdot \left[ B + C \ln \left( E + \frac{\dot{\varepsilon}}{\dot{\varepsilon}_0} \right) \right] \cdot [1 - \zeta (\eta - \eta_0)] \quad \eta = \frac{\sigma_m}{\bar{\sigma}}$$

Thermal softening was not considered because:

- The heat generation due to inelastic heat fraction during the experimental tests, unto which models are based, already account for heat generation in the small time scale: we are not machining a preheated material;
- Temperature in the primary deformation zone hardly reaches  $400^\circ C$  due to the chip mass transport.

However the preheating thermal effects are important in the secondary deformation zone, which characterizes contact responses and wear behaviour of the insert. A JC damage evolution model without thermal effects was also used:

$$\bar{\varepsilon}_i^p = \left[ D_1 + D_2 e^{D_3 \eta} \right] \cdot \left[ 1 + D_4 \ln \left( \frac{\dot{\varepsilon}}{\dot{\varepsilon}_0} \right) \right] \quad \bar{\sigma} = (1 - D) \bar{\sigma}, \quad D = \int_{\bar{\varepsilon}_i^p}^{\bar{\varepsilon}^p} \frac{\bar{\sigma}}{G_f} \cdot d\bar{\varepsilon}^p, \quad G_f = \int_{\bar{\varepsilon}_i^p}^{\bar{\varepsilon}_f^p} \bar{\sigma} \cdot d\bar{\varepsilon}_p$$



where  $D_i$  are damage model constants,  $D$  is the damage variable,  $G_f$  the fracture energy. To set up the model coefficients, three types of specimens were used: cylinder ( $\eta = -0.33$ ), smooth round bar ( $\eta = 0.33$ ), double notched specimen ( $\eta$  variable). The coefficient they found are showed in the table below:

Material Model							
Coefficient	$A$	$m$	$n$	$B$	$C$	$E$	$\zeta$
Value	232,1	439,6	0,199	1,193	0.227	367.9	0.05

Damage model					
Coefficient	$D_1$	$D_2$	$D_3$	$D_4$	$G_f$
Value	0.061	0.064	-1.065	0.027	$50 \text{ MJ/m}^3$

	Experiment	Simulation
Peak ( $\mu\text{m}$ )	$226.7 \pm 12.1$	139.5
Valley ( $\mu\text{m}$ )	$116.6 \pm 13.1$	81.9
Pitch ( $\mu\text{m}$ )	$161.3 \pm 24.3$	100.5
CCR	$1.51 \pm 0.08$	0.93

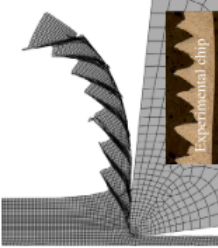


Table 5.3.3: [149, Cheng 2018], coefficients of the stress triaxiality modified JC model for Ti6Al4V

[150, Bertolini 2019] and his teammates aimed at the low temperature characterization of the material flow stress for cutting simulations. In cryogenic machining, economic performances are achieved for small flow rates, highly localized on the tool insert. Therefore, the work material is left (or this is the aim) substantially unaffected, plastic work raises temperature above ambient values for the most portion of the interested material. Nevertheless, the workmaterial is observed to freeze after milling experiments. Split Hopkinson Tension Bar tests were performed after a cryogenic bath with  $1 \text{ mm}$  sheets of Ti6Al4V.

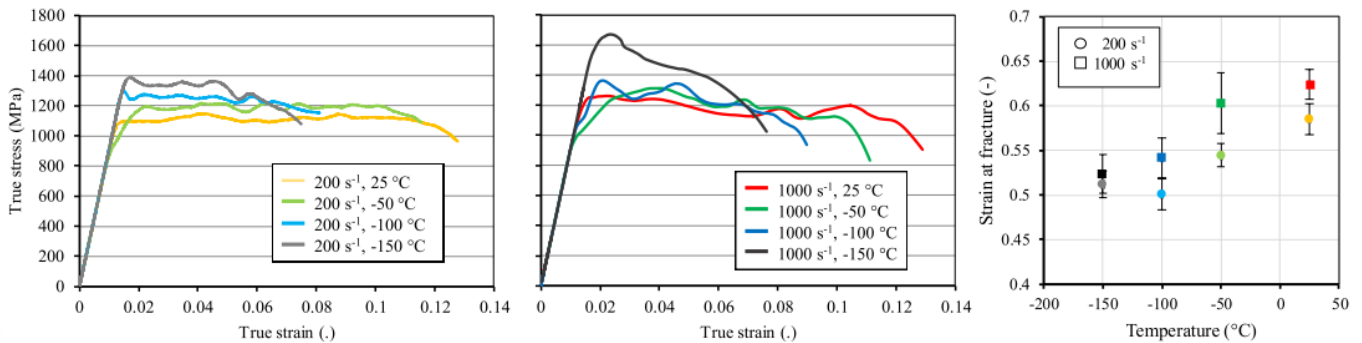


Figure 5.3.20: [150, Bertolini 2019] SHTB at cryogenic temperatures results

## 5.4 Computational Fluid Dynamics

CFD analysis have been carried out to understand how flow properties would help in maximizing heat transfer coefficients of impinging jets. It has been found that jet velocity and pressure strongly influence the ability of breaking the vapour layer in contact with the hot surfaces, limiting its insulating nature and increasing the heat transfer. On the other side, high pressure and velocity result in high discharge coefficient along delivery lines, which lowers the useful fluid phase at the exit of the nozzle. Optimizing both delivery variables and cutting parameters for the best tool life is too expensive and time demanding, therefore CFD optimization of the delivery lines and of the HTC at the impingement is necessary.

[151, Obikawa 2012] and teammates studied the effect of flank directed compressed air jet in turning Inconel 718 in synergy with emulsion. Continuum equations, Navier-stokes and Volume of Fluid equations for gradual change between liquid and vapor phase were applied with  $k - \epsilon$  turbulence model. The cutting fluid proved to be unable in penetrating the flank gap, due to contrary velocity of the workpiece and the narrow space. Nevertheless, compressed air improved turbulence and allowed for better penetration. Higher pressure fluids were advised for increased efficiency.

[152, Lu 2013] and colleagues studied the cooling effect of cryogenic jets on Aluminium with a geometry resembling the crevice between workpiece and tool. Cooling rates of thermocouples placed at regular distance on the flat workpiece side were measured. The device posed problems due to ice formation and clogging. Moreover, the heat source at tool tip was not considered. Added to the geometry, the overheat temperature of the walls is of crucial importance.

[48, Pusavec 2016] et al. analysed the effect of Nitrogen phase on the HTC of the impinging jet. They underline as the HTC must be temperature dependent, based on the temperature of the tool surface. They summarized the values of the HTC found in literature:

Heat transfer coefficient of LN2 impinging jets				
Article	[8]	[153]	Jin 2009	Rotella & Umbrello 2014
$HTC_{LN2} [W/m^2K]$	23270 ÷ 46750	48270 ÷ 74950	0 – 3500	20000

Table 5.4.1: [48, Pusavec 2016], HTC found in literature

The values differ very much among different works, the average value being around  $30kW/m^2K$ . One of the problems related to the variability of results is the phase in which Nitrogen is delivered. Another one is the particular nozzle configuration (distance, spot size, angle) and eventually the flow parameters (jet speed, delivery pressure). The authors developed a sensor capable of detecting the Nitrogen phase, based on the different light transmission of liquid and vapour phase. By switching on the system it can be seen how at least one minute is needed to achieve a stable liquid flow. By inverse heat transfer determination and an experimental specimen with geometries similar to the flank face of a tool on a workpiece, they obtained HTC values as a function of wall overheat temperature. It is interesting to note that after a certain overheating temperature ( $200^\circ C$ ), the HTC can be assumed constant around

$20000\text{W}/\text{m}^2\text{K}$ . Being the temperature of the chips or the tool faces usually higher than  $0^\circ\text{C}$  it means that a constant value for the HTC of  $20\text{kW}/\text{m}^2\text{K}$  is at least a decent approximation.

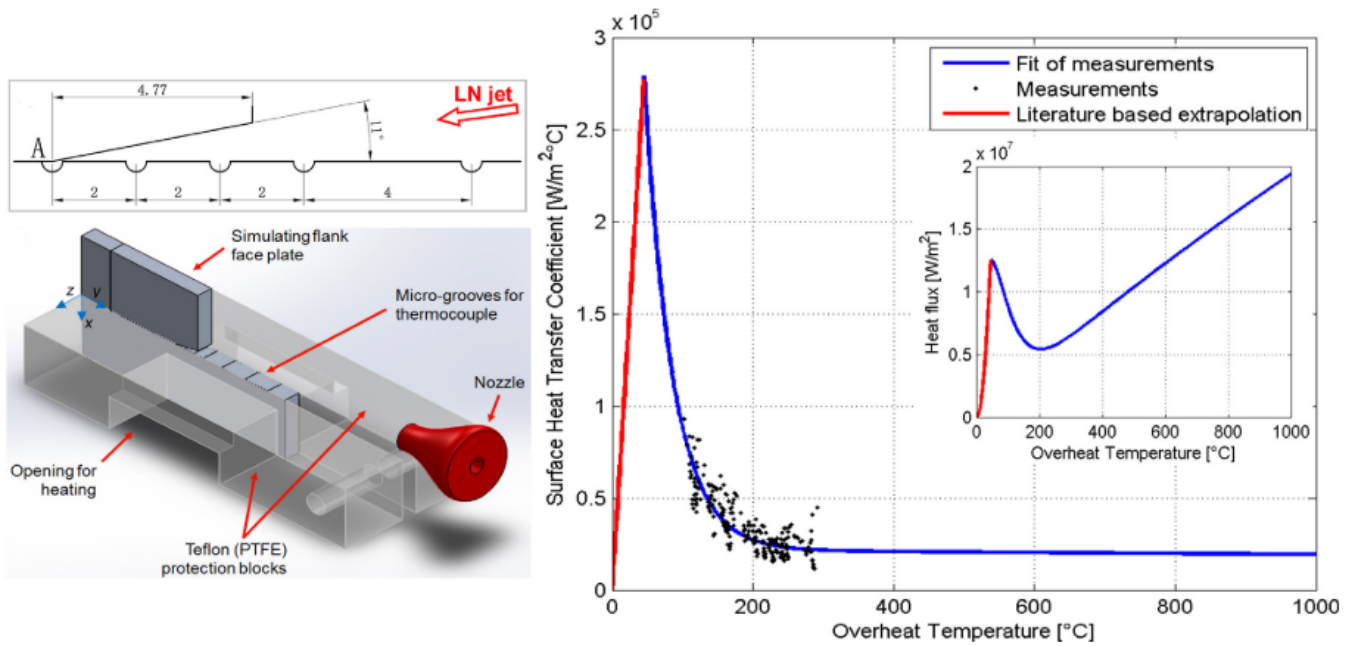


Figure 5.4.1: [48, Pusavec 2016] testing geometry and HTC as a function of wall overheat temperature

The jet speed was between  $4.5 \div 7.4\text{m}/\text{s}$ , the pressure  $1\text{bar}$  and the flow rate unstated, as the distance from which the jet was sprayed. Workpiece drag-out movement was not considered as influential. Nevertheless, the article provides precious insight and data for cutting simulations.

[154, Hribersek 2017] and colleagues, after revising literature results in terms of HTC values, developed an experimental and simulated model so to obtain, by inverse methodology, the HTC in case of normal impinging LN<sub>2</sub> jet on an Inconel 718 plate. They modeled of plate, thermocouple and thermopaste, and a moving area of assumed dimensions for the imprint of the impinging jet onto the plate, to which they manually varied the HTC to match the experimental temperatures registered by the thermocouples. They confirmed the trend underlined by [48, Pusavec 2016]. The highest value of  $75\text{kW}/\text{m}^2\text{K}$  is found for a wall temperature which keeps Nitrogen liquid. After  $\Delta T > 160^\circ\text{C}$  the HTC drops at a value around  $15\text{kW}/\text{m}^2\text{K}$ .

[155, Tahri 2017] et al. investigated the behaviour of liquid Nitrogen in the delivery tubes. As the cooling effectiveness depends on: pressure, velocity, temperature, gas/fluid fraction and pipe geometry, a correct design is needed to avoid unnecessary losses. The pressure of the liquid Nitrogen was varied between 2, 4 and 6 bar, the gas phase between 10, 30 and 50%, also the angle of the final pipe bend was changed. Along the rectilinear pipe, the lower temperature increase at steady state is obtained for the higher liquid quality, the pressure is almost irrelevant. Low angles for the final delivery sector to the nozzle are preferable. Their model didn't consider the wall roughness, and there is no mention of the cavitation effect, it mainly referred to the heat transfer with the

walls.

[156, Lequien 2018] and colleagues made a comprehensive analysis on the HTC for impinging LN2 jet on a plate as a function of different angles, distance, nozzle diameter and pressure. The experimental tests were carried on a plate with a moving nozzle as in [154, Hribersek 2017]. They simulated the heat transfer problem through CFD analysis making iterations on the liquid quality and assuming the heat flow with a Gaussian Normal distribution. They obtained the HTC and a correlation with the input variables. Best results were obtained for high pressure, large diameter, low distance perpendicular jet. The highest HTC reached is around  $15\text{ kW/m}^2\text{K}$ .

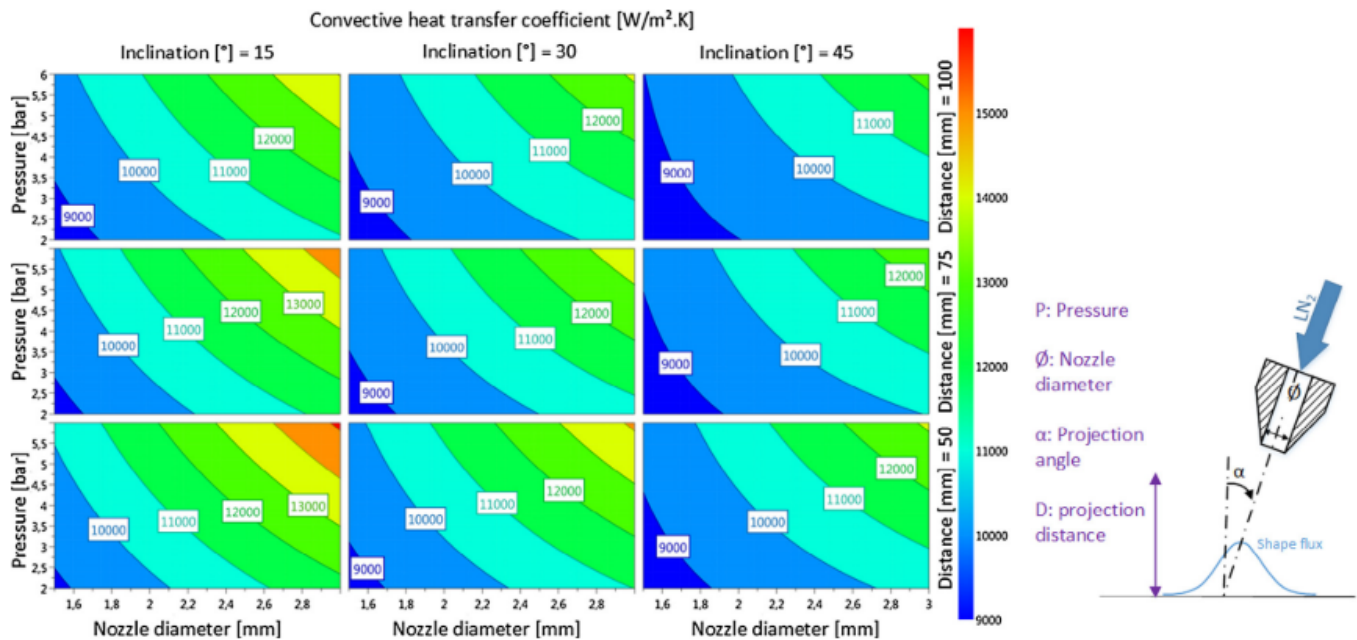


Figure 5.4.2: [156, Lequien 2018] LN2 jet HTC dependence on jet parameters

Since now we have seen how HTC determination articles refer to geometries similar to cutting processes or totally dissimilar (nozzle on a flat plate), no one has tried to solve an inverse heat transfer problem from experimental data that considered a real geometry and working nozzle configuration with the proper heat generation, looking at the HTC at the tool and not at the work material surface.

[49, Tahmasebi 2019] et al. made an exhaustive evaluation of LN2 behaviour in tubes and open air. For internal flow they considered especially cavitation boiling effect, which degraded the liquid quality and clogged the tubes with vaporous bubbles promoting unstable flow, and thermal exchange with the tube walls. For external flow they studied how the jet interacts with air and the insert. Internal flow of a two phase liquid is a complex phenomena and can be arranged as a single phase liquid flow, then vapour bubbles begin to generate as the liquid exchange heat and start to evaporate. Bubbles grow larger and bubble flow is seen, when boiling become important, slug flow and clogging of the tube section by vapour is seen. Annular flow with liquid on the walls is also possible.

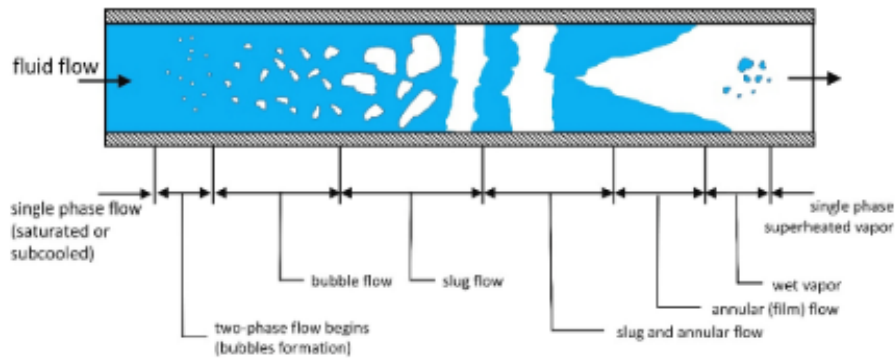


Figure 5.4.3: [49, Tahmasebi 2019] two phase flow behaviour

Internal flow was studied looking at the delivery pipes, the spindle collector and the tool holder channels. The external flow consisted with the jet in air and the interaction with the cutting zone. For what concerns the internal flow, even if the delivery line is completely adiabatic, hydrodynamic cavitation would lead to losses. Cavitation effects were modeled with the Homogeneous equilibrium model, HEM. By assuming non slip conditions with the tube walls and pressures of 2, 4, 6, 8 bar discharge coefficient were calculated. Raising pressure the losses increase due to the cavitation effect.

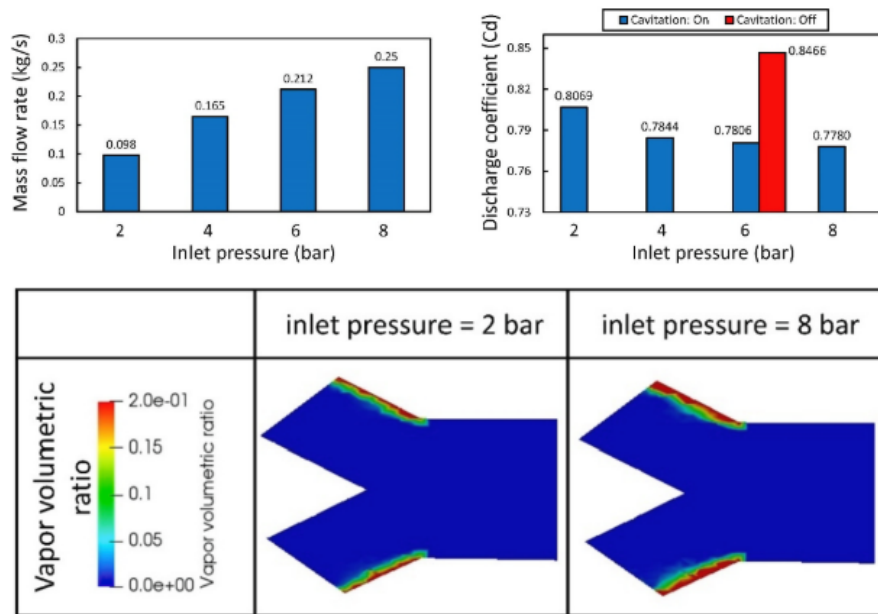


Figure 5.4.4: [49, Tahmasebi 2019] discharge coefficient at variable pressures and importance of cavitation

The low pressure developed in case of strong bends cause the liquid Nitrogen to vaporize and influence the jet behaviour. For what concerns the simulation inside the spindle collector the main problems were related to the large contact area of non insulated steel. Experimental and simulated flow rate at the ring exit were strongly different, meaning that the hypothesis of full liquid state at the beginning of the ring

was not real. What become evident is that a Nitrogen supply system should be designed with the minimal amount of surfaces for the liquid to exchange heat with. For what concerns external flow,  $2 \div 10 \text{ bar}$  flow pressures were tested. The highest pressure resulted poor because it washed liquid away too fast from the hot surfaces and was reflected back from the insert faces. The cutting zone was surrounded by more liquid if the pressure was maintained low.

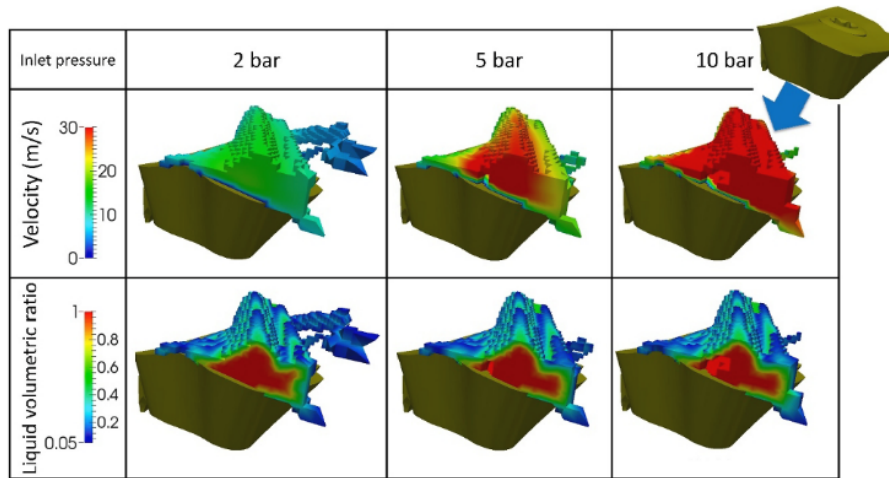


Figure 5.4.5: [49, Tahmasebi 2019] distribution of Nitrogen jet splashed on the insert face

Experimental tests were performed to verify the CFD simulation findings. High pressure LN2 cutting was similar to dry cutting while low pressure delivery generated the lower forces. In conclusion, the Authors' advice is to provide flows with pressures around  $2 \div 4 \text{ bar}$ , making a careful design of the delivery line to avoid strong bends that increase cavitation, and limit the surface heat exchange areas. This would not only provide better cutting performances but economic LN2 consumption as well. Rotation effects and insert high temperature must be considered for a complete evaluation. Then distribution of jets on tool and workpiece surface could be used to set thermal boundaries of FEM analyses.

[157, Golda 2019] et al. concentrated on the gas layer formed when a LN2 jet goes in contact with a hot surface. When a liquid Nitrogen stream comes in contact with a hot surface it evaporates suddenly, the time of liquid contact with the surface being almost null if compared to the gas contact.

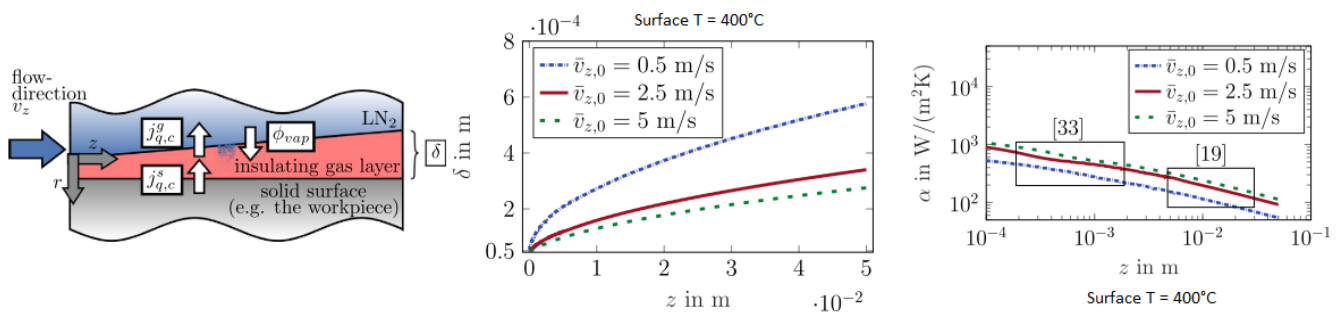


Figure 5.4.6: [157, Golda 2019] gas layer and HTC

The author stated that no contact between liquid and the cutting zone take place during machining, due to the high surface temperature, therefore determining the behavior of the gas layer is fundamental. They also accounted for the fact that, in most applications, the jets are parallel to the tool and workpiece surfaces, because they need to reach the flank and rake crevices. Therefore they modeled the evolution of the gas layer for a jet parallel to the surface, considering a heat transfer in the vertical direction. The gas layer grows proportional to the distance from the nozzle, the lower the speed (pressure) the larger the growth, the more the evaporated LN2, the lower the HTC due to the insulation of the gas layer. The heat transfer coefficient for a jet sliding on a tool face would be in the order of  $1kW/m^2K$ . So for what concerns a cutting simulation, for the portion of jet sliding on tool and workpiece surfaces the heat transfer would be much lower than what stated by other studies. At the end of crevices, the abrupt stop experienced by the jet may cause stirring and breaking of the gas layer, which could provide an increase in the cooling capacity.

## 5.5 Cryogenic machining simulations

*Chip formation simulations require a lot of information for the set up. Even the mere choice of the appropriate material and damage models must be done carefully. Friction models are often adopted as Coulomb-Tresca, for their simplicity and accuracy after having tuned the coefficients. Heat transfer coefficients with ambient air have little influence on the results due to the short simulated process time, interface conductance is often applied much high so to speed up thermal convergence. Cryogenic machining simulation increase the complexity of the problem: proper HTC and heat exchange windows need to be created, material behaviour at low temperature need to be characterized, if not for the shear zones, for the outer chip surface and workpiece skin. Friction condition will also vary. In this section we present the state of the art for cryogenic machining simulations.*

[71, Melkote 2017] and coworkers deeply investigate modeling techniques for metal machining. They reported results in which strain and strain rate fields were measured with Particle Image Velocimetry (PIV) and found to be larger than 10 and  $4 \cdot 10^5 1/s$  for  $1m/s$  cutting speed. Researchers at the NIST developed a system for high speed infrared thermography capable of detecting thermal fields in the shear zone. However, this advances are not yet applied for studying shear bands formation. Based on literature research, they suggest the use of a material model depending on strain, strain rates, temperature, stress state (triaxiality) and microstructure. Due to the complexity and lack of performance of these models, generally phenomenological models are adopted, like the JC (and its modifications), Power Law, strain path models.

Investigating friction modeling, they underlined the complexity of the problem, being influenced by motion, pressure, temperature, stiffness and vibrations. Friction is the most important parameter governing temperature distribution in the tool-chip interface, the best would be to model with  $\tau_f = f(\sigma_n, V_{sliding}, T_{interface}, \sigma_{flow})$ . However, accurate measurements of thermal fields in the interface cannot be done, therefore the danger of making a lot of effort for nothing is tangible. Researches also show as friction increase with tool wear. Research is needed in understanding the variability of results depending on friction modeling. Another issue is to understand the interaction between friction and material models.

Regarding thermal modeling, they suggest implementing HTC distributions instead of average values. Also, care in modeling thermal conductance in the tool-chip interface should be given as well.

Microstructure transformations affect material behaviour: recovery, recrystallization, grain growth, twinning, solid state transformations. These phenomena need to be described and understood so to update the flow stress of the material.

[158, Bordin 2015] and coworkers developed a FEM model to reproduce the performance of dry and cryogenic cutting of Ti6Al4V. They used a full Calamaz modification, as in [143, Sima 2010] model 2:

$$\bar{\sigma} = [A + B\varepsilon^n] \left[ 1 + C \ln \frac{\dot{\varepsilon}}{\dot{\varepsilon}_0} \right] \cdot \left[ 1 - \left( \frac{T - T_r}{T_m - T_r} \right)^m \right] \cdot \left[ D + (1 - D) \cdot \tanh \left( \frac{1}{(\varepsilon + p)^r} \right)^s \right]$$

$$D = 1 - \frac{T}{T_m}, \quad p = \left( \frac{T}{T_m} \right)^s$$

For the values of the parameters we address to the article literature (as the authors have done in turn). Coulomb-Tresca friction model was adopted, with  $m = 0.4, \mu = 0.3$  for cryogenic and  $m = 0.3, \mu = 0.2$  for dry cutting. A cryogenic window was set with  $h_{cryo} = 20 \text{ kW/m}^2\text{K}$ . Results showed agreement with the cutting force, less accuracy was found for the feed force and the temperature measurements, obtained experimentally with an embedded thermocouple. The model was also used to investigate the depth of the deformed layer left on the surface of the workpiece, however no comparison with an experimental value was added. Interesting is that the tool was cut and an adiabatic boundary was set to limit the mesh size.

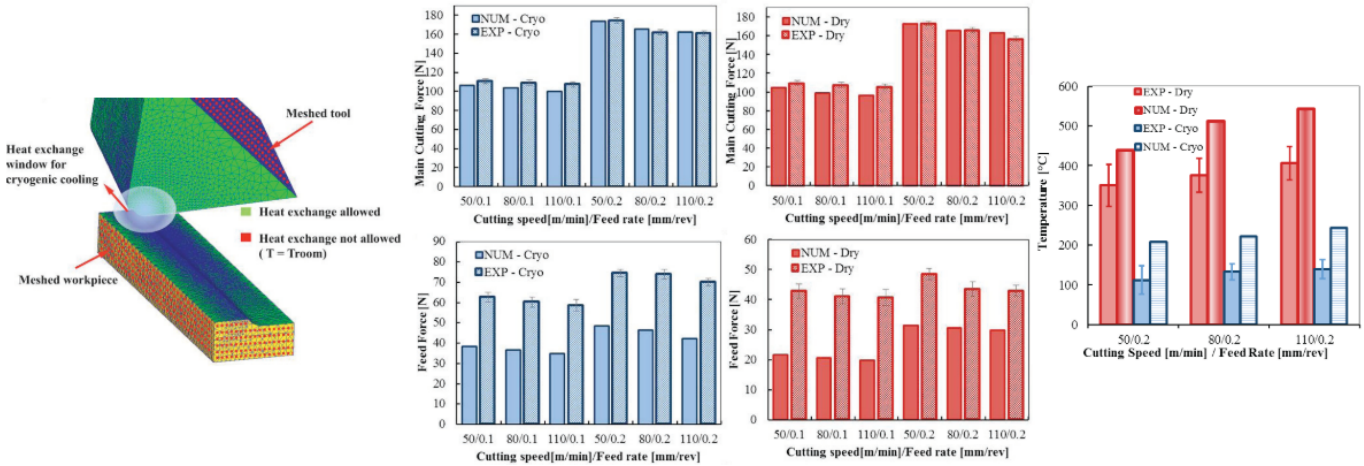


Figure 5.5.1: [158, Bordin 2015] FEM model, force and temperature predictions

[159, Davoudinejad 2015] and colleagues simulated dry and cryogenic chip formation in orthogonal cutting for Ti6Al4V. The material model was introduced in tabular form, however no indication of the source was presented. Coulomb friction model was adopted, with  $\mu = 0.55$  for the dry case and  $\mu = 0.62$  for cryogenic. They tested different jet spot diameter on the rake face and heat transfer coefficients, choosing  $2000 \text{ kW/m}^2\text{K}$ . This value is much higher than literature evaluations done later and



is justified by the rapid convergence of thermal fields. Cutting and feed forces agree well with experimental results, from which friction coefficients were taken. Chip morphology was averagely well predicted, however no clear comparison of simulated and experimental chip segmentation have been done in the article.

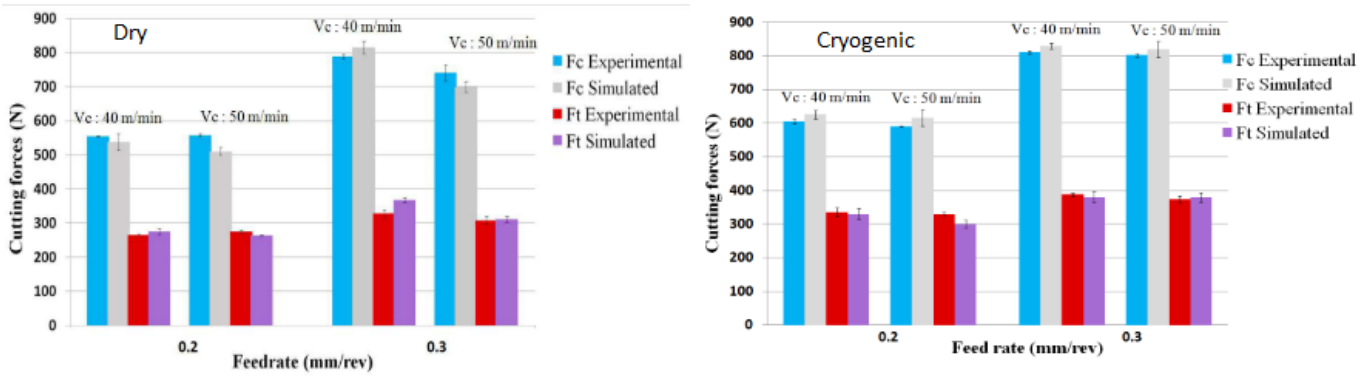


Figure 5.5.2: [159, Davoudinejad 2015] FEM model, force predictions

[160, Imbrogno 2017] and teammates simulated turning of Ti6Al4V for dry and cryogenic cases. They adopted a full Calamaz modification with  $A, B, C, n, m$  coefficients from Lee and Lin’s study and  $a, b, c, d$  parameters from [143, Sima 2010]. They adopted Coulomb-Tresca friction model and with  $[m, \mu] = [0.95, 0.8]$  for dry and  $[m, \mu] = [0.6, 0.5]$  for the cryogenic case, obtained after the calibration phase. Cylindrical windows were set up to represent the cryogenic jets, the HTC was interpolated as in [161, Umbrello 2016],  $20 \text{ kW/m}^2 \text{ K}$  was adopted as HTC with air as in most studies.

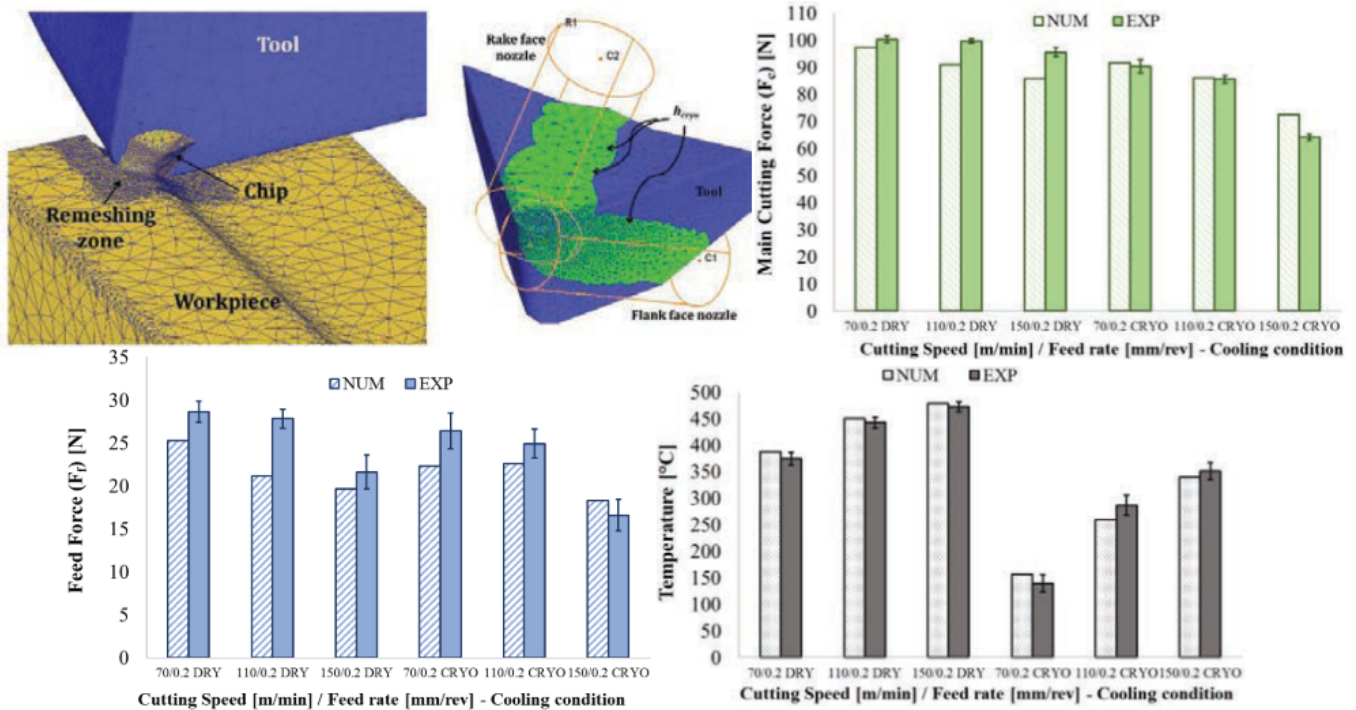


Figure 5.5.3: [160, Imbrogno 2017] FEM model, force and temperature predictions

Cutting, feed forces and chip front temperature showed good agreement with the experimental results. Accurate prediction of the deformed layer was also achieved. [162, Stampfer 2019] and colleagues simulated different applications of cryogenic flux in machining. External and internal delivery for cryogenic jets were tested. A variable HTC function of surface temperature was implemented in the model, however it represent an increasing trend with the surface temperature, which is contrary to some literature findings. The internal jet configuration was based on a micro hole in the insert at variable position and of variable diameter. A user remeshing algorithm was launched every  $5\mu\text{m}$  of machined material, updating heat transfer coefficients as well. To promote thermal steady state in the tool with small simulation time, the specific heat capacity of the tool was reduced. Heat exchange with air was modeled with  $100\text{W}/\text{m}^2\text{K}$  HTC, a value a little higher than usual that accounts for the cooler  $\text{N}_2$  environment. Tool temperatures were found lowest with a combined effect of internal channel at  $1.5\text{mm}$  from flank face and external jet providing  $1.5\text{mm}$  of cooling length contact. Moreover, the most efficient internal channel was found to be the farthest from the flank face, which result also in lower weakening effect of the edge.

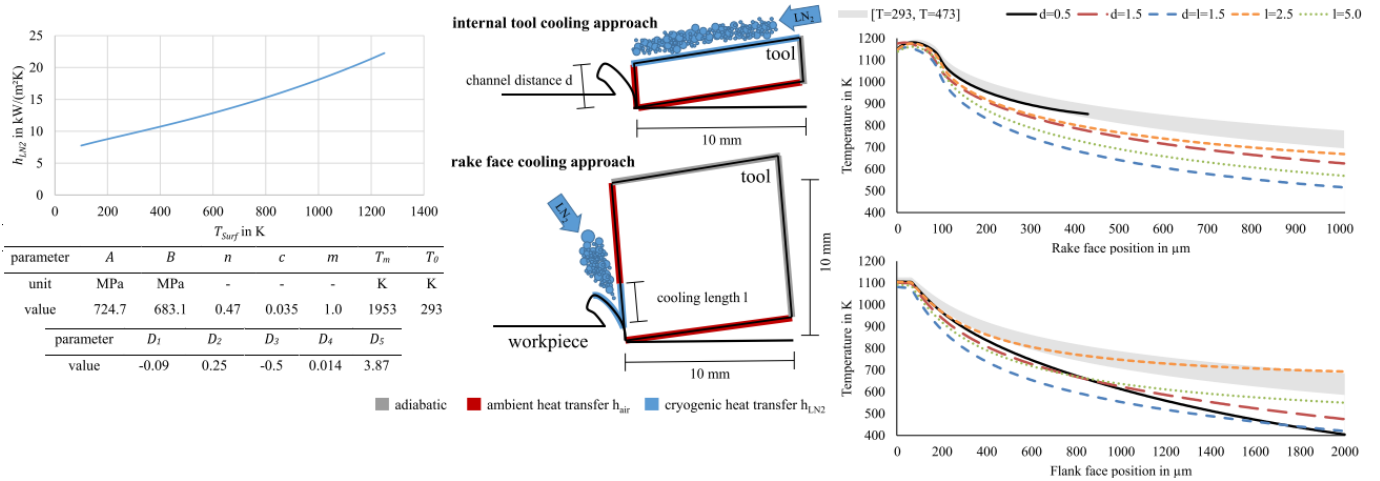


Figure 5.5.4: [162, Stampfer 2019] FEM model and thermal results

## 5.6 Hybrid Modeling

Analytical and numerical models have been combined to better characterize complex machining processes. Thermal, fluid-dynamic and mechanical processes have been implemented contemporarily or in separate stages of modeling. Different heat transfer models could be used to predict heat transfer coefficients then used to compute cutting forces into a mechanical model. [163, Salame 2019] and colleagues analysed cryogenic machining by means of FEM and CFD simulations. The thermal fields resulting from an orthogonal cutting simulation of Ti6Al4V ( $V = 150\text{m}/\text{min}$ ,  $0.3\text{mm}$  feed,  $\mu = 0.3$ ) were then applied to a CFD model studying the HTC of LCO2 jets. JC material and Damage models were used. For the heat generation, a simple model was adopted where the heat generated in the primary and secondary deformation zones are:

$$q_{shear} = F_v \cdot V \quad q_{friction} = \frac{F_{fr} \cdot V}{r}$$

with  $[F_v, V, r]$  are respectively average cutting force, cutting speed, chip ratio  $t_{chip}/t_{undeformed}$  and  $F_{fr} = F_v \sin \alpha + F_f \cos \alpha$ , with  $F_f$  average feed force. For what concerns the CFD analysis, VOF equations were adopted to model the phase transfer in the LCO2, however only liquid and gas phase were considered, whereas LCO2 jets exhibits also solid phase. A  $k - \epsilon$  turbulence model was adopted. The jets had  $8bar$  pressure (strange for LCO2) and distance between the target of 4 and 8 mm. Interestingly the  $8mm$  distant jet proved to be more effective. The higher distance allowed for lower speed and broke the conductive heat transfer in the jet, guaranteeing higher liquid phase at the stagnation point. The HTC were found to be  $38.8$  and  $49.8 kW/m^2K$  respectively for 4 and  $8mm$  distant nozzles. However, the simulated geometry is not corresponding to a real cutting tool. Moreover, the FEM and CFD models were considered totally uncoupled, whereas cryogenic machining could affect friction and cutting temperature, affecting the HTC in his turn.

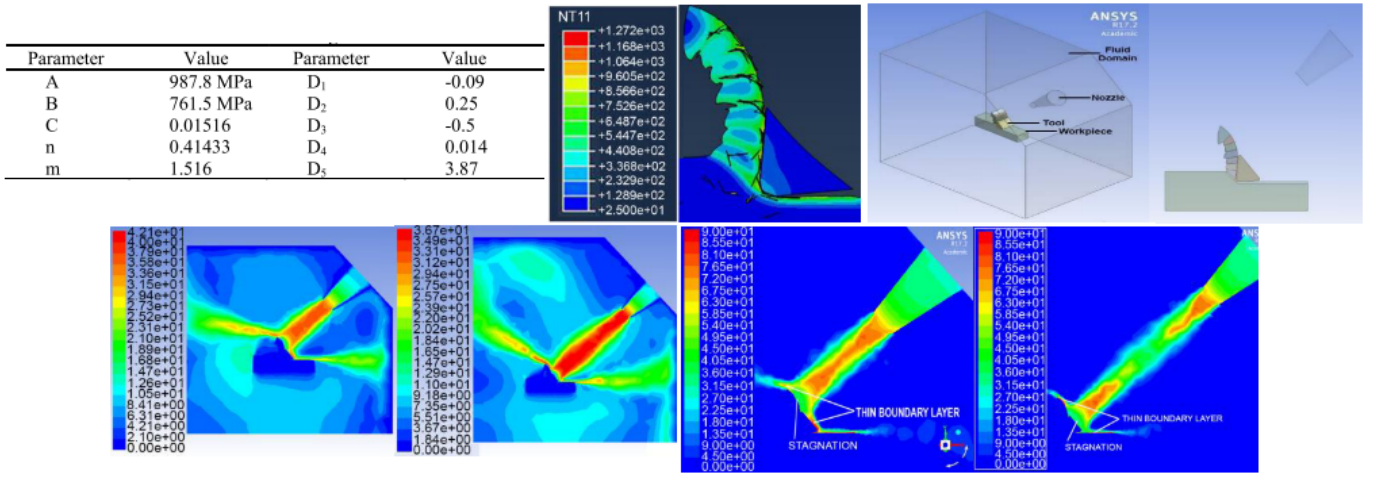


Figure 5.6.1: [163, Salame 2019] hybrid model set up and results

[164, Shi 2019] and coworkers analysed cryogenic machining of Ti6Al4V with a hybrid modeling technique. RANS with TKE (Turbulence Kinetic Energy) model were adopted, added by Multiphase Cavitation Model approach for the double phase LN2 flow. The HTC is calculated by  $h_{cryo} = \frac{q}{\Delta T}$  where  $\Delta T = T_{surface} - T_{fluid}$ ,  $q = k \frac{\partial T}{\partial x}$  with  $k$  conductivity of the hot target and  $\frac{\partial T}{\partial x}$  the temperature gradient in the hot target. The CFD simulation consisted in a jet-on-plate configuration, with a hot target at  $700^\circ K$ , nozzle of  $1mm$  diameter, placed at  $20mm$  distance from the target,  $1l/min$  flow and  $20m/s$  flow speed out of the nozzle. The HTC was found between  $24 \div 50 kW/m^2K$ . FEM simulations were run with  $h_{cryo} = 32 kW/m^2K$ ,  $\mu = 0.28$  and Voce Power Law:

$$\bar{\sigma} = [a - be^{c\bar{\epsilon}}] \cdot \left[ \left( \frac{\dot{\bar{\epsilon}}}{\dot{\bar{\epsilon}}_0} \right)^d \right] \cdot \left[ \left( \frac{T}{T_0} \right)^v \right], \quad [a, b, c, d, v] = [1705.2, 837.6, -1.92, 0.0048, -0.86]$$

Force results matched very well the experimental findings. Since thermal convergence in a 3D cutting simulation is time and resource demanding, a 2D orthogonal model was set up for analyzing the thermal build up in the tool-chip interface. The temperature profiles were used to estimate tool wear with Usui law:

$$\frac{\partial w}{\partial t} = A \cdot \sigma_n \cdot V_s \cdot e^{Q/T}, \quad A = 7.8 \cdot 10^4 \frac{1}{MPa}, Q = 2500^\circ K$$

where the adhesive wear rate is related to the normal pressure, sliding velocity and temperature. The wear rate is an increasing exponential function of temperature, therefore lower temperature results in lower wear rate. The article aims at characterizing cryogenic machining in a complete way, from CFD to FEM modeling and wear prediction. Furthermore it offers interesting thermal profiles on rake and flank faces.

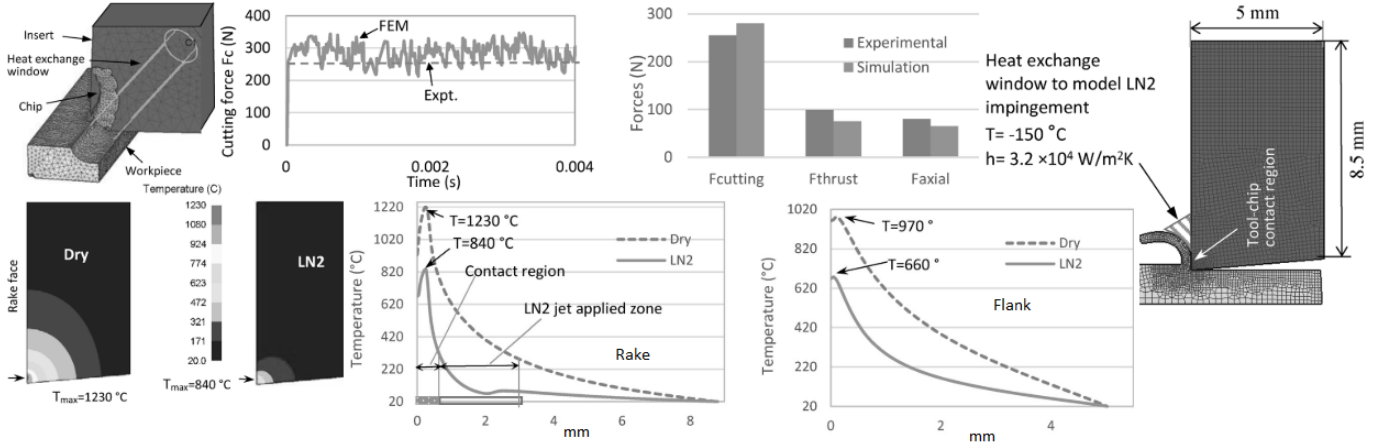


Figure 5.6.2: [164, Shi 2019] 3D FEM model and results, 2D model and thermal profiles

## 5.7 Surface integrity prediction models

One of the desired outcome of machining process simulations is the prediction of surface characteristics. Models have been implemented with sub routines that can predict metallurgical morphology, dynamic recrystallization, phase transformation and residual stresses onto the machined surface. In this section we will briefly analyse the state of the art and the strategies adopted to simulate surface alterations.

[165, Rotella 2014] and Umbrello developed a user subroutine to predict grain size and hardness variation, influencing material flow stress, for dry and cryogenic machining of Ti6Al4V:

$$\bar{\sigma} = \left[ a + \frac{k}{\sqrt{d}} + B\varepsilon^n \right] \left[ 1 + C \ln \frac{\dot{\varepsilon}}{\dot{\varepsilon}_0} \right] \cdot \left[ 1 - \left( \frac{T - T_r}{T_m - T_r} \right)^m \right] \cdot \left[ D + (1 - D) \cdot \tanh \left( \frac{1}{(\varepsilon + p)^r} \right)^s \right]$$

where only the  $\alpha$ -phase grain size is considered (carrying almost three times the strength of the  $\beta$ -phase).  $a, k$  are material constants. Grain size is modeled depending on dynamic recrystallization from the Zener-Hollomon law, while hardness follows the Hall-Petch law:

$$d = d_0 \cdot b \left( \dot{\varepsilon} e^{\frac{Q}{RT}} \right)^m, \quad HV = C_0 + \frac{C_1}{\sqrt{d}}$$

Cutting forces were found quite accurate when compared to the experiments. Grain size distribution along the depth of the workpiece was steeper than the experimental case, however the values quite agreed.

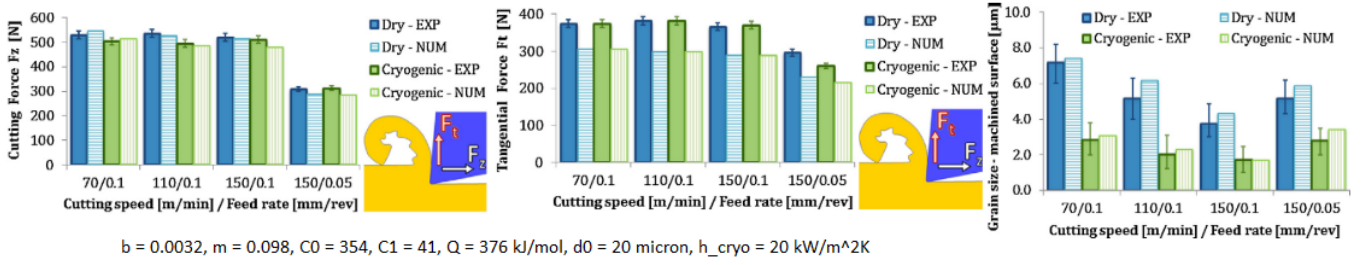


Figure 5.7.1: [165, Rotella 2014] grain size prediction model

[161, Umbrello 2016] and coworkers analysed microstructural changes like grain size and hardness for dry and cryogenic machining of AISI 52100 bearing steel. Interestingly, they provided a correlation for the HTC of a cryogenic jet depending on fluid properties and implemented a heat transfer coefficient variable in temperature:

$$h_{cryo} = \frac{0.2}{e^{0.35} g^{0.33}} \frac{V_f^{0.65} k_f^{0.67} c_p^{0.33} \gamma_f^{0.33}}{\nu_f^{0.32}} = -8 \cdot 10^{-6} \cdot T^3 - 0.0149 \cdot T^2 + 44.397 \cdot T + 10162$$

The temperature in question was not clear to whom it belong, probably the temperature on the impinging surface. The Brozzo fracture model was adopted, where the maximum tensile stress is normalized by the difference with the idrostatic stress:

$$D = \int_0^{\bar{\epsilon}_f} \frac{2\sigma_1}{3(\sigma_1 - \sigma_m)} d\bar{\epsilon}$$

The author further developed an hardness based flow stress model for the bearing steel, adding grain size and hardness variation:

$$\sigma = B(T) \cdot \left[ \left( a + \frac{k}{\sqrt{d}} \right) \epsilon^n + F + G \cdot \epsilon \right] \cdot \left\{ 1 + \left[ \log(\dot{\epsilon})^m - A \right] \right\}$$

$$d = \begin{cases} d_0 & \epsilon < \epsilon_c = C_0 Z^{n_Z} \\ d_{DRX} = bZ^p = b \left( \dot{\epsilon} e^{\frac{Q}{RT}} \right)^p, & \epsilon > \epsilon_c \end{cases}, \quad HRC = C_1 + \frac{C_2}{\sqrt{d}}$$

where  $d$  is the new grain size, to be updated after a recrystallization strain threshold. The parameters  $F, G$  are dependent on hardness,  $B(T), A, m, n$  are other model parameters described in the previous articles,  $C_1, C_2$  are derived by metallurgical experiments, as  $a, k$ . The constants  $p, b, C_0, n_Z$  are calibrated by comparing with experimental results. The model has got more than 13 constants, that have been calibrated in different studies. The goodness of the model is shown by the ability to predict grain size and hardness of the surface layer.

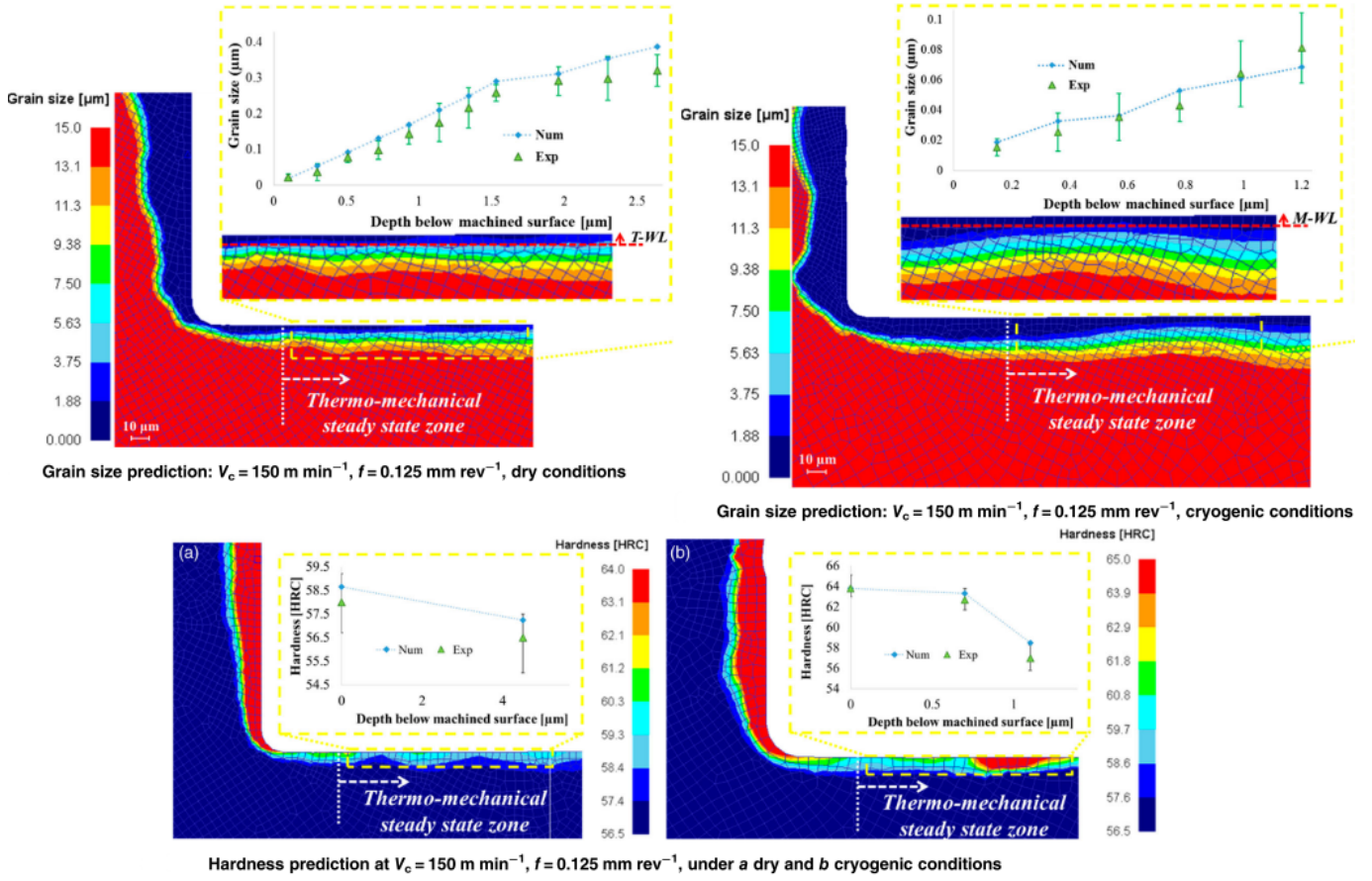


Figure 5.7.2: [161, Umbrello 2016] grain size and hardness prediction model

[166, Umbrello 2017] and colleagues investigate surface modification simulating turning of Ti6Al4V. They modeled the alpha phase lamellae orientation and thickness in the deformed layer. They implemented a Calamaz modified JC model, substituting the term  $A$  with a strain rate and temperature dependent function, depending on the alpha phase lamellae thickness:

$$\bar{\sigma} = \left[ a + \frac{k}{\sqrt{t}} + B\varepsilon^n \right] \left[ 1 + C \ln \frac{\dot{\varepsilon}}{\dot{\varepsilon}_0} \right] \cdot \left[ 1 - \left( \frac{T - T_r}{T_m - T_r} \right)^m \right] \cdot \left[ D + (1 - D) \cdot \tanh \left( \frac{1}{(\varepsilon + p)^r} \right)^s \right]$$

with  $[a, k] = [708.73 \text{ MPa}, 265.57 \text{ MPa} \sqrt{\mu\text{m}}]$ .  $B, C, n, m$  parameters were taken from Lee and Lin's work,  $s = 0.05, r = 2, d = 1, b = 5$ . The value of  $t$  was obtained through a Matlab regression with experimental lamellae thicknesses and FEM calculated strain rate and temperatures. The hardness value was represented by a Hall-Petch law  $H = C_1 + \frac{C_2}{\sqrt{t}}$ . The cryogenic case was added by a window on the flank face with a variable HTC as in [161, Umbrello 2016]. Friction coefficient (pure Coulomb model) were found between  $0.2 \div 0.3$  for the dry case and  $0.3 \div 0.4$  for the cryogenic.

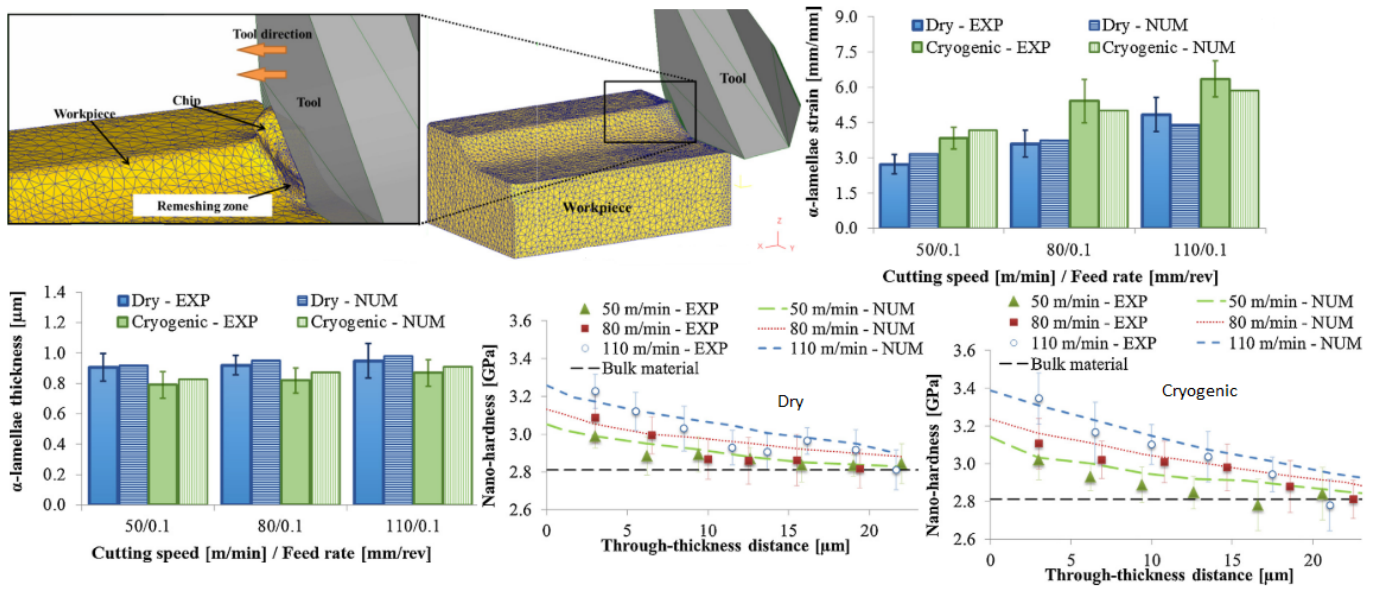


Figure 5.7.3: [166, Umbrello 2017] FEM model, alpha lamella thickness, strain and hardness prediction model

# Chapter 6

## FEM models for Cryogenic Milling

In this chapter, cryogenic milling FEM modeling will take place. It will deal with cryogenic milling tests using a tool with positive angles and square shoulder design. A model has been already set up by a previous student, however its material was lost. A new model need to be prepared, more robust (covering more feed and speed combinations) and guarantee lower calculation time. The main objective of the work was to analyse tool mechanical and thermal stresses between a square shoulder inserts and an high feed mill design with rounded inserts. Experimentally, the square shoulder design exhibit poor tool life performances in cryogenic environment against dry and wet cutting, while the high feed behaved slightly better for cryogenic than emulsion cooling. However, the aim proved to be too demanding. Several problems were encountered which made imperative a comprehensive analysis of the literature and the set up of a new, more robust, faster, trustful model. No time was left for setting up the high feed model, neither for running a square shoulder simulation with deformable insert so to extract tool stresses and thermal cycles, nor even a simulation which could provide a completion of the cutting arc.

The main problems have been: the lack of a reliable material model, necessity of iterations to determine optimal mesh sizes, iterations for damage model fitting, force fitting with friction coefficients, added to a lack of experimental data especially for the thermal boundaries (workpiece and tool bulk temperatures, cryogenic environment temperature).

The main drawback of the work is that simulations are run in dry and cryogenic environment only. That was due to availability of experimental results, and process complexity reduction. Simulations are not meant to underline dry, cryogenic or emulsion superiority, but only to reproduce experiments. Moreover, the model set up had so many issues that was easier to calibrate it at first for dry than for emulsion, getting rid of a media to be characterized with relative jet HTC, ambient HTC, etc.

We strongly hope the model to be useful for future speculations on tool stresses between the two milling approaches previously described.

### 6.1 “Square shoulder” model

Numerical machining models require a calculation mesh, which could be based on a CAD file, defining the geometry of the cutting process. Files are then imported into



a FEM program and the set up is added by the material model, the necessary fixturing and motions, the interaction between parts, friction and heat exchange properties. FORGE Nx T 3.0 has been chosen as FEM program. The software is dedicated to forging simulations and easily deal with large deformation, friction and heat exchange phenomena, allowing to chain simulations one after the other, designing an entire process. Dies (rigid or deformable) and deformable objects are easy to deal with and can move from one simulation to another carrying their field history. It uses Lagrangian formulation and a built-in remesher. Remeshing could be regulated by the user, following strain, strain rate, temperature gradients. The software allows the computation on multiple cores, depending on the license. Calculation were often done with 16 cores on a 60 core - 4 processors workstation with 2.5 GHz base clock speed and 356 GB DDR3 RAM.

### 6.1.1 Geometry generation

The geometry of the model is made by the part to cut and the cutting insert. Two additional features are needed: the workpiece fixturing system and the tool fixturing system (tool holder plate). This two latter geometries are required by the program to deal with deformable objects. There will be no necessity to use the tool holder plate to deal with a rigid insert, but the plate will be needed when dealing with a deformable insert. Autodesk Fusion 360 have been used for the CAD generation. It is an online CAD program offering the possibility to share and work simultaneously on the same project with different people, without downloading heavy packages on personal devices. Tool geometries are retrieved from producer websites. Assemblies are comprehensive of tool-holder and fixturing bolts. Only the inserts are loaded for the cutting model assembly. After some initial simulations, insert geometries are further reduced to what is interested by the cutting process. Simple cuts are done so that it would be easy to place thermal boundaries in case of tool thermal computation. Only small Tetrahedral tool portion is kept, while for the WP a semicircular one. This allows for the most limited amount of volume mesh obtainable which guarantees thermal uniformity (thermal gradients never reaches the boundary too steeply within the simulation time).

For a correct simulation of forces, prior insert pass along the arc is needed. This is generated with the aid of a sweep extruded cut in Autodesk Fusion 360. Unfortunately the CAD program didn't allow a sweep extrude cut of a 3D object along a profile, but the sweep of a 2D planar sketch only. Therefore, the insert was placed considering the tool holder mounting (correct insert angles) and the trajectory and then projected on a plane. The plane projection have been used as a profile for the sweep cut.

The tool follows a cycloid trajectory: the centre of the tool holder translates while the insert rotate around the holder centre:

$$\bar{x}(t) = \begin{bmatrix} x(t) \\ y(t) \end{bmatrix} = \begin{bmatrix} -Re\{d \cdot e^{j\vartheta}\} + S_f - S_t \\ -Im\{d \cdot e^{j\vartheta}\} \end{bmatrix}, \quad \begin{cases} \vartheta &= (\frac{\pi}{2} - \theta) + \omega \cdot t - S_\theta \\ S_f &= v_f \cdot t \end{cases}$$

where:  $d$  is the radius of the trajectory, defined as the distance from tool holder centre and insert fixing bolt centre,  $S_\theta, S_t$  are respectively engagement shift (along the arc) and translation shift (along the holder feed direction) of the tool centre,  $v_f$  is the linear advancement feed in  $mm/s$ .

PARAMETERS	SYMBOL	UNIT	VALUE
<b>TOOL</b>			
DIAMETER	D	[mm]	20
INSERT N°	Z	[-]	2
RADIAL ANGLE		[deg]	9.052
AXIAL ANGLE		[deg]	10.026
<b>CUTTING CONDITIONS</b>			
SPEED	Vc	[m/min]	50
FEED	Fz	[mm/(rev*tooth)]	0.15
ADOC	ADOC	[mm]	3
ENGAGEMENT	Eng	[%]	25%
RDOC	RDOC	[mm]	5
ENG. ANGLE	$\theta$	[rad]	1.05
SPINDLE SPEED	SS	[rev/min]	795.77
SPINDLE ROTATION	$\Omega$	[rad/s]	83.33
LINEAR FEED	F	[mm/min]	238.73
MRR	MRR	[cm <sup>3</sup> /min]	3.58

<b>CYCLOID PARAMETERS</b>			
HOLDER TO INSERT CENTRE	d	[mm]	6.385
ADVANCING SPEED	Vf	[mm/s]	3.979
REVOLUTION SPEED	$\omega$	[1/s]	83.333
INSERT CENTRE TO SURFACE	z	[mm]	5.642
TOOL CENTRE SHIFT	g	[mm]	1.182
ENGAGEMENT SHIFT	S $\theta$	[rad]	0.3
TRASLATION SHIFT	St	[mm]	0
<b>SIMULATION PARAMETERS</b>			
SIMULATION TIME	t	[s]	0.01257
LINEAR FEED	F	[mm/s]	3.9789
SPINDLE SPEED	SS	[rpm]	795.77
ROTATION CENTRE ALONG X	Ox	[mm]	-0.15
COOLING TIME	CT	[s]	0.06283

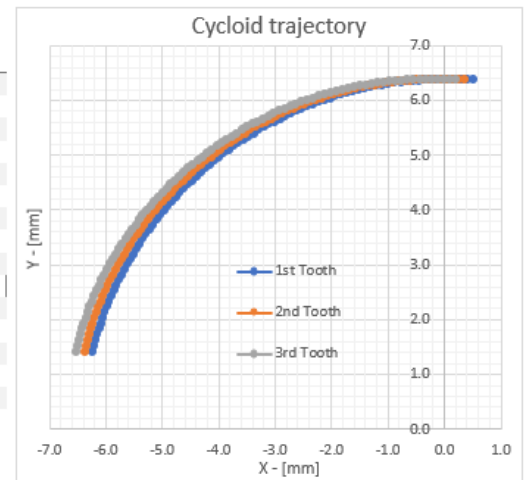


Figure 6.1.1: Process parameters and trajectory generation for the 0.15 mm/tooth feed, 3 mm depth, 50 m/min speed simulation

PARAMETERS	SYMBOL	UNIT	VALUE
<b>TOOL</b>			
DIAMETER	D	[mm]	20
INSERT N°	Z	[-]	3
RADIAL ANGLE		[Deg]	0
AXIAL ANGLE		[Deg]	4.1
<b>CUTTING CONDITIONS</b>			
SPEED	Vc	[m/min]	125
FEED	Fz	[mm/(rev*tooth)]	0.7
ADOC	ADOC	[mm]	1
ENGAGEMENT	Eng	[%]	75%
RDOC	RDOC	[mm]	15
ENG. ANGLE	$\theta$	[rad]	2.094
SPINDLE SPEED	SS	[rev/min]	1989.44
SPINDLE ROTATION	$\Omega$	[rad/s]	208.33
LINEAR FEED	F	[mm/min]	4177.82
MRR	MRR	[cm <sup>3</sup> /min]	62.667

<b>CYCLOID PARAMETERS</b>			
HOLDER TO INSERT CENTRE	d	[mm]	6.388
ADVANCING SPEED	Vf	[mm/s]	69.630
REVOLUTION SPEED	$\omega$	[1/s]	208.333
INSERT CENTRE TO SURFACE	z	[mm]	3.167
TOOL CENTRE SHIFT	s	[mm]	0.9
ENGAGEMENT SHIFT		[rad]	1
TRANSLATION SHIFT		[mm]	1
<b>SIMULATION PARAMETERS</b>			
SIMULATION TIME	t	[s]	0.010053
LINEAR FEED	F	[mm/s]	69.630
SPINDLE SPEED	SS	[rpm]	1989.44
ROTATION CENTRE ALONG X	Ox	[mm]	1.7

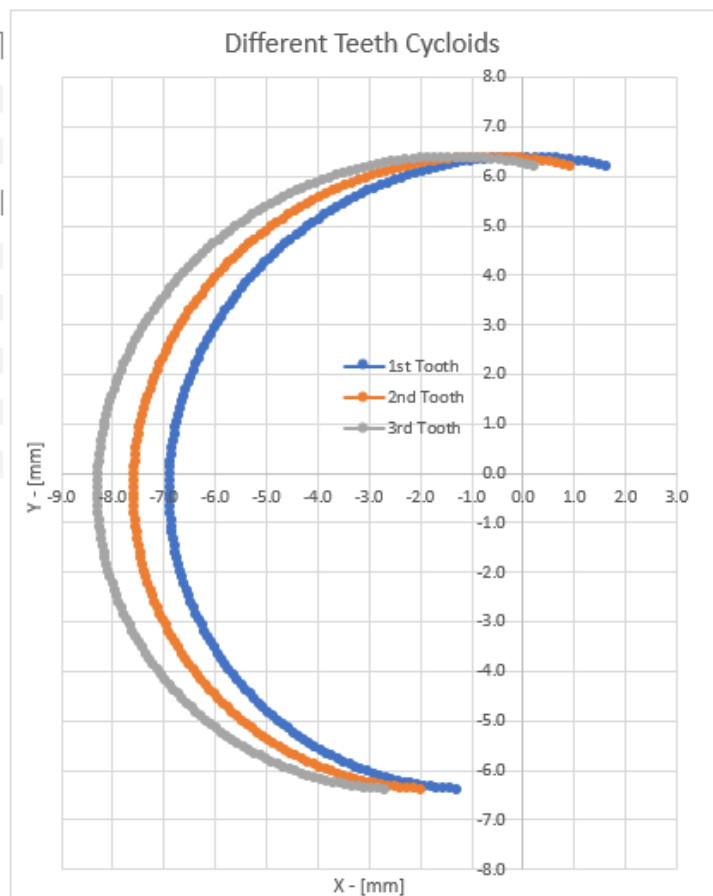


Figure 6.1.2: Process parameters and trajectory generation for the 0.7 mm/tooth feed, 1 mm depth, 125 m/min speed simulation

Other quantities are needed to place the insert in the correct 3D position along the trajectory. Very important is the coordinate system chosen. The tool holder centre at

the first insert passage was placed at the origin, plus a little shift (translational and in rotation angle) in order to extrude a complete cut arc in the first passage and supply enough arc so to simulate a complete cut (amount of which chosen after trials). The piece was placed at  $+5\text{mm}$  along the Y direction so to obtain a 25% engagement of the mill. The 2D trajectory is then added by a Z coordinate accounting for the depth of cut needed, related to the height of the insert centre.

The trajectory is imported in Fusion 360 as a CSV spline. The tool is positioned at the starting point of the cycloid with the correct rotation angles matching its orientation at the time instant at which the constructed trajectory starts. Then a plane is built on the starting point of the trajectory upon which the rake face is projected. The projection is used as a 2D planar profile for the sweep cut extrusion along the cycloidal trajectory.

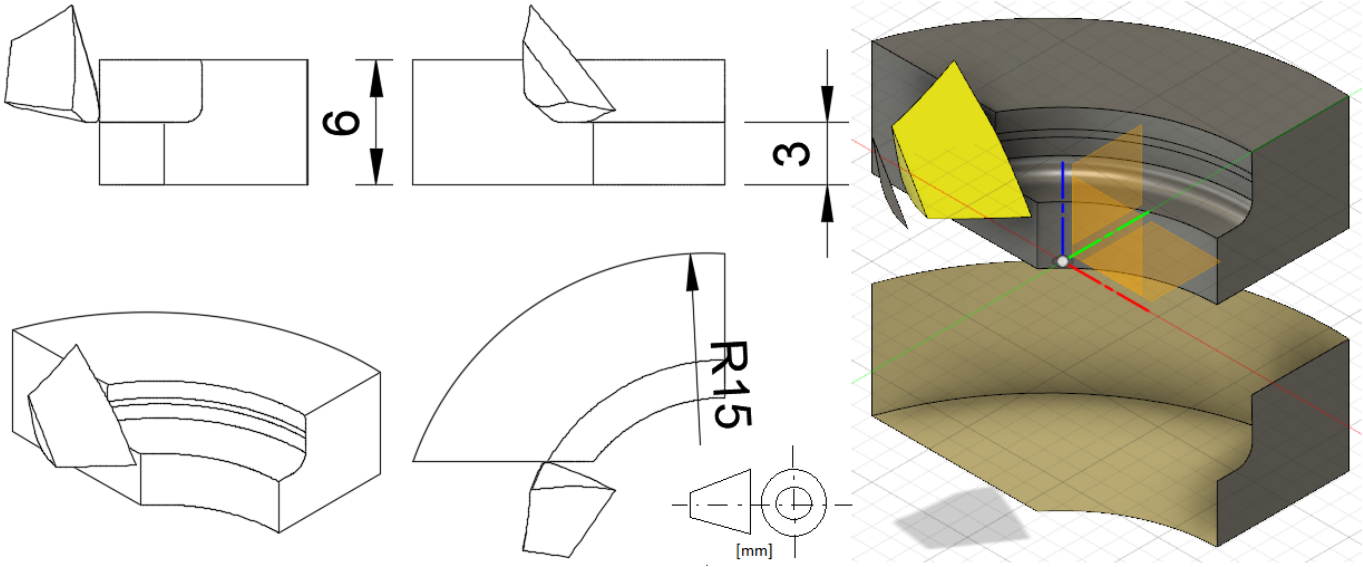


Figure 6.1.3: Final tool, workpiece and fixturing assembly for the “Square Shoulder” case

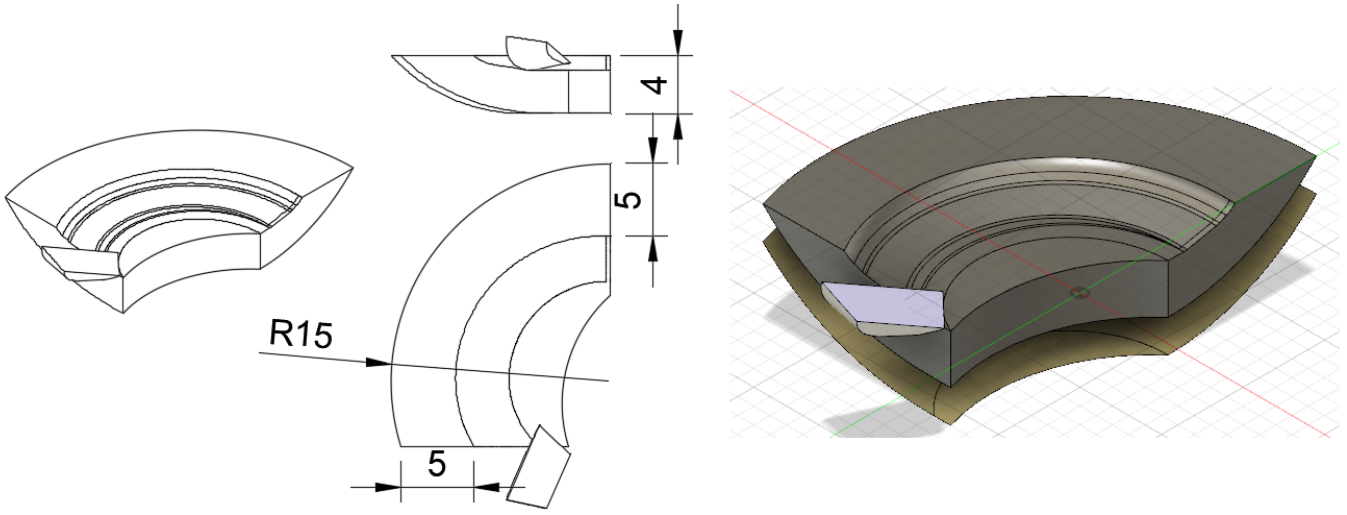


Figure 6.1.4: Final tool, workpiece and fixturing assembly for the “High Feed” case

The dimension of the workpiece (external radius and height) are such that temperature increase at the boundary due to conduction never goes much above ( $\pm 50^{\circ}\text{C}$ ) the initial temperature.

### 6.1.2 Mesh generation

The CAD assembly is imported in FORGE NxT 3.0, then the mesh is generated. Forge allows the use of handy mesh refinement windows which can be fixed to standing or moving objects. A meshing window fixed to the insert is used to refine the tool-chip contact region on the tool. A mesh size of  $50\ \mu\text{m}$  has been chosen and never changed, but should be refined if the insert is modeled as deformable. For the workpiece, wide  $1\ \text{mm}$  mesh triangles have been placed and refined to  $300\ \mu\text{m}$  along the cutting arc,  $80\ \mu\text{m}$  for the formed chip and  $40\ \mu\text{m}$  for the primary shear deformation zone. Remeshing on the workpiece has been triggered by a starting deformation value of 1. The latter two meshing windows on the workpiece have been attached to the insert and moved with it as it was seen that the time needed to remesh was lower than the one needed to the thermomechanical calculations over a fully refined arc.

This final mesh set was the result of improvements and experience gained during the material model set up phase, not the mesh of the initial trials. Meshing and remeshing are the most influencing variables affecting simulation results, above material models.

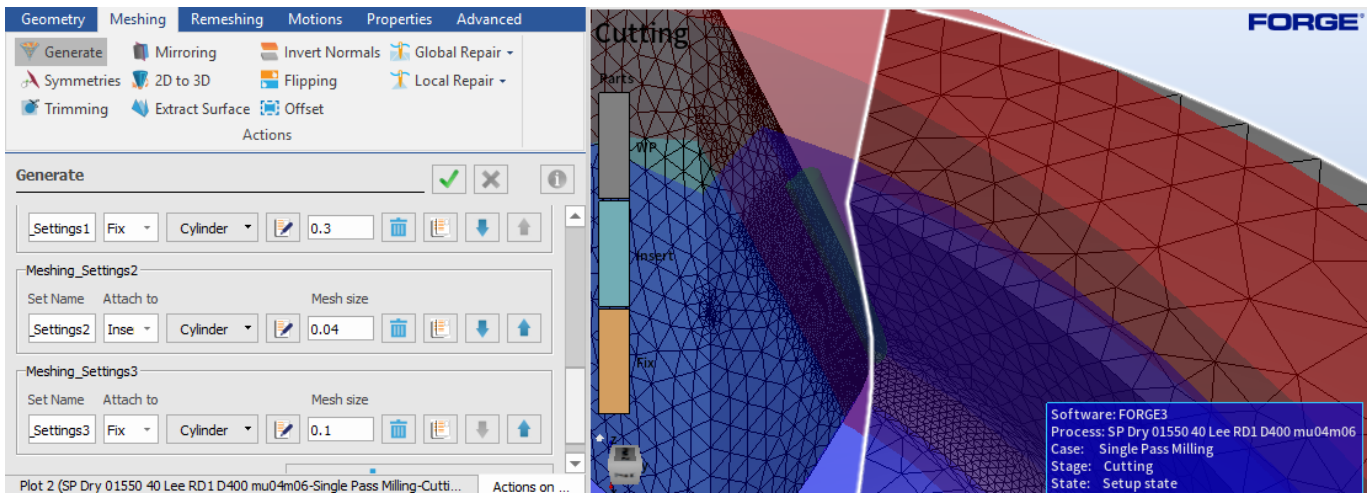


Figure 6.1.5: Meshing the geometries, example

### 6.1.3 Material and thermal properties

Material models in FORGE Nx T 3.0 can be applied from library, as Hans-Spittel equations, material tables, or by external “.tmf” files. Those files can call a coded material model expression (Johnson-Cook, Hans-Spittel and others), or structured tables describing the stress flow as a function of strain, strain rate and temperature. Material properties such as Young modulus, Poisson ratio, density, specific heat capacity, thermal conductivity, linear expansion can be coded with single constants values or temperature variable distributions, also tabular forms summing up all thermal related data can be called. The choice of the material model, as the choice of the friction

behaviour is described carefully in the “Model Fitting” section.

Added to the material model, a damage model have been considered. The Latham-Cockcroft damage model have been initially chosen for its simplicity and lack of material data. However, the criterion is decoupled, which means that one element is deleted once reached the threshold damage value, while it keeps all its strength before the threshold is reached. This behaviour does not correctly model the evolution of fractures in the material. Nevertheless, simulations are run with this criteria. Initial thermal fields were set to  $50^{\circ}C$  for the piece and fix,  $100^{\circ}C$  for the insert,  $30^{\circ}C$  was also the temperature of ambient air. This considered heat build up in the small simulated area after process warm up.

#### 6.1.4 Motions

The workpiece is fixed to the undeformable Fix die. To the tool, a translation along -X direction equal to the linear feed speed in  $mm/s$  is given, added by a rotation along the -Z axis with revolution speed in  $rpm$ , centre of rotation being placed at  $[-0.15, 0.0, 0.0]$ . All this can be easily done in FORGE thanks to the choice of the master die press movement as “Generic Press”. The motion of the dies can be easily checked in “Animation” with the “Kinematic preview”. Measurements have been done checking that effectively the uncut chip thickness answered to the theoretical value. The simulation time have been initially fixed to  $5ms$ , which corresponded to almost  $1/2$  of theoretical engagement ( $12ms$ ).

#### 6.1.5 Interactions

Thermal exchange was set with ambient air blown at  $500kW/m^2K$ , a value higher than usual (Chapter 5). This because the simulated area is very small (less than  $1cm^3$  of workpiece) so we suppose the ambient to be hot, and air strongly agitated by the mill rotation. Nevertheless, the heat transferred with ambient media varies far below  $30W$  with HTC values from  $10 \div 500W/m^2K$ , also ambient temperature has a role. Between workpiece and Fix adiabatic thermal exchange was set, then was checked that the temperature at the interface did not substantially change, if it did, the CAD was modified so to enlarge a bit the modeled workpiece.

Contact properties in FORGE include thermal contact behaviour. The chosen friction model was a stick and slip Coulomb-Tresca friction model, with coefficient  $m$  and  $\mu$  to be fitted with respect to experimental findings. In FORGE, the heat exchange between two bodies in contact, in which one is rigid, is treated by referring to the body effusivity:  $e = \sqrt{\rho \cdot k \cdot c_p} = 1111 \frac{W}{\sqrt{K}} \sqrt{\frac{s}{m}}$  by using  $k = 44.03W/m^{\circ}K$ ,  $\rho = 15250kg/m^3$ ,  $c_p = 188J/kg^{\circ}K$  for the carbide insert. Moreover, the temperature distribution on the rigid body is not calculated. It was assumed of constant temperature of  $300^{\circ}C$ , as an average representative tool skin temperature for the initial part of the cutting arc.

Partitioning the heat at the interface with the ratio between the material effusivities have been discussed in the literature, and the experimental results show that the portion of heat coming into the tool is overestimated, [120, Bonnet 2008a] (Chapter 5: Modeling). However, for initial setting up of the simulation with rigid insert this method was adopted. Moreover, no thermal data have been extracted during the experimental

campaign. This added to the fact that, often, more sophisticated models don't give much more accurate predictions, induced to use the simpler effusivity model.

### Cryogenic machining interactions

For cryogenic machining simulations, a low temperature and high heat exchange window was set up. With the shape of a cylinder, it was designed to reproduce the space occupied by the LN2 jet coming out from the tool holder delivery. A temperature of  $-195^{\circ}C$  was applied to the material surfaces in the window, while the heat transfer coefficient was applied depending on surface temperature as in [48, Pusavec 2016]. Also heat transfer with ambient media considers the presence of cold gases in the neighbourhood of the cutting zone, so the ambient temperature is reduced to  $-150^{\circ}C$  and the HTC with ambient air and LN2 gas is raised to  $1500W/m^2K$ , [48, Pusavec 2016].

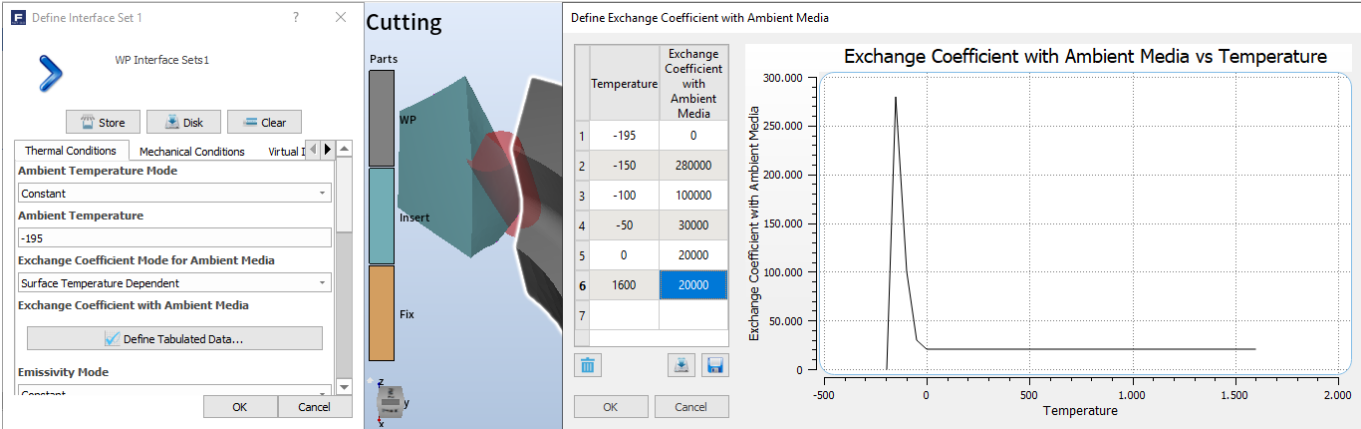


Figure 6.1.6: Cryogenic machining jet window TO CHANGE

Furthermore, the tool temperature is reduced to  $100^{\circ}C$  as the workpiece small simulated portion. This values are mere hypothesis considering qualitative observations during cutting processes and not precise values coming from experiments. The workpiece was left deeply frozen after the cutting trials. Also the cutting period is only 1/8 of rotation, therefore for 7/8 of the circle the tool is subjected to the intense cooling effect of the cold environment plus LN2 jet.

Both concerning literature and experiments at MUSP lab, there is general lack of data regarding thermal conditions in the neighbourhood of the cutting zone (workpiece, ambient and tool side). Also literature often simplify a cryogenic simulation by simply adding a window for the cryogenic jet, not considering the possible colder environment, neither the possible colder tool, neither the possible colder workpiece. Some just set arbitrary values for the initial temperature of the workpiece, unless this values could be actually measured.

For sure, the limitation that arises here is the aim of reproducing a steady state condition cut starting from scratch and with absolutely no information of the boundary conditions. Experiments should help on this side, measuring the average environment temperature, the workpiece thermal field before cut, and the tool thermal conditions while approaching the piece after having been cooled by the jet during the non-cutting phase.

Whereas information of the latter phenomena can be deduced from [37, Augspurger 2019] for the LCO2 case, no studies to the Author knowledge present data for LN2. Here some discussion on the solution of the thermal problem must be done. As we have said, FORGE treats rigid dies as surface meshed bodies with an effusivity. The effusivity is used to calculate the shared portion of friction heat through the formula:

$$q_{tool} = \frac{\sqrt{K_t \rho_t c_t}}{\sqrt{K_t \rho_t c_t} + \sqrt{K_w \rho_w c_w}} \cdot q_f = \frac{eff_{tool}}{eff_{tool} + eff_{wp}} q_f = \beta \cdot q_f \quad q_f = \tau_f \cdot v_{sl}$$

Then  $q_{wp} = q_f - q_{tool} = q_f (1 - \beta)$  is the heat flowing into the tool, used as a heat source for the thermal problem in the workpiece. The conductance at the interface is used to share the heat generated by material plastic deformation:  $q_{tool} = K \cdot (T_{wp} - T_{tool})$ ,  $T_{wp}$  and  $T_{tool}$  are workpiece and tool skin temperatures respectively. Both the effusivity of tool and conductance are therefore important in determining the heat extracted from the contact zones, we will present them carefully in the next sections. Another important factor is the tool temperature. Being the tool meshed only in surface, the tool temperature should reproduce the insert skin temperature during the cutting arc, and this also holds for the dry case. For fitting simulations however, a constant temperature value have been set, representative of the initial part of the cut.

A simulation with deformable insert could be done considering the tool thermal properties and a 3D mesh calculating its thermal fields. However, due to the high computational burden, this would have been done only after the fitting of the model, in fact at the end we run out of time and couldn't do it. Another solution we succeeded to implement is to give the tool a temporal thermal distribution so to mimic its skin temperature evolution during the arc. This solution method will be described in the Result section.

### 6.1.6 Calculation settings

Calculated fields were stored each  $0.1\text{ ms}$  so to conserve 50 points per simulation, avoiding the results to be too heavy. On 16 cores @2.5 GHz Workstation,  $5\text{ ms}$  of simulation (almost 1/2 of engagement arc) needed from 30 to 200 hour of calculations, depending on the level of occupation of the WS by other users. Produced results for each simulation weighted around 6 Gb.

## 6.2 Experimental Campaigns

### 6.2.1 Shoulder milling tests

In this section, results regarding the experimental campaign are presented. In particular, cutting forces would be used to compare simulation results for the square shoulder milling case. In August 2020 also an experimental campaign has been performed with the high feed setup. Since the author had knowledge on this experimental trials only by third parties and never actively tool part in the tests, trials are briefly introduced for what is meaningful for the simulations.

## Equipment and test parameters

Shoulder milling trials were performed at MUSP lab, with the cooperation of SIAD (Cryogenic Liquid supplier), Jobs S.p.a on a Mandelli M5 four axis, horizontal spindle, milling machine. The machine is equipped with a Siemens CNC system. Spindle and axes characteristics are showed below. Measuring system and tool specifications are displayed in the next table.



Figure 6.2.1: Experimental equipment, from left to right: Mandelli M5 horizontal spindle MT and workpiece mounted on dynamometric table, LN2 Dewar, Prototype spindle, working assembly

Component	Model	Additional Specs
Kistler Dynamometric Table	9255B	3kHz max frequency
Kistler Amplifier	5070A	
National Instruments Data Acquisition System	PXI-6259	10kHz max sampling rate
Sandvik Coromant Milling Tool	R390-020B20-11L	2 teeth, 20mm diameter
Sandvik Coromant Cutting Inserts	R390-11 T308M-MMS30T	PVD coated Carbide
Statebourne Cryogenics Dewar	CC800	800l, 3.5 bar
Cryogenic Spindle Delivery Unit	Prototype	Jobs S.p.a

Table 6.2.1: Equipment specifications

Inserts and tool holder were chosen under producer advice for semiroughing to finishing operations of aeronautical Ti6Al4V workpieces. Dry cutting, medium pressure emulsion cooling (“Wet”) and LN2 cryogenic cooling (“Cry”) were tested. Emulsion and cryogenic characteristics are reported afterwards.

The LN2 delivery system consisted in an external Dewar, time-weighted so to provide flow rate indications, a double jacketed vacuum insulated pipe system (drastic reduction of heat losses), gas separator (guaranteeing poor vapour title at the exit) and a newly designed spindle for cryogenic delivery. To avoid the excessive cooling of the spindle and its bearings, with consequent loss of dimensional stability and tolerances, an external AISI 304 low conductive ring collector was developed. Preliminary delivery



tests showed marked cavitation tendency in correspondence of critical delivery zones (bends, valves, change in section). CFD analysis ([49, Tahmasebi 2019]) confirmed this tendency: being the LN2 in its saturation state with vapour (in temperature and pressure), any heat source or drop in pressure cause a fraction of it to evaporate. The optimal delivery pressure was found to be around  $3bar$ . Higher and lower pressure resulted in intermittent flow due to high evaporation rates. This is good example showing that high flow is better from a cooling point of view, but considering the equipment and the sustainability of the process, an optimum must be found.

Experimental runs were taken in down milling, at a random order, with parameters expressed in the following table. The depth of cut was fixed at  $3mm$ . Runs were repeated for dry cutting and cryogenic cutting with  $1kg/min$  flow rate and  $3.5bar$  Dewar pressure. Wet runs at  $70m/min$  were run at different feeds of  $0.057$  and  $0.107mm/tooth$ , while wet runs at  $50m/min$  had the same feed of the other two cooling techniques. Emulsion pressure was measured around  $37bar$ , concentrate level at  $10\%$  as industrial practice for Titanium alloys suggested by the industrial partner.

Experimental run	Cutting Speed -[ $m/min$ ]	Cutting feed -[ $mm/tooth$ ]	Spindle Speed -[ $rpm$ ]
#1	70	0.20	1114.08
#2	50	0.08	795.77
#3	50	0.15	795.77
#4	50	0.20	795.77
#5	70	0.15	1114.08
#6	70	0.08	1114.08

Table 6.2.2: Cutting tests parameters

## Results

Important results for simulation purposes were cutting forces and chip morphology. Unfortunately no temperature measurements were taken.

Cutting forces are x, y and z components from the point of view of the tool. Signals obtained from the dynamometric tables were converted as Newton force values as a function of sample number. Single tooth passes were isolated, then a number of samples representative of the duration of the cut were taken, averaged, and the mean x, y and z force during the cutting arc was obtained using Matlab software:

$$\Delta samples = \frac{1}{2} \frac{1}{\Omega/60} \cdot F_s, \quad N_{samples} = \Delta t_{cut} \cdot F_s$$

$$F_{average,j}(t) = \frac{\sum_{i=1}^{N_{pass}} F_{i,j}(t)}{N_{pass}}, \quad 0 < t < \Delta t_{cut}, \quad j = x, y, z$$

$$S = \sqrt{\frac{\sum_{i=1}^{N_{pass}} |F_j(t) - F_{average,j}(t)|^2}{N-1}}, \quad (1-\alpha) = 95\%, \quad j = x, y, z$$

$$F_{sup/inf,j}(t) = F_{average,j}(t) \pm p \cdot \frac{S}{\sqrt{N_{pass}}}, \quad j = x, y, z$$

being  $N_{pass}$  the number of tool passes chosen (variable, depending on duration of the test cut and achieved stable values),  $\Omega$  the spindle speed,  $F_s$  the sampling frequency ( $5kHz$ ),  $\Delta samples$  the span of samples covering one half of a single revolution,  $N_{samples}$  the number of samples for one cutting arc lasting  $\Delta t_{cut}$ ,  $S$  the standard deviation,  $p$  the Normal distribution quantile for 95% confidence interval. The normal distribution was chosen because the number of passes always exceeded 25.

It became clear how there was something wrong in both the tool and the measuring table. For the dry and cryogenic case there exhibit a run-out, afterwards measured of  $40\mu m$ , which caused one insert to cut more material than the other. Therefore, passages with higher force signal were followed by passages with lower force signals. It was decided to average the two group of passes (as logic suggest) to obtain what it should have been obtained without the run out. For sure, the deviation of measurements is larger with respect to wet machining, in which no run-out happened. On the other hand, wet machining exhibit marked presence of systems dynamics in two main harmonics.

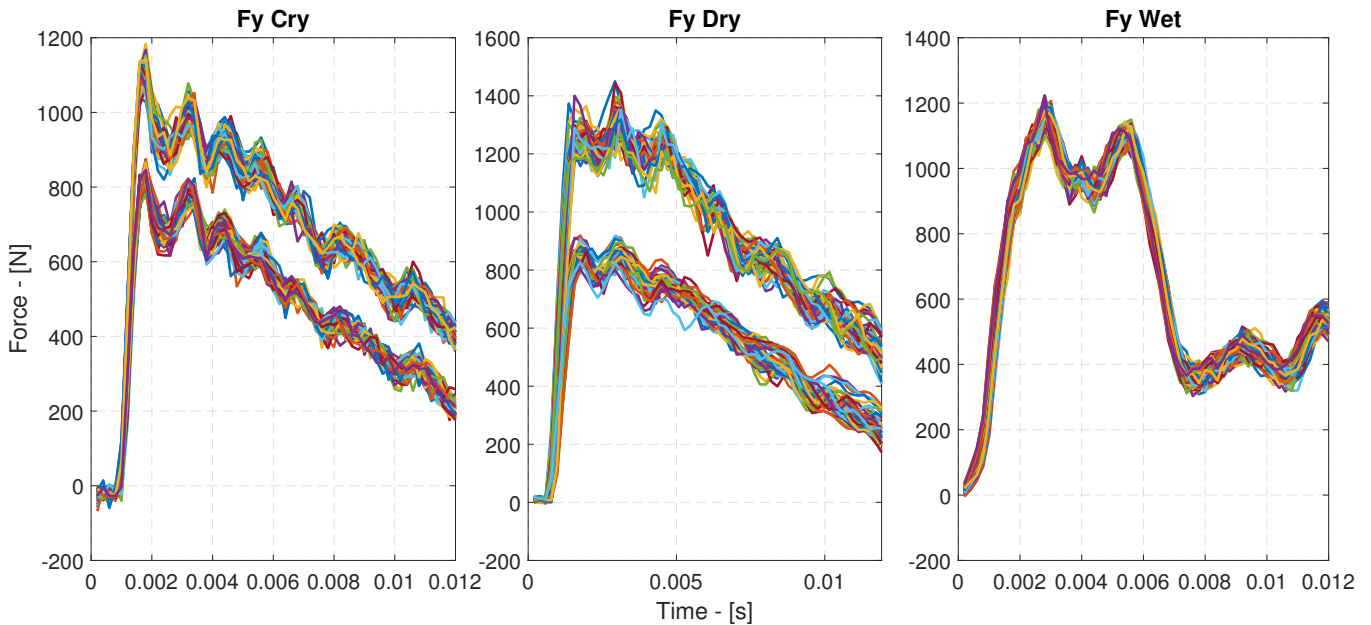


Figure 6.2.2: Insert Run-out during dry and cryogenic cuts, no Run-out for the wet cut but marked apparatus dynamics

Another problem regarded the response of the measurement table with the Titanium block. The block was huge ( $70kg$ ), meaning it decreased the natural frequency of the table. In particular, the x force measurement was affected by a low frequency peak in the FRF of the “table+workpiece” system. Also the z and y direction were slightly influenced by oscillatory response of the table. However, the z force can be considered of small relevance in the shoulder milling process, and the magnitude of the y force is high so that in comparison the oscillations of the table are low. Nevertheless, the x force measurement is to be considered wrong.

The oscillatory response of the system has probably been excited by the nature of the

process and the tool design. The chip is rapidly formed and spread all over the cutting edge before  $1\text{ ms}$ , excitation paragonable to hammering. The generated pulse (frequency content spread over initial hundreds of Hertz) means probably some component to have fallen in the resonance region, being amplified and shifting the phase of the signal. Only a dynamic reconstruction of the signal through the system FRF could improve the obtained x force.

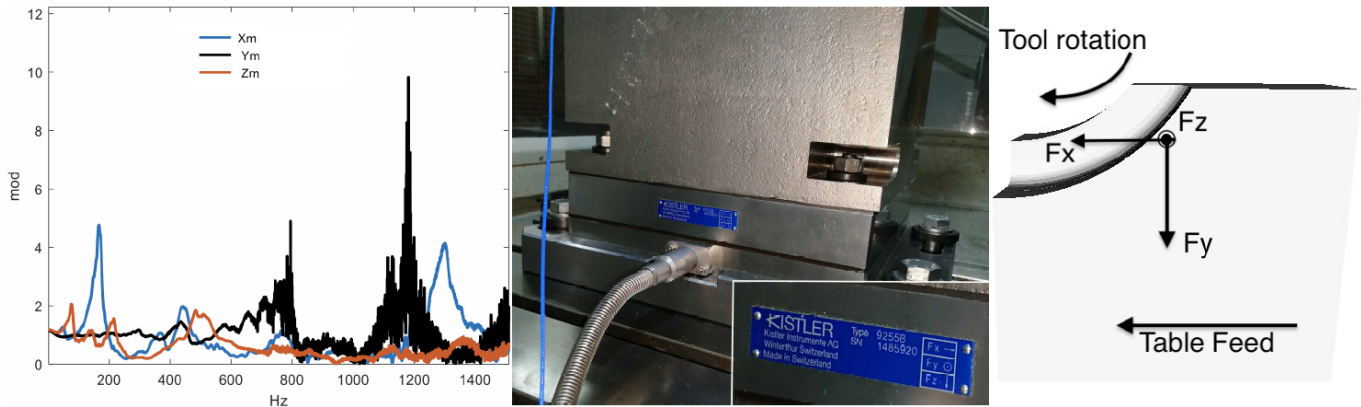


Figure 6.2.3: Measuring-table + MT table + sample dynamics, process scheme

Averaged cutting forces are displayed in the following pages. Some combination of feed and speed are not displayed to reduce the length of the document and enhance the visibility of the pictures shown. Direct comparison of forces are done only with the y component, which is the one representing the more the cutting force for the initial part of the cut. Forces are in Newton and the time scale is in seconds.

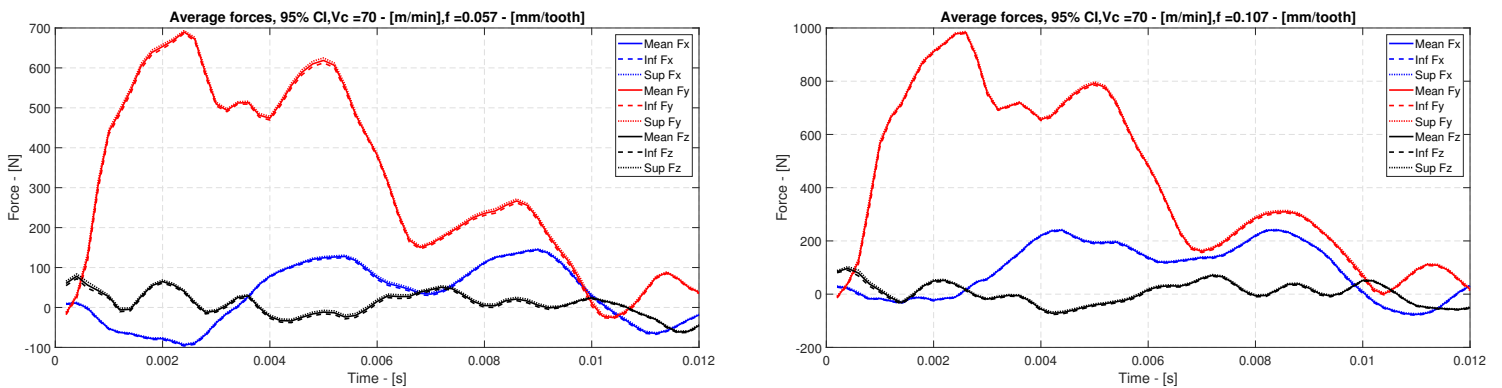


Figure 6.2.4: X, Y and Z forces on Tool for wet runs, feeds:  $0.057\text{ mm/tooth}$  (first column),  $0.107\text{ mm/tooth}$  (second column)

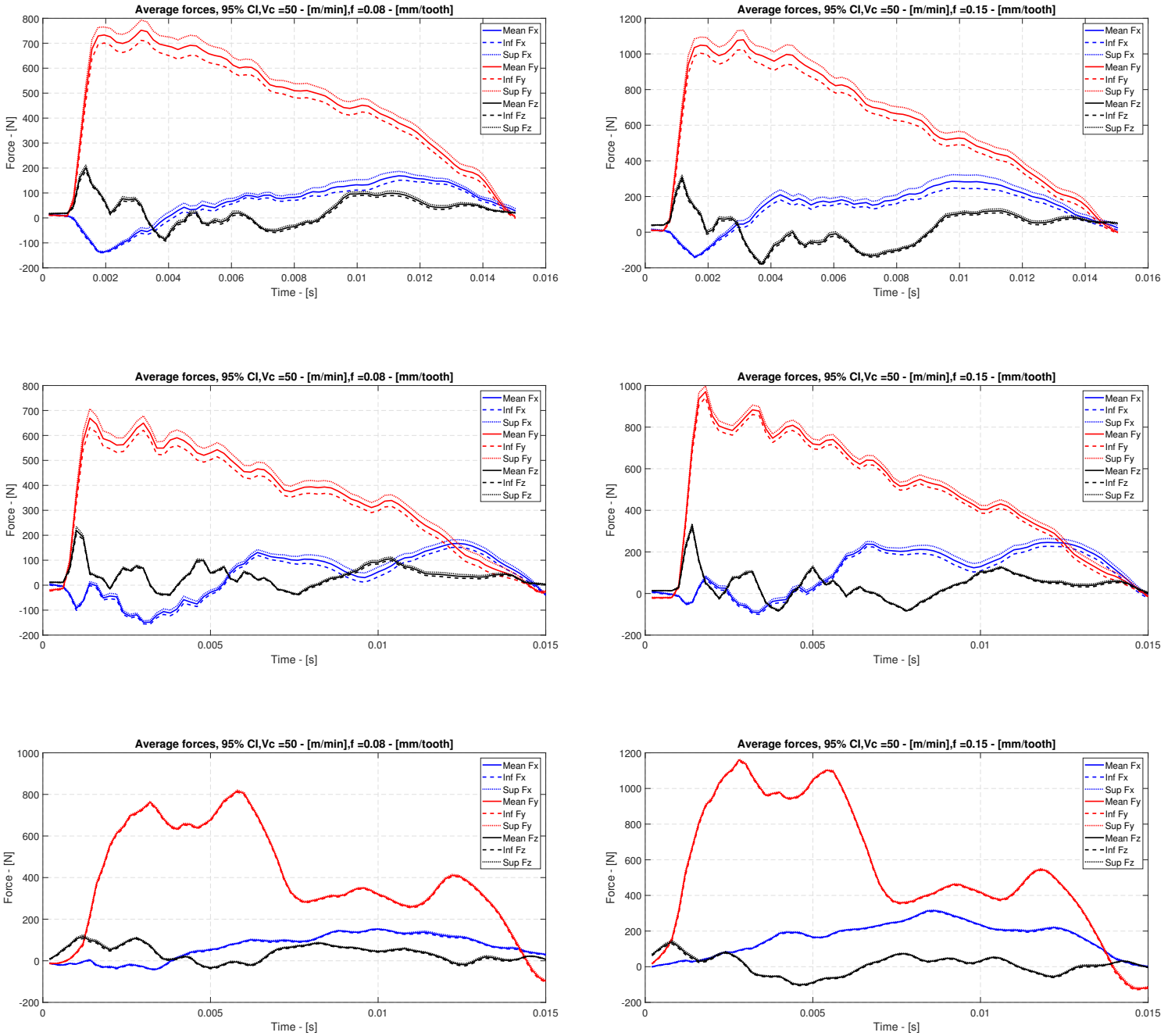


Figure 6.2.5: X, Y and Z forces on Tool for: dry cutting (first row), cryogenic (second row), wet runs (third row), feeds:  $0.08\text{ mm/tooth}$  (first column),  $0.15\text{ mm/tooth}$  (second column),  $0.2\text{ mm/tooth}$  missing for visibility issues

Time scale was considered of  $12\text{ ms}$  for the high speed cut, while  $15\text{ ms}$  for the lower speed one. This for the experimental forces to reach zero. However, theoretical cutting arcs should have lasted  $\Delta t_{cut} = \Omega \cdot \frac{2\pi}{60} \cdot \text{acos}(1/2) = 8.57$  and  $12.57\text{ ms}$  respectively. Forces are still higher than zero afterwards due to uncertainties in the cycle starting point, real cutting edge geometry and inertia of the measuring system.

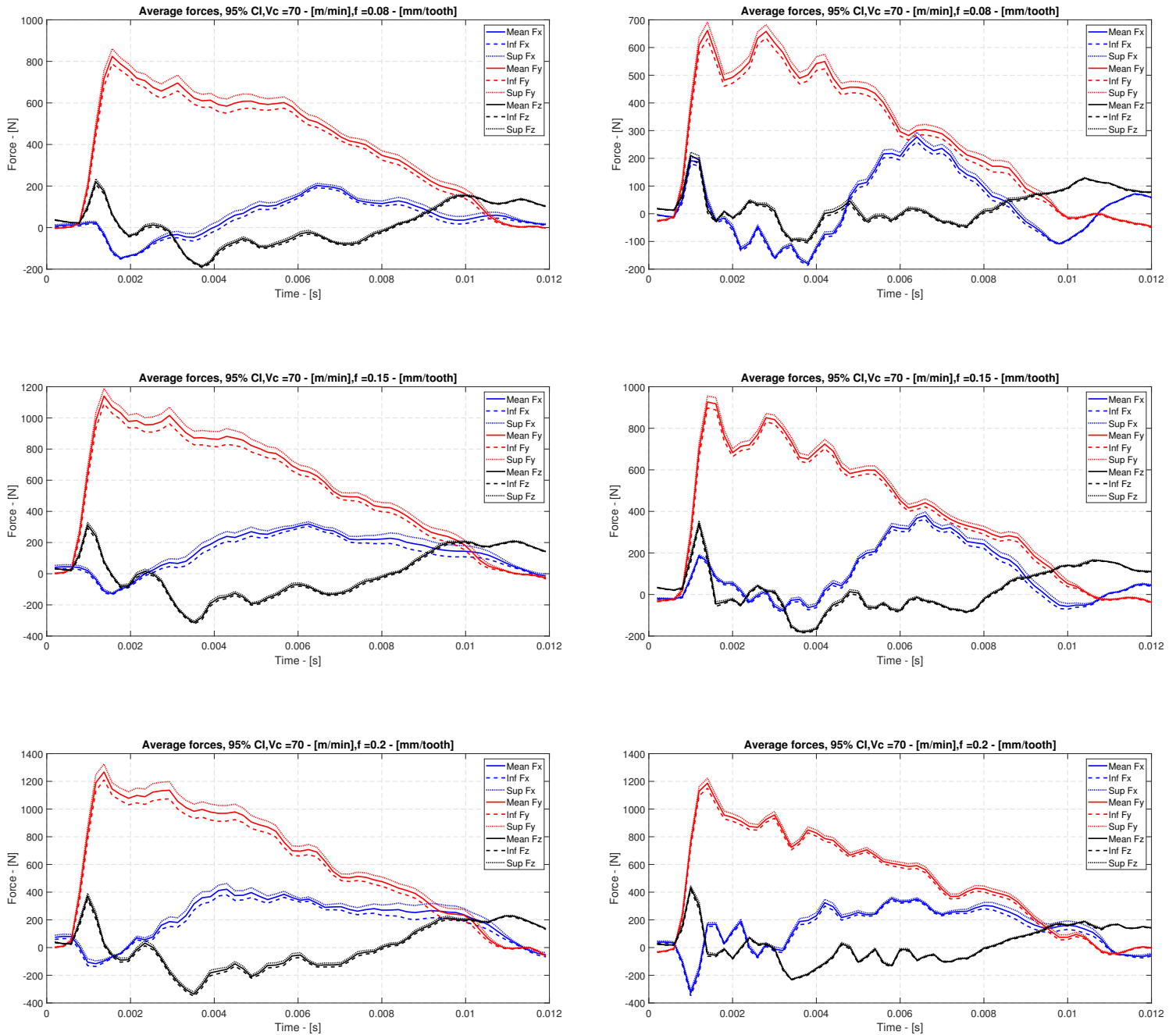


Figure 6.2.6: X, Y and Z forces on Tool for: dry cutting (first column), cryogenic (second column), feeds:  $0.08\text{ mm/tooth}$  (first row),  $0.15\text{ mm/tooth}$  (second row),  $0.2\text{ mm/tooth}$  (third row)

When Fy forces are compared there is difference in the time shift due to calculations and signal extraction that does not correspond to the test. The noticeable difference from the test is the lower magnitude of the force during all arc for cryogenic and the different shapes of the forces. Chips were also collected and photographed (Nikon D3300 with AF-S Micro NIKKOR 60mm f/2.8G ED lens) on a white screen. Noticeable is the higher defect concentration for the cryogenic case.

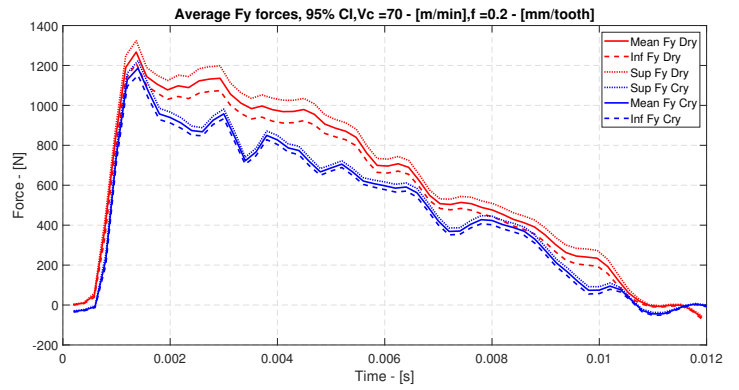
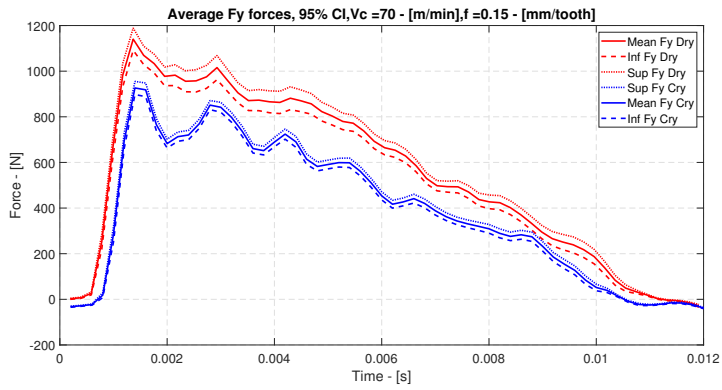
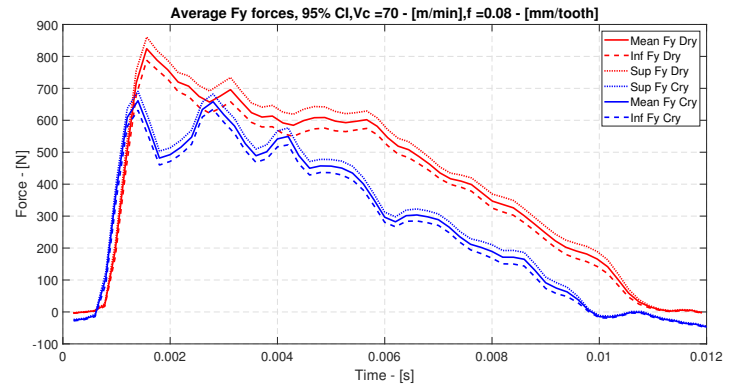
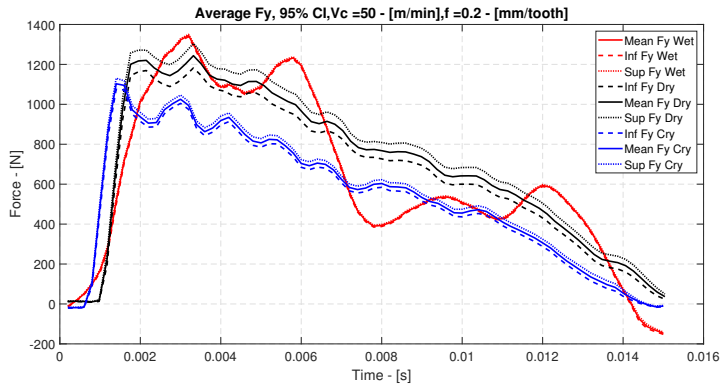
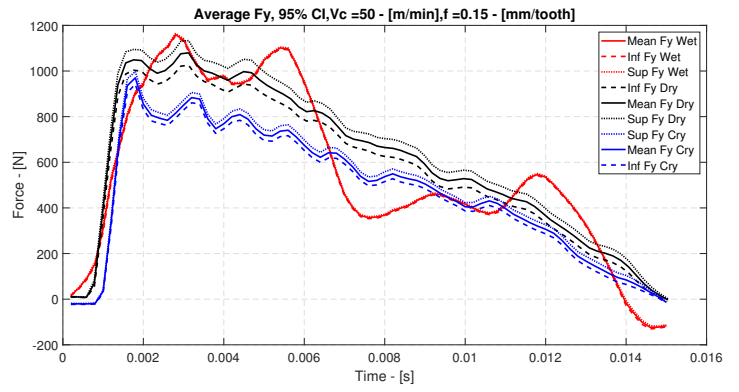
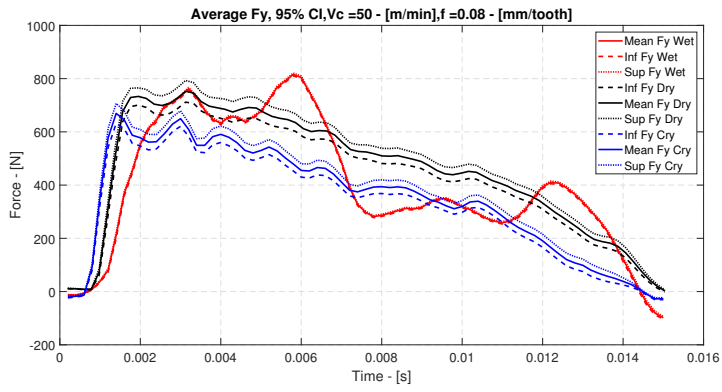


Figure 6.2.7: Comparison of Y forces between environments

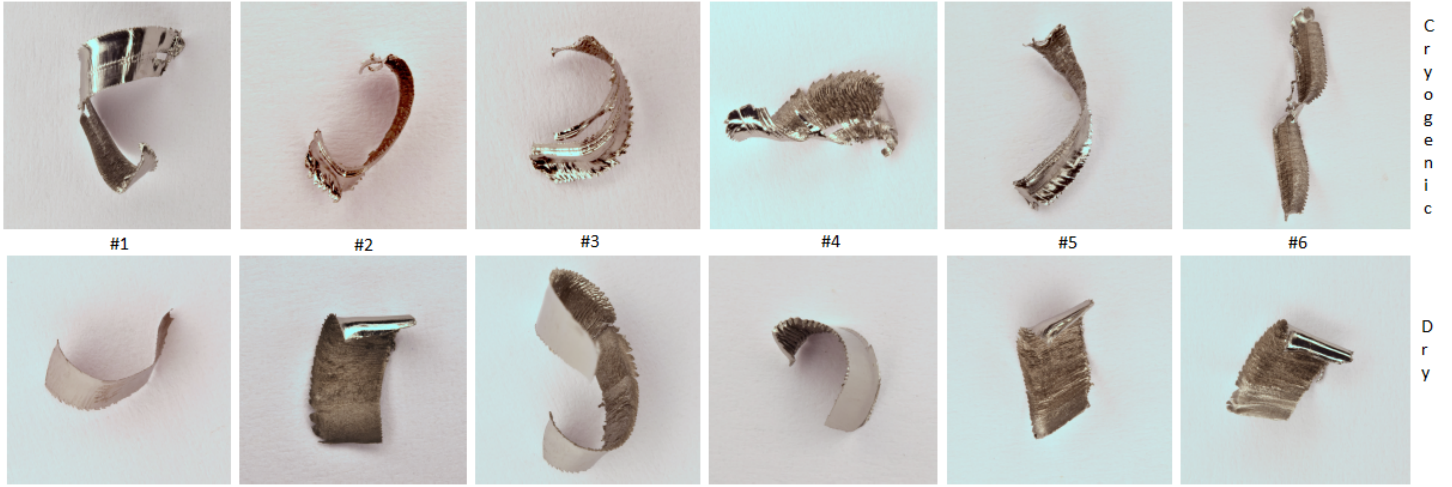


Figure 6.2.8: Collected chip photos

### Discussion of results

As can be seen from the force plot, lower forces have been found for the cryogenic case with respect to flood and dry cutting. Moreover, wet cutting exhibit smoother profiles. The quantification of this aspects along the cutting arc is not trivial. A first comparison can be drawn by considering the maxima of the forces along the arc. However, the peaks are influenced by the dynamic response of the table (lower effect on  $F_y$ , higher on  $F_x$  and  $F_z$ ). Therefore, the average on time can better characterize the variation of the force with respect to the machining environment along the whole arc. Making the average or the approximated (mean point) normalized integral on time, is the same:

$$F_{j,average} = \frac{\sum_{t=0}^{t=\Delta t_{cut}} F_j [t]}{N_{samples}} = \frac{\sum_{t=0}^{t=\Delta t_{cut}} F_j [t]}{\Delta t_{cut} \cdot F_s} = \frac{\sum_{t=0}^{t=\Delta t_{cut}} F_j [t] \cdot 1/F_s}{\Delta t_{cut}} \simeq \frac{I}{\Delta t_{cut}}$$

As it is the same to compare average forces and mean point integrals in time so to look at overall differences during the cutting arc:

$$\Delta F_{\%,j} = \frac{\sum_{t=0}^{t=\Delta t_{cut}} (F_j^{Dry} [t] - F_j^{Cry} [t])}{\sum_{t=0}^{t=\Delta t_{cut}} F_j^{Dry} [t]} = \frac{\sum_{t=0}^{t=\Delta t_{cut}} (F_j^{Dry} [t] - F_j^{Cry} [t])}{\frac{\sum_{t=0}^{t=\Delta t_{cut}} F_j^{Dry} [t]}{N_{samples}}} = \frac{F_{j,av}^{Dry} - F_{j,av}^{Cry}}{F_{j,av}^{Dry}}$$

It needs to be underlined that for lack of data in wet cutting at the higher speed and problems in visualization of data the order of the runs has been modified:

$$[\#1, \#2, \#3, \#4, \#5, \#6] = \left[ 50 \frac{m}{min} \setminus 0.08 \frac{mm}{tooth}, \quad 50 \setminus 0.15, \quad 50 \setminus 0.20, \quad 70 \setminus 0.08, \quad 70 \setminus 0.15, \quad 70 \setminus 0.20 \right]$$

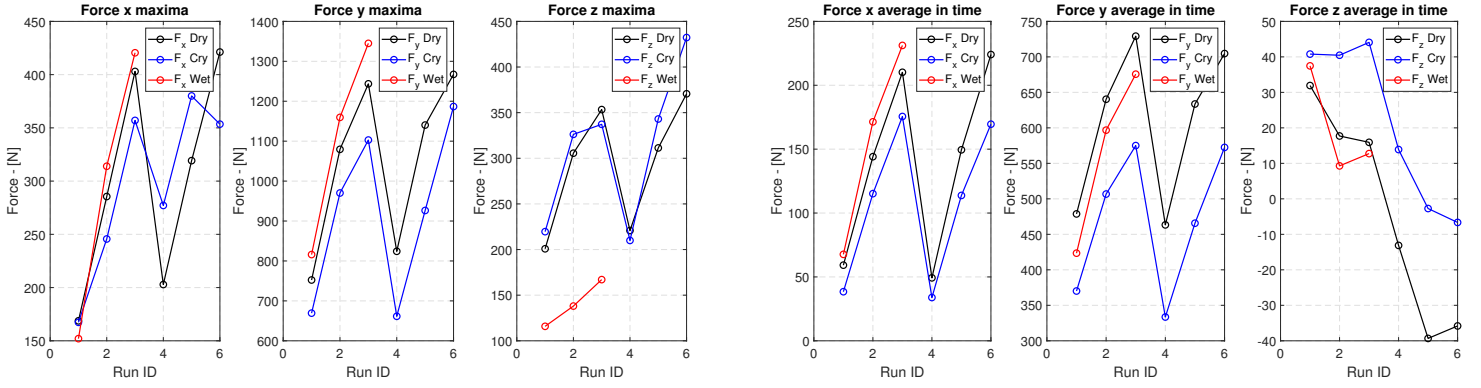


Figure 6.2.9: Comparison of maximum and average forces for the three environments, various speed and feed. The test ID are rearranged so that  $[\#1, \#2, \#3, \#4, \#5, \#6] = [50 \frac{m}{min} \setminus 0.08 \frac{mm}{tooth}, 50 \setminus 0.15, 50 \setminus 0.20, 70 \setminus 0.08, 70 \setminus 0.15, 70 \setminus 0.20]$

The values for  $F_y$  cutting force for cryogenic cutting with respect to dry and wet cutting are shown in the table below.

Run ID	Speed $-\frac{m}{min}$	Feed $-\frac{mm}{tooth}$	$F_y$ av. Wet $-\text{[N]}$	$F_y$ av. Dry $-\text{[N]}$ , $\Delta F_{y\%}^{wet-dry}$	$F_y$ av. Cryo $-\text{[N]}$ , $\Delta F_{y\%}^{wet-cry}$ , $\Delta F_{y\%}^{dry-cry}$
#1	50	0.08	423.46	478.76, +13.1%	370.16, -12.6%, -22.7%
#2	50	0.15	596.77	640.32, +7.3%	506.73, -15.1%, -20.9%
#3	50	0.20	675.64	729.19, +7.9%	575.03, -14.9%, -21.1%
#4	70	0.08	—	463.32, -%	333.51, -%, -28.0%
#5	70	0.15	—	633.60, -%	465.65, -%, -26.6%
#6	70	0.20	—	704.70, -%	572.47, -%, -18.8%

Table 6.2.3: Average  $F_y$  force comparison between cutting environments

Due to uncertainties in the measurement system, it is believed not productive to advance more speculations on cutting forces. Actually, the only experimental reliable values were the  $F_y$  forces and chip morphology. Therefore the two variables, one quantitative, the other qualitative, will be used to fit the FE models.

### 6.3 “Square shoulder” Model Fitting

Chip forming numerical model set up require a robust methodology. Firstly, material models were tested. Then based on the achieved performances, 3D simulations were run iterating for the suitable Latham-Cockcroft damage constant. Finally, friction coefficient were tailored so to match experimental forces. The following scheme describe the procedure. Details will be given in the following sections.



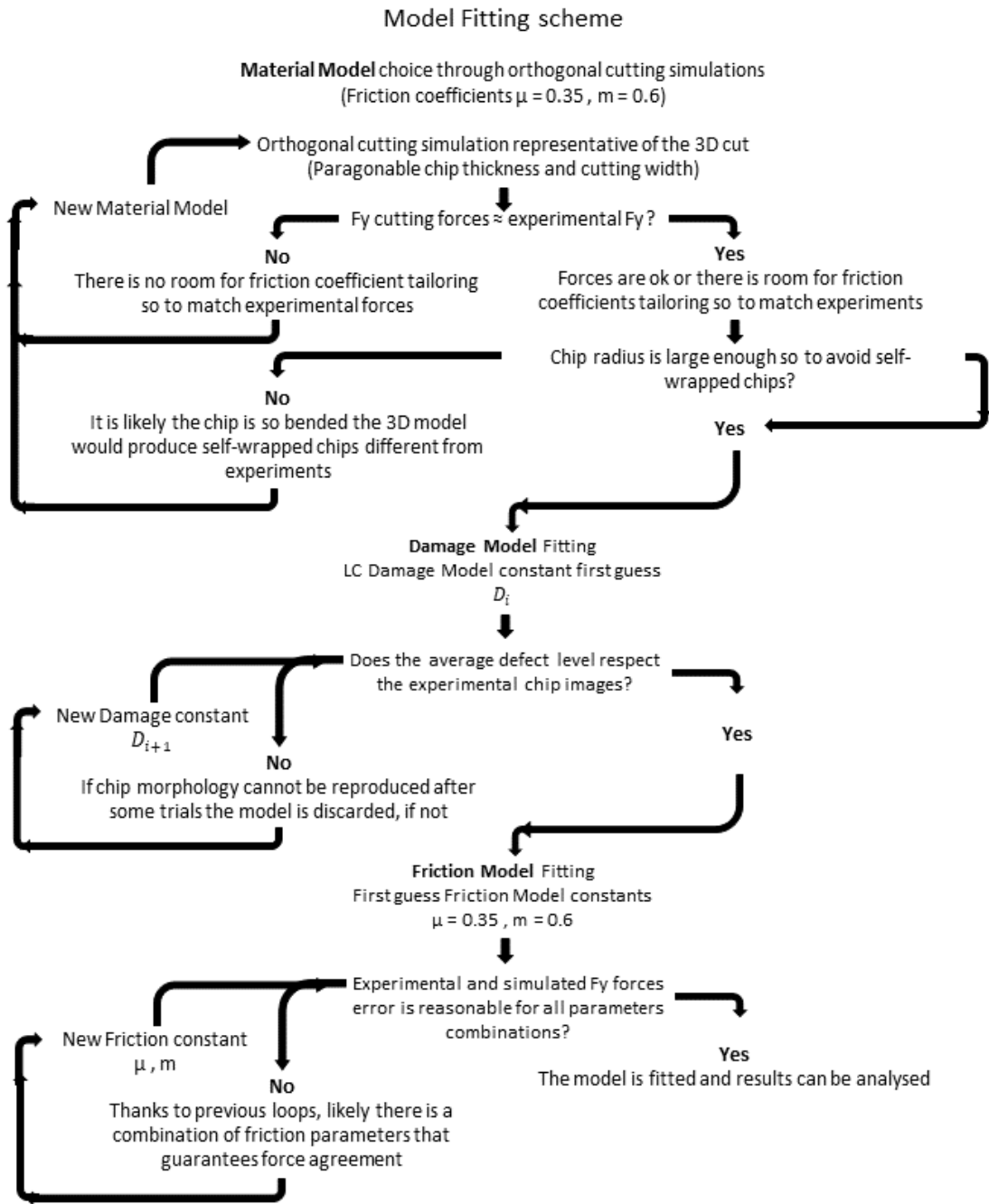


Figure 6.3.1: Model Fitting Scheme

### 6.3.1 Material model and mesh size fitting

#### Material model choice

First trials were done with [167, Pittala 2011] and Monno material model. The choice came from the work of a previous student. In the article, a milling operation is modeled by an orthogonal cutting process with variable uncut chip thickness. The coefficients for the JC material models are found by using OXCUT, a program based on the Oxley theory (cutting theory) which inversely determines the JC coefficients by initial guesses,

comparing the calculated cutting forces to the experimental ones. The parameter  $A$  is purposely set to zero to avoid the convergence to different coefficients set of the OXCUT routine, starting from different initial guesses, due to high non linearity. Also, the reference strain rate is very high. The doubts concerning the model reveal to be founded when preliminary simulations are run. The material refuse the cut, a characteristic of Ti alloys, which, however, doesn't happen with the observed magnitude, neither happened in the experimental trials. The problem is related to the parameter  $A$  being zero and  $\dot{\epsilon}_0 = 1000$  which in FORGE generates an ambiguous transition from elastic to plastic behaviour.

Discarded the initial material model there opened an entire universe of choice. After an exhaustive literature research, presented in the previous chapter (Chapter 5), material models were chosen, based on the claimed performances and the ease of implementation. Regarding the latter aspect, material model that required stress flow update during calculation were not adopted. Material models were implemented in matrix or tabular form. The implementation with self developed routines required too much time and effort for what concerns a thesis work, also given the fact that no prove sustained of marked superiority of a hard-implementable model against a simpler one. Chosen material models are shown in the table below. The Tabular model comes from the software database and is suitable for forging simulations, therefore the behaviour is very refined for strain rates up to  $10^4$ , however nothing is said for what happens afterwards.

Material Models Selection			
N°	Article	Model	Coefficients
1	[168, Lee 1998]	JC	$[A, B, C, n, m, \epsilon_0] =$ [782.7, 498.4, 0.028, 0.28, 1.0, $10^{-5}$ ]
2	[169, Meyer 2001]	JC	$[A, B, C, n, m, \epsilon_0] =$ [862.5, 331.2, 0.012, 0.34, 0.8, 1]
3	[132, Ozel 2006a]	JC	$[A, B, C, n, m] =$ [860, 640, $2.2 \cdot 10^{-6}$ , 0.23, 1.112]
4	[135, 143, Calamaz 2008, Sima 2010]	Modified JC	$[A, B, C, n, m, \epsilon_0, a, b, d, r, s] =$ [782.7, 498.4, 0.028, 0.28, 1, $10^{-5}$ , 2, 5, 1, 1, 0.05]
5	[144, Calamaz 2010a]	Modified JC	$[A, B, C, n, m, \epsilon_0, p, Tr_{ec}, r, q] =$ [870, 990, 0.011, 0.25, 1, 0.7, 0.6, 600, 1, 5]
6	[145, Karpát 2011]	Modified ZA	$[a, n^*, b, c, d, e, q, l, p, \epsilon_0, s, k, r, \epsilon_{cr}] =$ [590, 0.27, 740, $7.20E - 05$ , -0.021, 1.64, 0.035, 1.1, 0.08, 800, 0.6, 2, 2, 0.35]
7	[130, Wang 2014]	JC + JC damage	$[A, B, C, n, m, D_{1 \rightarrow 5}] =$ [862, 331, 0.34, 0.012, 0.8, -0.09, 0.25, -0.5, 0.014, 3.87]
8	Tabular model	-	-

Table 6.3.1: Material models selection, tabular model available in the additional information

Regarding material properties (Young's modulus, Thermal conductivity, Poisson's ratio, Density, Specific heat, Linear expansion), they are given in tabular form for

temperatures from ambient to  $1500^{\circ}\text{C}$  from the software database. With respect to cryogenic temperatures no data were available. We expect the material cooled down at very low temperatures to be far from the high deformation region, where the calculations influence slightly the problem. After some trials, a general increase in simulation time was found due to the time required to update the thermal properties (149 temperature points). Therefore, the search by the FORGE algorithm was eased by summarizing the properties with less data points, including them in the same file of the rheological model (where possible).

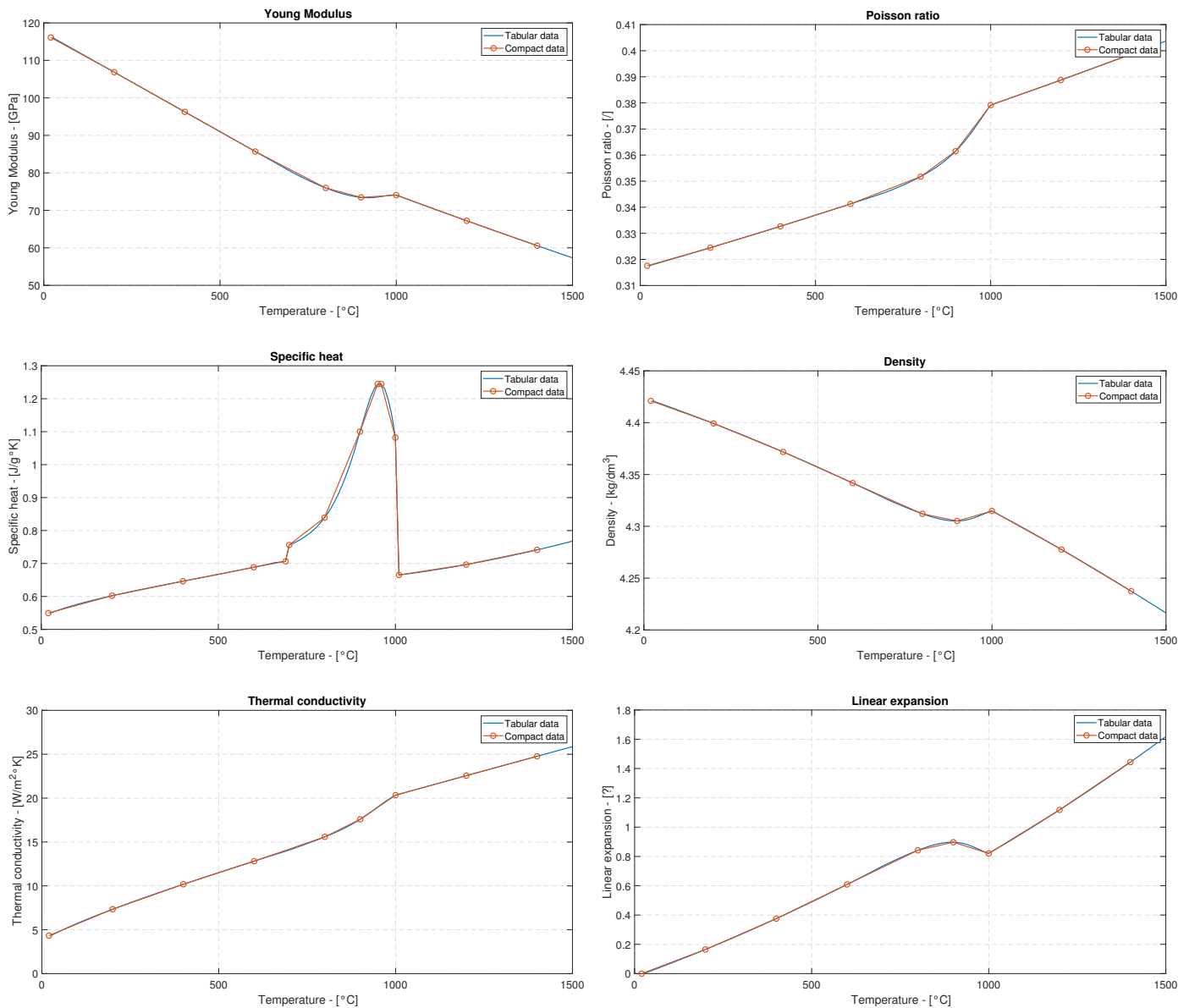


Figure 6.3.2: Ti6Al4V thermal dependent material properties, reduced data set over the tabular data from FORGE

## Mesh

As have been introduced, mesh is the main factor influencing simulations. Large mesh size and remeshing intervals lead to wrong results, fine mesh and frequent remeshing

to excessive precision, slow convergence, machine time wasting. Being 3D simulation so resource demanding, orthogonal cutting simulation were performed to analyse the development of shear bands as a function of mesh size. They also helped in choosing the most suitable material model looking at cutting forces and chip morphology (bending chip radius, segmentation).

The experimental chip shows evident segmentation which, however, it is hardly achievable with a so heavy simulation. Chip segmentation simulations are always done with orthogonal 2D plain strain cutting models and mesh size below  $5\mu m$ . Modified material models for chip segmentation are physical or analytical based models which are artificially altered so to promote shear banding without damage models. Conventional material models can be added by a Damage model, see Chapter 5, Material Models.

Shear bands are activated by an initial strain, from a certain strain rate on. Progressive localization, dynamic recrystallization and void/fracture coalescence cause band propagation. Researchers have tried to develop different modification to materials models that allow for a certain degree of softening in the material, after certain thresholds, to mimic shear band formation in FEM. It became clear that those thresholds are impossible to be obtained with coarse mesh size, necessary for a suitable calculation time of our model. Moreover, it is to be noticed that the literature implementation of modified models for chip segmentation on 3D turning or milling simulations are performed with a mesh so large that the segmentation cannot occur. Modified models are therefore used without being able to satisfy the objective they've been realized for, but that is normal, due to the high calculation burden it would require having small mesh sizes in 3D environments.

A solution could be to increase softening the more. With respect to this, material models were modified. A new family of material models consisted on a highly marked softening behaviour, including strain and strain rate thresholds deduced from simulation with large mesh. Indeed the material model have been developed into four different variants.

$$\bar{\sigma} = [A + B\varepsilon^n] \cdot \left[ 1 + C \ln \frac{\dot{\varepsilon}}{\dot{\varepsilon}_0} \right] \cdot \left[ 1 - \left( \frac{T - T_r}{T_m - T_r} \right)^{m - g(\varepsilon, \dot{\varepsilon})} \right], \quad g_1(\varepsilon, \dot{\varepsilon}) = W \cdot \left\{ \tanh \left( b \frac{\varepsilon}{\varepsilon_{cr}} \right) \cdot \tanh \left( b \frac{\dot{\varepsilon}}{\dot{\varepsilon}_{cr}} \right) \right\}$$

$$\bar{\sigma} = JC(\varepsilon) \cdot JC(\dot{\varepsilon}) \cdot JC(T) \cdot (1 - g_1(\varepsilon, \dot{\varepsilon}))$$

$$g_3(\varepsilon, \dot{\varepsilon}) = \frac{1}{2} \left\{ 1 + \tanh \left[ a \cdot \ln \left( \frac{\dot{\varepsilon}}{\dot{\varepsilon}_{cr}} \right) \right] \right\} \cdot \frac{1}{2} \left\{ 1 + \tanh [b(\varepsilon - \varepsilon_{cr})] \right\}$$

$$g_4(\varepsilon, \dot{\varepsilon}) = \frac{1}{2} \left\{ 1 + \tanh \left[ a \cdot \ln \left( \frac{\dot{\varepsilon}}{\dot{\varepsilon}_{cr}} \right) \right] \right\} \cdot \frac{1}{2} \left\{ 1 + \tanh [b(\varepsilon - \varepsilon_{cr})] \right\}, \quad \dot{\varepsilon}_{cr} = \dot{\varepsilon}_{cr0} \cdot f(T), \quad \varepsilon_{cr} = \varepsilon_{cr0} \cdot f(T)$$

The first model added only some additional softening through the thermal function, after a certain strain guaranteed a certain strain rate. The second separate the effect on a different function. The third, refines the shape of the softening functions, the fourth introduces thermal dependent strain and strain rate limits. Results and model parameters are displayed in the following figures. The idea was that, even with a large mesh, the threshold could be reached and the material softened. Summing up, 12 material models were analysed with orthogonal simulations.

The simulations were set up with  $0.1\text{ mm}$  undeformed chip thickness,  $50\text{ m/min}$  cutting speed, coulomb tresca friction model with  $\mu = 0.6$ ,  $m = .035$ . The thermal conductance at the interface was  $10\text{ kW/m}^2\text{K}$ , and a constant tool effusivity of  $e = \sqrt{\rho \cdot k \cdot c_p} = 1111 \frac{\text{W}}{\text{K}} \sqrt{\frac{\text{s}}{\text{m}}}$  was used for tool-workpiece heat partition (as for the 3D simulation). Ambient temperature was set at  $20^\circ\text{C}$ , convection with ambient air was set at  $20\text{ W/m}^2\text{K}$ , the tool was rigid. Refined moving windows for meshing the shear zone and keep a refined mesh on the machined surface were applied. The model thickness was  $1\text{ mm}$ , plain strain condition assumed. The cut lasted from  $0.6$  to  $0.8\text{ ms}$ , time in which forces and maximum temperature in the tool reached the steady state. Remeshing on deformation was applied as the only option available for 2D simulations.

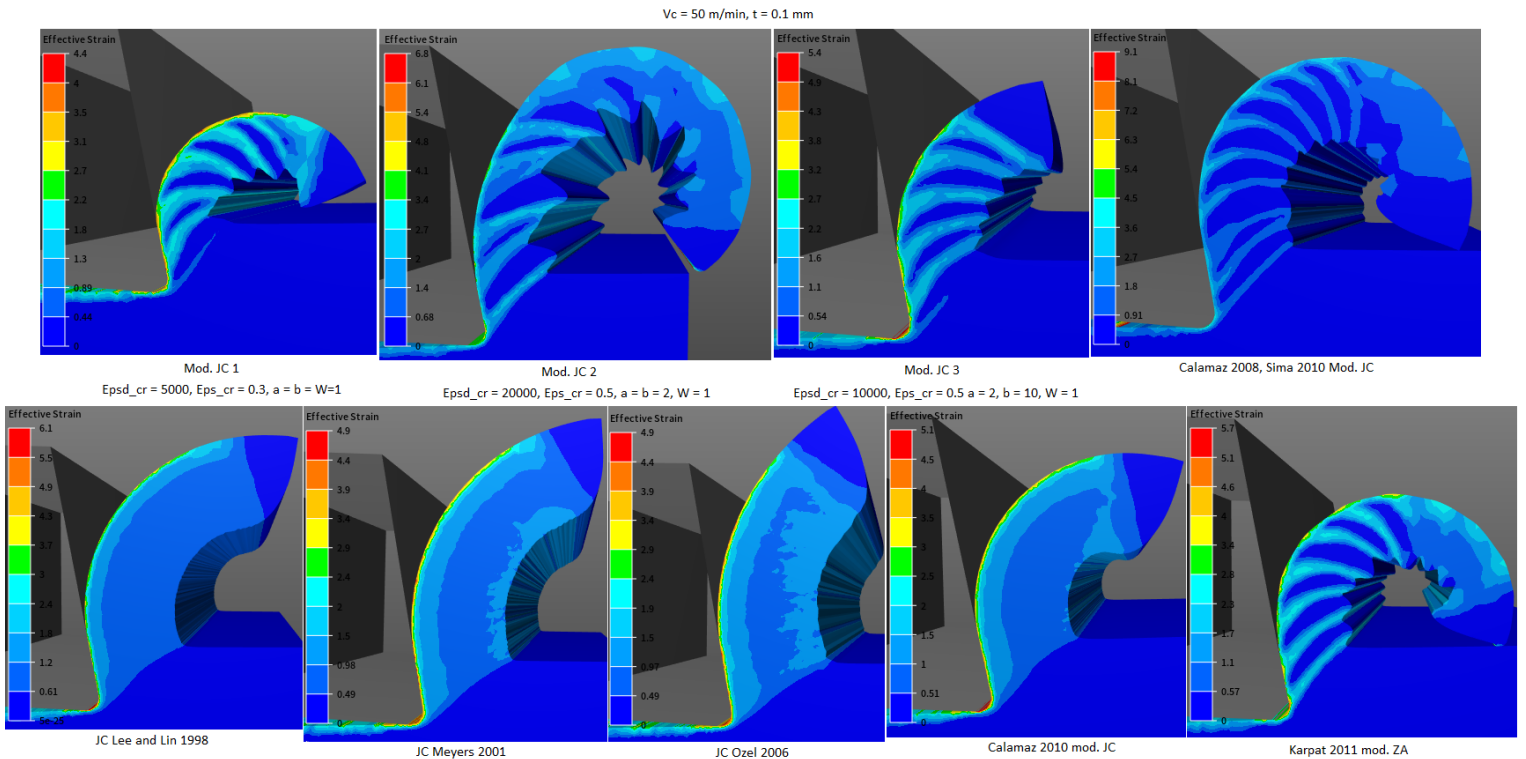


Figure 6.3.3: Results for  $5\mu\text{m}$  mesh size, different material models, dry cutting

Results show that shear localization is difficult even with a quite refined mesh size. Chip bending radius increase after the chip scratches the surface of the piece. Friction was quite irrelevant on the chip morphology phenomena. The various self developed material models and the Calamaz modified JC struggled in representing shear localization, even if fair serration degrees were produced. Model 2 was able to produce consistent serrations with a larger mesh. However, as we will see, the mesh size is still too refined for achieving results within bearable time in the 3D simulation. The problem was that the softening region was too coarse. This due to the initial coarser mesh size which prevented strain localization. Moreover, if softening was further increased, temperature localization was impaired, as the stress flow of the material was very low and even at large strains the temperature generation due to inelastic heat fraction was too low to promote further softening. In brief, the process was not

progressive, chip formation dynamics different, forces very low and chip bending too pronounced. The remaining material models were tried at  $5\ \mu m$  mesh size as well. None of them but the Karpat one was able to produce serrations, unless with non localized shear bands promoting excessive chip bending.

Even if, for the self developed model, an increased capacity in degree of serration of the material at  $5\ \mu m$  is seen, with coarser mesh this capacity is rapidly lost. The ability of shear localization at very refined mesh size of the Calamaz model is optimal. Nevertheless, even by adopting  $30\ \mu m$  mesh size in the primary shear zone only, for the 3D simulation, shear bands aren't obtained at all.

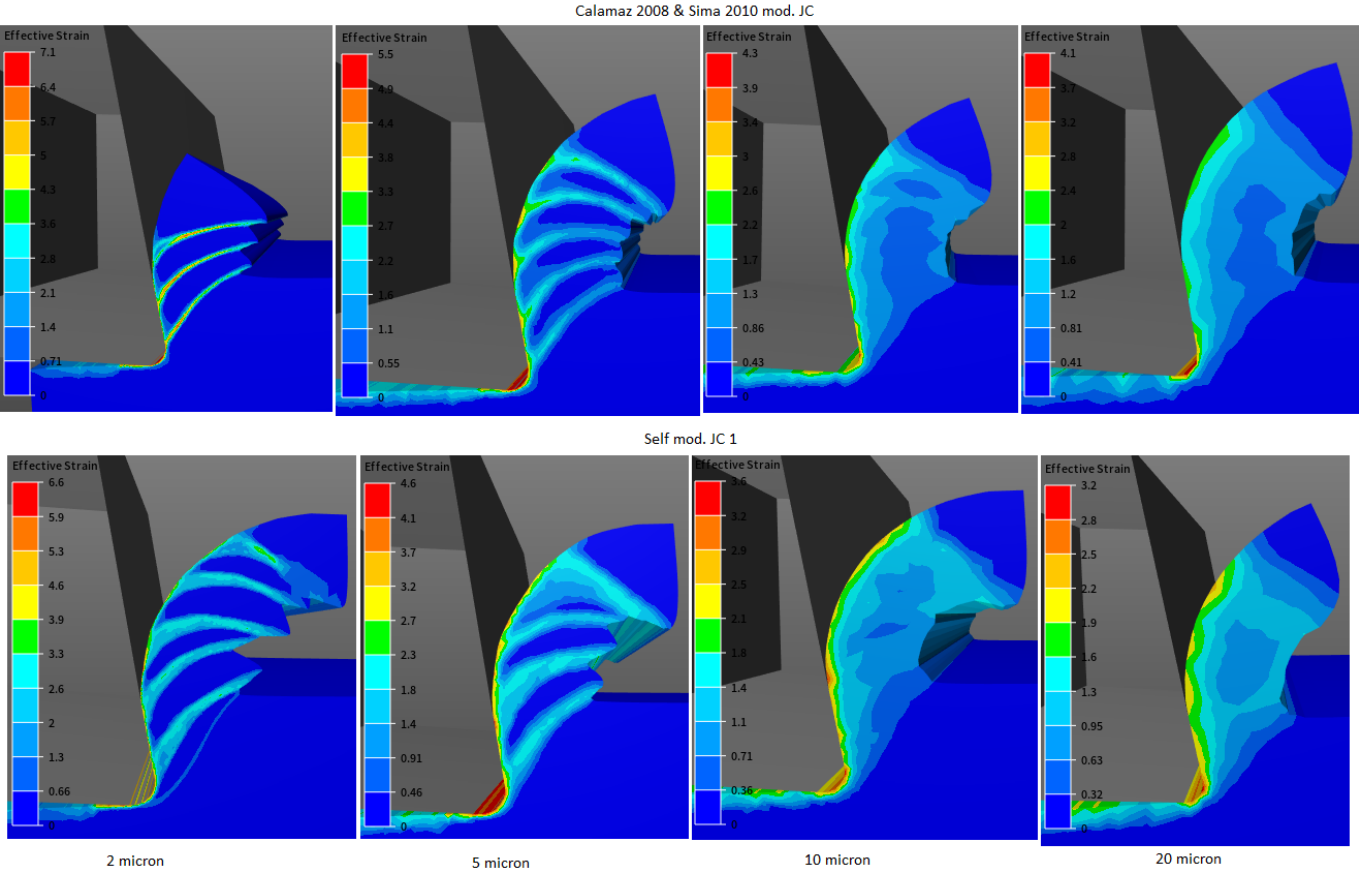


Figure 6.3.4: Results for variable mesh size, dry cutting

It is believed, by the author, that there is hardly a way to modify material models so to obtain shear bands as they happen in reality with coarser mesh adopted for heavy industrial simulations. This is still for what concerns the Author (limited) knowledge a research gap.

A remeshing algorithm triggered by recrystallization and recovery limits could be implemented so to generate the shear band highly localized starting from an initial larger mesh. This allows to refine the calculations in the shear band in response to the strong stress, strain, strain rate and temperature gradients developing there. Outside the band, mesh can be coarsened to avoid excessive refinement burden. This finds evidence in obtained chips, as the areas outside a certain distance from the shear band present

almost undeformed material grains. On the other hand, these remeshing techniques could strongly increase the calculation time due to frequent and heavy remeshing for Refinement and Derefinement.

This sort of algorithms are more than what time and purpose of this study would justify, therefore the idea was not investigated further. Shear band morphology in the 3D simulated chip was only considered to produce similar chip bending radius, average shape and paragonable defect levels.

A Matlab routine was implemented to visually investigate the differences between the most promising chosen models. From the figure below it can be seen that even between the simple JC models there is plenty of difference. Concerning the three modified models, much more variability is seen. It is remarkable that such a difference can be found in material models regarding the same material grade.

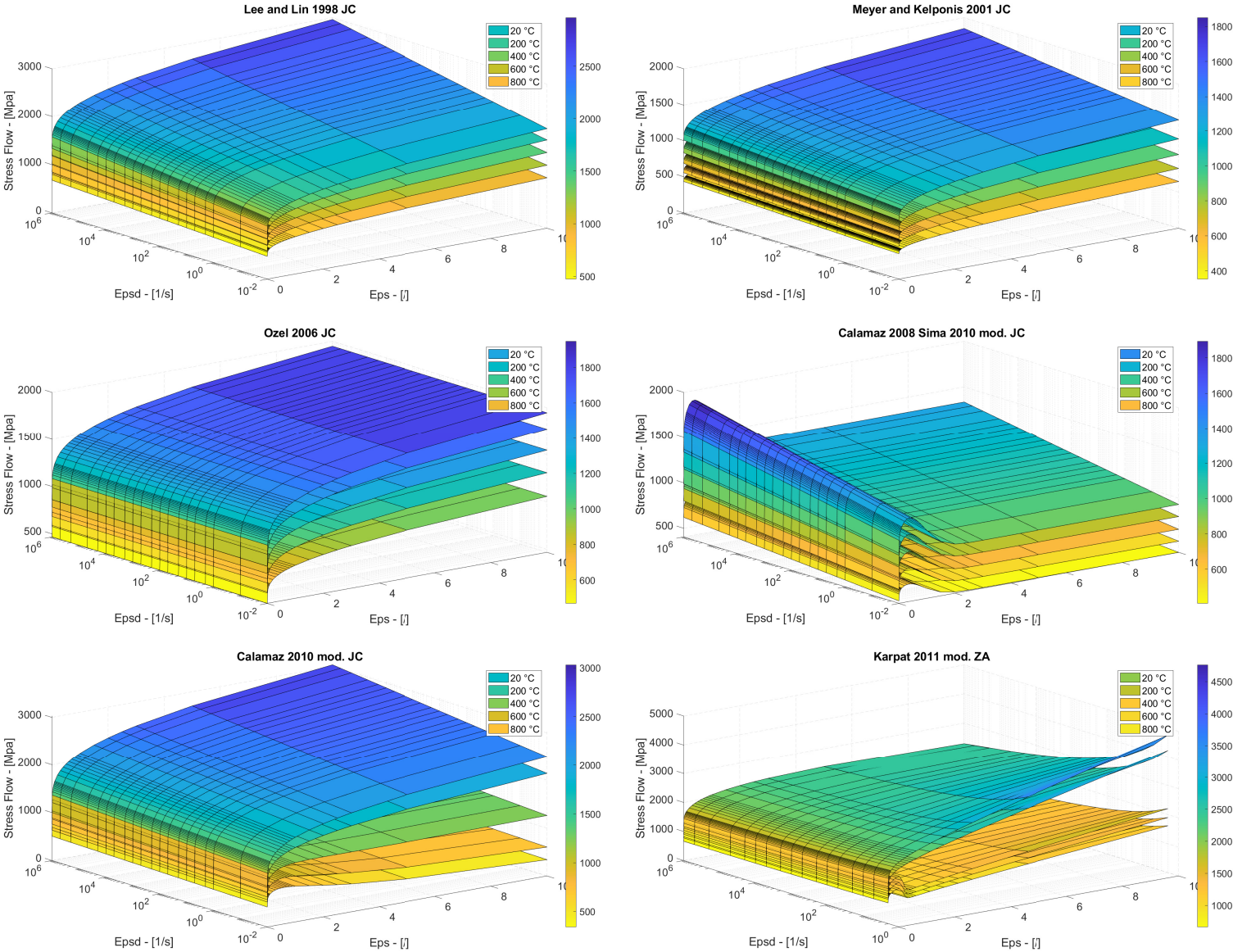


Figure 6.3.5: Stress flow of different models comparison

Orthogonal cutting simulations were set up with  $20\ \mu m$  mesh size for the 7 presented material models. Unfortunately, JC fracture model with ductile fracture propagation criteria was not implemented in FORGE Nx T 3.0, therefore the promising model of [130, Wang 2014] couldn't be investigated. The 7 material models were compared regarding cutting force, temperature and chip morphology behaviour at large mesh. Models were discarded if the cutting force was much lower than  $0.02T_{onns} - (200\ N)$ . The 3D model's depth of cut is three times the Orthogonal model width. The chip thickness of the orthogonal model is  $0.1\ mm$ , paragonable to the 3D model at 1/3 of engagement. Therefore  $200\ N$  force would approximately result in  $600\ N$  for the 3D simulation. This, looking at the experimental forces, proved to be the lower value acceptable. Models that exhibit lower force values couldn't be adjusted to experimental forces by friction model tailoring.

The Meyers JC coefficient set proved to be too soft. The Calamaz and Karpas modified models, even if performing well in force prediction, produced chips that curled and self entangled with themselves, totally dissimilar to the experimental ones. This proves how modified materials models for orthogonal simulations are not suitable for 3D calculations. The tabular, Ozel and Lee models produced the larger radiused chips, with paragonable forces and maximum temperature prediction. Those models were implemented in 3D cutting simulations, varying damage model coefficient as explained in the next chapter.

Proofs of the results now discussed are shown in images we have not reported due to space issues but can be found in the additional information.

### 6.3.2 Damage model

Damage model influence on shear band formation in relation with mesh size was also studied. In the majority of cases with large mesh, adding a simple Latham-Cockcroft normalized criterion, had the result to enhance shear band formation without control. High fragmentation and considerable volume loss is generated by eliminated elements. Again, the use of a damage model to promote shear banding is justified only with the use of a properly refined mesh.

A damage model was implemented in the simulation with the main aim to reproduce the level of fractures of the experimental chip. It was not introduced to get shear bands, unless it proved to produce their shape but precise morphology was not investigated. The damage model chosen for the simulation is the simplest Latham-Cockcroft. It is decoupled from the stress flow of the material which means an element keeps its full strength until it fractures and it is eliminated from the calculations. More accurate criteria, such as the JC damage model, modify the strength of the element from the onset to the failure of the element, thus providing a realistic and gradual fracture evolution. A lot of different damage models are implemented in the program: Oyane, Lemaitre (5 decoupled and 5 coupled), Rice and Tracey and Transvalor self modified LC damage model. In the literature, LC or JC damage models are always used. The Brozzo model is also adopted (sort of developed LC). Interesting would be to try different damage models, coupled and uncoupled, reporting the effort (coefficient tailoring) to benefit (calculation time, chip morphology) ratio relative to their implementation. In the present work, the Author has neither time nor data to undertake this interesting task.



The model of Lee and Lin proved to produce good chips with all damage values, the  $F_y$  force was well predicted for high value of  $D$  (500 MPa) but average chip morphology was better for lower values (400 – 450 MPa). Maximum cutting temperatures on the workpiece were quite high  $\cong 1200^\circ C$ , unless on the tool could be lower. As no experimental values on temperature were recorded, any reasonable value according to literature could be acceptable.

Tabular model could produce promising chip radius, overall chip shape and damage levels, added to quite acceptable shear band levels, but for one single combination of mesh size and remeshing frequency, that proved the model not robust. Due to the promising results in terms of chip morphology, an effort was made to visualize its flow stress, translating it in analytical form (quite long one):

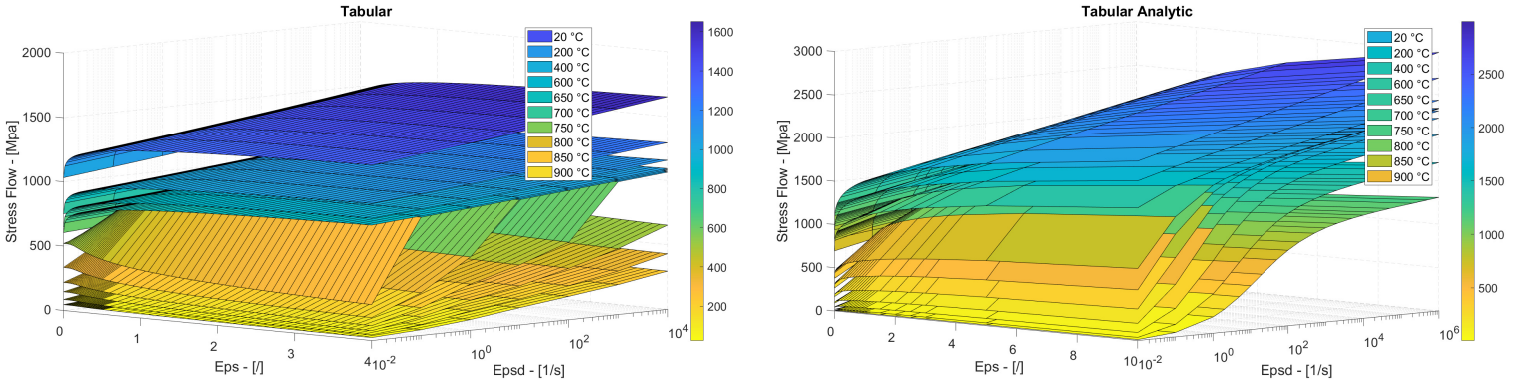


Figure 6.3.6: Material Models comparison

$$\bar{\sigma} = JC(\varepsilon) \cdot JC(\dot{\varepsilon}) \cdot h(T) \cdot g(\dot{\varepsilon}, T)$$

$$g(\dot{\varepsilon}, T) = \frac{1}{2} \left[ 1 - \text{Tanh} \left( b \cdot \ln \left( \frac{\dot{\varepsilon}}{\dot{\varepsilon}_{cr}} \right) \right) \right]$$

$$\dot{\varepsilon}_{cr} = \frac{\dot{\varepsilon}_{cr,0}}{[JC(T)]^e}, \quad JC(T) = 1 - \left( \frac{T - T_r}{T_m - T_r} \right)$$

$$h(T) = JC(T) \cdot \left[ 1 - \text{Tanh} \left( \frac{T - T_{beta}}{w_T} \right) \cdot \text{Sech} \left( \frac{T - T_{beta}}{w_T} \right) \cdot a \right]$$

where  $h(T)$  is a thermal softening function considering the beta phase softening after  $T_{beta} = 900^\circ C$ ,  $\dot{\varepsilon}_{cr}$  the strain rate onset of hardening, temperature dependent,  $g(\dot{\varepsilon}, T)$  the hardening or softening function in strain rate. This analytic representation tries to mimic the behaviour of the Tabular model, even if not perfectly. Unfortunately, the Author had no resources left to investigate the aspect further, given the fact that the model couldn't provide acceptable results: chip morphology was well predicted for low damage constant values, while cutting force was too low for effective friction coefficient tuning over experimental values.

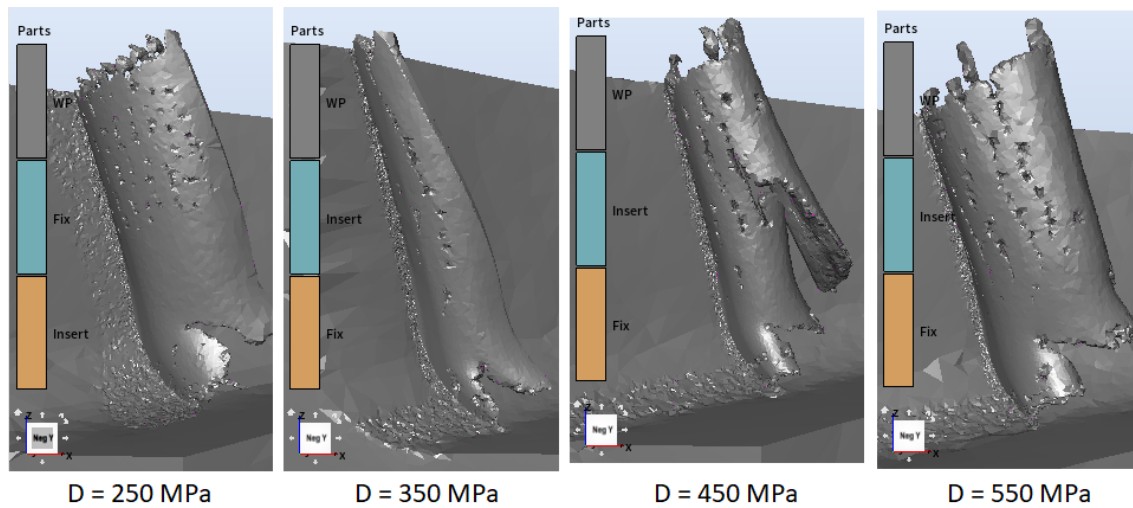


Figure 6.3.7: Tabular material model, 3D trials with variable damage constants

However, the development of a material model comprehensive of low and high strain rates, with more accurate temperature effects (phase softening and below zero behaviour) remains a very interesting research perspective. Ozel model produced much defects for low D values, while for high ones promoted chip features different from experimental findings.

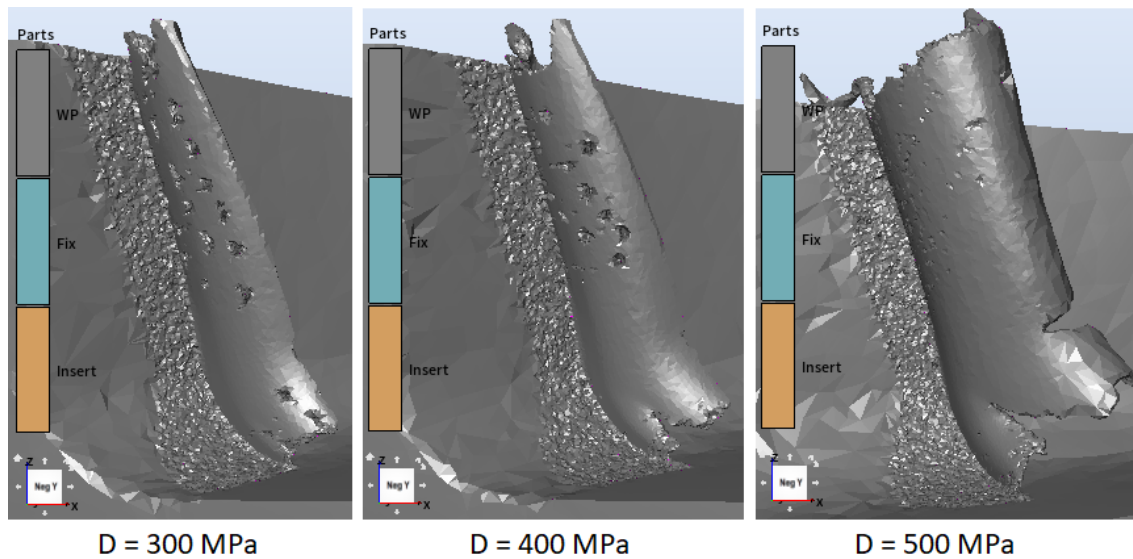


Figure 6.3.8: Ozel 2006 material model, 3D trials with variable damage constants

### 6.3.3 Contact model set up

Contact model plays a minor role in the determination of cutting forces, whereas it influences directly the thermal fields and stress development on the insert. This trend was also confirmed by first simulation trials. Chip morphology remained almost unchanged by varying, the friction coefficients. The contact model should include interfacial friction and conductance evolution as a function of tool-chip interactions such as normal pressure, temperature, sliding speed.

In milling, each tool pass provide force data with variable chip thickness, so that an experimental friction coefficient could be determined as in [119, Arrazola 2008] (Chapter 5, Friction Modeling). Average rake and radial mounting angles were used in order to calculate cutting and feed forces from x, y experimental forces:

$$\omega = \Omega [rpm] \cdot \frac{2\pi}{60} \quad [rad/s], \quad \theta(t) = t \cdot \omega + \theta_{st} \quad [rad]$$

$$F_C = Fy \cdot \cos(\theta(t) + \alpha_{rake}) + Fx \cdot \sin(\theta(t) + \alpha_{rake}) \quad F_f = -Fy \cdot \sin(\theta(t) + \alpha_{rake}) + Fx \cdot \cos(\theta(t) + \alpha_{rake})$$

$$F_N = F_C \cdot \cos(\alpha_{twist}), \quad F_\mu = \sqrt{F_f^2 + (F_C \cdot \sin(\alpha_{twist}))^2}$$

$$\mu = \frac{F_\mu}{F_N}$$

where  $\Omega$  is the spindle speed,  $\theta_{st}$  the starting engagement  $\theta_{st} = atan(1/2)$  for our case (“Square shoulder” 25% engagement),  $\alpha_{rake}$  is the rake angle,  $\alpha_{twist}$  is the axial mounting bend of the insert,  $F_N$  is the normal force on rake,  $F_C$  and  $F_f$  are the cutting and feed forces.

However, the uncertainties due to the measuring set up added to the forced simplicity of the model (average angles over the whole depth of cut), caused the calculated average friction coefficient to be incoherent: the actual value often was larger than one, with no physical meaning.

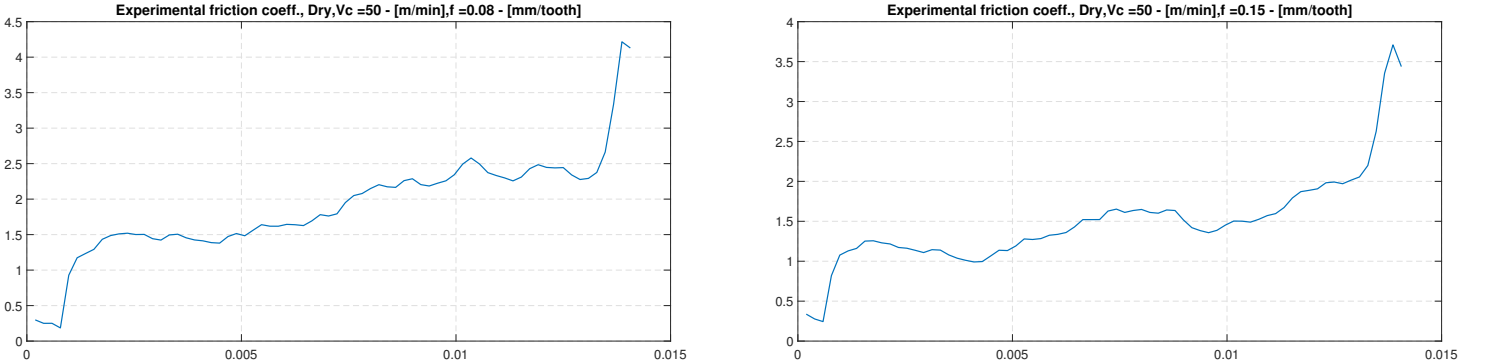


Figure 6.3.9: Experimentally derived friction coefficients along the cut

A temperature dependent contact behaviour could be implemented in FORGE, regarding the friction coefficient and the thermal conductance at the interface. Therefore, following the example of [104, Moufki 1998], [108, Haglund 2008] and the experience of [111, 112, Molinari 2011, Molinari 2012] a thermal dependent contact model was developed. The idea was that a friction model needs to be based on experimental values to be reliable. Too often, friction models with very different values between cryogenic and dry cutting are used. This is often the result of cutting force tailoring using friction coefficients. On the contrary, average friction coefficients found from reliable tribo-tests give quite agreeing values.

Friction and heat partition coefficient measurement test often provide average coefficients as a function of average contact pressures and macroscopic sliding speed. They would also correspond to an average interface temperature. A friction model is implemented that returns the average experimental friction coefficient at a temperature equal to the average experimental interface temperature. For other temperatures friction coefficient is modified as follows:

$$\mu = \bar{\mu} \cdot \left( 1 - \left( \frac{T - \bar{T}}{T_{melt} - \bar{T}} \right) \right)$$

where  $\bar{\mu}$  is the average experimental friction coefficient,  $\bar{T}$  the correspondent average temperature. The idea is that friction shear stress would reduce at high temperature and increase at low temperatures. The average contact pressure and sliding speed (relative to the test for the determination of the average friction coefficient) need to be near the real cutting ones for the following model to be realistic. The model condensate the effect of contact pressure and sliding speed in the effect of temperature: higher contact pressure and sliding speed translates in higher temperature. However the effect of pressure is already considered when shear stress is calculated by:  $\tau = \mu \cdot \sigma_n$ . The effect of speed on temperature is implemented as dissipative contact. Therefore the model accounts only for modification of friction coefficient with temperature.

FORGE looks at undeformable objects through their effusivity regarding the thermal problem. The effusivity of the tool is given constant (look previous sections), while the effusivity of the workpiece varies with its thermal properties. The result is that the HPC decrease with temperature increase.

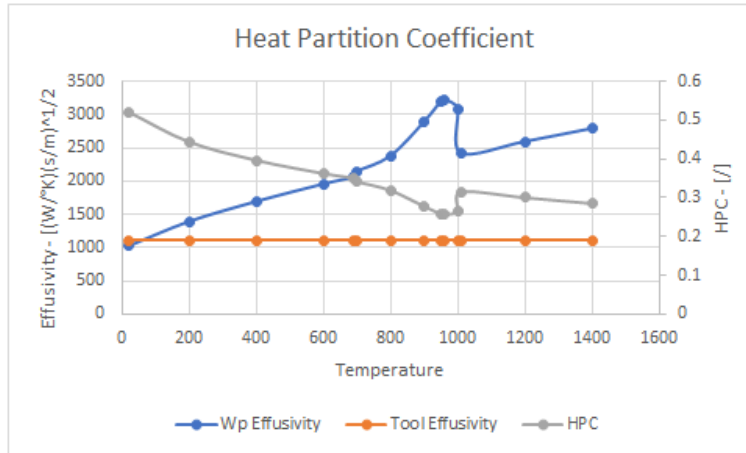


Figure 6.3.10: HPC variations with workpiece temperature, Material properties coming from FORGE

Experimental findings shows that the HPC increase for higher normal pressure and decrease for higher sliding speed (mass transport of the chip). Thus regarding the particular sliding speed and normal pressure distribution on the interface, the heat partition should increase from the detaching region until the sticking region, and then remain almost constant or increase due to increased pressure.

While the HPC regulates the amount of friction heat flowing into the tool, the conductance determines the plastic heat directed to the insert  $Q''_{tool} = K \cdot (T_{wp} - T_{tool})$ .

The interface conductance can be modeled as a function of temperature and pressure. However, we can implement easily only temperature variation, therefore, interface conductance is modeled as follows:

$$k = k_{max} \left( 1 + \alpha - \left( \frac{T_{melt} - T}{T_{melt}} \right) \right)$$

where  $\alpha$  is the percentage of maximum conductance  $k_{max}$  that makes it equal to the conductance at ambient temperature. Assuming a plausible temperature profile along the interface, the conductance would exhibit a maximum at the highest temperature point and decrease toward the tool tip. A more accurate modeling would consider it to increase due to the increase of pressure.

$$k = k_{max} \left( 1 + \alpha - \left( \frac{T_{melt} - T}{T_{melt}} \right) \cdot \left( \frac{\sigma_{max} - \sigma}{\sigma_{max}} \right) \right)$$

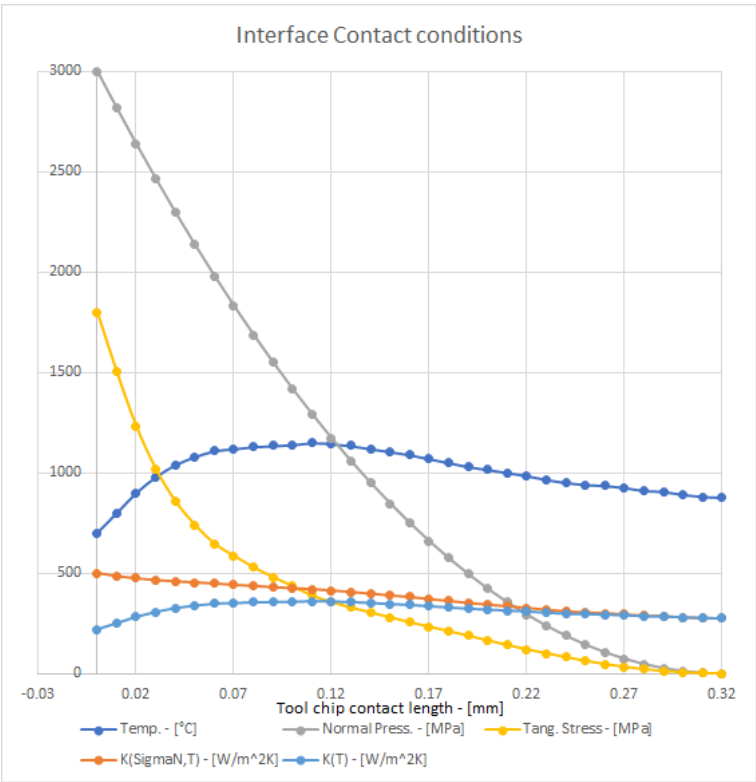


Figure 6.3.11: Thermal dependent Contact Model

Mind that there is no sense in raising the conductance at high levels for a milling simulation. The practice is performed in orthogonal cutting, a continuous process lasting decades of seconds while simulations are meant to reproduce its steady state in milliseconds. In our case we want to reproduce the real temperature build up for a tool pass that lasts milliseconds. The conductance must have real physical data. The temperature in the tool would reach stable cycle values after some tool passes probably, so not in the first one. The only way to simulate a realistic steady state cycle with a single pass is to start the simulation with a thermal field paragonable to the thermal

conditions of the tool at the end of the non cutting phase.

This model and procedure was developed from literature analysis of contact models and availability of experimental data coming from practical tribometers. However, to keep complexity of the problem under control, simulations were set up with a simple Coulomb-Tresca model with constant coefficients:

Environment	Tresca coeff. -[-]	Friction coeff. -[-]
Dry	0.8	0.3
Cryo	0.6	0.25

Table 6.3.2: Contact model coefficients for 3D model fitting

This simplicity is justified by the necessity of getting rid of some variables, identifying on the Damage coefficient a single quantity onto which iterate. The contact models are meant to be refined after material and damage models are set. Is not worth having intricate contact models while material and damage ones need to be tailored. Values of contact model coefficients were taken considering literature simulation and experimental studies. Those represent initial values onto which iterate to match experimental cutting forces.

# Chapter 7

## Model results

### 7.1 Dry Environment

Lee and Lin model, shear zone mesh refinement of  $40\mu m$ , average chip mesh size of  $80\mu m$ , remeshing on deformation from  $1m/m$  and LC damage models with  $D = 425MPa$  proved to be effective in modeling average shape and defect level of experimental chips, and  $Fy$  cutting force. Simulated time was set  $5ms$  which correspond to less than half of the engagement arc. Simulations lasted 30 hours and more, if the workstation (60 cores @ 2.5 GHz, 365 GB ram DDR3, hard drive 4 TB) was crowded.

Firstly  $Fy$  cutting forces and chip morphology are compared to the experimental results. As we have anticipated,  $Fx$  and  $Fz$  experimental and cutting forces exhibit strong variation in both amplitude and shape. Following the evolution of chip thickness, theoretical force evolution is correctly predicted by the FEM. Experimental forces are subjected to strong measurement issues, one of all the resonance peaks of the assembly MT table - measuring table - bulk Titanium piece, suitable for wear tests but not for force measurements. More accurate force measurements would be obtained by limiting the mass of the Titanium sample, also because force measurements only require a minimum material removal. Fortunately, the  $Fy$  force could provide a reasonable comparison between experiments and simulations. Forces displayed in the following are the results of friction coefficient tailoring, which became:

Environment	Tresca coeff. $m$ [-]	Friction coeff. $\mu$ [-]
Dry	0.6	0.4
Cry	0.4	0.25

Table 7.1.1: Final contact model coefficients

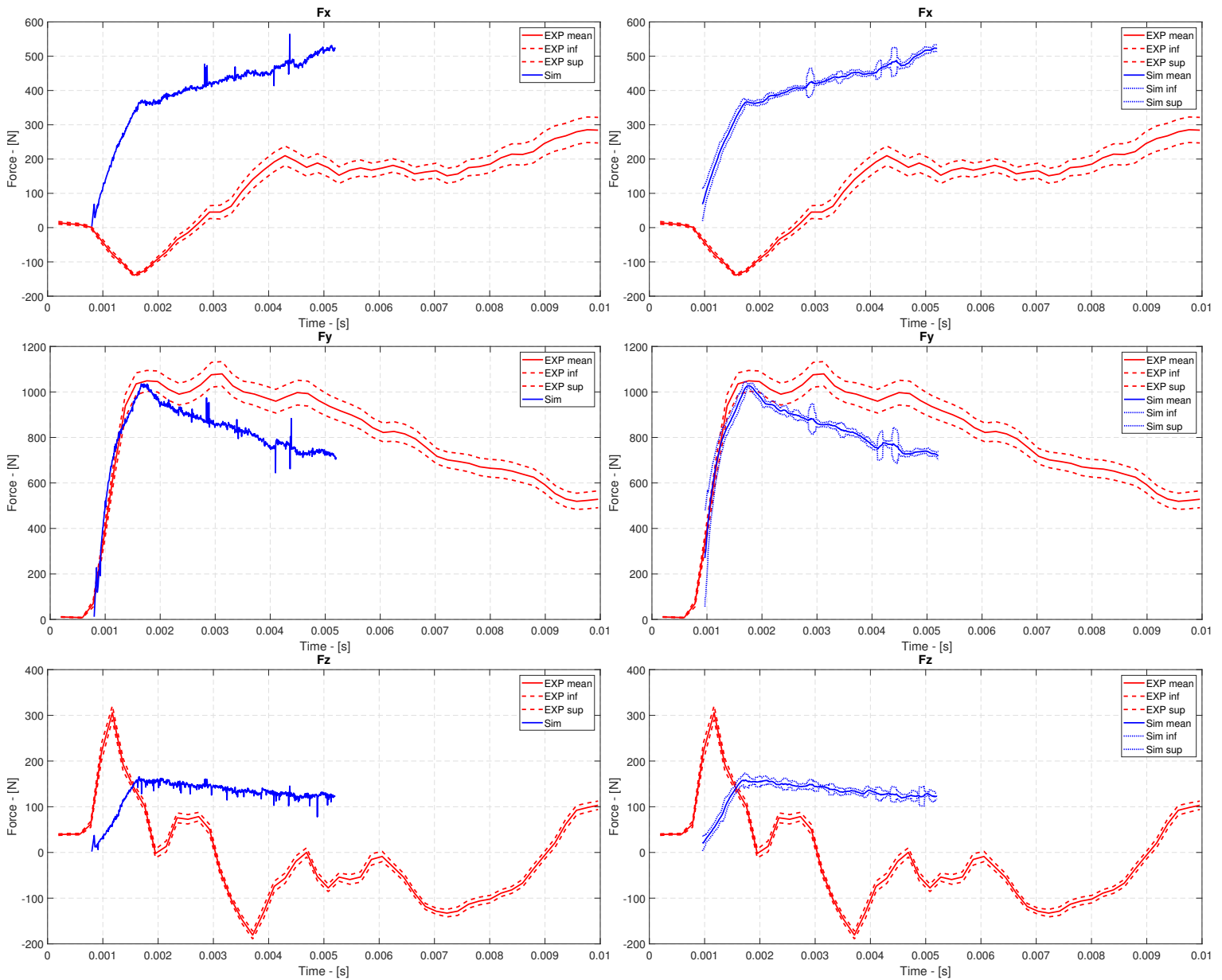


Figure 7.1.1: Simulated and experimental cutting forces comparisons, right column windowed,  $0.15\text{mm/tooth}, 50\text{m/min}$

Simulated quantities often exhibit large variations between time steps due to numerical issues, but have abundant resolution and can be windowed. Windowing generates smoother profiles with high probability of getting rid of numerical noise. The value in the centre of the window is obtained by averaging the values inside the window, which then moves its center to the following value of the vector:

$$F_i^{wdw} = \frac{\sum_{i=-k}^k F_i}{2k}, \quad S_i^{wdw} = \sqrt{\frac{\sum_{i=-k}^k |F_i - F_i^{wdw}|^2}{2k - 1}}, \quad (1 - \alpha) = 95\%$$

$$F^{wdw}(t) = F^{wdw}(t) \pm p \cdot \frac{S^{wdw}(t)}{\sqrt{2k}}$$



Secondly, chip morphology between experiments and simulations is compared. Limitations in this case are the simulation shortness and the limited quantity of experimental images. In the first simulated case (#ID 3,  $0.15\text{ mm/tooth}$ ,  $50\text{ m/min}$ ), the experimental chip is certainly a pair of chips stick together. In general, the simulated chip reproduces the lower defected areas (a) and upper segmentation (b). The latter characteristic is better predicted than the first one, probably due to coarser mesh size around the tool corner edge (additional meshing windows required following precisely the edge). The chip also includes segmentations traveling for the whole depth of cut. Chip bending is reasonably in accordance with the experiments. We have to underline that the experimental chip has been collected from the MT chip storage after cool down and could have modified its shape, while the simulated one is still very hot.

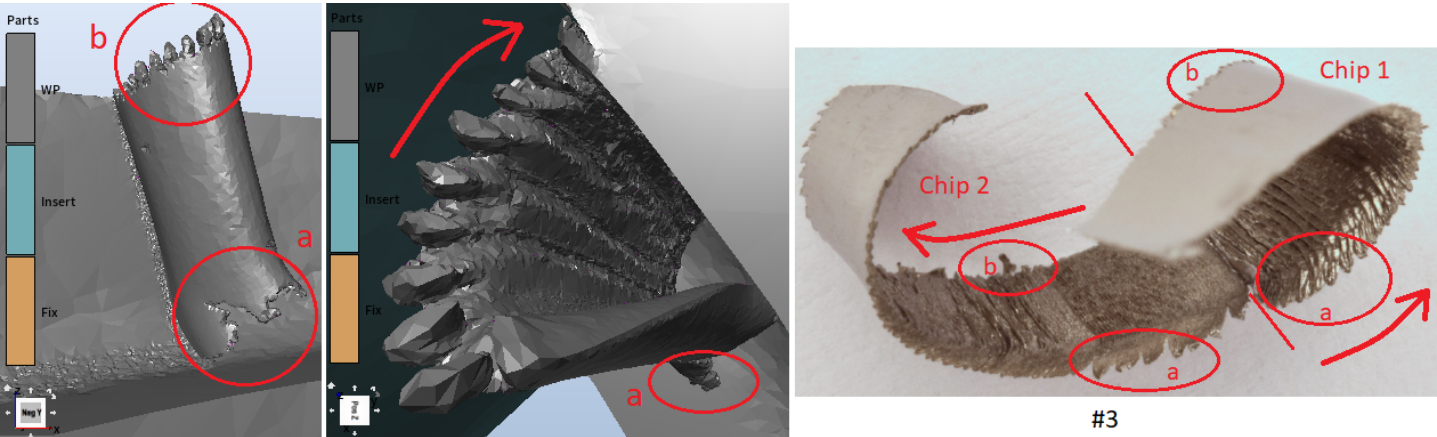


Figure 7.1.2: Simulated and experimental chip morphology: a) lower chip part, b) upper chip part, #ID 3  $0.15\text{ mm/tooth}$ ,  $50\text{ m/min}$ . The arrows indicate chip formation direction

Lower LC damage constant values ( $D < 400\text{ MPa}$ ) cause the serration fractures to reach the back surface for the whole chip height, causing it to fragment in pieces. Larger LC constants result in too ductile chips with no characteristic upper and lower fragmentation.

FORGE offers a variety of other results in the form of time curves or volume dispersed quantities. The maximum temperature in the workpiece gives an idea of the maximum temperature reached in the tool, that is lower due to heat partition, conductance, and short contact duration. However, the software doesn't allow thermal calculation of a rigid die, as any rigid object has a surface mesh only. To calculate thermal fields only in the insert (not the mechanical ones), the insert could have been modeled as deformable while preventing its mechanical computation (option available in Forge). However, that introduce a 3D mesh on the tool for the thermal computation that can slow by 20% the calculations. For sake of simplicity, we decided for a rigid tool, at least for model fitting purposes.

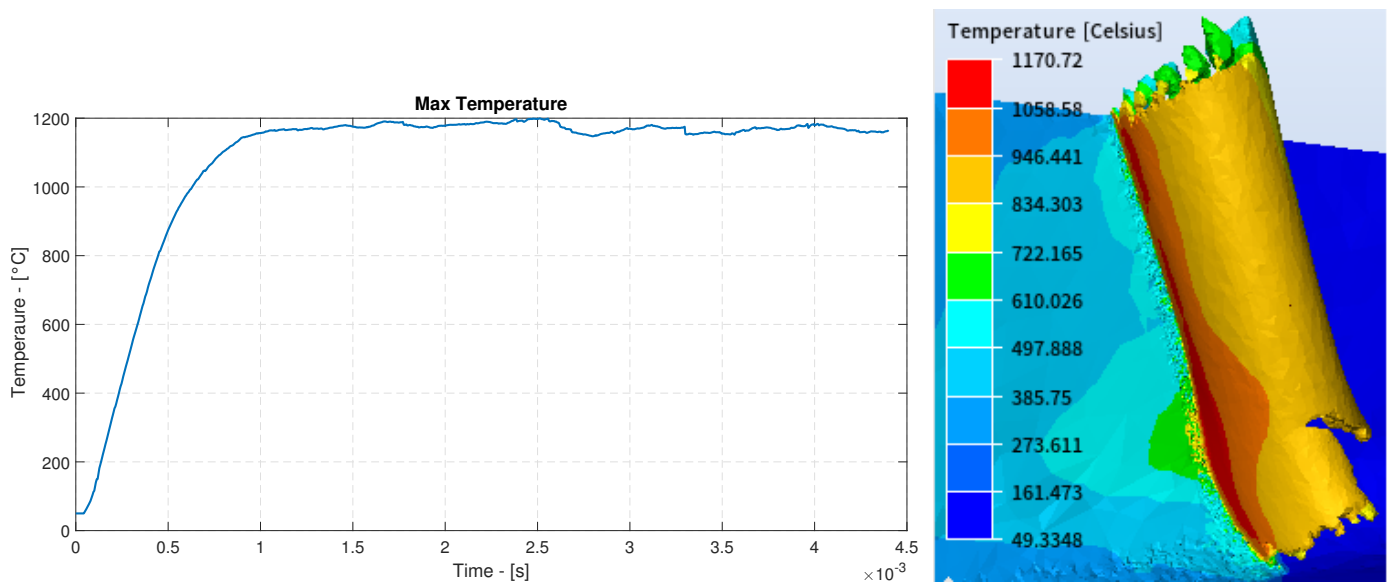


Figure 7.1.3: Max Temperature profile, and location at 3.2ms, #ID 3 0.15mm/tooth, 50m/min

Total model volume gives an idea of the amount of volume loss due to element deletion. The Element Deletion Areas inform on the location of element deletion. The “Latandco” value informs of the LC damage value reached by elements; elements that reach the value of the LC damage constants are excluded from the computation. We can see as the Element Deletion Areas and “Latandco” values rise in correspondence of shear bands. Therefore, using a LC damage model to reproduce shear bands is, all simplifications considered, a first fair choice.

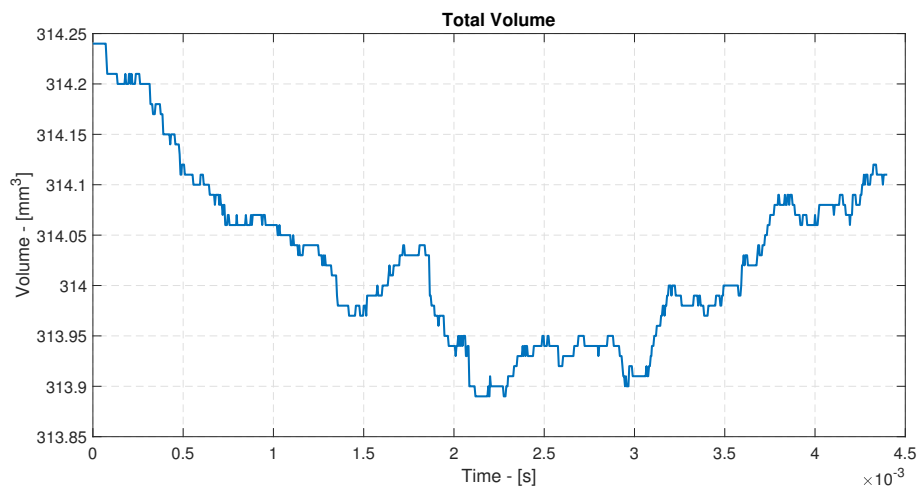


Figure 7.1.4: Volume loss, #ID 3 0.15mm/tooth, 50m/min

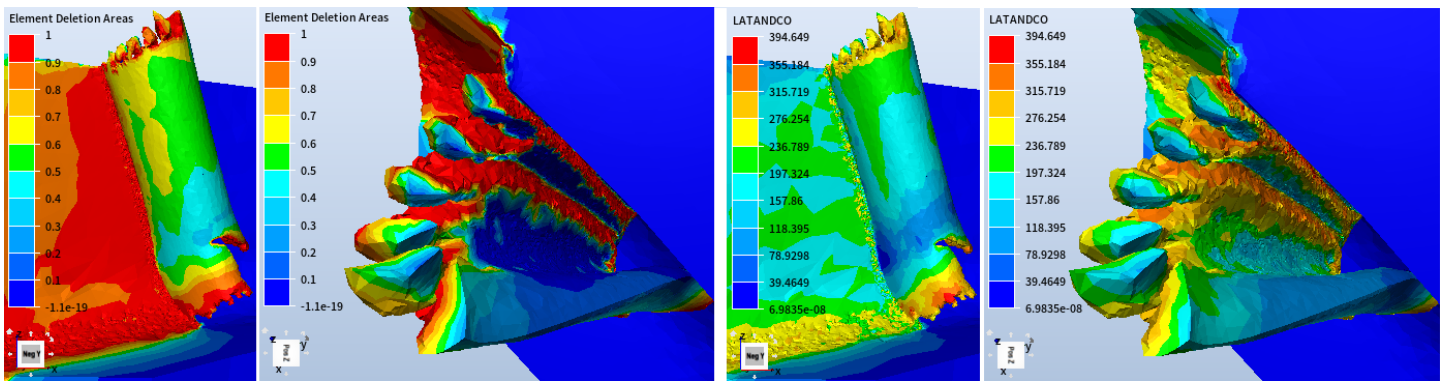


Figure 7.1.5: “EDA” and “Latandco” at 3ms, #ID 3 0.15mm/tooth, 50m/min

Heat Exchanges with dies, with ambient for convection and radiation, and due to friction are plotted. It can be seen how the Exchange with ambient media for both radiation and convection is quite negligible. Heat exchange with dies is also small due to the short simulation time. This data is highly dependent on the conductance value, affected by some uncertainties, and in general by the contact model. Mechanical Exchanges include elastic, plastic and friction power as the energies dissipated by elastic, plastic strains and friction. As a chip removal process, plastic power has a major role, followed by friction power. This is parallel to the importance of material and friction models while simulating chip formation processes: material models have more influence on mechanical results (cutting forces) while contact models have major impact in regulating the Heat Exchange.

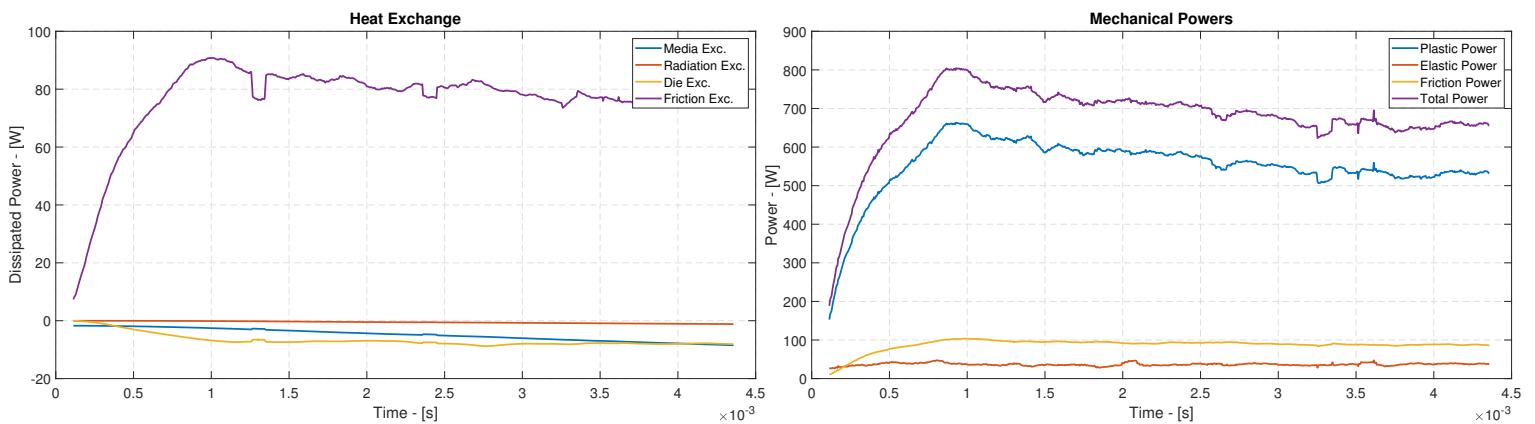


Figure 7.1.6: Heat and Mechanical Exchanges, #ID3 0.15mm/tooth, 50m/min

### 7.1.1 Cutting parameters influence

Dry cutting simulations were run reproducing experimental runs #1, #3, #4, #5 as shown in the table below.

ID	Speed -[m/min]	Feed -[mm/tooth]	MRR - [cm <sup>3</sup> /min]
#3	50	0.15	3.58
#5	70	0.15	5.01
#4	50	0.2	4.77
#1	70	0.2	6.68

Table 7.1.2: Simulation runs parameters

Cutting forces along y axis are displayed below. Two main issues are present: **Feed trend.** The model approximates from below the low feed experiments while from above the higher feed measurements (peak force). Possible explanations can be that at higher feed, the material to be sheared increase, tool-chip interface increase, temperature increase and may cause friction variations. Anyway we believe exaggerate to develop dedicated friction coefficients for different feeds, so it haven't been done. Different ratio  $N^{\circ}_{elements}/Chip_{thickness}$  could also cause variation in force accuracy in feed. Refining the shear mesh size could bring to better result for the lower feed. Cutting simulations do not account for MT compliance, which excitation changes with the feed and speed.

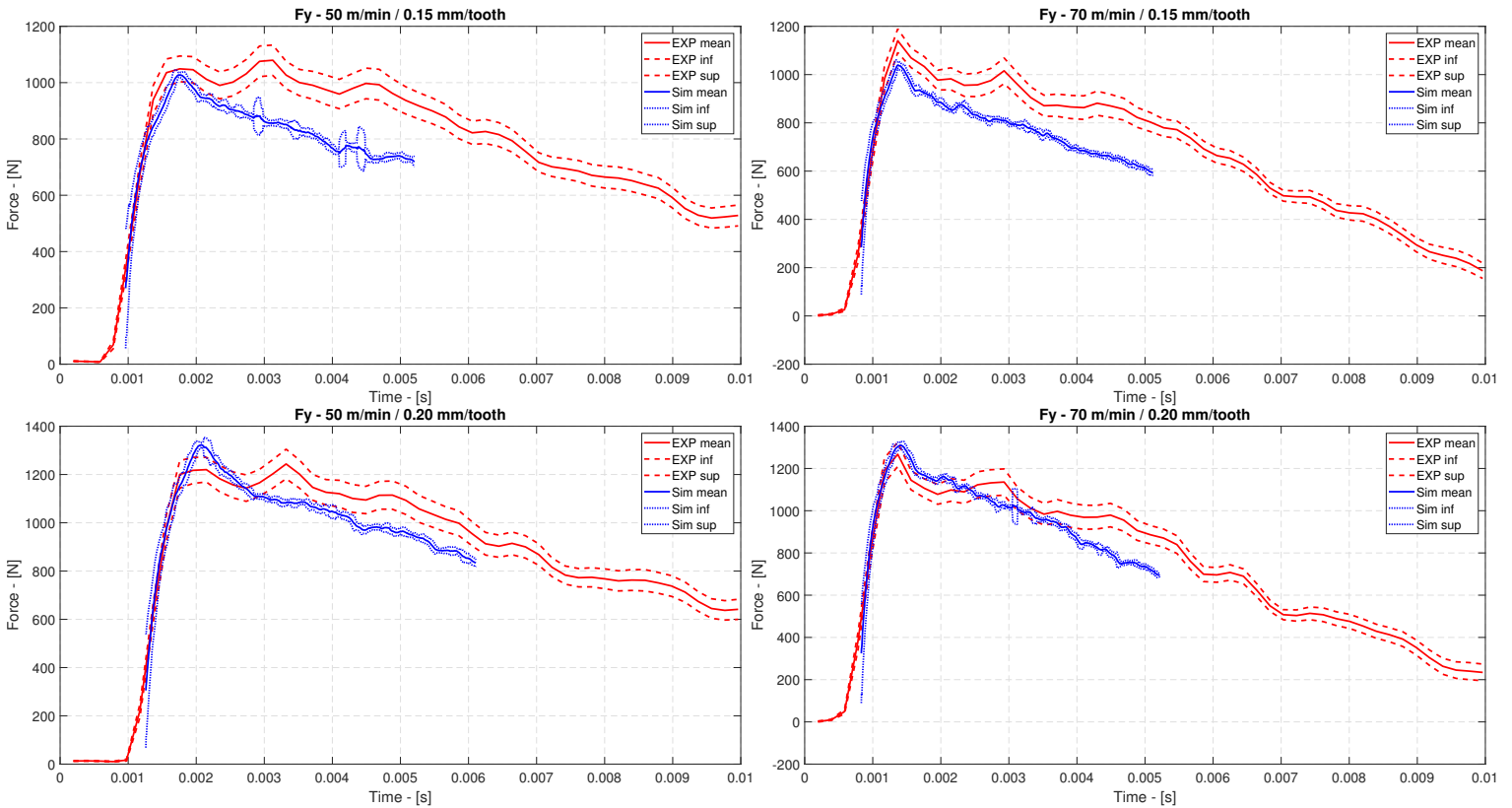


Figure 7.1.7: Simulated windowed and experimental cutting forces comparisons

**Decreasing slope.** All simulated forces exhibit a steeper decrease with respect to experimental measurements. Possible answers for this could again take into the plot

the compliance of the MT. The actual cutting chip thickness could vary according to MT dynamics. Another explanation could be an approximate modeling of workpiece compliance, for example in the low strain rate ranges. We know the JC model have been designed for impact loading. Simulated chip thickness seems to decrease more rapidly than in reality.

A numerical comparison of forces is performed. Simulated and experimental force were subtracted and integrated in time with trapezoidal approximation, then normalized by the experimental force time integral. Also peak force values are compared:

$$Err_{trapez} = \frac{\int_0^{t_{sim}} (F_y^{Sim} - F_y^{Exp}) dt}{\int_0^{t_{sim}} F_y^{Exp} dt}, \quad Err_{peak} = \frac{max(F_y^{Sim}) - max(F_y^{Exp})}{max(F_y^{Exp})}$$

Exp ID	$Err_{trapez}$	$Err_{peak}$
#3	-16.0%	-4.8%
#5	-14.6%	-8.8%
#4	-5.8%	+6.4%
#1	-6.6%	+3.4%

Table 7.1.3: Numerical Fy forces prediction accuracy

Force prediction accuracy is believed to be acceptable, as errors below 10% are paragonable with modeling approximations such as MT perfect rigidity, thermal boundaries, friction behaviour assumptions and consistent with literature results. Fitting for lower integral error would have caused overestimation of peak error in all runs. We believe of importance understanding phenomena underneath the highlighted problems than trying to fit perfectly experimental data with time demanding iterations on friction coefficients.

Simulated chip bending radius and average upper and lower defect levels are reproduced with an acceptable level of accuracy. Moreover, the model is capable of reproducing the trend in speed and feed observed in literature and experiments. Serration frequency increases (narrower bands) for increased speed, while decrease for higher feed. Experimental serrations seems to be reproduced accurately for the #4 run, however, from experimental chip #1 hardly any peculiar feature can be discerned.

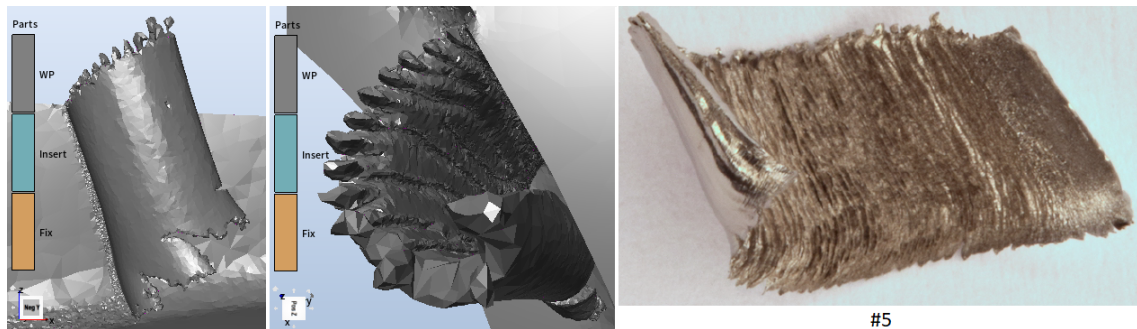


Figure 7.1.8: Chip morphology comparison, #5

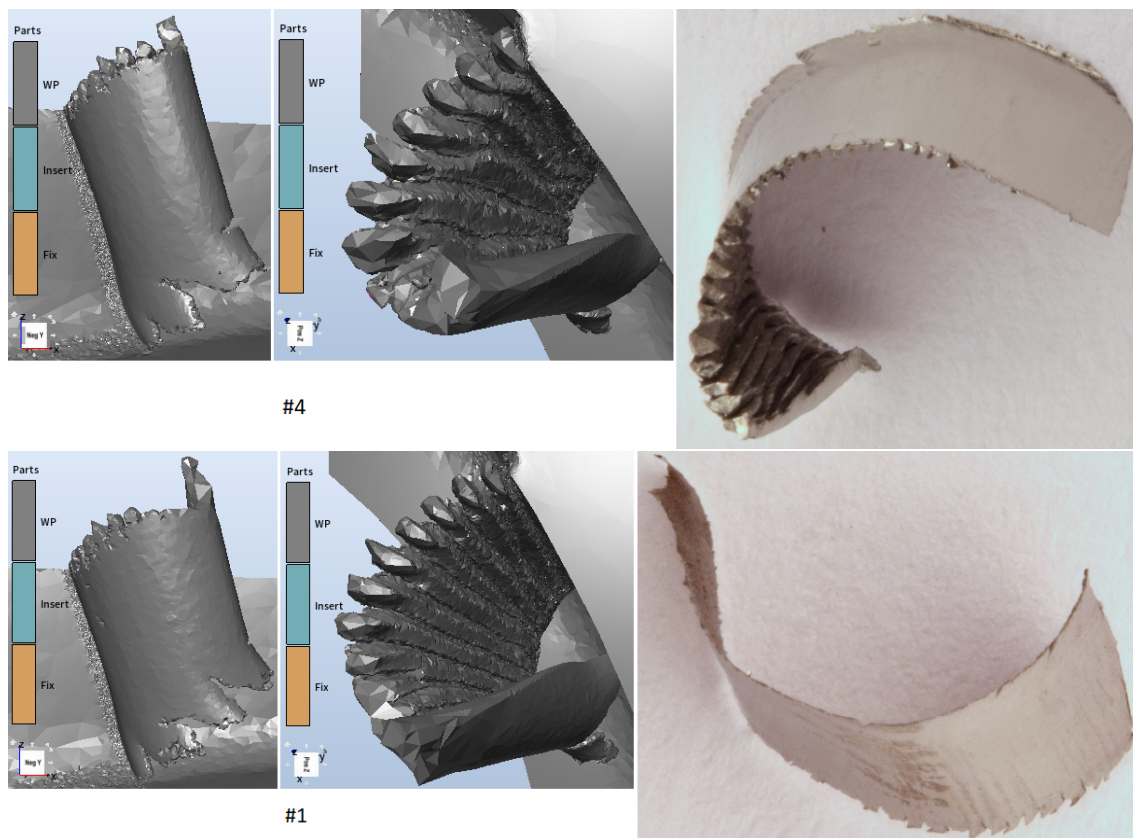


Figure 7.1.9: Chip morphology comparison, #4, #1

Maximum cutting temperature and location among different parameter combination varies as shown in the following figures.

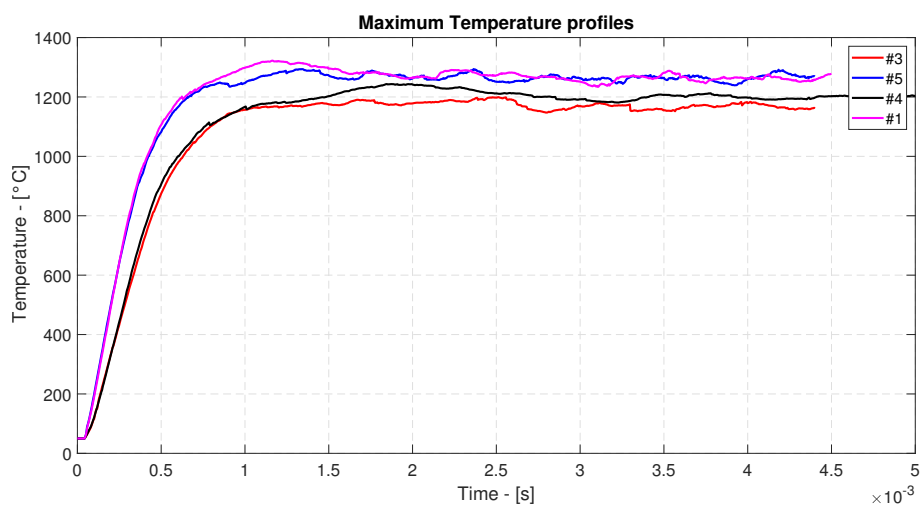


Figure 7.1.10: Maximum temperature comparison between simulated runs

We can see that the maximum temperature in the tool is always located in the same spot. It is likely that diffusion and adhesion wear would take place at accelerate pace there. The increase in speed heightens temperature more than the increase in feed. The latter cause the highest temperature region to be wider. Temperature values seem

quite high, but there is to be said that few have managed to obtain reliable temperature measurements in that location, on workpiece side.

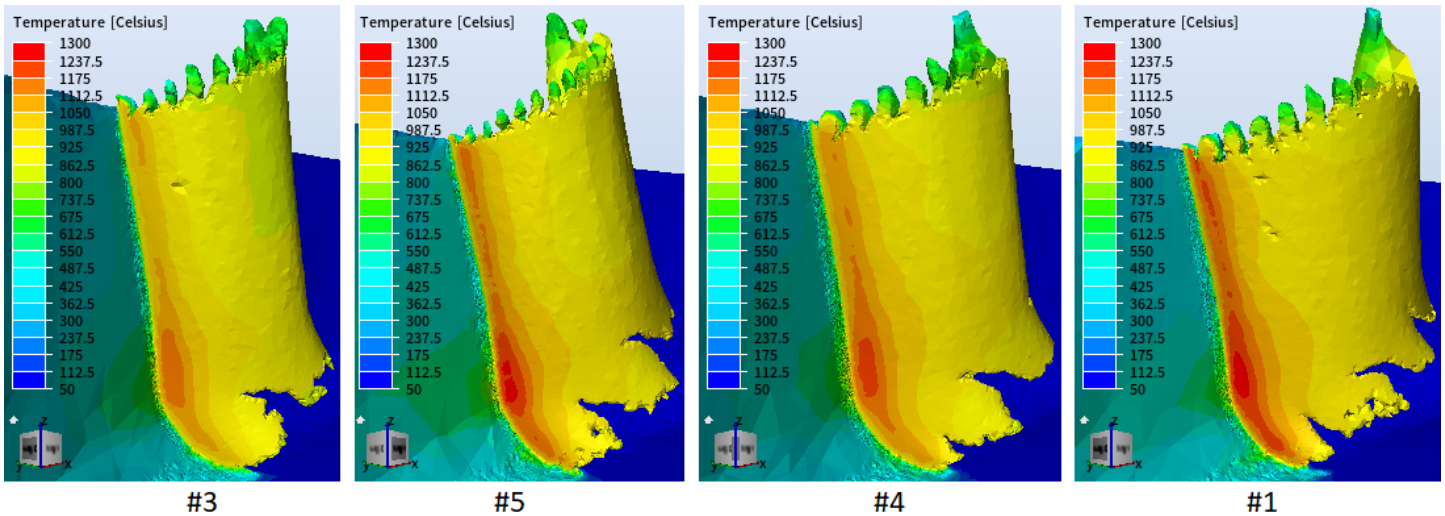


Figure 7.1.11: Temperature fields comparison between simulated runs

Concerning the front side of the chip, temperatures are variable and comparable to measurements obtained with Thermocameras.

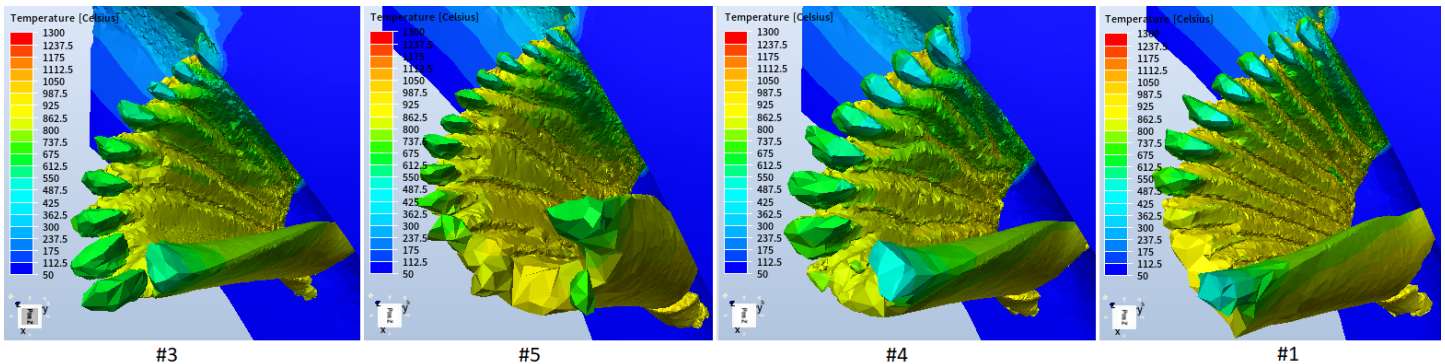


Figure 7.1.12: Front surface chip temperature

Heat Exchange by convection and radiation toward the environment are but very small portion of the thermal energy exchanged in the process. It can be seen how the magnitude of heat convection and radiation raises with cutting speed. Heat exchange with tool (die) is also quite small due to short process time and conductance at the interface. The heat transferred to the tool is mainly governed by the feed, so the portion of contact surface (larger tool chip contact length). Same behaviour is observed for the heat generated by friction. Elastic power has a very noisy signal, even if windowed, and raises almost with equal manner with speed and feed. Friction power is more influenced by tool chip contact area, so feed than speed. Plastic power has the highest influence in the total cutting power. It seems to raise in equal manner with feed and speed, it would be therefore convenient to go at higher speed than feed, due to the increase in the MRR, causing, however, higher temperature and tool wear.

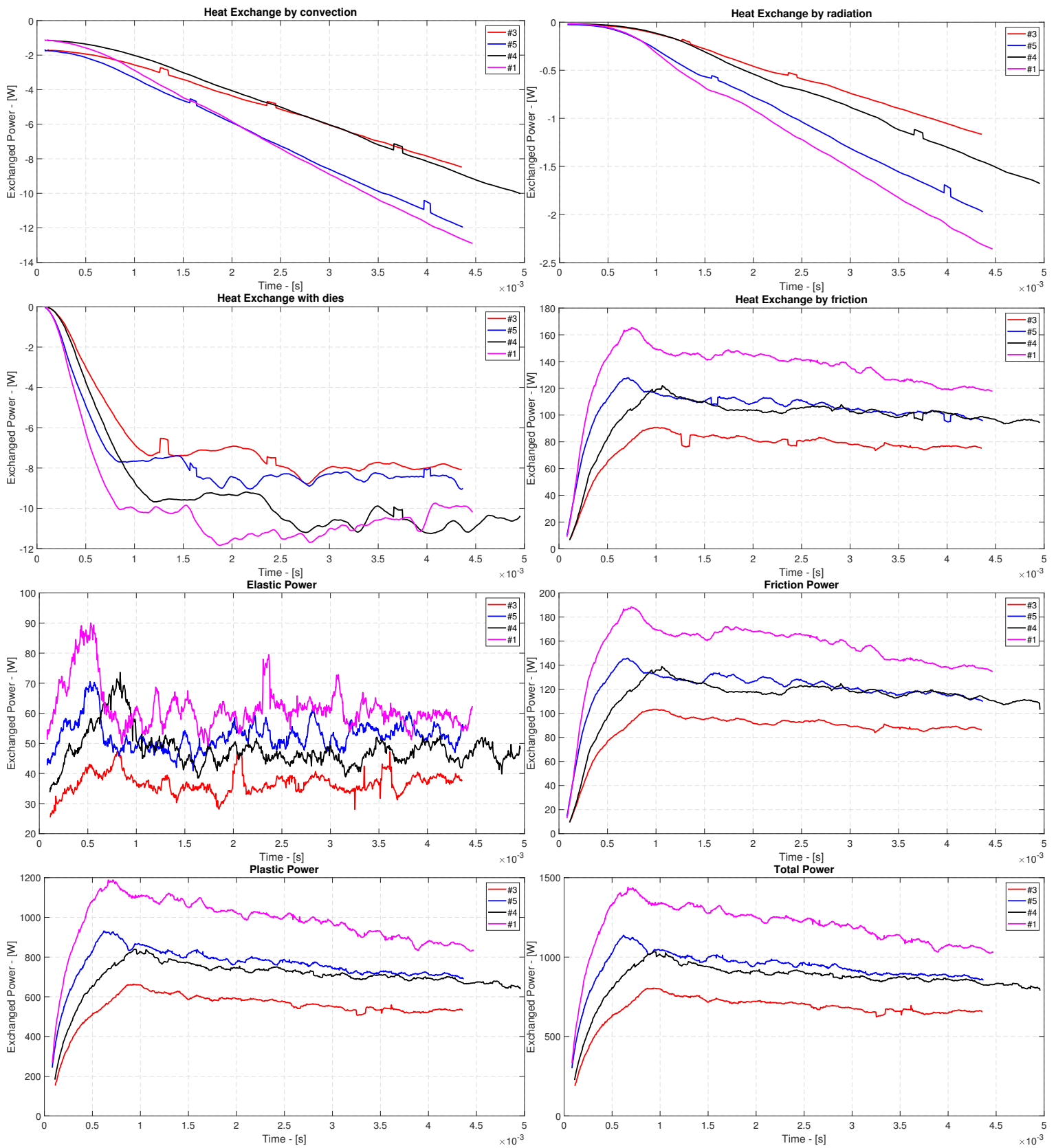


Figure 7.1.13: Simulated windowed and experimental Heat Exchanges and Mechanical Powers comparison



## 7.1.2 Cutting mechanics and tool stress analysis

It is interesting to compare specific material and tool related features in variable cutting parameters. Strain remain almost unchanged with local maxima around 8, while keeping from 3 to 6 in the secondary deformation zone.

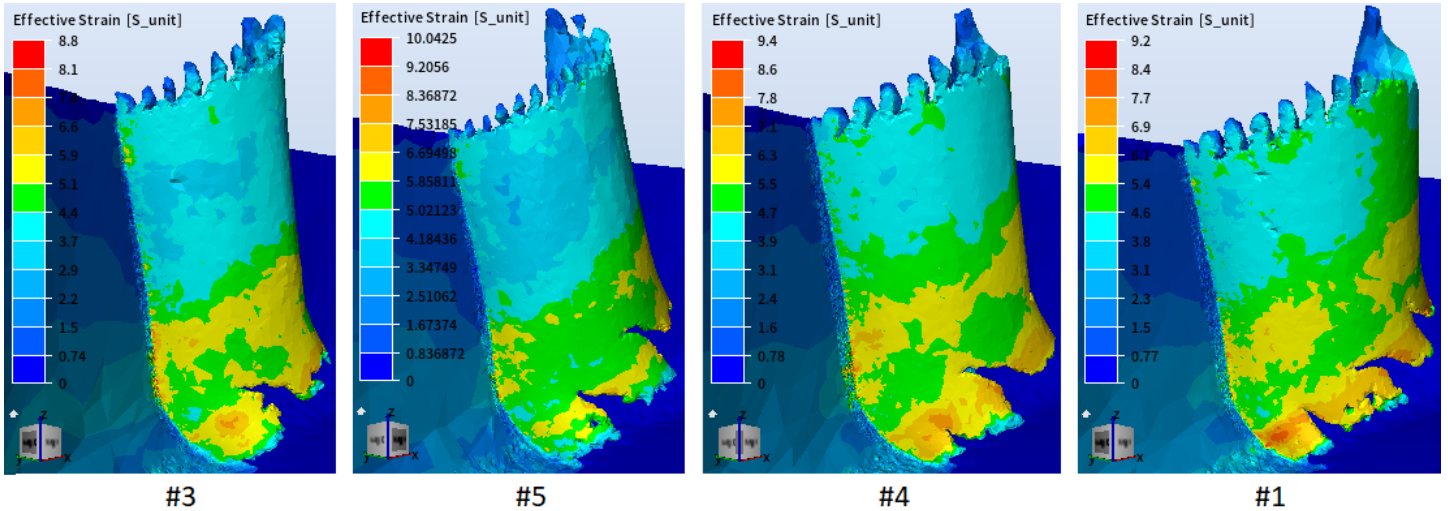


Figure 7.1.14: Strain fields around  $4ms$  for the simulation runs

Strain rate visualization in 3D is complex. By applying filtering thresholds, logarithmic scales and cutting planes the shear zone peculiar strain rate path is visible and average values can be obtained. Strain rate increase at higher speed as cutting cinematic would suggest. It decrease with higher feed probably because of the increased chip thickness, so wider material portion can share the loading rate. Anyway, the images represent only a portion of the edge, and a single time instant. They could therefore depict a particular case

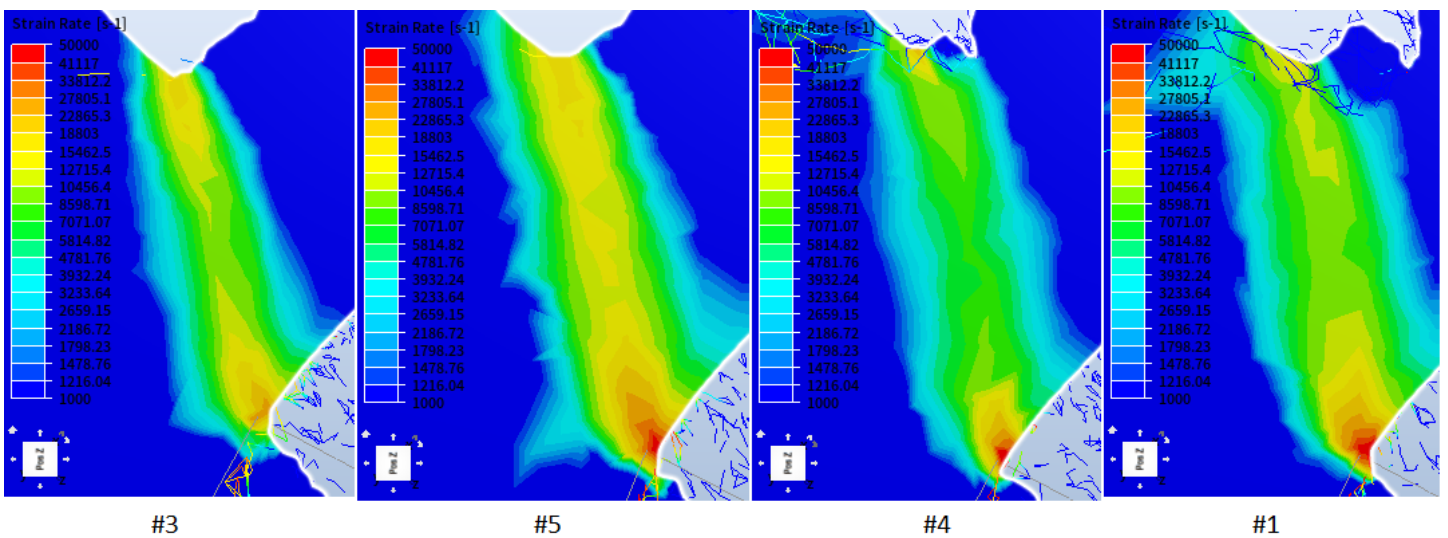


Figure 7.1.15: Strain Rate fields in the shear zone around  $2.3ms$  for the simulation runs #1, #4 and  $3.2ms$  for #3, #5

Looking at tool side, it can firstly be noted the contact time between workpiece and insert. It gives an idea of the area with higher probability of wear development and geometry of the contact area. “Normal stress on die”, “All die relative tangent speed” and “All relative tangent stress vectors” display the magnitude of the relative vectorial fields. Normal stress can reach up to  $3.5\text{GPa}$  for the higher feed parameters. Tangential speed evidence a small area of sticking near the tool tip.

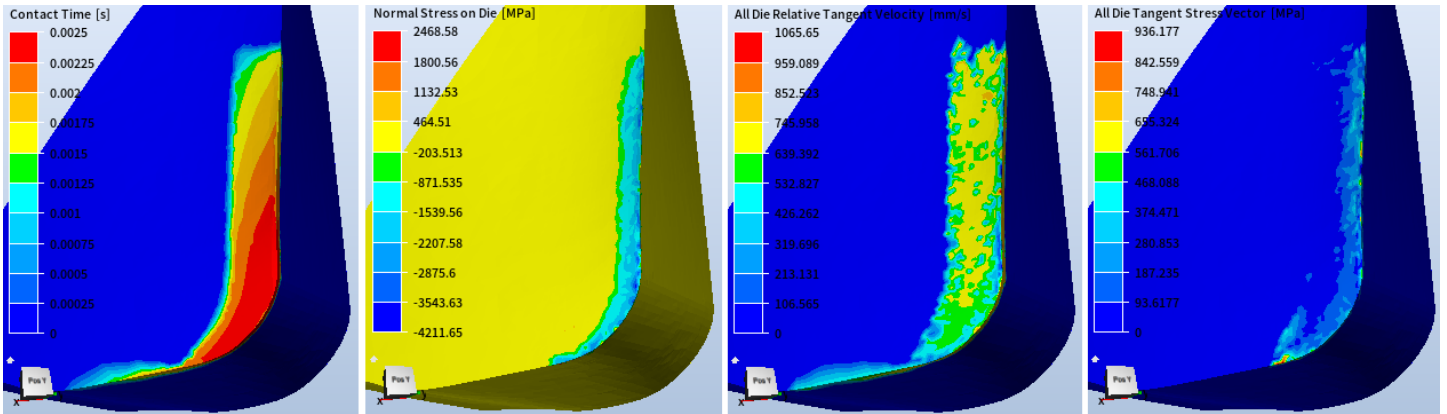


Figure 7.1.16: Insert related fields: contact time, normal stress magnitude, tangential speed magnitude, tangential stress magnitude, #4  $50\text{m/min}0.20\text{mm/tooth}$

However, tool computed stresses and tangential speeds are subjected to strong averaging. By analyzing in depth, with the use of paths, the normal stress, tangential speed and stress, it can be seen how noisy the signal are. Below the case for run #4 is reported, but the same holds for all simulations. The two graphs should be equal.

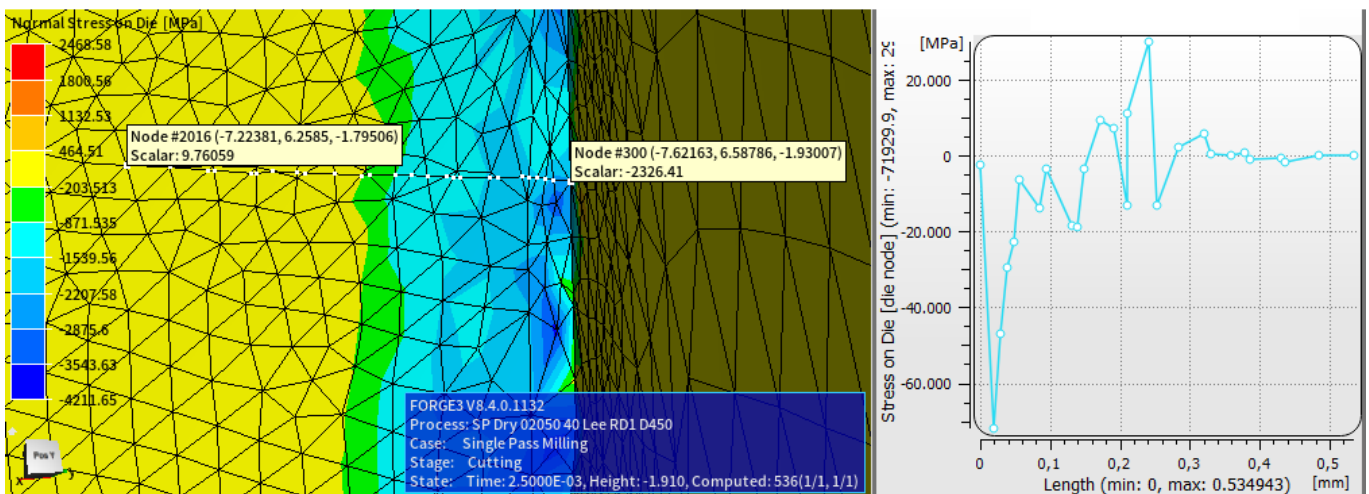


Figure 7.1.17: Normal stress high variability on tool side, #1  $70\text{m/min}0.2\text{mm/tooth}$

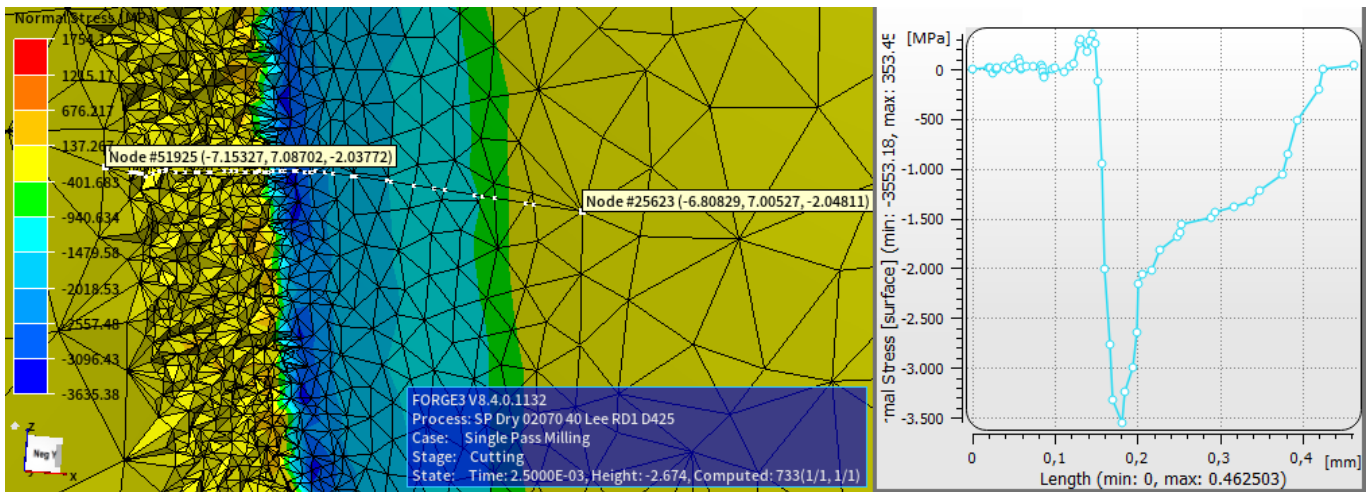


Figure 7.1.18: Normal stress on WP side, #1 70m/min 0.2mm/tooth

The tool computed quantities are simple projection on tool mesh of deformable object results, it is clear something happens causing the high variability. It has more sense to look at the workpiece side. Normal stress and temperature fields can be extracted along paths and displayed as a function of the chip contact length. As an example, it is reported below the normal pressure calculated on the workpiece, far more fair looking than the one calculated on tool side.

Tool-Chip contact paths were drawn and normal pressure and temperature on workpiece side were extracted. For all simulation runs, the chosen time steps corresponded to the same position along the cutting arc, so to evidence difference in tool chip contact length due to the variable feed rate and provide the same time for thermal field stabilization. For the highest cutting speed this corresponded to 2.3ms while it was 3.2ms for the 50m/min case.

As the quantities are taken from the workpiece side, it is necessary to recognize where does the flank and rake separates (b). Intuitively this would happen in correspondence of the maximum normal pressure value. Also, being flank wear null (tool modeled as perfectly sharp), flank contact length is minimal (ab) compared to the rake tool-chip contact length (bc).

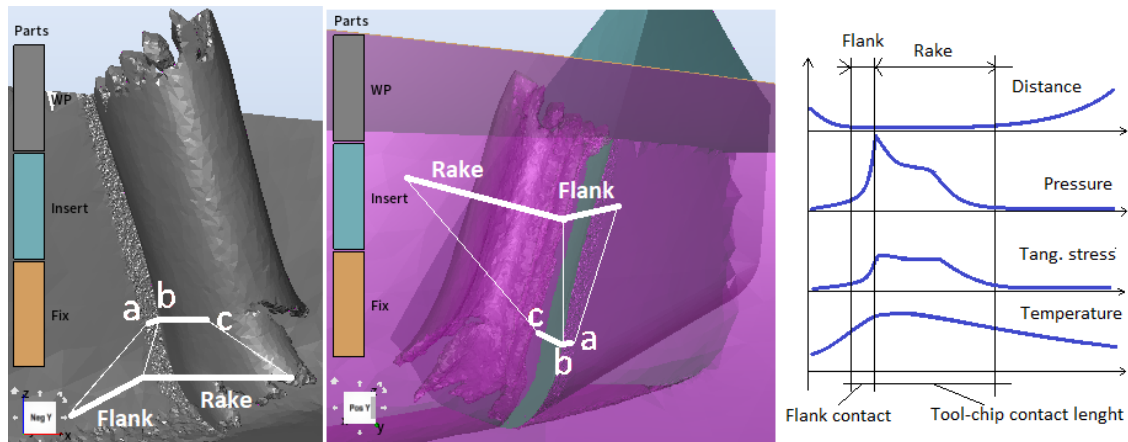


Figure 7.1.19: Tool chip contact path scheme

Concerning the normal stress, XY stress tensor component was considered, given the orientation of the chip sliding on the tool. It was not possible to extract surface tangent stresses like it was possible with normal ones, this causes some issues:

- There is an almost constant shift of  $200\text{ MPa}$  that can be seen at the left and right, also when the workpiece surface and the chip surface has detached;
- There is a sign inversion that can be guessed as the almost  $90^\circ$  solid tool angle from rake to flank. This also can be used to detect the passage from flank to rake or vice versa. However, data around the tool edge, being a sharp corner, can be inaccurate.

Said so, the tangential stress is highly dependent on the contact model choice, any result is therefore biased by the Coulomb Tresca model choice. Anyway, we can see that its behavior is acceptable according to literature.

Normal pressure, on the other hand, has a different behaviour from what is known in literature, usually approximated by a simple decreasing exponential function on the rake. It exhibits a slope change which seems to be linked with the uncut chip thickness, influencing also the temperature profile. This feature has been found in all and every path tried by the author to extract contact variables. It would be interesting to investigate this effect further.

Tool chip contact length behaves well in relation with cutting parameters, as reported in literature, increasing with the feed while decreasing slightly with speed.

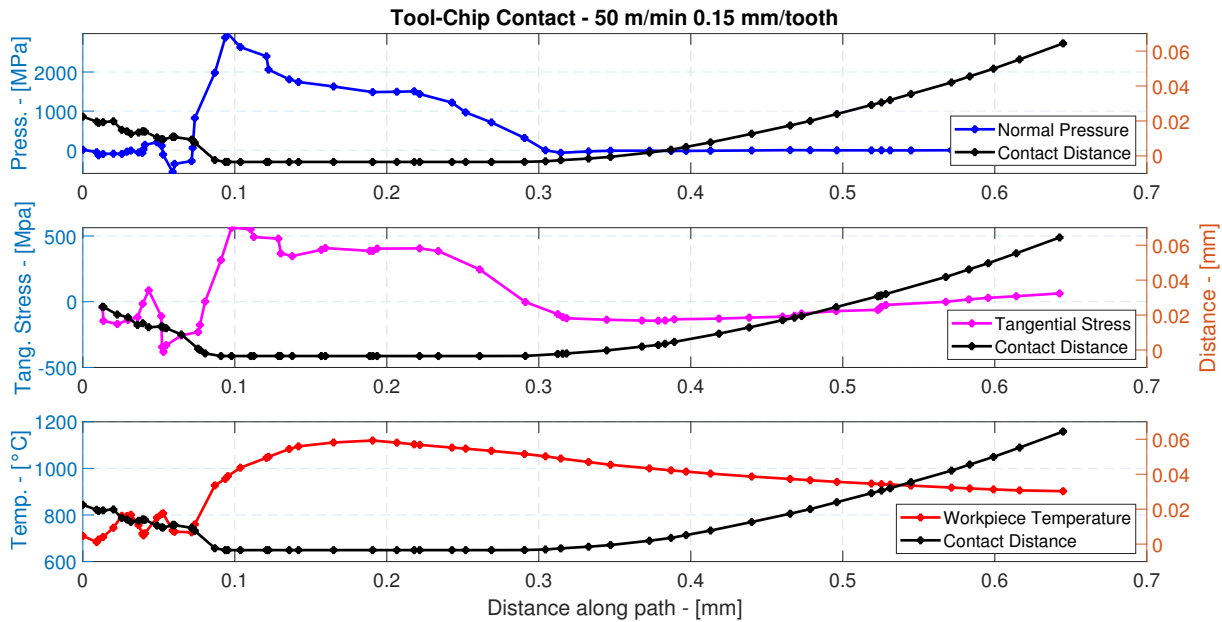


Figure 7.1.20: Tool-Chip contact variables, #3

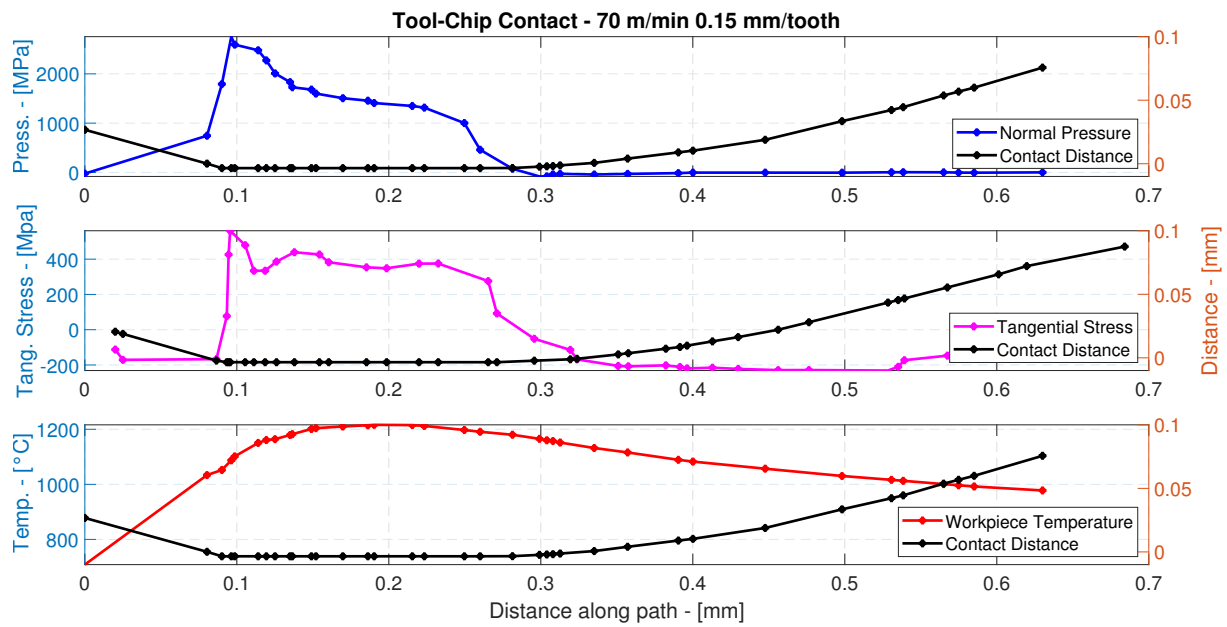


Figure 7.1.21: Tool-Chip contact variables, #5

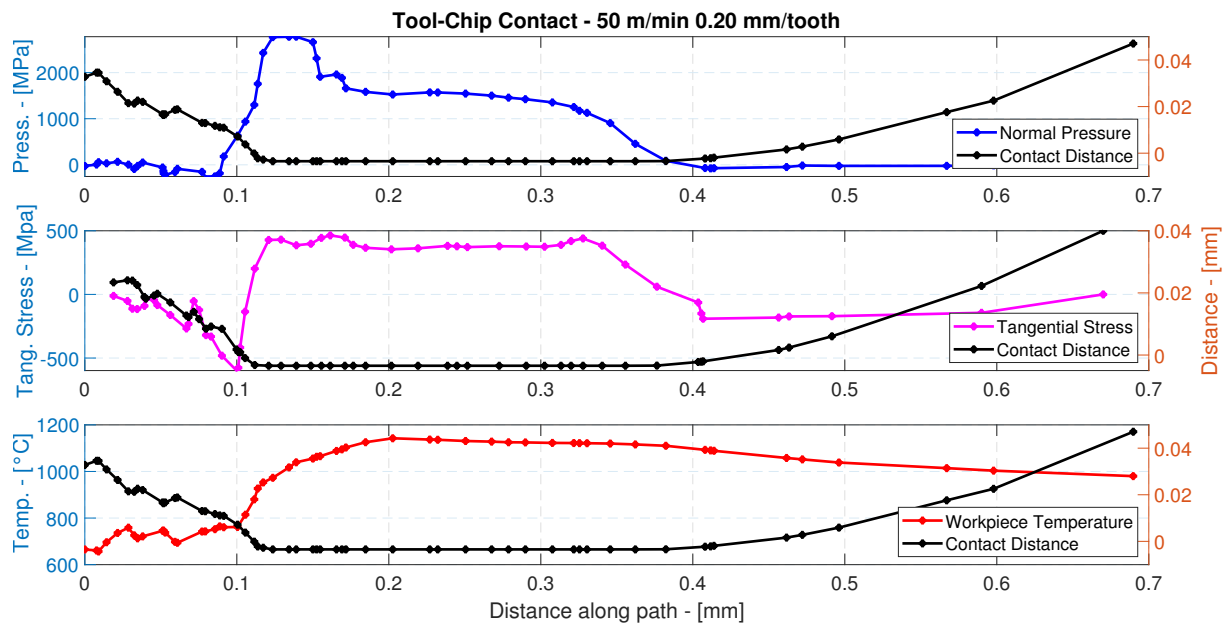


Figure 7.1.22: Tool-Chip contact variables, #4

This paths are extracted in the region of the peak temperature along the tool edge. The tool edge is long, it could have been more complete to extract paths along the whole engaged edge length at precise intervals one from another. The single curves could have been then averaged, for example, on three main paths (with mean and deviation) to be attributed to the linear vertical edge, the round corner, and the linear bottom horizontal edge. It would have been so lengthy we decided to show only the highest loaded spot, likely to be subjected to the most intense wear rates.

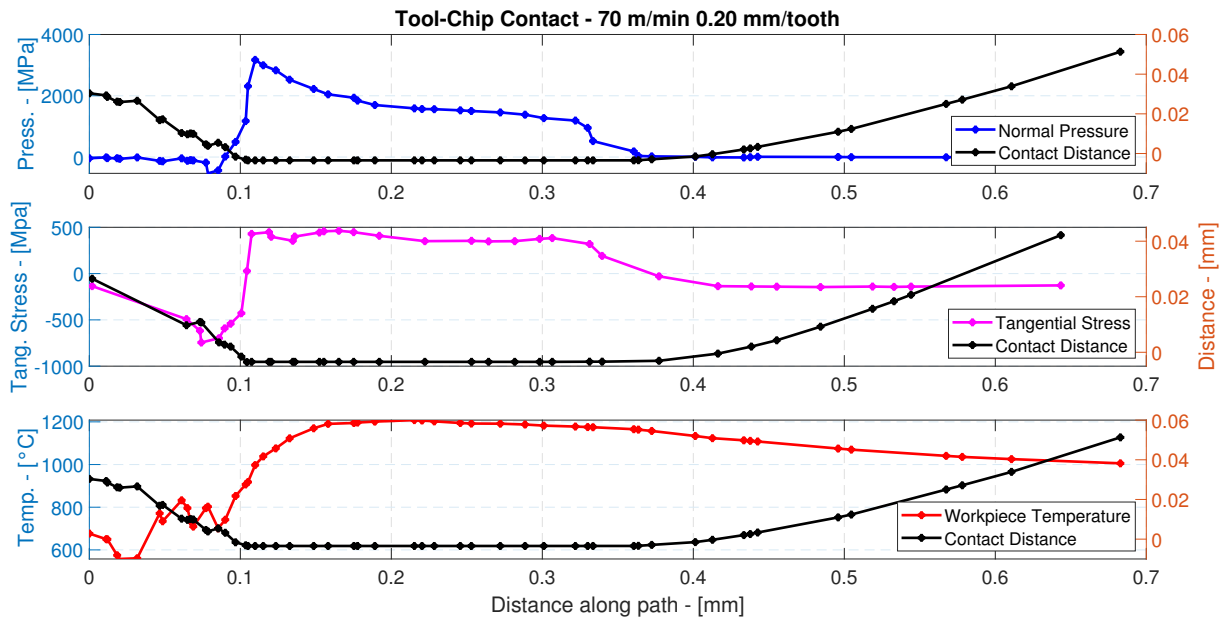


Figure 7.1.23: Tool-Chip contact variables, #1

## 7.2 Cryogenic Environment

Simulations were run in cryogenic environment as described in the section for model set up. A cryogenic window at  $-195^{\circ}\text{C}$  with variable HTC was added. Workpiece initial temperature was set below zero ( $-20^{\circ}\text{C}$ ), tool temperature to  $-100^{\circ}\text{C}$  (approximation), ambient at  $-150^{\circ}\text{C}$ , HTC  $1500\text{W}/\text{m}^2\text{K}$ . Contact model fitting with experimental results gave  $\mu = 0.25$ ,  $m = 0.4$ . Cutting force along Y axis and errors (along the arc and peak discrepancies) are shown below. Forces along X and Z axis exhibit same issues as dry forces, see section 1.2.

Cryogenic Environment			Dry Environment		
Exp ID	$Err_{trapz}$	$Err_{peak}$	Exp ID	$Err_{trapz}$	$Err_{peak}$
#3	-3.9%	-4.3%	#3	-16.0%	-4.8%
#5	-4.3%	+1.2%	#5	-14.6%	-8.8%
#4	+7.2%	+13.2%	#4	-5.8%	+6.4%
#1	+7.9%	+7.0%	#1	-6.6%	+3.4%

Table 7.2.1: Cryogenic Numerical Fy forces prediction accuracy

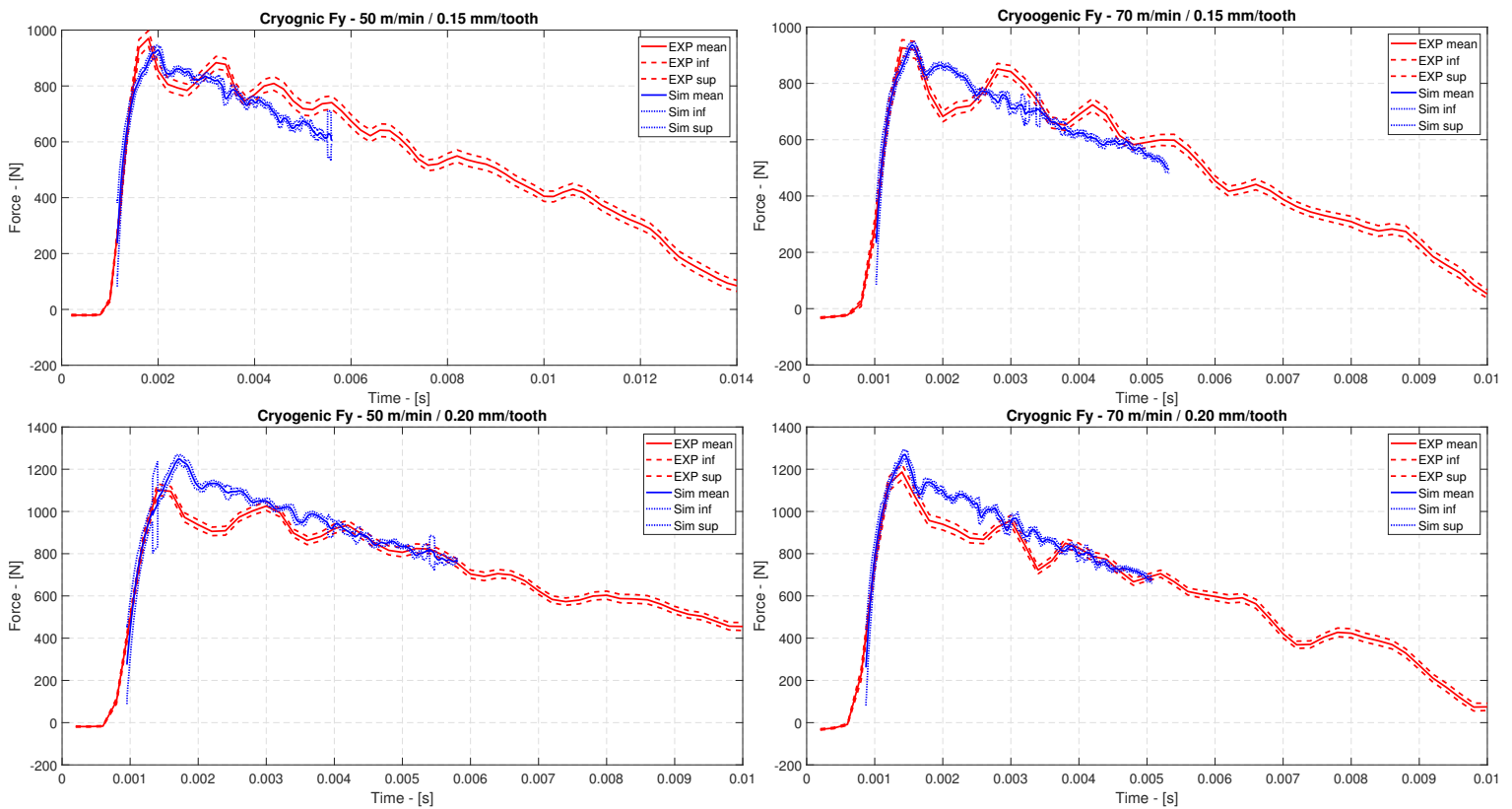


Figure 7.2.1: Simulated windowed and experimental cryogenic cutting forces comparisons

Fy cutting force is considered well predicted. Case #4 present the highest peak error but after that the force behaviour is well predicted. For the cryogenic case we have a better prediction of force evolution and peak forces with respect to the dry case. This could be due to higher MT stiffness at low temperatures so that the rigid approximation of the FEM is more accurate.

Chip morphology is in line with average defect levels of experimental chips. However, the model is not able to reproduce the correct development of those defects. In simulations, strong fragmentation is generated by serration fractures reaching the back chip surface. Proof of this is the “EDA” and “LatandCo” fields being concentrated on shear bands, who have then become fractures.

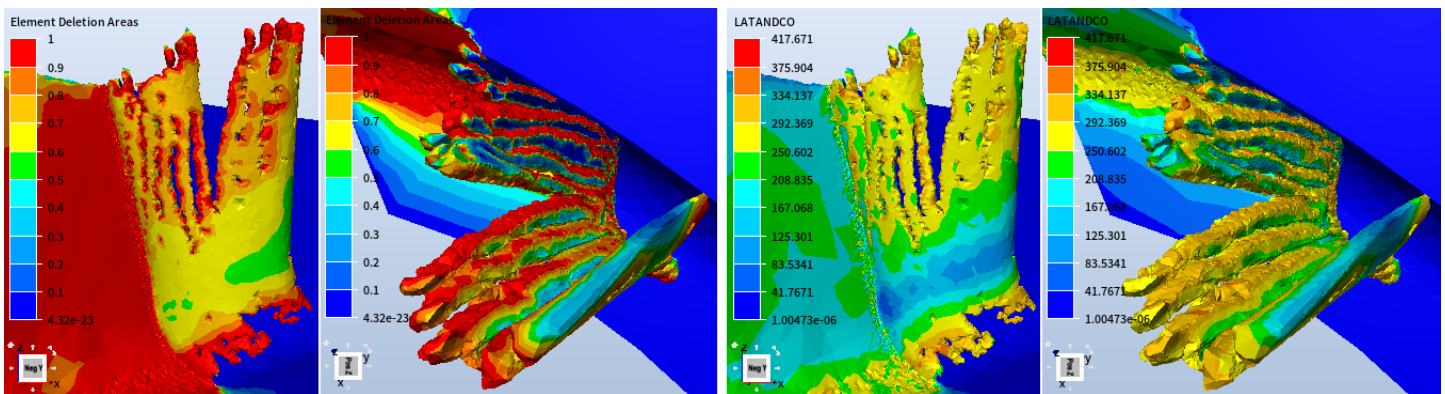


Figure 7.2.2: “EDA” and “Latandco”, Cryogenic simulation, #ID 3 0.15mm/tooth, 50m/min

Also higher fragmentation is seen in the lower chip part. Defects presents in dry chips are here increased in magnitude. A recurrent feature of experimental cryogenic chips is a horizontal fracture propagating after the first chip portion has formed. Chip #5 is much longer than other collected chips, it could miss completely that chip portion which turn the comparison difficult. In general, no simulation is able to reproduce that horizontal fracture. It is to be said that 5ms of cutting couldn't be enough for the formation of that fracture. Chips #4 and #1 predict the lower defect level of initial chip portions.

With respect to dry cutting, cryogenic (parameters matched simulations) chip thickness is lower and shear band frequency is increased, according to literature (see chapter 4, Turning, Chip Morphology). A general issue regarded keeping at a reasonable refined level the newly formed chip without undergo excessive calculation deceleration. A 80 μm formed chip mesh window size caused cryogenic simulations to last 40 ÷ 100 hours.

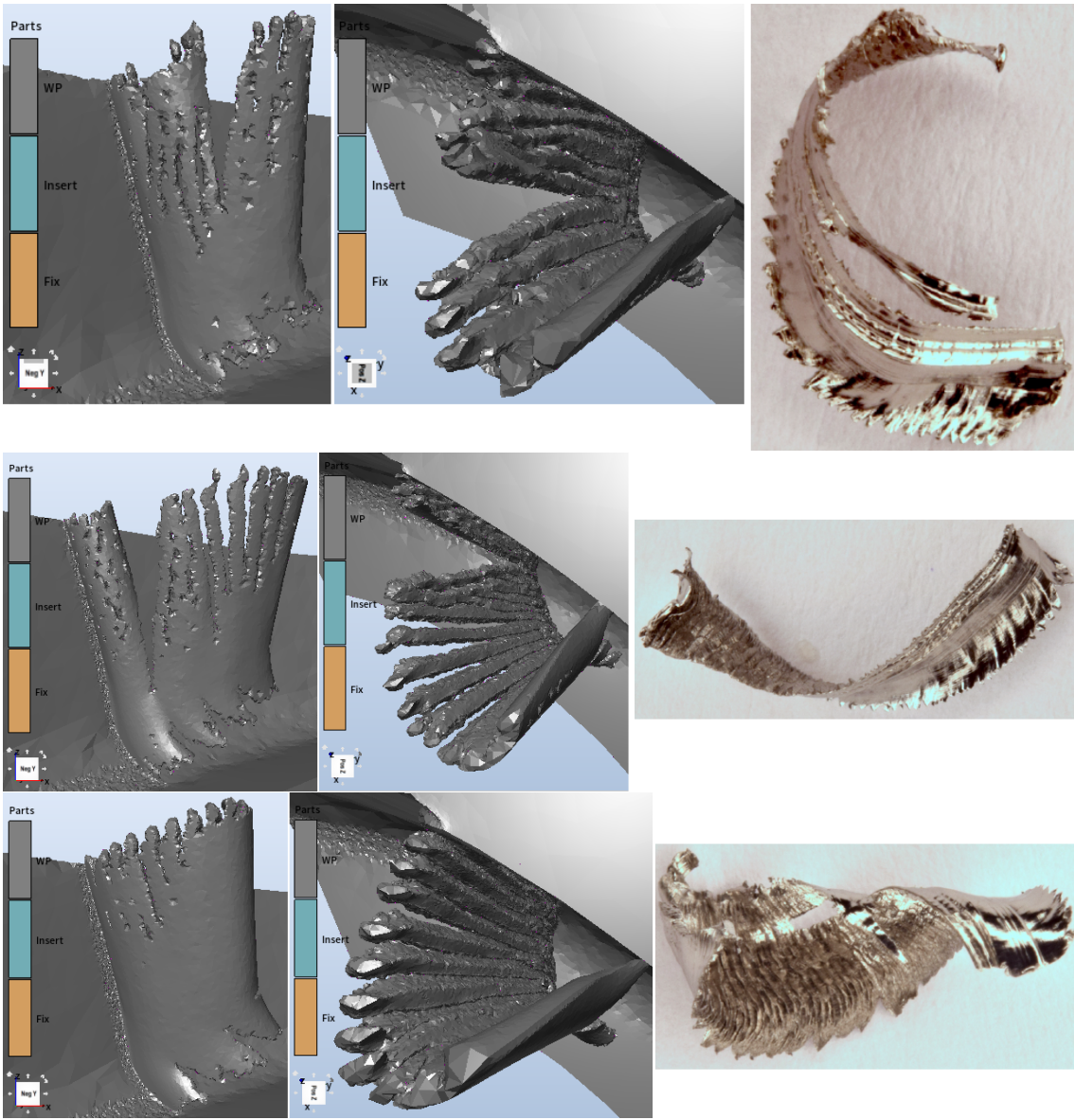


Figure 7.2.3: Cryogenic chip morphology prediction, #3, #5, #4



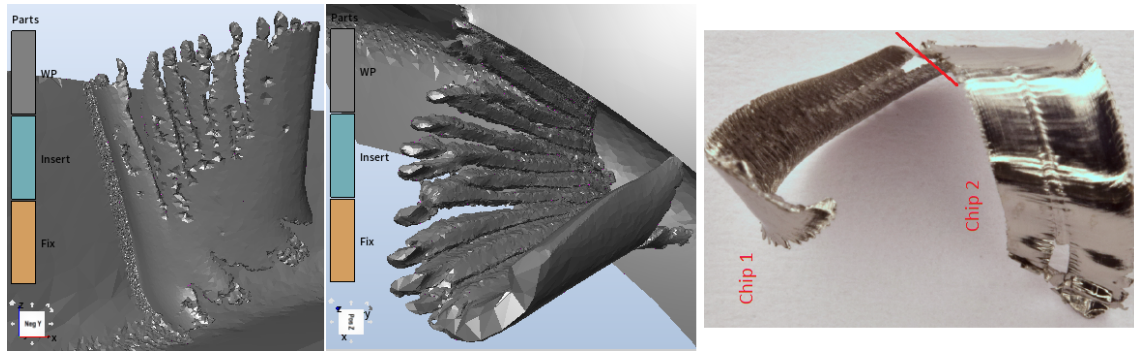


Figure 7.2.4: Cryogenic chip morphology prediction, #1

It is to be said that the model was able to automatically predict higher defect level of cryogenic chips without acting on stress flow or damage model modification. Lower temperature meant higher stress flow response. More elements reached the Damage limit value and have been deleted from the computation. On the same time, this phenomena brings forward meshing issues problems. Large mesh size with frequent element deletion causes chip holes, fractures, material voids. This lead to longitudinal fragmentation of chips at higher level than experimental observations.

Other than mesh refinement, simplicity of the LC criterion and JC material model description could appear when so intense defectivity is present. All considered, the model fairly describes the main phenomena leading to higher chip fragmentation and accurately reproduces the cutting force.

Maximum temperatures observed a variation around  $-100 \div 150^{\circ}\text{C}$  with respect to dry cutting. The hot spot is still concentrated in the same region and still at quite high temperature. Thermal related wear rates would therefore be retarded but not blocked.

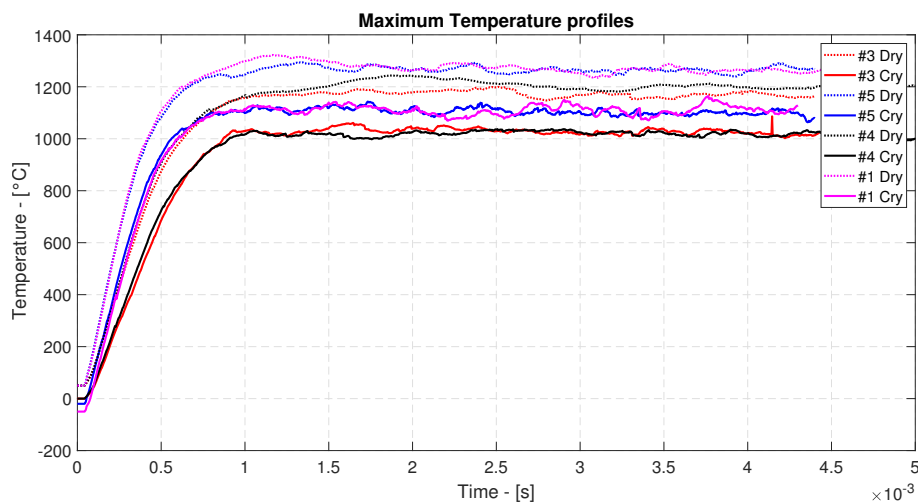


Figure 7.2.5: Maximum temperature comparison between dry and cryogenic simulated runs

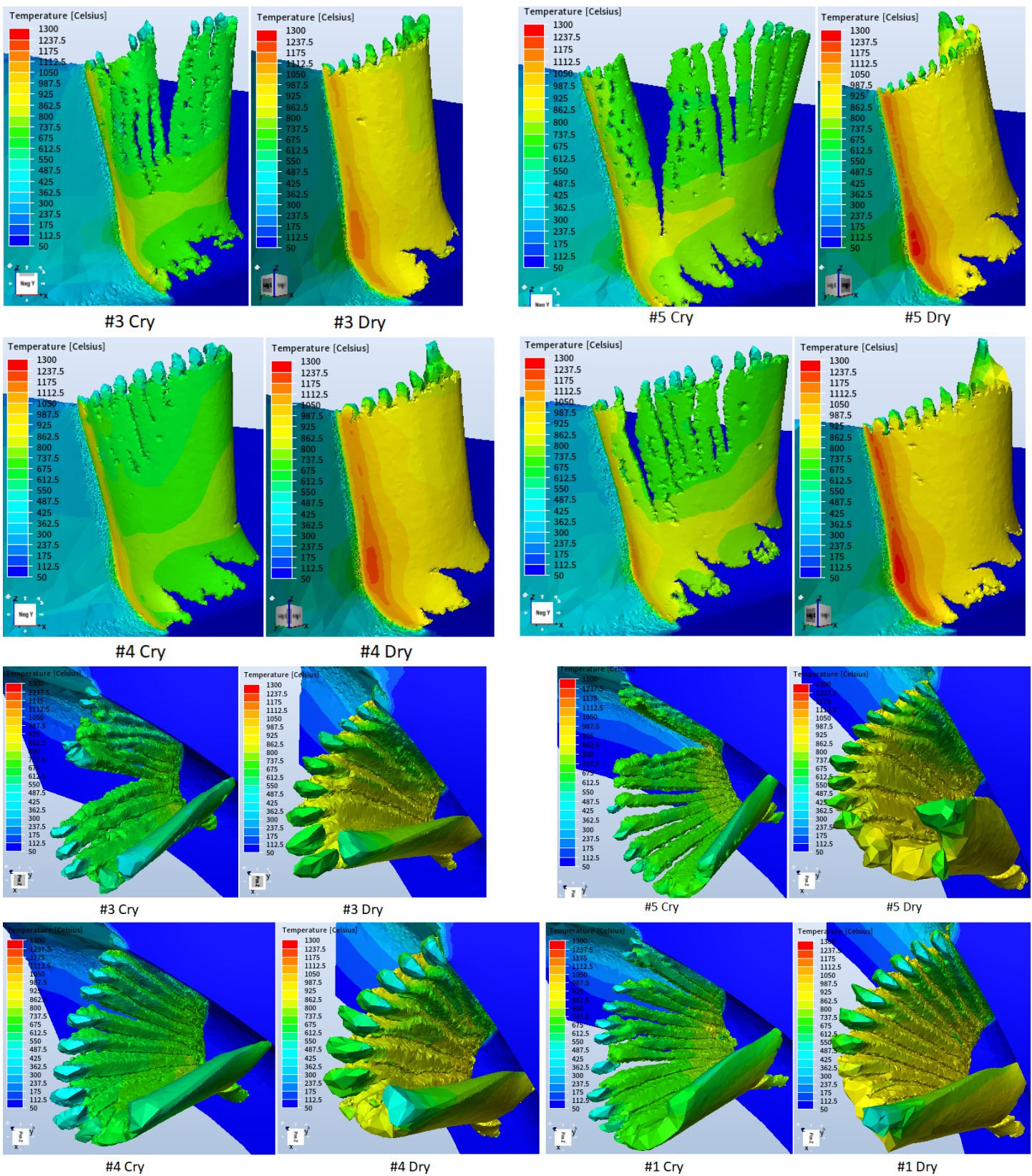


Figure 7.2.6: Temperature fields comparison between dry and cryogenic simulated runs

Cryogenic cuts exhibit higher heat exchange toward the environment (given the

higher HTC and lower temperature of ambient gaseous N<sub>2</sub>). Exchange by radiation is lower but absolutely negligible. Exchange with dies is much higher in cryogenic case. This is biased by the low temperature of the tool skin kept constant during all simulation time, but since it is the same for dry case a comparison can be drawn. Friction heat exchange and power are lower due to imposed lower contact coefficients. Plastic power is reduced for cryogenic machining. This is interesting as the material isn't able to exploit all his ductility and needed less energy to be sheared. Total power is lower, being in line with experimental findings.

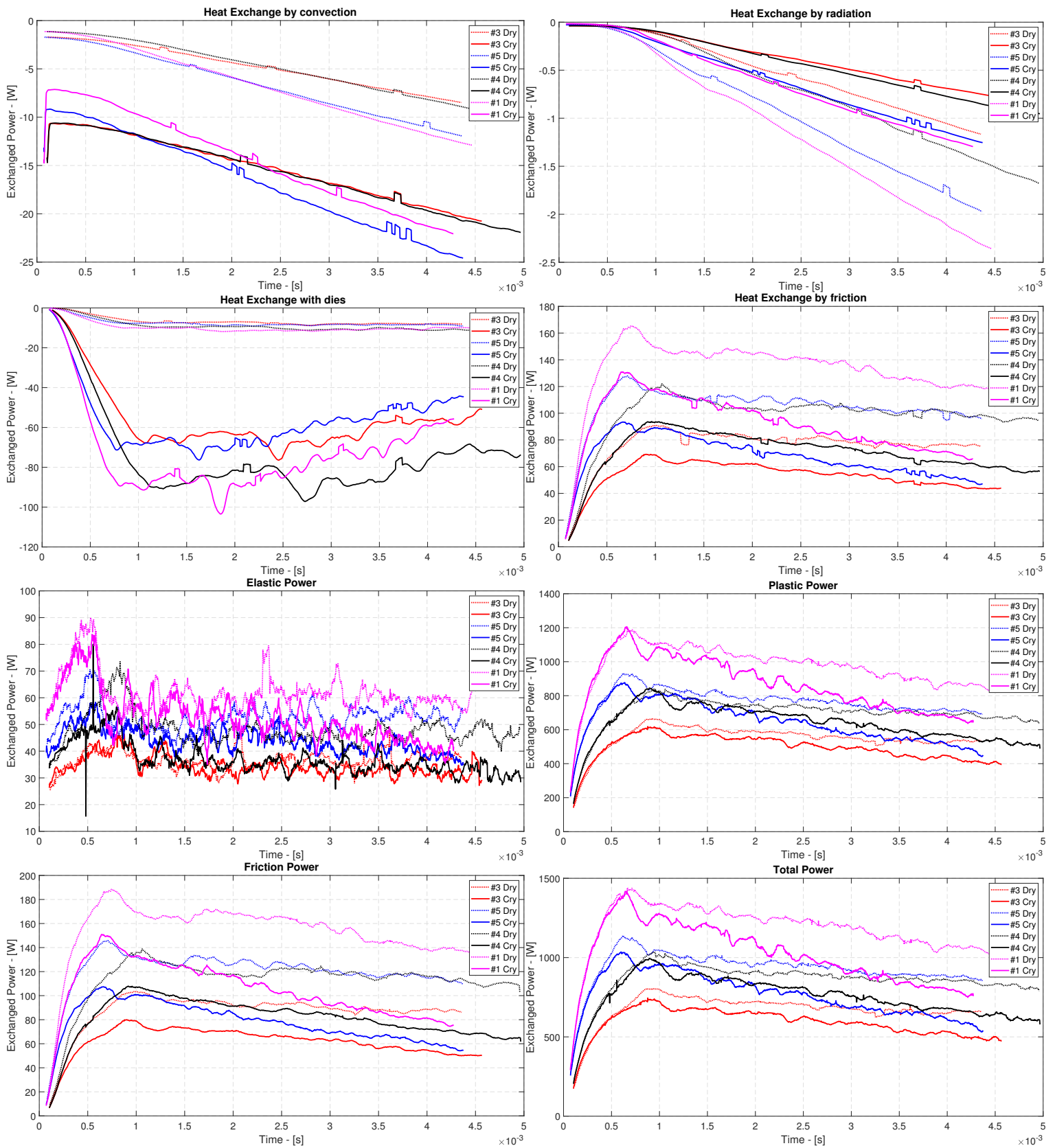


Figure 7.2.7: Simulated windowed and experimental Heat Exchanges and Mechanical Powers comparison, cryogenic and dry comparisons

## 7.2.1 Cryogenic cutting mechanics and tool stress analysis

Strains level remain almost unchanged from dry conditions, reaching localized maximum of 8 but keeping around  $3 \div 6$  along the edge. What is different from dry conditions, is a more definite colour banding (compare the image in section 7.1.2). Also higher strain levels are present. This could have been the cause for the formation of the horizontal crack through the chip length. In the model a crack is not initiated there because temperature is much higher than the upper chip part, and stress flow levels are too low to activate element deletion of the LC damage model, in poor words, the material is too soft there to fracture. The model would therefore lack of a maximum strain driven fracture level, which is plausible and interesting.

The primary cause of this strain band concentration could be the cutting edge geometry or the cooling jet chip-bending action.

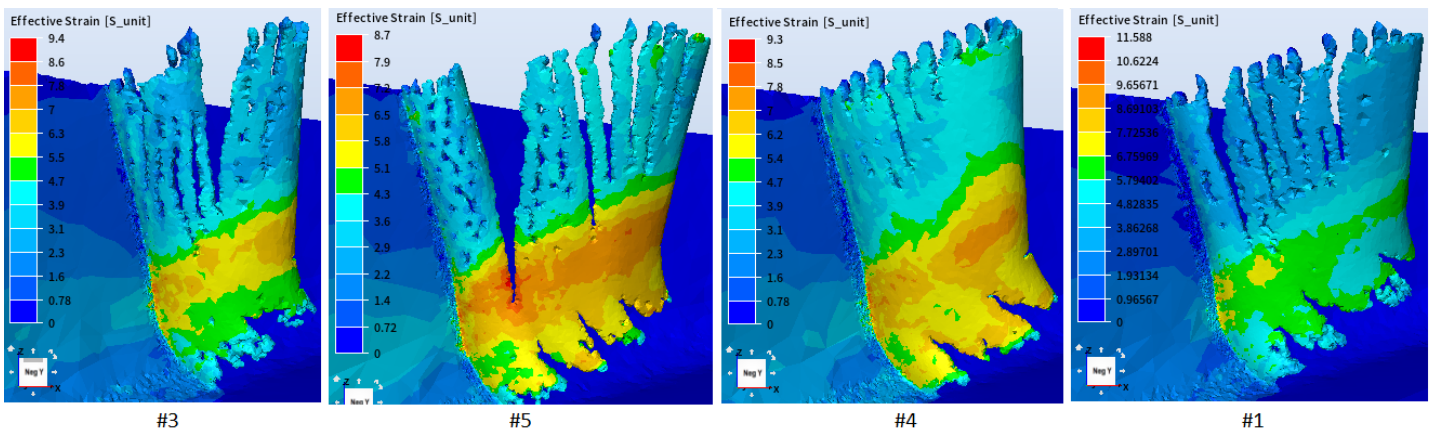


Figure 7.2.8: Strain fields for the cryogenic simulation runs

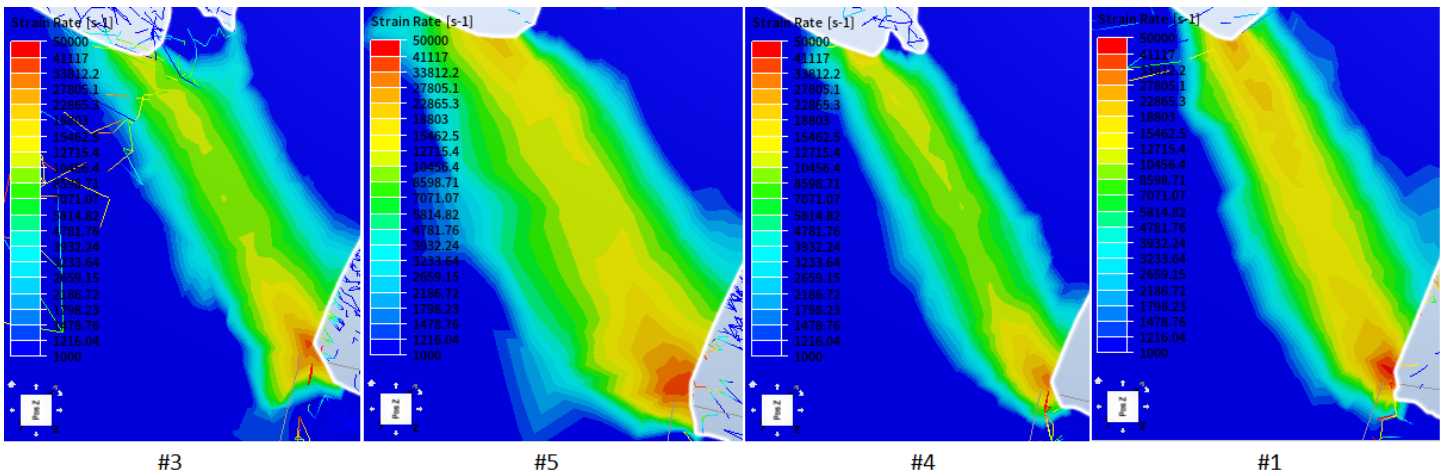


Figure 7.2.9: Strain Rate fields in the shear zone around  $2.3ms$  for the cryogenic simulation runs #1, #4 and  $3.2ms$  for #3, #5

Strain rates exhibit lower influence of feed compared to dry cutting, and seems to increase for the higher feed runs. Given the fact that strain rate fields is a complex tridi-

mensional and time variant, a fixed space and time visualization can be misleading. Tool-chip interface paths were extracted trying to consider the same position along the vertical cutting edge, in the vicinity of the maximum temperature spot, before the round corner.

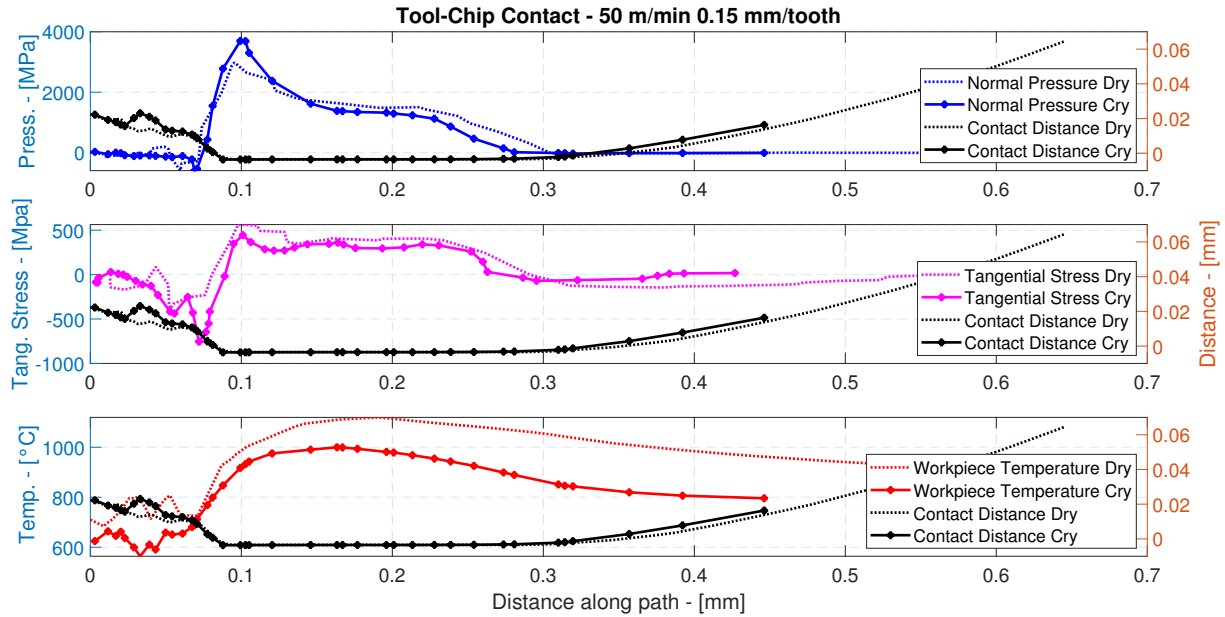


Figure 7.2.10: Tool-Chip contact variables, cry versus dry #3

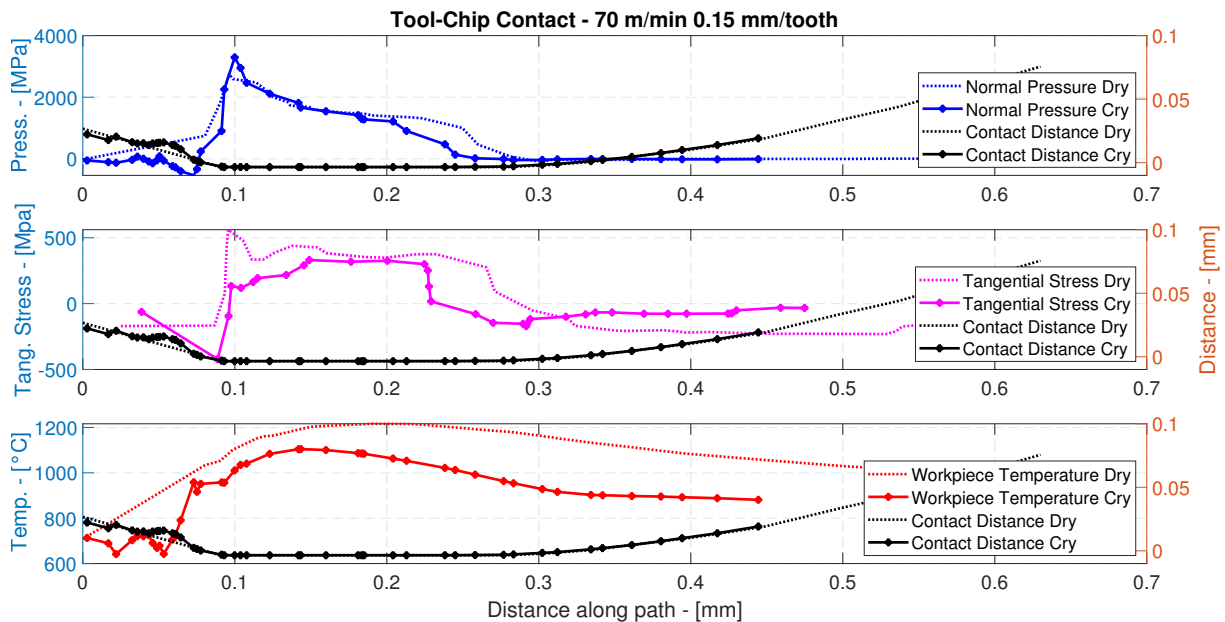


Figure 7.2.11: Tool-Chip contact variables, cry versus dry #5

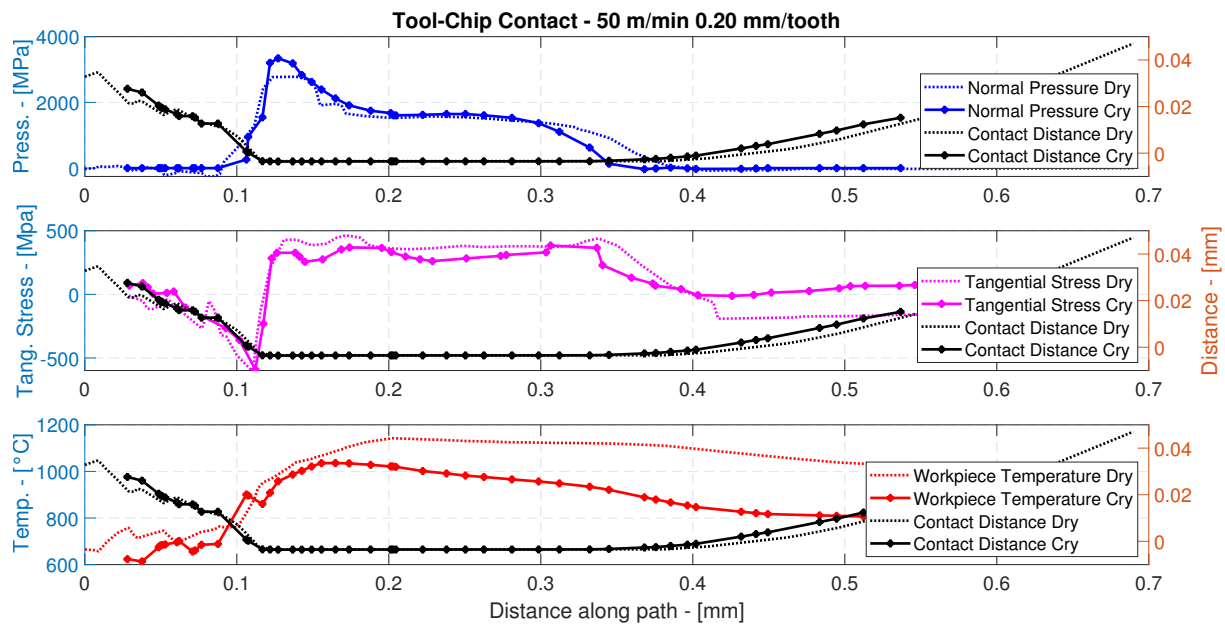


Figure 7.2.12: Tool-Chip contact variables, cry versus dry #4

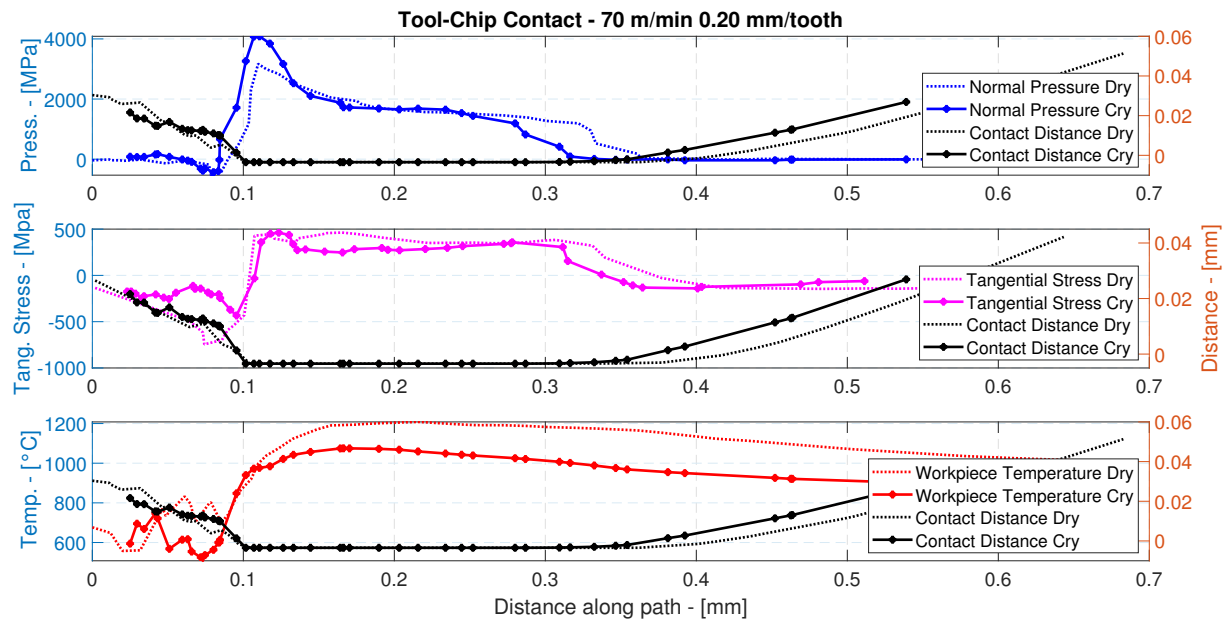


Figure 7.2.13: Tool-Chip contact variables, cry versus dry #1

A part from a net interface temperature decrease, the graphs show an important finding regarding normal pressure: Normal pressure distribution are reduced in length. They are also a bit increased in magnitude, but we prefer not to trust this too much. Profiles should be taken at regular interval over the whole edge and statistical analysis would tell if really there exhibit normal pressure increase. On the other hand we can say that normal pressure, being not lower than in the dry cases, acts on a reduced length. This means the cutting edge is loaded in a way that enhances its weakness.

The tool-chip interface length reduces? From the normal pressure and tangential stress distributions this is evident in all combinations. Less evident considering the distance between the workpiece and the tool. However, two bodies can be very near each other without touching. The threshold of contact in FE models is activated when little interpenetration is reached. Said so we can say with reasonable confidence that interface length reduces.

The following field images show how the cryogenic normal pressure gradients are steeper (narrow yellow and green bands).

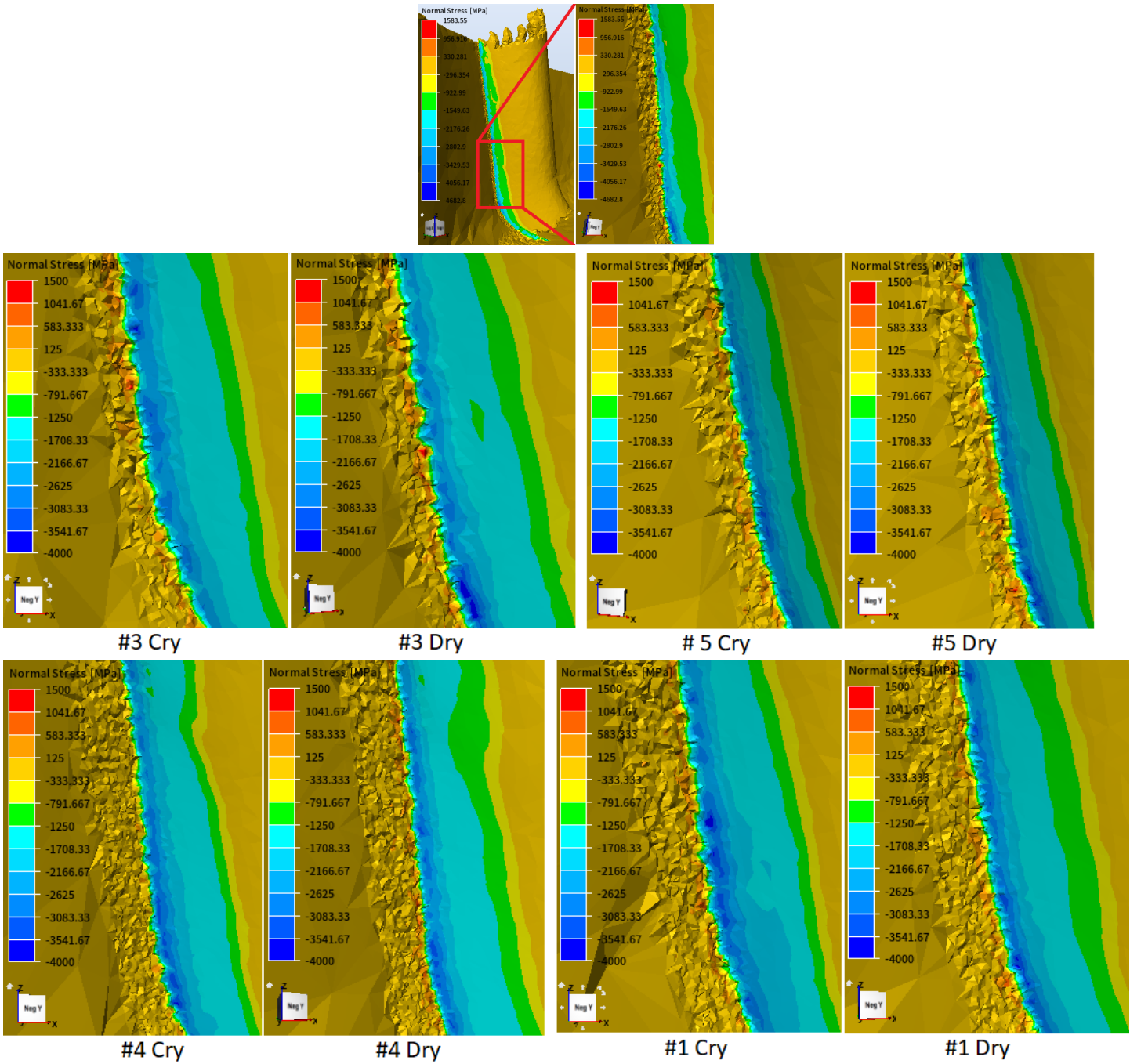


Figure 7.2.14: Normal pressure distribution comparison between dry and cryogenic runs



Cryogenic insert loading is therefore more localized, not lower, more sudden with respect to dry cutting.

### 7.3 Summary

We believe handy to resume the achieved result in a schematic way. Both cryogenic and dry cutting simulations were run with Johnson-Cook material model, Latham-Cockcroft damage model with  $D = 400 \text{ MPa}$  constant, same material properties and interface conductance values of  $10 \text{ kW/m}^2\text{K}$ . The effusivity of the tool was also kept constant. The changes in the model between the cutting strategies are summarized in the following table.

Cutting Environment	Dry	Cryogenic
Friction coefficients	$\mu = 0.4, m = 0.6$	$\mu = 0.25, m = 0.4$
Workpiece initial temperature	$50^\circ\text{C}$	$0^\circ\text{C}$
Ambient temperature	$50^\circ\text{C}$	$-150^\circ\text{C}$
HTC with Ambient media	$500 \text{ W/m}^2\text{K}$	$1500 \text{ W/m}^2\text{K}$
Tool constant temperature	$300^\circ\text{C}$	$100^\circ\text{C}$
HTC jet window	–	Variable, see Chapter 6
HTC jet window temperature	–	$-195^\circ\text{C}$

Table 7.3.1: Resuming table for model coefficients and boundaries

The main findings coming from numerical model and experimental results regarding different cutting environments are summarized in the following table.

Issue	Finding
Friction coefficients	Lower for cryogenic machining
Cutting Forces	20% lower for cryogenic with respect to dry, 10% lower against wet cutting
Ambient temperature	Lower workpiece and environment temperature for cryogenic
Insert loading	Higher edge loading, higher normal pressure gradients on edge for cryogenic
Tool-Chip contact length	Lower for cryogenic
Workpiece temperature	Negative shift $\simeq -150^\circ\text{C}$ for cryogenic
Chip defect levels	Much higher for cryogenic
Tool temperature	Negative shift in the thermal cycle of inserts due to idle phase cooling for cryogenic

Table 7.3.2: Resuming table for findings regarding comparisons between cutting environments

# Chapter 8

## Summary and Conclusion

An extensive, and one of the few quantitatively oriented, literature analysis on cryogenic machining experimental trials on Ti6Al4V alloy has shown how, unless the high number of articles, is very difficult to extract trends or understand phenomena causing tool life problems, cutting force and friction inconsistent results, optimal cryogenic flow parameters depending on cutting parameters.

The complexity generated by the numerous available tool geometries, coating layers, cutting approaches, cryogenic flow parameters (often unstated) is added by the total diversity of cryogenic flow delivery designs. Cryogenic flow parameters have been scientifically justified by few, with the result that very different pressures and flow rates are applied without knowing if optimal under economic and ecologic point of view. On the same side, lack of scientific justification of nozzle designs resulted in a variety of application strategies without knowing if optimal in targeting the heat affected zones. Additional process complexity in milling is the answer for the poor and discontinuous obtained performances of the cryogenic alternative.

Cutting simulations are a fundamental aid to experimental runs, and in synergy with them, capable of industrial development of new technologies. Chip forming numerical modeling is a complex subject involving material response to intense and differentiate loading rate and conditions, complex contact/ thermal interactions, high number of input variables and need of reliable experimental/literature data. Process, software and FEM behaviour knowledge is compulsory to discriminate the reliability of results.

Many studies focused on orthogonal cutting simulations and have contributed to develop the knowledge on material, friction, damage, thermal models. However, we believe it is time to move the attention toward realistic cutting processes.

### **FE Modeling of heavy industrial cutting processes**

This work underlines how **Material models** developed for orthogonal cutting simulations have been used in 3D models with mesh sizes by far larger than needed to exploit the peculiarity of the models, which does not justify their use. Simpler Johnson-Cook material model could be used instead.

For all simulations, a correct chip radius was obtained after the chip scratched against the workpiece. The chip must not be too bent or self-wrapped since then. This study highlighted how Material models developed for orthogonal cutting promoted wrapped chips different from experimental ones. It was also observed that chip radii are seldom

considered when those studies compare experimental and numerical chip morphology. During the research it emerged how **Damage models** are often applied as final model refinements or simple additions to match experimental values through iterations, with exception of the Johnson-Cook damage model. In our case, a simple Latham-Cockcroft damage model offer a first order approximation of shear band modeling for Ti6Al4V. However, to avoid unnecessary iterations and advance knowledge on material behaviour, damage model need to be systematically compared and their effectivity studied. Material and damage models should be condensed in a single material description, as for the Johnson-Cook case.

It was also depicted how Stress flow description for Ti6Al4V show large variations. Same alloy material grades should be described by less variable parameters set. Efforts need to be addressed to more precise material description over strains, strain rates and temperature ranges of machining interests.

While proceeding with model fitting it became clear how **Friction modeling** in simulations should be based on experimental trials, avoiding further iterations (lengthy for 3D heavy simulations). As literature suggests, there are in fact more material model-friction model couples giving accurate force and chip morphology predictions. The choice depend on practical issues such as time, implementation in codes, model coefficients availability.

During model tailoring we were able to understand that Friction fitting on cutting force is mainly related to material models strength fitting. Changes in  $m$  are related to the uncertainties in the shear stress limit determination depending on the material flow stress. For static loading we can say  $\tau_{lim} = \sigma/\sqrt{3}$  but what exactly happens to the shear limits at high strains, strain rates and extreme pressure conditions? In general  $m \neq 1/\sqrt{3} \cong 0.58$ , and based on that researchers are free to change  $m$  so to fit experiments. The value of  $\mu$  on the other hand is fixed to experimental findings with tribometers with Ti6Al4V-Carbide tools couples ( $0.2 \div 0.4$ ). Our model proves to be realistic also considering this aspect.

## Cryogenic Machining understanding from numerical simulations

Our model shows that cryogenic machining fitting needed lower **friction** coefficients, at least suggesting that contact conditions must change. Material behaviour was influenced only by  $100 \div 150^\circ C$  shift, which, on the other hand, would even rise cutting forces (less thermal softening). Eventually, lower contact conditions are expected so to match the experimental results.

Metallurgical motivations for the phenomena the simulations do not give. The tool would be cooler than in dry conditions, extracting much more heat. This mean it keeps stronger, harder and more slippery than a hotter tool while dry cutting. Hardly any penetration of LN2 is supposed possible, given the vertical orientation of the jet.

A new insight, coming from recent surface quality analysis at MUSP, suggest that a different surface morphology can be another portion of the answer. Tearing is more definite for cryogenic machining, promoting higher macro rugosity (higher peaks and valleys). During material loading the peaks are smoothed but valleys could remain, trapping gas and lowering the contact area.

The present model, as in literature, showed contact length to reduce slightly, leading to lower friction power and heat generation in turn.

One of the most important findings of the study concerned **Tool load**. It raised with cryogenic application as tool-chip contact length reduce and normal pressure on rake does not diminish. Normal pressure distribution is steeper and localized on the very edge of the cutting tool. The phenomena offers an important key to look at square shoulder tool life early failure in experimental trials, and in general, at early failures observed in milling. Generally milling inserts are less bulky than turning cutters. This linked to tool geometries promoting sudden edge engagement causes intense loading impulse. Edge chipping due to strong thermo-mechanical load would be increased for the cryogenic case, causing refused cut and severe flank rubbing action. Poor tool life would result.

Sturdy tool geometries promoting gradual engagement with the workpiece would smooth mechanical loads, achieving higher tool life. High feed tools, made with more expensive materials and complex manufacturing procedures have bulky geometries and are strong so to withstand high chip loads. Their use in cryogenic machining would be beneficial not only at high feed, but at moderate as well due to their tough nature.

The present work demonstrates how the work material express lower ductility due to the lower temperature, lower friction, increased stress flow and material damage levels. This leads to increased defect level in chips and reduced cutting power.

### **Cryogenic Machining improvements from cutting simulations**

The Numerical model underline as the cooling jet has limited action in cooling the tool-chip interface affected regions. While fitting cryogenic simulations it became clear how the addition of a cooling window only, whatever physical approximation of the HTC ( $10 \div 150 kW/m^2 \circ K$ ) demonstrated slow cooling action. The heat generated in the process and the rotation speed caused the jet to have limited time for cooling down the affected area.

Good results in terms of chip morphology have been achieved with low temperature of the workpiece. This in line with the frozen conditions of specimens at the end of cutting trials. The piece would freeze due to the extreme cold environment developing in the vicinity of the cutting area. The cold environment would be generated by the continuous addition of cold Nitrogen vapours in the same area, tool pass, after pass, after pass. Higher level of defects in chips would be due to a negative shift in temperature of the process by some hundredth degrees.

The jet would contribute to newly formed chip cooling as well as tool cooling during the idle phase, promoting a negative shift for the insert skin temperature cycle. Also simulations do not consider the thrusting action of jets onto chips. The pure mechanical power of the high pressure jet could bend chips and promote lifting actions so to limit the more the interface length and increase the interface cooling action.

Regarding this final phenomena, chip lifting action would be increased by orientating smartly the jet. In our case the best way, as literature suggest, would be perpendicularly to chip flow on the rake face.

Finally, we must not forget to discuss about flank wear. Tool life tests are based on flank wear. Literature studies suggest how rake cooling could influence flank wear through edge recession rate limitation. The lower tool temperature would decrease crater wear rate and slow down edge recession. The lower workpiece temperature and definite tearing of the material could lower flank abrasion. In any case flank wear limitation

is indirect, while for many turning applications flank cooling have always been applied directly.

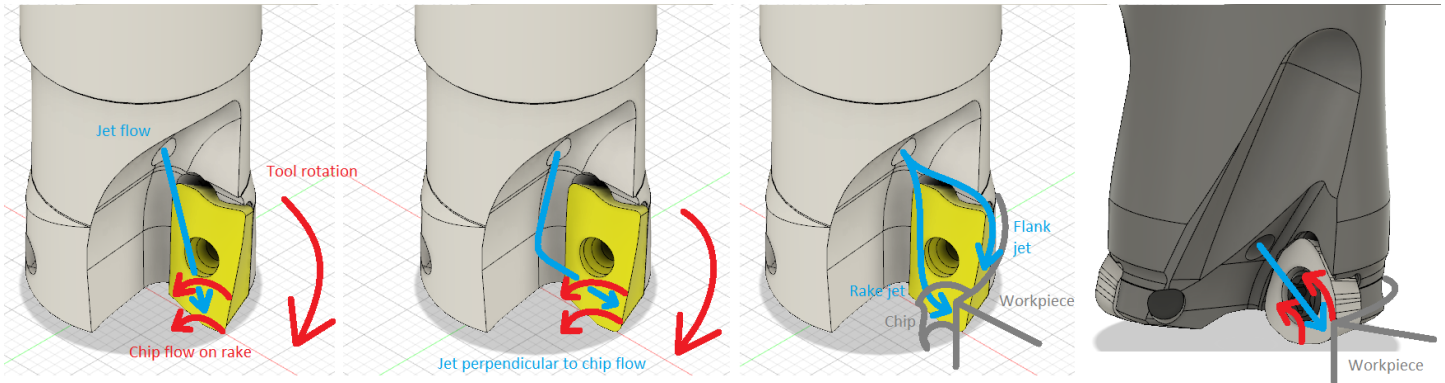


Figure 8.0.1: Jet orientation versus chip forming direction, high feed tool (last picture) has favorable jet orientation

## Modeling procedure

Setting up a model from zero means facing a wide horizon of choice. The main procedure we have been subjected to is to keep complexity at a reasonable level during the working period. In the first phase, being a lot of unknown variables present (material models, friction values, damage values, thermal boundaries, mesh sizes, remeshing frequency, remeshing mode...) it was not worth to complicate the problem by adding other source of complexity such as variable friction models, accurate thermal fields. In a second phase, in which material, damage models, friction average values and meshing were set, refined friction and thermal modeling could have been applied. The only problem we faced was time. There was barely time left to refine models, but that is the nature of things.

## Future work

### Complete Engagement simulations

For sake of simplicity, whole engagement simulations have not been tried. Calculations progressively slow down while the newly formed chip adds elements to the model. Machined surface was not kept refined for same reasons. Once the tool flank left, machined layer should have kept at a reasonable small mesh size. This would have translated into another source of element addition and calculation deceleration.

Keeping a reasonable  $N^{\circ}_{elements}/Chip_{thickness}$  ratio for meaningful results is necessary. This means that, for the final part of the engagement, mesh size needs to be much smaller than what would be necessary for the first part. Starting with that small final-mesh-requirement would result in excessively slow computations. FORGE can helps us, as a separate step can be set up within the same process, allowing to stop the calculations, change the mesh size of the shear refined zone, and continue automatically. Mind that this procedure is necessary to obtain a complete reliable engagement in reasonable time, for example two days, computer power dependent of course but still a bit to much for industrial purposes.

An ambitious aim we had to renounce was the whole cutting arc + cooling + second passage, we believe FORGE to be a good program to do it.

### FORGE capabilities

The software offers a lot of useful tools but mainly two alternatives were available for tool stress/thermal calculations. Simulation finished, a decoupled thermo-mechanical calculation could be done on the tool by applying the simulated fields through the contact interface. The second solution is to run a thermal or thermo-mechanical coupled simulation in which the tool is either thermal meshed, or thermo-mechanical calculated. Lower frequency of mechanical calculations could also be given so to avoid slowing down too much the simulation. Tool-chip contact area, pressure and tangential stress on tool could have been extracted giving more precise indications.

An interesting option could have been used to calculate the temperature of the work-piece after the tool passage. Even in a simulation with partial engagement, the “Final Cooling” option could have been activated. Setting up the time until the next insert would have engaged the cut, we could have let the thermal field evolve until the next tool approach.

### Experimental targets

For what concerns cryogenic cutting trials and tool life tests, delivery design in the vicinity of the cutting zone need to be optimized. In milling, no one tried to reproduce the excellent results of Hong and colleagues [13, Hong 2001c] of the end of the nineties, with very localized nozzle positions. In parallel, there is no study regarding the precise application of cryogen to the flank face of milling inserts. The development of fixturing bolts with additional integrated micro liquid delivery have never been applied in milling. Nozzle orientation need to be adjusted with respect to chip flow on rake.

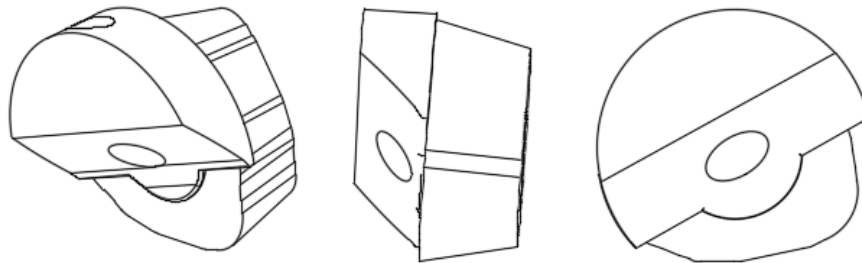


Figure 8.0.2: Insert dedicated nozzle design example

Few studies analysed the importance of thermal cycles felt by the insert and their link with tool life. Thermal cycling and stress distributions on the insert need to be studied in relation with cryogenic flow. No experimental or analytic study have tried to produce data regarding tool temperature variation caused by the addition of LN2.

## Numerical modeling related experiments

Simulations set up is still dependent on particular cutting data that need to be obtained ad hoc, or necessitate long and demanding iterations. Material models are often a choice based on the mere performance observed in the literature, probably dependent on the particular application (for example orthogonal cutting), with no warranty of success when applied in other circumstances.

Specifically regarding material models, new robust experimental methods need to be developed in order to measure the flow stress of the material at strain and strain rates levels observed in machining and link them with damage models.

**Friction models** need to be set up so that experimentally obtained friction coefficient can be applied as a function of temperature, normal pressure, sliding speed. In parallel, conductance behaviour needs to be modeled as well.

**Thermal boundary measurements** are crucial for setting up reliable steady state cutting models. Workpiece, tool, ambient temperature need to be monitored. Also punctual average values out of cutting regions can help when setting up a model.

Scientific research is a continuous flow nourished by implicit agreement between subsequent students, researchers, generations. We have done our best and strongly hope to have offered future researchers a solid base for their efforts.

## Acknowledgments

*Despite the aim of the author in analyzing the complete available literature up to date, some articles have not been included either because not found or under charge. Also it is very likely some have been missed during the research.*

*More in general, this work doesn't even claim to be complete, because it is mainly the outcome of a single mind. As any product which is not the offspring of cooperation between minds, it would certainly miss something, a lack which Corona Virus worsened.*

I would like to thank my family and Sara first, for the patience they often turned to me when I lacked to fulfill my duties during intense study periods. I also thank them for offering me, at times, evasion and necessary relax.

This work has required a non trivial amount of time and effort, the good part of the hysteria being associated with technical issues related to the program. With respect to this I would like to personally thank Massimo for its careful and prompt support. For the same reason, special thanks to Federico.

Finally, a last but not least thank goes to Riccardo, thesis companion with whom I shared worries and efforts during my thesis work, hoping I acted similarly for him.



# Tables

In this section we add some interesting tables, useful to provide a different visualization of the biblical mess otherwise known as bibliography. Tables ordering articles for tools and workpiece materials or subjects (review, experiments, modeling, optimization, tribology etc) have been organized. However, not all of those tables are presented, because I had no time to look at the articles within. I concentrated only on Ti6Al4V studies, stick to the point that is not worth filling up pages with information I couldn't check if complete. The hope is that others would grab the challenge and reorder the high number of studies for cryogenic machining regarding other groups of materials. For instance, good performances are obtained by cutting Inconel 718 and similar. Interesting, as some researchers report, would be the application of cryogenics while cutting aluminum, magnesium alloys, and, for machinists, non-metallic exotic forms of matter also known as polymers and ceramics.

A first table summarizing the reviews on cryogenic machining is presented. Some of them are very professional, others only tables containing some articles. Then, a table containing articles regarding tool life experimental analysis for Ti6Al4V is reported. The articles have been used to analyse the cryogenic machining performance in Chapter 3. Since used tools are mainly coated and uncoated Carbides, and the geometry regarding turning is always quite bulky (while for milling differences in tool design are already treated in Chapter 3) tool specifications are not displayed. Other great variables, such as delivery design, flow media and properties are however included. Achieved performances and process parameters are not included, due to limited space, the results can be found reading Chapter 3 or looking directly at the cited articles (my excel database is not written politely, let's say).

Consequently, articles regarding pure thermal, FEM and CFD models are organized. Tables also include articles concerning friction and material models. Finally, thanks to the work done on a case study regarding sustainability of cryogenic machining, the author include also a table regarding Sustainable related issues useful for the study of economic and ecologic performance of cryogenic machining. If there is not it is because I run out of time.

Reviews on Cryogenic Machining			
N°	Reference	Title	Content
1	[2, Yildiz 2008]	<i>“A review of cryogenic cooling in machining processes”</i>	Provides tables containing research experiments ordered by cooling strategy
2	[12, Yasa 2012]	<i>“Overview of cryogenic cooling in machining of Ti alloys and a case study”</i>	-
3	[?, Shokrani 2013]	<i>“State of the art of cryogenic machining and processing”</i>	Provides tables of experimental articles sorted for materials
4	[1, Jawahir 2016]	<i>“Cryogenic manufacturing processes”</i>	Detailed explanation of recent findings, Flow properties analysis
5	[?, Deshpande 2018]	<i>“How cryogenic techniques help in machining of nickel alloys? A review”</i>	Review on Nickel alloys, with tables ordering experiments for Dry, Cryogenic, Hybrid machining and Cryogenic Processing
6	[?, Haron 2018]	<i>“A review on future implementation of cryogenic machining in manufacturing industry”</i>	Detailed and complete study offering alternative insights on chip morphology and surface integrity
7	[34, Benedicto 2017]	<i>“Technical, Economic and Environmental Review of the Lubrication/Cooling Systems Used in Machining Processes”</i>	Provides an excellent review and insight regarding cutting fluid alternatives and related issues
8	[86, Rubio 2015]	<i>“Cooling Systems Based on Cold Compressed Air: A Review of the Applications in Machining Processes”</i>	Useful for understanding and referencing for chilled air applications
9	[5, Pusavec 2009]	<i>“The role of cryogenics in machining processes”</i>	-
10	[46, Madhukar 2016]	<i>“A critical review on cryogenic machining of titanium alloy (TI-6AL-4V)”</i>	Historical insights, LN2 delivery systems and flow rates general order of magnitude
11	[?, Senevirathne 2016]	<i>“Effect of Cryogenic Cooling on Machining Performance on Hard to Cut Metals - A Literature Review”</i>	Adds really small contribution to previous works
12	[?, Kale 2017]	<i>“A Review on Cryogenic Machining of Super Alloys Used in Aerospace Industry”</i>	Manage past studies for geographical area, gives additional insights
13	[170, Sharma 2019]	<i>“Impact of cryogenic cooling during machining: A Literature Review”</i>	Lists in table some previous articles and summarize their findings
14	[171, Ahmad-Yazid 2010]	<i>“A review of cryogenic cooling in high speed machining (HSM) of mold and die steels”</i>	Provide extensive review in the analysis of RHVT
15	[?, Abele 2011]	<i>“High speed milling of titanium alloy”</i>	Review on the general machinability of Ti alloys

Table 8.0.1: Literature reviews on Cryogenic Machining

Titanium Alloy Ti6Al4V Tool Life Performances Articles

N°	Reference	Approach	Cooling Media	Delivery Design	Flow Properties
1	[12, Yasa 2012]	Turning	LN2	Flood	-
2	[15, Wang 2000]	Turning	LN2	Indirect rake cooling	-
3	[70, 13, Hong 2001a&c]	Turning	LN2	MicroR&F	24bar, 0.65kg/min
4	[10, 47, 172, Paul 2006, Venugopal 2007]	Turning	LN2	Localized R&F	-
5	[63, Dhananchezian 2011]	Turning	LN2	Micro R&F	3bar
6	[55, Bermingham 2011]	Turning	LN2	Rake Cap	8.27bar
7	[57, Bermingham 2012]	Turning	LN2	Rake Cap	8bar
9	[173, 174, Shokrani 2012]	Milling (Carbide Helix)	LN2	External Spray	-
10	[72, 73, Jerold&Kumar 2013]	Turning	LN2&LCO2	External Spray	-
11	[32, Strano 2013]	Turning	LN2	Localized R&F	1.6bar
12	[65, 66, Deiab&Raza 2014]	Turning	LN2	Unknown	-
13	[51, 52, Park 2015, Suhaimi 2018]	Milling (Carbide Helix)	LN2	Through Holder	3bar
14	[61, Shokrani 2016a]	Milling (Carbide Helix)	LN2	External Spray	1.5bar, 0.32kg/min
15	[69, Ayed 2017]	Turning	LN2	Rake Cap	4.5/9bar 1.29/2.5kg/min
16	[39, 40, Sadik 2016&2017]	Milling (Indexable)	LCO2	Through Holder	50bar, 0.65kg/min
17	[77, Shokrani 2015]	Milling (Carbide Helix)	LN2	External Spray	0.16/0.33/0.5kg/min
18	[29, Nimel 2019]	Milling (Ball Insert)	LCO2	External Spray	2.5bar – (?)
19	[64, Mia 2019]	Turning	LN2	Localized R&F	50bar, 2.4kg/min
20	[36, Tapoglou 2017]	Milling (Indexable)	LCO2	Through Holder	-
21	[74, Bordin 2017]	Turning	LN2	Localized R&F	15bar
22	[75, Bordin 2015a]	Turning	LN2	Localized R&F	15bar, 0.9kg/min
23	[83, Kramer 2014]	Turning	LN2&LCO2	Unknown	-
24	[67, Tirelli 2015]	Turning	LN2	Localized R&F	1.6bar, 0.75kg/min
25	[80, Pittala 2018]	Milling (Carbide Helix)	LCO2	Mill Channels	50bar, 2.7kg/min
26	[175, Lee 2015]	Micro-Milling	LN2+Preheating	External Spray	0.5bar – (?)
27	[76, Bruschi 2016]	Turning	LN2	Localized R&F	6bar

N°	Reference	Approach	Cooling Media	Delivery Design	Flow Properties
28	[176, Damir 2018]	Turning	LN2	Localized R&F	0.8 kg/min
29	[42, Kirsch 2018]	Turning	LN2 LCO2	External Spray	2 bar, 1.1 kg/min 60 bar, 1.75 kg/min
30	[79, Shokrani 2019]	Milling (Carbide Helix)	LN2	Micro R&F	1 bar, 0.33 kg/min
31	[177, Biermann 2015]	Turning	LCO2	Rake Cap	-
32	[78, Shokrani 2018]	Milling	LN2	Micro R&F	1 bar
33	[84, Iqbal 2019]	Face Turning	LN2 LCO2	External Spray	1 bar 62.5 bar

Table 8.0.2: Studies on Cryogenic tool life performances during Ti6Al4V cutting

Thermal Models. Temperature Measurements, Thermal Oriented FEM			
N°	Reference	Description	Content
1	[8, Hong 2001b] Turning Ti-6Al-4V	Thermal modeling 2D steady state heat transfer	Temperature control effectiveness of dry, emulsion, cryogenic back, rake, flank, flank& rake cooling and WP precooling
2	[89, Ay 1998] Turning Al, Cu, Cast Iron, AISI1045	Temperature measurement	Thermal profile as first order exponential, max tool temperature shifted from the tip
3	[90, Dhar 2002a] Turning C40 Steel	Temperature measurement Cryogenic vs Dry Tool-WP thermocouple	Tool max temperature shift due to chip drag and friction heat build up
4	[91, O'Sullivan 2001]	Temperature measurement	Review
5	[92, Bacci da Silva 1999]	Temperature measurement	Review
6	[94, Ng 1999] Turning AISI H13	Temperature measurement	Optical fibre pyrometer
7	[95, Davies 2007]	Temperature measurements	Review
8	[96, Komanduri 2000] Turning	Thermal modeling	First of three articles on analytical thermal modeling of tool chip interface
9	[6, Abukhshim 2006] Turning	Thermal modeling	Review
10	[98, Liu 2007] Turning A390 Al	3D thermal model	Chilled air cooling

N°	Reference	Description	Content
11	[99, Kitagawa 1997] Milling Inconel 718, Ti-6Al-6V-2Sn	Temperature measurement	Maximum temperature is lower in interrupted cutting, but thermal oscillation is high
12	[93, Yang 2014] Milling Ti6Al4V	Temperature measurement	Constantan Band thermocouple on workpiece
13	[45, Sato 2011] Milling Ti6Al4V	Thermal modeling and measurement	Optical fiber pyrometer and Green's function thermal transient model
14	[43, Jiang 2013] Milling AISI1045	Thermal modeling and measurement	Larger engagement result in larger thermal cycling
15	[44, Karaguzel 2016] Milling AISI1050	Thermal modeling and measurement	Larger engagement lead to larger maximum and average temperature in the cycle. Higher speed reduce the thermal oscillations
16	[100, Baohai 2016] Milling Inconel 718	Thermal modeling and measurement	Variable heat source considering stick-slip model, interface quantities obtained from simulations
17	[37, Augspurger 2019] Milling Ti6Al4V	Thermal modeling and measurement	LCO2 can reduce the maximum thermal load on inserts
18	[101, Augspurger 2020] Milling AISI1050	Thermal modeling and measurement	Heat toward the insert decreases by rising the cutting speed
19	[102, Umbrello 2007] Turning AISI1045	2D orthogonal cutting and 3D pure thermal FEM	Conductance value can be raised artificially to reproduce in small time the thermal field on insert skin at steady state
20	[178, Ceretti 2007] Turning AISI1045	2D orthogonal cutting and 3D pure thermal FEM	Physical conductance is dependent on feed and speed

Table 8.0.3: Studies on Thermal modeling and measurements in metal cutting

Tribology and Friction Models			
N°	Reference	Description	Content
1	[104, Moufki 1998] Orthogonal Cutting CRS 1018 Steel	Friction modeling	Friction is primarily governed by temperature at the interface
2	[106, Ozel 2006] Orthogonal Cutting Low Carbon Steel	Friction models comparison	Variable friction coefficient along the interface preferable for accurate results
3	[107, Filice 2007] Orthogonal Cutting AISI1045	Friction models comparison	Good material models are needed as starting point to speculate on friction models, new conductance models need to be studied
4	[108, Haglund 2008] Orthogonal Cutting AISI4140	Friction models comparison	Thermal dependent friction coefficient is the most accurate
5	[109, Shi 2009] Orthogonal Cutting AISI1045	Friction modeling	Precise and detailed models can perform worse than simple constant friction coefficients
6	[110, Arrazola 2010] Orthogonal Cutting AISI 4340	Friction models comparison	Coulomb-Tresca stick-slip models need accurate shear stress limit depending on $T, \varepsilon, \dot{\varepsilon}$ depending stress flow
7	[111, 112, Molinari 2011, Molinari 2012] Orthogonal Cutting 42CrMo4	Friction modeling and testing	Dependence of sticking region by sliding friction, by speed and consequent thermal softening
8	[113, Ulutan 2013] Orthogonal Cutting Inconel 100, Ti6Al4V	Friction and tool stress modeling	The most complete friction analysis on tool

Table 8.0.4: Studies on Friction Modeling

Friction Determination			
N°	Reference	Description	Content
1	[115, Hong 2002] AISI1018, Ti64	Closed tribometer	Reduction in case of LN2 but problems for the “favourable” equipment layout
2	[7, 116, Hong 2001d, Jun 2005]AISI1018, Ti64	Force elaboration	Reduction in case of LN2, difficult separation of workpiece material properties variation
3	[117, Hong 2006] AISI1018, Ti64	Closed tribometer	-
4	[105, Childs 2006] Turning	Tool-Split technique results	-
5	[118, El-Tayeb 2009] Ti6Al4V, Ti5Al4V	Closed tribometer	Friction coefficient dependent on sliding speed and normal pressure, however far from normal cutting ranges
6	[119, Arrazola 2008] AISI 4140	Force elaboration	Original force elaboration, variable friction along the interface give best results
7	[120, Bonnet 2008a] AISI 316 L	Pin on rod open tribometer	Sliding speed dependent friction coefficient and heat partition coefficients
8	[121, Bonnet 2008] AISI 316 L	FEM simulation with previous friction model	-
9	[122, Egana 2012] Ti6Al4V	Open pin on rod tribometer	Variable pressure and sliding speed determined friction and HP coefficients
10	[123, Puls 2012] AISI 1045	Closed tribometer, deformable disk	Constant friction coefficient relating varying normal and friction forces
11	[19, Courbon 2013] Inconel 718, Ti64	Pin on rod open tribometer	Friction and HP coefficients for variable speed and cooling approaches
12	[124, Rech 2013a] Several materials	Pin on rod open tribometer	HP and Friction coeff. determination, then application of sliding speed dependent friction coefficient in FEM
13	[125, Yousfi 2017] Ti6Al4V	Pin on rod open tribometer	The main influence to the friction coeff. is rugosity
14	[126, Sterle 2019] Ti6Al4V, 42CrMo4	Comparison between open and closed tribometers	For cryogenic friction determination, open tribometers are preferable

Table 8.0.5: Studies on Experimental Friction Determination

## Rehology and Material Models for Ti6Al4V simulations

N°	Reference	Model	Content
1	[127, Johnson 1983]	Johnson-Cook material model	-
2	[128, Johnson 1985]	Johnson-Cook damage model	-
3	[129, 130, 114, Chen 2011, Wang 2014, Atlati2014]	JC damage model with ductile fracture propagation criteria	-
4	[131, Cockcroft 1968]	Latham-Cockcroft damage model	-
5	[132, Ozel 2006a] Ti64 and others	JC experimental model	Model coefficients determined inversely through cutting tests and Oxley theory
6	[133, Guo 2006] AISI 52100	Baumann-Chiesa-Johnson	Long determination of coefficients
7	[134, Anurag 2007] Ti64 and others	Internal State Variable model	Not tested in any cutting simulation
8	[135, Calamaz 2008] Ti6Al4V	Calamaz Modified JC	Softening effect at high strains to reproduce shear banding
9	[137, Umbrello 2008] Ti6Al4V	LC damage criterion	A good material model is necessary to iterate on damage and friction models
10	[138, Ozel 2009] Ti6Al4V	Comparison of JC model coefficients	Large variability on results for different JC model coefficients sets is observed
11	[139, Sun 2009a] Ti6Al4V	JC model sensitivity analysis	Important effect of inelastic heat fraction coefficient and stress state in the fracture behaviour
12	[140, Shi 2010] AISI1045	Distributed Primary Zone Deformation model	Z-A accurate in describing the shear zone stress-strain state. Unique solution to inverse JC model determination is possible with designed tests
13	[143, Sima 2010] Ti6Al4V	Calamaz Modified JC model tuning	The best accuracy can be obtained with a complete Calamaz modification
14	[144, Calamaz 2010a] Ti6Al4V	New modified JC model	With refined mesh accurately describe strain localization in shear bands
15	[145, Karpat 2011] Ti6Al4V	Karpat Modified Z-A	Excellent results in reproduction of two separate experimental campaigns
16	[129, Chen 2011] Ti6Al4V	JC material and Damage models with ductile fracture propagation	Accuracy in shear band prediction and chip bending radius, no remeshing
17	[146, Calamaz 2011] Ti6Al4V	New modified JC model	Strain and strain rate dependent softening
18	[147, Shrot 2012] AISI52100	Inverse JC coefficient determination	Difficulties in converging to the same set from different initial guesses



N°	Reference	Model	Content
19	[148, Liu 2013] Ti6Al4V	Modified ZA	-
20	[130, Wang 2014] Ti6Al4V	JC material and Damage models with ductile fracture propagation	No remeshing and orientation of the initial mesh so to avoid distortion
21	[149, Cheng 2018] Ti6Al4V	Modified JC material model and JC damage model	-
22	[150, Bertolini 2019]	SHPB testing at cryogenic temperatures	-

Table 8.0.6: Studies on Material Models for cutting simulations

CF Properties and CFD Models			
N°	Reference	Description	Content
1	[151, Obikawa 2012]	Evaluation of compressed air to flank face effect	Increase in turbulence and penetration of emulsion
2	[152, Lu 2013]	Inverse determination of HTC of cryogenic jet toward tool flank	Development of a specimen and procedure for inverse HTC determination from TC cooling rate
3	[48, Pusavec 2016]	Inverse HTC determination, Fluid/Gas phase detection	HTC as a function of overheat temperature, importance of flux state
4	[154, Hribersek 2017]	Inverse HTC determination, jet on plate	Confirms the inverse proportionality of HTC and surface overheat
5	[155, Tahri 2017]	Heat transfer along the pipes for LN2	High liquid title and smooth bends are preferable, no roughness of tubes and no cavitation considered
6	[156, Lequien 2018]	Inverse HTC determination, various jet pressure, spot diameters, angles, distance	Preferable: high pressure, large diameter, low distance perpendicular jet
7	[49, Tahmasebi 2019]	Internal and external LN2 flow behaviour	No slip and cavitation, cavitation is preponderant for fluid evaporation. Pressure need to be optimized considering the delivery line
8	[157, Golda 2019]	Gas layer behaviour for parallel LN2 flows	The HTC in case of parallel (not perpendicular) impinging jet can be one order of magnitude lower than the usual literature values

Table 8.0.7: Studies on CFD Modeling of cryogenic and emulsion jets, flow properties of Cutting Fluids

Cryogenic Machining FE models, Hybrid FE-CFD models, Surface prediction Models			
N°	Reference	Description	Content
1	[136, Ozel 2011] Turning Inconel 718	Calamaz Modified JC	Accurate force results, lower temperatures prediction
2	[71, Melkote 2017]	Review on modeling of machining processes	-
3	[158, Bordin 2015] Turning Ti6Al4V	Force, temperature and deformed layer predictions, cryo vs dry	First full Calamaz modified JC, section of the tool to reduce computational burden
4	[159, Davoudinejad 2015] Orthogonal Cutting Ti6Al4V	Force and chip morphology prediction, cryo vs dry	Tabular material model, good result can be obtained by experimentally determined friction coefficients
5	[160, Imbrogno 2017] Turning Ti6Al4V	Force, temperature and deformed layer prediction	First full Calamaz mod. JC, cylindrical window for cryogenic jet,
6	[162, Stampfer 2019] Orthogonal Cutting Ti6Al4V	Cryogenic delivery design simulation	The only simulation in which an alternative design is simulated, reduction of tool heat capacity, higher ambient HTC, variable LN2 HTC
7	[163, Salame 2019] Orthogonal Cutting Ti6Al4V	Decoupled CFD and FEM simulation	Thermal fields of the FEM reported on the CFD model, no coupled effects considered, LCO2 HTC
8	[164, Shi 2019] Turning Ti6Al4V	Inverse HTC determination with jet on plate, 3D FEM for force prediction, 2D FEM for interface temperature prediction	Voce Power Law and Usui wear model
9	[165, Rotella 2014] Orthogonal Cutting Ti6Al4V	Grain size and hardness prediction	Grain size and hardness updated material model
10	[161, Umbrello 2016] Orthogonal Cutting AISI 52100	Grain size and hardness prediction	Variable cryogenic HTC, Brozzo fracture model, Hardness based material model updated by grain size and hardness
11	[166, Umbrello 2017] Turning Ti6Al4V	Metallurgical alpha grain orientation and surface hardness	First Calamaz modification with hardness and alpha deformation updated flow stress

Table 8.0.8: Studies on Cryogenic FE Models

## Additional information

Cryogenic Sustainability Evaluation:

FORGE NxT 3.0 User Guide: [http://docs.transvalor.com/forge/en/nxt3\\_0/](http://docs.transvalor.com/forge/en/nxt3_0/)



# Bibliography

- [1] I. Jawahir, H. Attia, D. Biermann, J. Duflou, F. Klocke, D. Meyer, S. Newman, F. Pusavec, M. Putz, J. Rech, V. Schulze, and D. Umbrello, "Cryogenic manufacturing processes," *CIRP Annals*, vol. 65, pp. 713–736, jan 2016. 1.1, 1.1.1, 1.1.2, 2.1.3, 2.2.3, 2.2.3, 2.2.3, 2.4.2, 3.3.2, 4.3.2, 8
- [2] Y. Yildiz and M. Nalbant, "A review of cryogenic cooling in machining processes," *International Journal of Machine Tools and Manufacture*, vol. 48, pp. 947–964, jul 2008. 1.1.2, 2.1.3, 2.1.3, 2.2, 2.2.1, 2.2.2, 2.2.3, 2.3.1, 2.3.2, 2.4.2, 2.5.1, 3, 8
- [3] A. Shokrani, V. Dhokia, P. Muñoz-Escalona, and S. T. Newman, "State-of-the-art cryogenic machining and processing," *International Journal of Computer Integrated Manufacturing*, vol. 26, no. 7, pp. 616–648, 2013. 1.1.2, 2.1, 2.1.3, 2.2, 2.2.1, 2.2.2, 2.2.3, 2.3.1, 2.3.2, 2.4.1, 3
- [4] Y. V. Deshpande, A. B. Andhare, and P. M. Padole, "How cryogenic techniques help in machining of nickel alloys? A review," *Machining Science and Technology*, vol. 22, no. 4, pp. 543–584, 2018. 1.1.2, 2.2.1, 2.2.3, 2.3.1, 2.3.2, 2.5, 5
- [5] F. Pušavec, A. Stoić, and J. Kopač, "The role of cryogenics in machining processes," *Tehnicki Vjesnik*, vol. 16, no. 4, pp. 3–10, 2009. 1.1.3, 2.5.1, 8
- [6] N. Abukhshim, P. Mativenga, and M. Sheikh, "Heat generation and temperature prediction in metal cutting: A review and implications for high speed machining," *International Journal of Machine Tools and Manufacture*, vol. 46, pp. 782–800, jun 2006. 2.1.1, 5.1.2, 8
- [7] S. Y. Hong, Y. Ding, and W.-c. Jeong, "Friction and cutting forces in cryogenic machining of Ti6Al4V," *International Journal of Machine Tools and Manufacture*, vol. 41, pp. 2271–2285, dec 2001. 2.1.2, 2.3.2, 2.3.3, 4.1.1, 5.2.2, 5.2.12, 8
- [8] S. Y. Hong and Y. Ding, "Cooling approaches and cutting temperatures in cryogenic machining of Ti-6Al-4V," *International Journal of Machine Tools and Manufacture*, vol. 41, pp. 1417–1437, aug 2001. 2.1.2, 3.3.2, 3.3.2, 3.3.10, 5.1.2, 5.1.2, 5.4, 8
- [9] S. Sun, M. Brandt, S. Palanisamy, and M. S. Dargusch, "Effect of cryogenic compressed air on the evolution of cutting force and tool wear during machining of Ti6Al4V alloy," *Journal of Materials Processing Technology*, vol. 221, pp. 243–254, jul 2015. 2.1.2, 4.1.1, 4.1.1, 4.1.12
- [10] K. Venugopal, S. Paul, and A. Chattopadhyay, "Tool wear in cryogenic turning of Ti-6Al-4V alloy," *Cryogenics*, vol. 47, pp. 12–18, jan 2007. 2.1.2, 4.1.1, 4.1.11, 8
- [11] S. Y. Hong and Z. Zhao, "Thermal aspects, material considerations and cooling strategies in cryogenic machining," *Clean Products and Processes*, vol. 1, pp. 107–116, 1999. 2.1.3, 2.1.4, 2.1.5, 4.2.2
- [12] E. Yasa, S. Pilatin, and O. Çolak, "Overview of cryogenic cooling in machining of Ti alloys and a case study," *Journal of Production Engineering*, vol. 2, no. July, pp. 1–9, 2012. 2.1.3, 2.1.3, 2.2.3, 2.3.1, 2.3.2, 2.5, 4.1.1, 4.3.1, 8, 8
- [13] S. Y. Hong, I. Markus, and W.-c. Jeong, "New cooling approach and tool life improvement in cryogenic machining of titanium alloy Ti-6Al-4V," *International Journal of Machine Tools and Manufacture*, vol. 41, pp. 2245–2260, dec 2001. 2.1.3, 3.3.2, 3.3.10, 4.1.1, 5.2.2, 8, 8
- [14] D. Biermann and M. Heilmann, "Improvement of workpiece quality in face milling of aluminum alloys," *Journal of Materials Processing Technology*, vol. 210, pp. 1968–1975, nov 2010. 2.2.1
- [15] Z. Wang and K. Rajurkar, "Cryogenic machining of hard-to-cut materials," *Wear*, vol. 239, pp. 168–175, apr 2000. 2.2.2, 3.3.2, 3.3.1, 5.1.2, 8
- [16] N. Dhar, S. Paul, and A. Chattopadhyay, "The influence of cryogenic cooling on tool wear, dimensional accuracy and surface finish in turning AISI 1040 and E4340C steels," *Wear*, vol. 249, pp. 932–942, nov 2001. 2.2.2
- [17] Z. Wang, K. Rajurkar, and M. Murugappan, "Cryogenic PCBN turning of ceramic (Si 3N 4)," *Wear*, vol. 195, pp. 1–6, jul 1996. 2.2.2, 3.3.2, 3.3.1, 5.1.2
- [18] C. H. C. Haron, S. S. Muhamad, and J. A. Ghani, "A review on future implementation of cryogenic machining in manufacturing industry," *Progress in Industrial Ecology, An International Journal*, vol. 12, no. 3, p. 260, 2018. 2.3.1, 2.3.3, 2.4.1
- [19] C. Courbon, F. Pusavec, F. Dumont, J. Rech, and J. Kopač, "Tribological behaviour of Ti6Al4V and Inconel718 under dry and cryogenic conditions—Application to the context of machining with carbide tools," *Tribology International*, vol. 66, pp. 72–82, oct 2013. 2.3.2, 5.2.2, 5.2.20, 8
- [20] M. Dhananchezian and M. P. Kumar, "Experimental investigation of cryogenic cooling by liquid nitrogen in the orthogonal machining of aluminium 6061-T6 alloy," *International Journal of Machining and Machinability of Materials*, vol. 7, no. 3-4, pp. 292–303, 2010. 2.3.3

- [21] C. Courbon, T. Mabrouki, J. Rech, D. Mazuyer, F. Perrard, and E. D'Eramo, "Towards a physical FE modelling of a dry cutting operation: Influence of dynamic recrystallization when machining AISI 1045," in *Procedia CIRP*, vol. 8, pp. 516–521, Elsevier B.V., jan 2013. 2.3.3, 2.3.1
- [22] Y. Xu, J. Zhang, Y. Bai, and M. A. Meyers, "Shear localization in dynamic deformation: Microstructural evolution," *Metallurgical and Materials Transactions A: Physical Metallurgy and Materials Science*, vol. 39 A, no. 4, pp. 811–843, 2008. 2.3.3, 2.3.2
- [23] G. G. Ye, S. F. Xue, M. Q. Jiang, X. H. Tong, and L. H. Dai, "Modeling periodic adiabatic shear band evolution during high speed machining Ti-6Al-4V alloy," *International Journal of Plasticity*, vol. 40, pp. 39–55, jan 2013. 2.3.2
- [24] M. Cotterell and G. Byrne, "Dynamics of chip formation during orthogonal cutting of titanium alloy Ti-6Al-4V," *CIRP Annals*, vol. 57, pp. 93–96, jan 2008. 2.3.3
- [25] A. Molinari, X. Soldani, and M. H. Miguélez, "Adiabatic shear banding and scaling laws in chip formation with application to cutting of Ti-6Al-4V," *Journal of the Mechanics and Physics of Solids*, vol. 61, pp. 2331–2359, nov 2013. 2.3.3
- [26] G. Krishnamurthy, S. Bhowmick, W. Altenhof, and A. Alpas, "Increasing efficiency of Ti-alloy machining by cryogenic cooling and using ethanol in MRF," *CIRP Journal of Manufacturing Science and Technology*, vol. 18, pp. 159–172, aug 2017. 2.3.3, 2.3.4
- [27] S. N. Kane, A. Mishra, and A. K. Dutta, "Preface: International Conference on Recent Trends in Physics (ICRTP 2016)," *Journal of Physics: Conference Series*, vol. 755, no. 1, pp. 6–13, 2016. 2.4.2
- [28] S. Isakson, M. I. Sadik, A. Malakizadi, and P. Krajnik, "Effect of cryogenic cooling and tool wear on surface integrity of turned Ti-6Al-4V," in *Procedia CIRP*, vol. 71, pp. 254–259, Elsevier B.V., jan 2018. 2.4.2
- [29] K. Nimel Sworna Ross and M. Ganesh, "Performance Analysis of Machining Ti-6Al-4V Under Cryogenic CO<sub>2</sub> Using PVD-TiN Coated Tool," *Journal of Failure Analysis and Prevention*, vol. 19, no. 3, pp. 821–831, 2019. 2.4.2, 3.3.2, 3.3.9, 8
- [30] R. Bertolini, L. Lizzul, L. Pezzato, A. Ghiotti, and S. Bruschi, "Improving surface integrity and corrosion resistance of additive manufactured Ti6Al4V alloy by cryogenic machining," *International Journal of Advanced Manufacturing Technology*, vol. 104, no. 5-8, pp. 2839–2850, 2019. 2.4.2
- [31] S. D. Supekar, D. J. Graziano, S. J. Skerlos, and J. Cresko, "Comparing energy and water use of aqueous and gas-based metalworking fluids," *Journal of Industrial Ecology*, pp. 1–13, 2020. 2.5, 4.3.1
- [32] M. Strano, E. Chiappini, S. Tirelli, P. Albertelli, and M. Monno, "Comparison of Ti6Al4V machining forces and tool life for cryogenic versus conventional cooling," *Proceedings of the Institution of Mechanical Engineers, Part B: Journal of Engineering Manufacture*, vol. 227, no. 9, pp. 1403–1408, 2013. 2.5, 3.3.2, 3.3.6, 4.1.1, 4.1.1, 4.1.12, 8
- [33] F. Pušavec and J. Kopač, "Sustainability assessment: Cryogenic machining of inconel 718," *Strojnikski Vestnik/Journal of Mechanical Engineering*, vol. 57, no. 9, pp. 637–647, 2011. 2.5
- [34] E. Benedicto, D. Carou, and E. Rubio, "Technical, Economic and Environmental Review of the Lubrication/Cooling Systems Used in Machining Processes," *Procedia Engineering*, vol. 184, pp. 99–116, jan 2017. 2.5.1, 2.5.1, 8
- [35] A. F. Clarens, J. B. Zimmerman, G. A. Keoleian, K. F. Hayes, and S. J. Skerlos, "Comparison of life cycle emissions and energy consumption for environmentally adapted metalworking fluid systems," *Environmental Science and Technology*, vol. 42, no. 22, pp. 8534–8540, 2008. 2.5.1
- [36] N. Tapoglou, M. I. A. Lopez, I. Cook, and C. M. Taylor, "Investigation of the Influence of CO<sub>2</sub> Cryogenic Coolant Application on Tool Wear," *Procedia CIRP*, vol. 63, pp. 745–749, jan 2017. 3.1.2, 4.1.2, 8
- [37] T. Augspurger, M. Koch, F. Klocke, and B. Döbbeler, "Investigation of transient temperature fields in the milling cutter under CO<sub>2</sub> cooling by means of an embedded thermocouple," in *Procedia CIRP*, vol. 79, pp. 33–38, Elsevier B.V., jan 2019. 3.1.2, 5.1.3, 5.1.8, 6.1.5, 8
- [38] D. Fernández, A. Sandá, and I. Bengoetxea, "Cryogenic milling: Study of the effect of CO<sub>2</sub> cooling on tool wear when machining Inconel 718, grade EA1N steel and Gamma TiAl," *Lubricants*, vol. 7, no. 1, pp. 1–10, 2019. 3.1.2, 3.3.2, 3.3.15, 4.3.2
- [39] M. I. Sadik, S. Isakson, A. Malakizadi, and L. Nyborg, "Influence of Coolant Flow Rate on Tool Life and Wear Development in Cryogenic and Wet Milling of Ti-6Al-4V," *Procedia CIRP*, vol. 46, pp. 91–94, 2016. 3.1.2, 3.3.2, 3.3.14, 4.1.2, 8
- [40] M. I. Sadik and S. Isakson, "The role of PVD coating and coolant nature in wear development and tool performance in cryogenic and wet milling of Ti-6Al-4V," *Wear*, vol. 386-387, pp. 204–210, sep 2017. 3.1.2, 4.1.2, 4.1.16, 8
- [41] F. Pušavec, D. Grguraš, M. Koch, and P. Krajnik, "Cooling capability of liquid nitrogen and carbon dioxide in cryogenic milling," *CIRP Annals*, vol. 68, pp. 73–76, jan 2019. 3.2.1, 4.3
- [42] B. Kirsch, S. Basten, H. Hasse, and J. C. Aurich, "Sub-zero cooling: A novel strategy for high performance cutting," *CIRP Annals*, vol. 67, pp. 95–98, jan 2018. 3.2.1, 4.1.1, 4.3, 8
- [43] F. Jiang, Z. Liu, Y. Wan, and Z. Shi, "Analytical modeling and experimental investigation of tool and workpiece temperatures for interrupted cutting 1045 steel by inverse heat conduction method," *Journal of Materials Processing Technology*, vol. 213, pp. 887–894, jun 2013. 3.2.1, 5.1.3, 5.1.6, 8
- [44] U. Karaguzel, M. Bakkal, and E. Budak, "Modeling and Measurement of Cutting Temperatures in Milling," *Procedia CIRP*, vol. 46, no. December, pp. 173–176, 2016. 3.2.1, 5.1.3, 5.1.7, 8
- [45] M. Sato, N. Tamura, and H. Tanaka, "Temperature variation in the cutting tool in end milling," *Journal of Manufacturing Science and Engineering, Transactions of the ASME*, vol. 133, no. 2, pp. 1–7, 2011. 3.2.1, 5.1.3, 5.1.5, 5.1.3, 8
- [46] S. Madhukar, A. Shravan, P. V. Sai, and V. V. Satyanarayana, "A critical review on cryogenic machining of titanium alloy (Ti-6Al-4V)," *International Journal of Mechanical Engineering and Technology*, vol. 7, no. 5, pp. 38–45, 2016. 3.2.2, 3.3.2, 8

- [47] K. Venugopal, S. Paul, and A. Chattopadhyay, "Growth of tool wear in turning of Ti-6Al-4V alloy under cryogenic cooling," *Wear*, vol. 262, pp. 1071–1078, apr 2007. 3.2.2, 4.1.1, 8
- [48] F. Pusavec, T. Lu, C. Courbon, J. Rech, U. Aljancic, J. Kopac, and I. Jawahir, "Analysis of the influence of nitrogen phase and surface heat transfer coefficient on cryogenic machining performance," *Journal of Materials Processing Technology*, vol. 233, pp. 19–28, jul 2016. 3.2.2, 3.2.3, 5.4, 5.4.1, 5.4.1, 5.4, 6.1.5, 8
- [49] E. Tahmasebi, P. Albertelli, T. Lucchini, M. Monno, and V. Mussi, "CFD and experimental analysis of the coolant flow in cryogenic milling," *International Journal of Machine Tools and Manufacture*, vol. 140, no. February, pp. 20–33, 2019. 3.3.2, 4.3, 4.3.1, 5.1, 5.4, 5.4.3, 5.4.4, 5.4.5, 6.2.1, 8
- [50] T. Minton, S. Ghani, F. Sammler, R. Bateman, P. Fürstmann, and M. Roeder, "Temperature of internally-cooled diamond-coated tools for dry-cutting titanium," *International Journal of Machine Tools and Manufacture*, vol. 75, pp. 27–35, dec 2013. 3.3.2
- [51] K. H. Park, G. D. Yang, M. A. Suhaimi, D. Y. Lee, T. G. Kim, D. W. Kim, and S. W. Lee, "The effect of cryogenic cooling and minimum quantity lubrication on end milling of titanium alloy Ti-6Al-4V," *Journal of Mechanical Science and Technology*, vol. 29, no. 12, pp. 5121–5126, 2015. 3.3.2, 3.3.2, 3.3.2, 3.3.13, 4.1.2, 8
- [52] M. A. Suhaimi, G.-D. D. Yang, K.-H. H. Park, M. J. Hisam, S. Sharif, and D.-W. W. Kim, "Effect of Cryogenic Machining for Titanium Alloy Based on Indirect, Internal and External Spray System," *Procedia Manufacturing*, vol. 17, pp. 158–165, jan 2018. 3.3.2, 3.3.2, 4.1.2, 8
- [53] Z. Zurecki, R. Ghosh, and J. H. Frey, "Finish-turning of hardened powder metallurgy steel using cryogenic cooling," *International Journal of Powder Metallurgy (Princeton, New Jersey)*, vol. 40, no. 1, pp. 19–31, 2004. 3.3.2, 3.3.3
- [54] Shokrani, V. Dhokia, S. Newman, and R. Imani-Asrai, "An Initial Study of the Effect of Using Liquid Nitrogen Coolant on the Surface Roughness of Inconel 718 Nickel-Based Alloy in CNC Milling," *Procedia CIRP*, vol. 3, pp. 121–125, jan 2012. 3.3.2
- [55] M. Bermingham, J. Kirsch, S. Sun, S. Palanisamy, and M. Dargusch, "New observations on tool life, cutting forces and chip morphology in cryogenic machining Ti-6Al-4V," *International Journal of Machine Tools and Manufacture*, vol. 51, pp. 500–511, jun 2011. 3.3.2, 3.3.4, 4.1.1, 4.1.1, 4.1.1, 4.1.9, 4.1.1, 4.1.10, 4.1.1, 8
- [56] C. Machai and D. Biermann, "Machining of  $\beta$ -titanium-alloy Ti-10V-2Fe-3Al under cryogenic conditions: Cooling with carbon dioxide snow," *Journal of Materials Processing Technology*, vol. 211, pp. 1175–1183, jun 2011. 3.3.2, 4.1.1, 4.1.11, 4.3.2
- [57] M. Bermingham, S. Palanisamy, D. Kent, and M. Dargusch, "A comparison of cryogenic and high pressure emulsion cooling technologies on tool life and chip morphology in Ti-6Al-4V cutting," *Journal of Materials Processing Technology*, vol. 212, pp. 752–765, apr 2012. 3.3.2, 3.3.5, 4.1.1, 4.1.1, 4.1.1, 4.3, 8
- [58] F. Klocke, L. Settineri, D. Lung, P. Claudio Priarone, and M. Arft, "High performance cutting of gamma titanium aluminides: Influence of lubricoolant strategy on tool wear and surface integrity," *Wear*, vol. 302, pp. 1136–1144, apr 2013. 3.3.2
- [59] Y. Kaynak, "Evaluation of machining performance in cryogenic machining of Inconel 718 and comparison with dry and MQL machining," *International Journal of Advanced Manufacturing Technology*, vol. 72, no. 5-8, pp. 919–933, 2014. 3.3.2, 3.3.7
- [60] A. Shokrani, V. Dhokia, and S. T. Newman, "Investigation of the effects of cryogenic machining on surface integrity in CNC end milling of Ti-6Al-4V titanium alloy," *Journal of Manufacturing Processes*, vol. 21, pp. 172–179, jan 2016. 3.3.2, 4.1.2
- [61] A. Shokrani, V. Dhokia, and S. T. Newman, "Comparative investigation on using cryogenic machining in CNC milling of Ti-6Al-4V titanium alloy," *Machining Science and Technology*, vol. 20, no. 3, pp. 475–494, 2016. 3.3.2, 3.3.8, 4.1.2, 4.1.15, 8
- [62] S. Y. Hong and M. Broome, "Economical and ecological cryogenic machining of AISI 304 austenitic stainless steel," *Clean Products and Processes*, vol. 2, no. 3, pp. 0157–0166, 2000. 3.3.2, 3.3.11
- [63] M. Dhananchezian and M. Pradeep Kumar, "Cryogenic turning of the Ti-6Al-4V alloy with modified cutting tool inserts," *Cryogenics*, vol. 51, pp. 34–40, jan 2011. 3.3.2, 3.3.12, 4.1.1, 4.1.1, 8
- [64] M. Mia, M. K. Gupta, J. A. Lozano, D. Carou, D. Y. Pimenov, G. Królczyk, A. M. Khan, and N. R. Dhar, "Multi-objective optimization and life cycle assessment of eco-friendly cryogenic N2 assisted turning of Ti-6Al-4V," *Journal of Cleaner Production*, vol. 210, pp. 121–133, feb 2019. 3.3.2, 3.3.16, 8
- [65] I. Deiab, S. W. Raza, and S. Pervaiz, "Analysis of Lubrication Strategies for Sustainable Machining during Turning of Titanium Ti-6Al-4V Alloy," *Procedia CIRP*, vol. 17, pp. 766–771, jan 2014. 4.1.1, 8
- [66] S. W. Raza, S. Pervaiz, and I. Deiab, "Tool wear patterns when turning of titanium alloy using sustainable lubrication strategies," *International Journal of Precision Engineering and Manufacturing*, vol. 15, no. 9, pp. 1979–1985, 2014. 4.1.1, 8
- [67] S. Tirelli, E. Chiappini, M. Strano, M. Monno, and Q. Semeraro, "Economical comparison of cryogenic vs. Traditional turning of Ti-6Al-4V: A case study," *Key Engineering Materials*, vol. 651-653, pp. 1204–1210, 2015. 4.1.1, 8
- [68] S. Sun, M. Brandt, and M. Dargusch, "Machining Ti-6Al-4V alloy with cryogenic compressed air cooling," *International Journal of Machine Tools and Manufacture*, vol. 50, pp. 933–942, nov 2010. 4.1.1, 4.3.3
- [69] Y. Ayed, G. Germain, A. P. Melsio, P. Kowalewski, and D. Locufier, "Impact of supply conditions of liquid nitrogen on tool wear and surface integrity when machining the Ti-6Al-4V titanium alloy," *International Journal of Advanced Manufacturing Technology*, vol. 93, no. 1-4, pp. 1199–1206, 2017. 4.1.1, 8
- [70] S. Y. Hong, "Economical and ecological cryogenic machining," *Journal of Manufacturing Science and Engineering, Transactions of the ASME*, vol. 123, no. 2, pp. 331–338, 2001. 4.1.1, 5.2.2, 8
- [71] S. N. Melkote, W. Grzesik, J. Outeiro, J. Rech, V. Schulze, H. Attia, P. J. Arrazola, R. M'Saoubi, and C. Saldana, "Advances in material and friction data for modelling of metal machining," *CIRP Annals - Manufacturing Technology*, vol. 66, pp. 731–754, jan 2017. 4.1.1, 5.5, 8

- [72] B. Dilip Jerold and M. Pradeep Kumar, "The influence of cryogenic coolants in machining of Ti-6Al-4V," *Journal of Manufacturing Science and Engineering, Transactions of the ASME*, vol. 135, no. 3, pp. 1–8, 2013. 4.1.1, 4.3, 8
- [73] M. P. Kumar and B. D. Jerold, "Effect of Cryogenic Cutting Coolants on Cutting Forces and Chip Morphology in Machining Ti-6Al-4V Alloy," *International Journal of Applied Science and Technology*, vol. 6, no. 2, pp. 1–7, 2013. 4.1.1, 4.3, 8
- [74] A. Bordin, S. Sartori, S. Bruschi, and A. Ghiotti, "Experimental investigation on the feasibility of dry and cryogenic machining as sustainable strategies when turning Ti6Al4V produced by Additive Manufacturing," *Journal of Cleaner Production*, vol. 142, pp. 4142–4151, jan 2017. 4.1.1, 4.1.10, 8
- [75] A. Bordin, S. Bruschi, A. Ghiotti, and P. F. Bariani, "Analysis of tool wear in cryogenic machining of additive manufactured Ti6Al4V alloy," *Wear*, vol. 328-329, pp. 89–99, apr 2015. 4.1.1, 4.1.1, 4.1.13, 8
- [76] S. Bruschi, R. Bertolini, A. Bordin, F. Medea, and A. Ghiotti, "Influence of the machining parameters and cooling strategies on the wear behavior of wrought and additive manufactured Ti6Al4V for biomedical applications," *Tribology International*, vol. 102, pp. 133–142, oct 2016. 4.1.1, 8
- [77] A. S. Shokrani, V. Dhokia, and S. T. Newman, "Investigation of Cutting Parameters in Sustainable Cryogenic End Milling," pp. 39–50, 2015. 4.1.2, 8
- [78] A. Shokrani, V. Dhokia, and S. T. Newman, "Energy conscious cryogenic machining of Ti-6Al-4V titanium alloy," *Proceedings of the Institution of Mechanical Engineers, Part B: Journal of Engineering Manufacture*, vol. 232, no. 10, pp. 1690–1706, 2018. 4.1.2, 8
- [79] A. Shokrani and S. T. Newman, "A new cutting tool design for cryogenic machining of Ti-6Al-4V titanium alloy," *Materials*, vol. 12, no. 3, pp. 1–14, 2019. 4.1.2, 8
- [80] G. M. Pittalà, "A study of the effect of CO2 cryogenic coolant in end milling of Ti-6Al-4V," in *Procedia CIRP*, vol. 77, pp. 445–448, Elsevier B.V., jan 2018. 4.1.2, 8
- [81] H. Safari, S. Sharif, S. Izman, H. Jafari, and D. Kurniawan, "Cutting force and surface roughness characterization in cryogenic high-speed end milling of Ti-6Al-4V ELI," *Materials and Manufacturing Processes*, vol. 29, no. 3, pp. 350–356, 2014. 4.2.2
- [82] K. A. Venugopal, R. Tawade, P. G. Prashanth, S. Paul, and A. B. Chattopadhyay, "Turning of titanium alloy with TiB2-coated carbides under cryogenic cooling," *Proceedings of the Institution of Mechanical Engineers, Part B: Journal of Engineering Manufacture*, vol. 217, no. 12, pp. 1697–1707, 2003. 4.2.2
- [83] A. Krämer, F. Klocke, H. Sangermann, and D. Lung, "Influence of the lubricoolant strategy on thermo-mechanical tool load," *CIRP Journal of Manufacturing Science and Technology*, vol. 7, pp. 40–47, jan 2014. 4.3, 8
- [84] A. Iqbal, W. Zhao, J. Zaini, N. He, M. M. Nauman, and H. Suhaimi, "Comparative analyses of multi-pass face-turning of a titanium alloy under various cryogenic cooling and micro-lubrication conditions," *International Journal of Lightweight Materials and Manufacture*, vol. 2, pp. 388–396, dec 2019. 4.3, 8
- [85] Y.-l. lin KE, H.-y. yue DONG, G. LIU, and M. ZHANG, "Use of nitrogen gas in high-speed milling of Ti-6Al-4V," vol. 19, pp. 530–534, jun 2009. 4.3.1
- [86] E. M. Rubio, B. Agustina, M. Marín, and A. Bericua, "Cooling Systems Based on Cold Compressed Air: A Review of the Applications in Machining Processes," *Procedia Engineering*, vol. 132, pp. 413–418, 2015. 4.3.3, 8
- [87] S. Yuan, L. Yan, W. Liu, and Q. Liu, "Effects of cooling air temperature on cryogenic machining of Ti6Al4V alloy," *Journal of Materials Processing Technology*, vol. 211, pp. 356–362, mar 2011. 4.3.3
- [88] F. Benabid, H. Benmoussa, and M. Arrouf, "A thermal modeling to predict and control the cutting temperature. The simulation of face-milling process," *Procedia Engineering*, vol. 74, no. 6, pp. 37–42, 2014. 5.1
- [89] H. Ay and W.-J. Yang, "Heat transfer and life of metal cutting tools in turning," *International Journal of Heat and Mass Transfer*, vol. 41, pp. 613–623, feb 1998. 5.1.1, 8
- [90] N. R. Dhar, S. Paul, and A. B. Chattopadhyay, "Role of cryogenic cooling on cutting temperature turning steel," *Journal of Manufacturing Science and Engineering, Transactions of the ASME*, vol. 124, no. 1, pp. 146–154, 2002. 5.1.1, 8
- [91] D. O'Sullivan and M. Cotterell, "Temperature measurement in single point turning," *Journal of Materials Processing Technology*, vol. 118, pp. 301–308, dec 2001. 5.1.1, 5.1.1, 8
- [92] M. Bacci da Silva and J. Wallbank, "Cutting temperature: prediction and measurement methods—a review," *Journal of Materials Processing Technology*, vol. 88, pp. 195–202, apr 1999. 5.1.1, 8
- [93] Y. Yang and W. Zhu, "Study on cutting temperature during milling of titanium alloy based on FEM and experiment," *International Journal of Advanced Manufacturing Technology*, vol. 73, no. 9-12, pp. 1511–1521, 2014. 5.1.1, 5.1.3, 5.1.4, 8
- [94] E.-G. Ng, D. Aspinwall, D. Brazil, and J. Monaghan, "Modelling of temperature and forces when orthogonally machining hardened steel," *International Journal of Machine Tools and Manufacture*, vol. 39, pp. 885–903, jun 1999. 5.1.1, 8
- [95] M. A. Davies, T. Ueda, R. M'Saoubi, B. Mullany, and A. L. Cooke, "On The Measurement of Temperature in Material Removal Processes," *CIRP Annals - Manufacturing Technology*, vol. 56, pp. 581–604, jan 2007. 5.1.1, 8
- [96] R. Komanduri and Z. B. Hou, "Thermal modeling of the metal cutting process Part I - temperature rise distribution due to shear plane heat source," *International Journal of Mechanical Sciences*, vol. 42, pp. 1715–1752, sep 2000. 5.1.2, 8
- [97] P. Majumdar, R. Jayaramachandran, and S. Ganesan, "Finite element analysis of temperature rise in metal cutting processes," *Applied Thermal Engineering*, vol. 25, pp. 2152–2168, oct 2005. 5.1.2
- [98] J. Liu and Y. Kevin Chou, "On temperatures and tool wear in machining hypereutectic AlSi alloys with vortex-tube cooling," *International Journal of Machine Tools and Manufacture*, vol. 47, pp. 635–645, mar 2007. 5.1.2, 8

- [99] T. Kitagawa, A. Kubo, and K. Maekawa, "Temperature and wear of cutting tools in high-speed machining of Inconel 718 and Ti-6Al-6V-2Sn," *Wear*, vol. 202, pp. 142–148, jan 1997. 5.1.3, 5.1.3, 8
- [100] W. Baohai, C. Di, H. Xiaodong, Z. Dinghua, and T. Kai, "Cutting tool temperature prediction method using analytical model for end milling," *Chinese Journal of Aeronautics*, vol. 29, pp. 1788–1794, dec 2016. 5.1.3, 8
- [101] T. Augspurger, G. Da Silva, D. Schraknepper, P. Mattfeld, and T. Bergs, "Model-based monitoring of temperatures and heat flows in the milling cutter," *The International Journal of Advanced Manufacturing Technology*, apr 2020. 5.1.3, 5.1.9, 8
- [102] D. Umbrello, L. Filice, S. Rizzuti, F. Micari, and L. Settineri, "On the effectiveness of Finite Element simulation of orthogonal cutting with particular reference to temperature prediction," *Journal of Materials Processing Technology*, vol. 189, pp. 284–291, jul 2007. 5.1.4, 5.1.10, 8
- [103] E. Ceretti, L. Filice, D. Umbrello, and F. Micari, "ALE simulation of orthogonal cutting: A new approach to model heat transfer phenomena at the tool-chip interface," *CIRP Annals - Manufacturing Technology*, vol. 56, pp. 69–72, jan 2007. 5.1.4, 5.1.11
- [104] A. Moufki, A. Molinari, and D. Dudzinski, "Modelling of orthogonal cutting with a temperature dependent friction law," *Journal of the Mechanics and Physics of Solids*, vol. 46, pp. 2103–2138, oct 1998. 5.2.1, 5.2.1, 6.3.3, 8
- [105] T. H. Childs, "Friction modelling in metal cutting," *Wear*, vol. 260, pp. 310–318, feb 2006. 5.2.1, 5.2.2, 8
- [106] T. Özel, "The influence of friction models on finite element simulations of machining," *International Journal of Machine Tools and Manufacture*, vol. 46, pp. 518–530, apr 2006. 5.2.1, 5.2.3, 5.2.4, 8
- [107] L. Filice, F. Micari, S. Rizzuti, and D. Umbrello, "A critical analysis on the friction modelling in orthogonal machining," *International Journal of Machine Tools and Manufacture*, vol. 47, pp. 709–714, mar 2007. 5.2.1, 5.2.5, 5.2.1, 8
- [108] A. J. Haglund, H. A. Kishawy, and R. J. Rogers, "An exploration of friction models for the chip-tool interface using an Arbitrary Lagrangian-Eulerian finite element model," *Wear*, vol. 265, pp. 452–460, jul 2008. 5.2.1, 5.2.6, 6.3.3, 8
- [109] B. Shi and H. Attia, "Modeling the thermal and tribological processes at the tool-chip interface in machining," *Machining Science and Technology*, vol. 13, no. 2, pp. 210–226, 2009. 5.2.1, 5.2.7, 8
- [110] P. J. Arrazola and T. Özel, "Investigations on the effects of friction modeling in finite element simulation of machining," *International Journal of Mechanical Sciences*, vol. 52, pp. 31–42, jan 2010. 5.2.1, 5.2.8, 8
- [111] A. Molinari, R. Cheriguene, and H. Miguelez, "Numerical and analytical modeling of orthogonal cutting: The link between local variables and global contact characteristics," *International Journal of Mechanical Sciences*, vol. 53, pp. 183–206, mar 2011. 5.2.1, 5.2.9, 6.3.3, 8
- [112] A. Molinari, R. Cheriguene, and H. Miguelez, "Contact variables and thermal effects at the tool-chip interface in orthogonal cutting," *International Journal of Solids and Structures*, vol. 49, pp. 3774–3796, dec 2012. 5.2.1, 5.2.9, 6.3.3, 8
- [113] D. Ulutan and T. Özel, "Determination of tool friction in presence of flank wear and stress distribution based validation using finite element simulations in machining of titanium and nickel based alloys," *Journal of Materials Processing Technology*, vol. 213, pp. 2217–2237, dec 2013. 5.2.1, 5.2.10, 5.2.11, 8
- [114] S. Atlati, B. Haddag, M. Nouari, and M. Zenasni, "Thermomechanical modelling of the tool-workmaterial interface in machining and its implementation using the ABAQUS VUINTER subroutine," *International Journal of Mechanical Sciences*, vol. 87, pp. 102–117, oct 2014. 5.2.1, 5.3.1, 8
- [115] S. Y. Hong, Y. Ding, and J. Jeong, "Experimental evaluation of friction coefficient and liquid nitrogen lubrication effect in cryogenic machining," *Machining Science and Technology*, vol. 6, no. 2, pp. 235–250, 2002. 5.2.2, 5.2.13, 8
- [116] S. C. Jun, "Lubrication effect of liquid nitrogen in cryogenic machining friction on the tool-chip interface," *Journal of Mechanical Science and Technology*, vol. 19, no. 4, pp. 936–946, 2005. 5.2.2, 8
- [117] S. Hong, "Lubrication mechanisms of LN2 in ecological cryogenic machining," *Machining Science and Technology*, vol. 10, no. 1, pp. 133–155, 2006. 5.2.2, 5.2.14, 8
- [118] N. El-Tayeb, T. Yap, V. Venkatesh, and P. Brevern, "Modeling of cryogenic frictional behaviour of titanium alloys using Response Surface Methodology approach," *Materials & Design*, vol. 30, pp. 4023–4034, dec 2009. 5.2.2, 8
- [119] P. J. Arrazola, D. Ugarte, and X. Domínguez, "A new approach for the friction identification during machining through the use of finite element modeling," *International Journal of Machine Tools and Manufacture*, vol. 48, pp. 173–183, feb 2008. 5.2.2, 5.2.15, 5.2.16, 6.3.3, 8
- [120] C. Bonnet, F. Valiorgue, J. Rech, C. Claudin, H. Hamdi, J. M. Bergheau, and P. Gilles, "Identification of a friction model-Application to the context of dry cutting of an AISI 316L austenitic stainless steel with a TiN coated carbide tool," *International Journal of Machine Tools and Manufacture*, vol. 48, pp. 1211–1223, sep 2008. 5.2.2, 5.2.17, 6.1.5, 8
- [121] C. Bonnet, F. Valiorgue, J. Rech, and H. Hamdi, "Improvement of the numerical modeling in orthogonal dry cutting of an AISI 316L stainless steel by the introduction of a new friction model," *CIRP Journal of Manufacturing Science and Technology*, vol. 1, pp. 114–118, jan 2008. 5.2.2, 5.2.17, 8
- [122] A. Egaña, J. Rech, and P. J. Arrazola, "Characterization of Friction and Heat Partition Coefficients during Machining of a TiAl6V4 Titanium Alloy and a Cemented Carbide," *Tribology Transactions*, vol. 55, no. 5, pp. 665–676, 2012. 5.2.2, 5.2.18, 8
- [123] H. Puls, F. Klocke, and D. Lung, "A new experimental methodology to analyse the friction behaviour at the tool-chip interface in metal cutting," *Production Engineering*, vol. 6, no. 4-5, pp. 349–354, 2012. 5.2.2, 5.2.19, 8
- [124] J. Rech, P. J. Arrazola, C. Claudin, C. Courbon, F. Pusavec, and J. Kopac, "Characterisation of friction and heat partition coefficients at the tool-work material interface in cutting," *CIRP Annals - Manufacturing Technology*, vol. 62, pp. 79–82, jan 2013. 5.2.2, 5.2.21, 8



- [125] M. Yousfi, J. Outeiro, C. Nouveau, B. Marcon, and B. Zouhair, "Tribological Behavior of PVD Hard Coated Cutting Tools under Cryogenic Cooling Conditions," *Procedia CIRP*, vol. 58, pp. 561–565, jan 2017. 5.2.2, 8
- [126] L. Sterle, F. Pušavec, and M. Kalin, "Determination of friction coefficient in cutting processes: comparison between open and closed tribometers," *Procedia CIRP*, vol. 82, pp. 101–106, jan 2019. 5.2.2, 5.2.22, 5.2.23, 8
- [127] G. R. Johnson and W. H. Cook, "A Computational Constitutive Model and Data for Metals Subjected to Large Strain, High Strain Rates and High Pressures," *the Seventh International Symposium on Ballistics*, pp. 541–547, 1983. 5.3, 8
- [128] G. R. Johnson and W. H. Cook, "Fracture characteristics of three metals subjected to various strains, strain rates, temperatures and pressures," *Engineering Fracture Mechanics*, vol. 21, no. 1, pp. 31–48, 1985. 5.3.1, 8
- [129] G. Chen, C. Ren, X. Yang, X. Jin, and T. Guo, "Finite element simulation of high-speed machining of titanium alloy (Ti-6Al-4V) based on ductile failure model," *International Journal of Advanced Manufacturing Technology*, vol. 56, no. 9-12, pp. 1027–1038, 2011. 5.3.1, 5.3.1, 5.3.2, 5.3.15, 8
- [130] B. Wang and Z. Liu, "Investigations on the chip formation mechanism and shear localization sensitivity of high-speed machining Ti6Al4V," *International Journal of Advanced Manufacturing Technology*, vol. 75, no. 5-8, pp. 1065–1076, 2014. 5.3.1, 5.3.1, 5.3.2, 5.3.19, 6.3.1, 6.3.1, 8
- [131] M. G. Cockcroft and D. J. Latham, "Ductility and the Workability of Metals," 1968. 5.3.1, 8
- [132] T. Özel and E. Zeren, "A methodology to determine work material flow stress and tool-chip interfacial friction properties by using analysis of machining," *Journal of Manufacturing Science and Engineering, Transactions of the ASME*, vol. 128, no. 1, pp. 119–129, 2006. 5.3.2, 5.3.2, 5.3.1, 6.3.1, 8
- [133] Y. B. Guo, Q. Wen, and K. A. Woodbury, "Dynamic material behavior modeling using internal state variable plasticity and its application in hard machining simulations," *Journal of Manufacturing Science and Engineering, Transactions of the ASME*, vol. 128, no. 3, pp. 749–759, 2006. 5.3.2, 5.3.3, 8
- [134] S. Anurag and Y. B. Guo, "A modified micromechanical approach to determine flow stress of work materials experiencing complex deformation histories in manufacturing processes," *International Journal of Mechanical Sciences*, vol. 49, pp. 909–918, sep 2007. 5.3.2, 5.3.2, 8
- [135] M. Calamaz, D. Coupard, and F. Girot, "A new material model for 2D numerical simulation of serrated chip formation when machining titanium alloy Ti-6Al-4V," *International Journal of Machine Tools and Manufacture*, vol. 48, pp. 275–288, mar 2008. 5.3.2, 5.3.4, 6.3.1, 8
- [136] T. Ozel, I. Llanos, J. Soriano, and P. J. Arrazola, "3d finite element modelling of chip formation process for machining inconel 718: Comparison of FE software predictions," *Machining Science and Technology*, vol. 15, no. 1, pp. 21–46, 2011. 5.3.2, 5.3.5, 8
- [137] D. Umbrello, "Finite element simulation of conventional and high speed machining of Ti6Al4V alloy," *Journal of Materials Processing Technology*, vol. 196, pp. 79–87, jan 2008. 5.3.2, 5.3.6, 8
- [138] T. Ozel, S. Yildiz, and J. Ciurana, "Influence of Material Models on Serrated Chip Formation in Simulation of Machining Ti-6Al-4V Titanium Alloy," 2009. 5.3.2, 5.3.7, 8
- [139] J. Sun and Y. B. Guo, "Material flow stress and failure in multiscale machining titanium alloy Ti-6Al-4V," *International Journal of Advanced Manufacturing Technology*, vol. 41, no. 7-8, pp. 651–659, 2009. 5.3.2, 5.3.8, 8
- [140] B. Shi and M. H. Attia, "Evaluation criteria of the constitutive law formulation for the metal-cutting process," *Proceedings of the Institution of Mechanical Engineers, Part B: Journal of Engineering Manufacture*, vol. 224, no. 9, pp. 1313–1328, 2010. 5.3.2, 5.3.9, 8
- [141] B. Shi, H. Attia, and N. Tounsi, "Identification of material constitutive laws for machining - Part I: An analytical model describing the stress, strain, strain rate, and temperature fields in the primary shear zone in orthogonal metal cutting," *Journal of Manufacturing Science and Engineering, Transactions of the ASME*, vol. 132, no. 5, 2010. 5.3.2
- [142] B. Shi, H. Attia, and N. Tounsi, "Identification of material constitutive laws for machining - Part II: Generation of the constitutive data and validation of the constitutive law," *Journal of Manufacturing Science and Engineering, Transactions of the ASME*, vol. 132, no. 5, pp. 1–9, 2010. 5.3.2
- [143] M. Sima and T. Özel, "Modified material constitutive models for serrated chip formation simulations and experimental validation in machining of titanium alloy Ti-6Al-4V," *International Journal of Machine Tools and Manufacture*, vol. 50, pp. 943–960, nov 2010. 5.3.2, 5.3.10, 5.3.11, 5.5, 5.5, 6.3.1, 8
- [144] M. Calamaz, D. Coupard, and F. Girot, "Numerical simulation of titanium alloy dry machining with a strain softening constitutive law," *Machining Science and Technology*, vol. 14, no. 2, pp. 244–257, 2010. 5.3.2, 5.3.12, 6.3.1, 8
- [145] Y. Karpap, "Temperature dependent flow softening of titanium alloy Ti6Al4V: An investigation using finite element simulation of machining," *Journal of Materials Processing Technology*, vol. 211, pp. 737–749, apr 2011. 5.3.2, 5.3.13, 5.3.14, 6.3.1, 8
- [146] M. Calamaz, D. Coupard, M. Nouari, and F. Girot, "Numerical analysis of chip formation and shear localisation processes in machining the Ti-6Al-4V titanium alloy," *International Journal of Advanced Manufacturing Technology*, vol. 52, no. 9-12, pp. 887–895, 2011. 5.3.2, 5.3.16, 8
- [147] A. Shrot and M. Bäker, "Determination of Johnson-Cook parameters from machining simulations," in *Computational Materials Science*, vol. 52, pp. 298–304, Elsevier, feb 2012. 5.3.2, 5.3.17, 8
- [148] R. Liu, S. Melkote, R. Pucha, J. Morehouse, X. Man, and T. Marusich, "An enhanced constitutive material model for machining of Ti-6Al-4V alloy," *Journal of Materials Processing Technology*, vol. 213, pp. 2238–2246, dec 2013. 5.3.2, 5.3.18, 8

- [149] W. Cheng, J. Outeiro, J. P. Costes, R. M'Saoubi, H. Karaoui, L. Denguir, V. Astakhov, and F. Auzenat, "Constitutive model incorporating the strain-rate and state of stress effects for machining simulation of titanium alloy Ti6Al4V," in *Procedia CIRP*, vol. 77, pp. 344–347, Elsevier B.V., jan 2018. 5.3.2, 5.3.3, 8
- [150] R. Bertolini, S. Bruschi, A. Ghiotti, G. Haugou, H. Morvan, and L. Dubar, "Material behaviour at low temperatures for calibrating cryogenic machining numerical simulations," *Procedia CIRP*, vol. 82, pp. 344–349, jan 2019. 5.3.2, 5.3.20, 8
- [151] T. Obikawa, M. Yamaguchi, K. Funai, Y. Kamata, and S. Yamada, "Air jet assisted machining of nickel-base superalloy," *International Journal of Machine Tools and Manufacture*, vol. 61, pp. 20–26, oct 2012. 5.4, 8
- [152] T. Lu, O. W. Dillon, and I. S. Jawahir, "A thermal analysis framework for cryogenic machining and its contribution to product and process sustainability," *11th Global Conference on Sustainable Manufacturing*, pp. 262–267, 2013. 5.4, 8
- [153] S. Y. Hong and Y. Ding, "Micro-temperature manipulation in cryogenic machining of low carbon steel," *Journal of Materials Processing Technology*, vol. 116, pp. 22–30, oct 2001. 5.4
- [154] M. Hribersek, V. Sajn, F. Pusavec, J. Rech, and J. Kopac, "The Procedure of Solving the Inverse Problem for Determining Surface Heat Transfer Coefficient between Liquefied Nitrogen and Inconel 718 Workpiece in Cryogenic Machining," *Procedia CIRP*, vol. 58, pp. 617–622, jan 2017. 5.4, 8
- [155] C. Tahri, P. Lequien, J. C. Outeiro, and G. Poulachon, "CFD Simulation and Optimize of LN2 Flow Inside Channels Used for Cryogenic Machining: Application to Milling of Titanium Alloy Ti-6Al-4V," *Procedia CIRP*, vol. 58, pp. 584–589, 2017. 5.4, 8
- [156] P. Lequien, G. Poulachon, J. C. Outeiro, and J. Rech, "Hybrid experimental/modelling methodology for identifying the convective heat transfer coefficient in cryogenic assisted machining," *Applied Thermal Engineering*, vol. 128, pp. 500–507, jan 2018. 5.4, 5.4.2, 8
- [157] P. Golda, R. Schießl, and U. Maas, "Heat transfer simulation of a cryogenic cooling stream in machining operation," *International Journal of Heat and Mass Transfer*, vol. 144, p. 118616, dec 2019. 5.4, 5.4.6, 8
- [158] A. Bordin, S. Imbrogno, G. Rotella, S. Bruschi, A. Ghiotti, and D. Umbrello, "Finite Element Simulation of Semi-finishing Turning of Electron Beam Melted Ti6Al4V Under Dry and Cryogenic Cooling," *Procedia CIRP*, vol. 31, pp. 551–556, jan 2015. 5.5, 5.5.1, 8
- [159] A. Davoudinejad, E. Chiappini, S. Tirelli, M. Annoni, and M. Strano, "Finite Element Simulation and Validation of Chip Formation and Cutting Forces in Dry and Cryogenic Cutting of Ti6Al4V," *Procedia Manufacturing*, vol. 1, pp. 728–739, jan 2015. 5.5, 5.5.2, 8
- [160] S. Imbrogno, S. Sartori, A. Bordin, S. Bruschi, and D. Umbrello, "Machining Simulation of Ti6Al4V under Dry and Cryogenic Conditions," *Procedia CIRP*, vol. 58, pp. 475–480, jan 2017. 5.5, 5.5.3, 8
- [161] D. Umbrello, S. Caruso, and S. Imbrogno, "Finite element modelling of microstructural changes in dry and cryogenic machining AISI 52100 steel," *Materials Science and Technology (United Kingdom)*, vol. 32, no. 11, pp. 1062–1070, 2016. 5.5, 5.7, 5.7.2, 5.7, 8
- [162] B. Stampfer, P. Golda, F. Zanger, R. Schießl, U. Maas, and V. Schulze, "Thermomechanically coupled numerical simulation of cryogenic orthogonal cutting," in *Procedia CIRP*, vol. 82, pp. 438–443, Elsevier B.V., jan 2019. 5.5, 5.5.4, 8
- [163] C. Salame, R. Bejjani, and P. Marimuthu, "A better understanding of cryogenic machining using CFD and FEM simulation," *Procedia CIRP*, vol. 81, pp. 1071–1076, jan 2019. 5.6, 5.6.1, 8
- [164] B. Shi, A. Elsayed, A. Damir, H. Attia, and R. M'Saoubi, "A Hybrid Modeling Approach for Characterization and Simulation of Cryogenic Machining of Ti-6Al-4V Alloy," *Journal of Manufacturing Science and Engineering, Transactions of the ASME*, vol. 141, no. 2, pp. 1–8, 2019. 5.6, 5.6.2, 8
- [165] G. Rotella and D. Umbrello, "Finite element modeling of microstructural changes in dry and cryogenic cutting of Ti6Al4V alloy," *CIRP Annals*, vol. 63, pp. 69–72, jan 2014. 5.7, 5.7.1, 8
- [166] D. Umbrello, A. Bordin, S. Imbrogno, and S. Bruschi, "3D finite element modelling of surface modification in dry and cryogenic machining of EBM Ti6Al4V alloy," *CIRP Journal of Manufacturing Science and Technology*, vol. 18, pp. 92–100, aug 2017. 5.7, 5.7.3, 8
- [167] G. M. Pittalà and M. Monno, "A new approach to the prediction of temperature of the workpiece of face milling operations of Ti-6Al-4V," *Applied Thermal Engineering*, vol. 31, pp. 173–180, feb 2011. 6.3.1
- [168] W. S. Lee and C. F. Lin, "High-temperature deformation behaviour of Ti6Al4V alloy evaluated by high strain-rate compression tests," *Journal of Materials Processing Technology*, vol. 75, pp. 127–136, mar 1998. 6.3.1
- [169] H. W. Meyer and D. S. Kleponis, "Modeling the high strain rate behavior of titanium undergoing ballistic impact and penetration," *International Journal of Impact Engineering*, vol. 26, pp. 509–521, dec 2001. 6.3.1
- [170] A. Sharma, R. C. Singh, and R. M. Singari, "Impact of cryogenic cooling during machining : A Literature Review," vol. 11, no. 2, pp. 1–6. 8
- [171] A. Ahmad-Yazid, Z. Taha, and I. P. Almanar, "A review of cryogenic cooling in high speed machining (HSM) of mold and die steels," *Scientific Research and Essays*, vol. 5, no. 5, pp. 412–427, 2010. 8
- [172] S. Paul and A. B. Chattopadhyay, "Environmentally conscious machining and grinding with cryogenic cooling," *Machining Science and Technology*, vol. 10, no. 1, pp. 87–131, 2006. 8
- [173] A. Shokrani, V. Dhokia, and S. T. Newman, "Evaluation of cryogenic CNC milling of Ti-6Al-4V titanium alloy," *22nd International conference on flexible automation and intelligent manufacturing, Helsinki-Stockholm*, pp. 1–4, 2012. 8

- [174] A. Shokrani, V. Dhokia, and S. T. Newman, "Study of the effects of cryogenic machining on the machinability of Ti-6Al-4V titanium alloy," *Proceedings of the 12th International Conference of the European Society for Precision Engineering and Nanotechnology, EUSPEN 2012*, vol. 2, no. June, pp. 283–286, 2012. 8
- [175] I. Lee, V. Bajpai, S. Moon, J. Byun, Y. Lee, and H. W. Park, "Tool life improvement in cryogenic cooled milling of the preheated Ti-6Al-4V," *International Journal of Advanced Manufacturing Technology*, vol. 79, no. 1-4, pp. 665–673, 2015. 8
- [176] A. Damir, A. Sadek, and H. Attia, "Characterization of Machinability and Environmental Impact of Cryogenic Turning of Ti-6Al-4V," *Procedia CIRP*, vol. 69, no. January, pp. 893–898, 2018. 8
- [177] D. Biermann, H. Abrahams, and M. Metzger, "Experimental investigation of tool wear and chip formation in cryogenic machining of titanium alloys," *Advances in Manufacturing*, vol. 3, no. 4, pp. 292–299, 2015. 8
- [178] E. Ceretti, L. Filice, D. Umbrello, and F. Micari, "ALE simulation of orthogonal cutting: A new approach to model heat transfer phenomena at the tool-chip interface," *CIRP Annals - Manufacturing Technology*, vol. 56, pp. 69–72, jan 2007. 8